THE
PHYSICAL REVIEW

A journal of experimental and theoretical physics established by E. L. Nichols in 1893

SECOND SERIES, VOL. 69, NOS. 7 AND 8 APRIL 1 AND 15, 1946

Some Experimental Results Concerning Mesotrons

R. P. SHUTT
The Bartol Research Foundation of the Franklin Institute, Swarthmore, Pennsylvania
(Received December 31, 1945)

In the first part of the article cross sections for anomalous, non-Coulombian single scattering of mesotrons are determined by a comparison of the scattering observed in two different lead thicknesses, a method partly described in a previous paper. For mesotrons with energies above $\sim 5\times 10^8$ ev it is found that the scattering through angles ranging from less than 5° up to 90° is predominantly anomalous. The second section concerns itself with showers of mesotrons. The phenomenon of saturation for the production of mesotron showers in lead as reported by Jánossy and Sinha is not confirmed. Some special photographs of mesotron and electron showers are reproduced and discussed. In the last section an analysis of the number of slow, heavily ionizing mesotrons and protons gives only slight and not conclusive evidence that mesotrons of very low energies (<20 Mev) disappear by a process other than any known so far.

1. APPARATUS

THE present article is intended to give a summary of results obtained from an analysis of about 40,000 cloud-chamber photographs taken several years ago by means of the apparatus described previously on several occasions.[1,2] The cloud chamber is 60 cm in diameter and 15 cm deep, and it contained argon at a pressure of 1.3 atmospheres saturated with a mixture of water and *n*-propyl alcohol vapors. Throughout the experiments to be described, three lead plates, 1 cm, 5 cm, and 1 cm thick, respectively, spaced 13 cm apart, were mounted horizontally inside the chamber. Expansions were controlled by coincidences of two counters located above the cloud chamber. All the photographs were stereoscopic.

The apparatus was operated in a sub-basement room under an estimated 60 cm of concrete. The position and amount of additional lead absorbers will be given in the course of the discussion.

For nearly half of the pictures, a homogeneous magnetic field of 1150 oersteds was maintained in the cloud chamber.

The photographs have been analyzed with particular regard to the effects of scattering and showers of cosmic-ray mesotrons, and to the number of mesotrons and protons of low energies.

2. ANOMALOUS SCATTERING

The angles α through which the rays were deflected while traversing one of the three lead plates were measured in the photograph taken along the axis of the cloud chamber. Distributions in α of the rays with the thicknesses t of the lead plates as parameters have thus been obtained. Since the magnetic field of 1150 oersteds is not sufficient to measure the energy of individual fast mesotrons, the distributions in

[1] T. H. Johnson, J. G. Barry, and R. P. Shutt, Phys. Rev. 59, 470A (1941).
[2] R. P. Shutt, Phys. Rev. 61, 6 (1942).

α involve the energy distribution of the particles inside the cloud chamber.

Mesotrons can be scattered by electrical forces as expressed by Coulomb's law or by short range nuclear and spin forces. When the deflections of the individual particles occur in one single act, the scattering is called single, while one speaks of multiple scattering when a large number of very small deflections is involved. Williams[3] has shown that the Coulomb scattering is predominantly multiple. For a given energy the distribution in α is Gaussian for multiple scattering, with only the mean value $\bar{\alpha}$ of the Gaussian depending on assumptions made concerning the kind and range of the scattering force. $\bar{\alpha}$ is of the form $kt^{\frac{1}{2}}$ where k is independent of the thickness t. The approximations involved are good as long as α is not too large. As discussed in a previous paper[2] introduction of the transformation $u=\alpha t^{-\frac{1}{2}}$ into the Gaussian distribution in α results in a function of u which is independent of t. It has also been shown[2] that even if the electrical scattering were single, the particular form of Coulomb's law would lead to an expression transformable in the same manner, provided the α are not too large. The following conclusions can be drawn. Provided the energy distributions of the particles in two lead plates of different thicknesses t are of the same shape, the distributions in α found experimentally in these thicknesses should become identical when expressed as functions of $u=\alpha t^{-\frac{1}{2}}$ if the scattering is purely multiple or purely of the Coulomb type (multiple or possibly single). Any departure from this rule shows that other forces are present besides the Coulomb force, and that scattering caused by these forces is single because single scattering is directly proportional to t, which with the one exception of single Coulomb scattering generally leads to distributions not transforming in the way described above. Since the actual paths taken by the rays are somewhat longer than t, and because of the approximations involved in Williams' theory, the values of the functions of u for $\alpha<30°$ may differ by an estimated 3 percent compared with actually observed departures of 40 percent or more. The object of the present discussion is to confirm and extend the conclusions drawn earlier making use of the new data.

The following illustrates how the number of mesotrons scattered anomalously, i.e., neither by any type of multiple process nor by a force varying with the square of the distance from the scattering center, can be determined from the experimental data. $A_1\big|_{u_1}^{u_2}$ and $A_2\big|_{u_1}^{u_2}$ shall designate the number of mesotrons scattered anomalously in the thicknesses t_1 and t_2, respectively, in the range $u_1 \leqq u \leqq u_2$. The letter E in place of A refers to the number of particles scattered electrically, and T is the total number deflected. According to the theory outlined above we then have

$$E_1\big|_{u_1}^{u_2}=E_2\big|_{u_1}^{u_2}, \tag{1}$$

and therefore

$$T_2\big|_{u_1}^{u_2}-T_1\big|_{u_1}^{u_2}=A_2\big|_{u_1}^{u_2}-A_1\big|_{u_1}^{u_2}. \tag{2}$$

T_1 and T_2 have been measured, A_1 and A_2 are unknown. Thus Eq. (2) is not sufficient, and further assumptions must be made. Transforming back to α we have from (2)

$$T_2\big|_{\alpha_{12}}^{\alpha_{22}}-T_1\big|_{\alpha_{11}}^{\alpha_{21}}=A_2\big|_{\alpha_{12}}^{\alpha_{22}}-A_1\big|_{\alpha_{11}}^{\alpha_{21}}, \tag{3}$$

where $\alpha_{11}=u_1t_1^{\frac{1}{2}}$, $\alpha_{21}=u_2t_1^{\frac{1}{2}}$, $\alpha_{12}=u_1t_2^{\frac{1}{2}}$, and $\alpha_{22}=u_2t_2^{\frac{1}{2}}$. Evidently one can write

$$A_1\big|_{\alpha_{11}}^{\alpha_{21}}=A_1\big|_{\alpha_{11}}^{\alpha_{12}}+A_1\big|_{\alpha_{12}}^{\alpha_{22}}-A_1\big|_{\alpha_{21}}^{\alpha_{22}}, \tag{4}$$

and thus from (3) and (4)

$$A_2\big|_{\alpha_{12}}^{\alpha_{22}}-A_1\big|_{\alpha_{12}}^{\alpha_{22}} = T_2\big|_{\alpha_{12}}^{\alpha_{22}}-T_1\big|_{\alpha_{11}}^{\alpha_{21}}+A_1\big|_{\alpha_{11}}^{\alpha_{12}}-A_1\big|_{\alpha_{21}}^{\alpha_{22}}. \tag{5}$$

The A_1 still present in Eq. (5) can easily be estimated. As pointed out before, any anomalous scattering observable by this method must be single, and therefore proportional to t. Thus generally

$$A_1\big|_{\alpha_a}^{\alpha_b}=(t_1/t_2)A_2\big|_{\alpha_a}^{\alpha_b}. \tag{6}$$

Furthermore we certainly have

$$0<A_2\big|_{\alpha_{11}}^{\alpha_{12}}<T_2\big|_{\alpha_{11}}^{\alpha_{12}} \tag{7}$$

[3] E. J. Williams, Proc. Roy. Soc. **A169**, 531 (1939).

TABLE I. Anomalous scattering between 4.5° and 27°.

	1 $T_1\|_0^{90}$ 1 cm Pb, traversals	2 $T_2\|_0^{90}$ 5 cm Pb, traversals	3 $T_1\|_2^{12}$ 1 cm Pb %	4 $T_2\|_{4.5}^{27}$ 5 cm Pb %	5 $T_2\|_2^{4.5}$ 5 cm Pb %	6 $T_2\|_{12}^{27}$ 5 cm Pb %	7 $A_{2\min}\|_{4.5}^{27}$ 5 cm Pb %	8 $A_{2\max}\|_{4.5}^{27}$ 5 cm Pb %	9 $\frac{A_{2\min}}{T_2}\|_{4.5}^{27}$ %	10 $\frac{A_{2\max}}{T_2}\|_{4.5}^{27}$ %	11 $E_{\min}$ 10^9 ev
a Observed under 15 cm Pb and 60 cm of concrete	27200	13800	4.8	7.8	10.0	1.3	4.9±0.5	(7.7±0.5) 6.3±0.5	48±5	(76±5) 63±5	0.2
b Same as a, selected pictures	6900	3700	5.0	7.4	8.9	1.3	3.9±0.8	(6.3±0.8) 5.1±0.8	41±8	(66±8) 53±8	0.2
c Same as a, with triple coincidences	5300	2700	1.6	3.3	9.8	0.0	2.8±0.7	(5.9±0.7) 4.3±0.7	65±16	(138±16) 100	4.5
d Observed under 88 cm Pb and 60 cm of concrete	5900	3100	2.0	5.9	8.3	0.8	6.3±0.8	(8.7±0.8) 7.7±0.8	82±10	(113±10) 100	0.2

TABLE II. Anomalous scattering between 9° and 27°.

	1 $T_1\|_0^{90}$ traversals	2 $T_2\|_0^{90}$ traversals	3 $T_1\|_4^{12}$ %	4 $T_2\|_9^{27}$ %	5 $T_2\|_4^{9}$ %	6 $T_2\|_{12}^{27}$ %	7 $A_{2\min}\|_9^{27}$ %	8 $A_{2\max}\|_9^{27}$ %	9 $\frac{A_{2\min}}{T_2}\|_9^{27}$ %	10 $\frac{A_{2\max}}{T_2}\|_9^{27}$ %	11 $E_{\min}$ 10^9 ev
a Observed under 15 cm Pb and 60 cm of concrete	27200	13800	2.0	2.4	6.4	1.3	0.6±0.3	(2.3±0.3) 1.5±0.3	19±10	(74±10) 49±10	0.2
d Observed under 88 cm Pb and 60 cm of concrete	5900	3100	0.8	1.7	4.9	0.8	1.5±0.3	(2.8±0.3) 2.2±0.3	68±13	(127±13) 100	0.2

and

$$0<A_2|_{\alpha_{21}}^{\alpha_{22}}<T_2|_{\alpha_{21}}^{\alpha_{22}}. \quad (8)$$

Finally, it appears to be an experimental fact that

$$T_2|_{\alpha_{11}}^{\alpha_{12}}>T_2|_{\alpha_{21}}^{\alpha_{22}}. \quad (9)$$

Making use of Eq. (6) and substituting the inequalities (7) to (9) into Eq. (5) we obtain

$$A_{2\min}|_{\alpha_{12}}^{\alpha_{22}}=[T_2|_{\alpha_{12}}^{\alpha_{22}}-T_1|_{\alpha_{11}}^{\alpha_{21}}]t_2/(t_2-t_1) \quad (10)$$

and

$$A_{2\max}|_{\alpha_{12}}^{\alpha_{22}}=[T_2|_{\alpha_{12}}^{\alpha_{22}}-T_1|_{\alpha_{11}}^{\alpha_{21}}+(T_2|_{\alpha_{11}}^{\alpha_{12}}-T_2|_{\alpha_{21}}^{\alpha_{22}})t_1/t_2]t_2/(t_2-t_1) \quad (11)$$

as upper and lower limits for A_2, the number of mesotrons scattered anomalously through angles $\alpha_{12}\leqq\alpha\leqq\alpha_{22}$.

Previously[2] only the lower limit $A_{2\min}$ had been calculated which appeared to be sufficient on account of the large statistical errors involved then.

The data as they are needed for the calculations have been compiled in Tables I and II, columns 1–6. In columns 7–10, the results are given. Observations on the two 1-cm lead plates have been combined. In Table I $\alpha_{11}=2°$ and $\alpha_{21}=12°$ have been chosen, leading to values of $\alpha_{12}=4.5°$ and $\alpha_{22}=27°$, respectively, using $t_1=1$ cm and $t_2=5$ cm. The choice of the lower limit α_{11} is determined by the accuracy with which the angles can be measured, while the upper

limit α_{21} is chosen such as to make $\alpha_{22}<30°$. In Table II $\alpha_{11}=4°$ has been selected, the upper limit being the same as in Table I.

An estimated correction of 30 percent has been added to all values of A_2 and the values of T_2 used for computation of columns 9 and 10 since only projections of the actual three-dimensional deflections onto the plane of the photographic camera have been measured.

The observations listed in row *a* of the tables were made under 15 cm of lead located immediately above the cloud chamber in addition to the 60 cm of concrete making up the structure of the building. For row *b* of Table I a number of pictures with particularly clear and straight tracks have been selected. Row *d* shows data obtained under 88 cm of lead in place of the 15 cm used before. Row *c* of Table I has been obtained in the following way. Again there were 15 cm of lead above the chamber, but in addition a large counter tray containing 56 counters was placed below the cloud chamber with 35 cm of lead interposed between chamber and tray. Double coincidences of the two upper counters still tripped the expansion mechanism regardless of the state of the lower counter tray. But, whenever a triple coincidence occurred between the top counters and the bottom tray, a small neon bulb mounted near the center of the front side of the chamber was lit up for a few seconds, thus indicating that the ray had penetrated 35 cm of lead after leaving the chamber. The light flash can be seen in Fig. 3.

The uncertainties indicated in columns 7–10 are standard errors calculated in the usual way.

Finally, the 11th column gives a lower limit for the kinetic energy of the particles as determined by the following criteria. In rows *a*, *b*, and *d* all tracks have been included except those which appeared to be heavily ionized. A mesotron ionizes appreciably more than normally when its energy falls below 0.2×10^8 ev. Thus the lower limit observed here is $E_{\min}=0.2\times10^8$ ev. However where a triple coincidence occurred the ray must have penetrated the 35 cm of lead below the cloud chamber. Here the theory of ionization leads to a value of $E_{\min}$ of 4.5×10^8 ev.

In columns 7 and 8, $A_{2\,\min}$ and $A_{2\,\max}$ have been tabulated showing the minimum and maximum percentages of mesotrons scattered anomalously in the 5-cm lead plate. These fractions refer to the total number of traversals through the plate. In columns 9 and 10 the fractions $A_{2\,\min}/T_2$ and $A_{2\,\max}/T_2$, respectively, are listed for comparison of the number of anomalously scattered particles with the total of rays scattered through the same range of angles.

Now, in column 10 there occurred two values for $A_{2\,\max}/T_2$ which were greater than 100 percent showing that the calculated $A_{2\,\max}$ is actually much too high. By putting the two values in question equal to 100 percent, all the other numbers involving $A_{2\,\max}$ have been reduced correspondingly by interpolation between $A_{2\,\min}$ and $A_{2\,\max}$. The original, too-high values have been enclosed in parentheses in the tables.

Comparing the results for A_2 obtained from the different sets of pictures, and noted in columns 7 and 8, one finds only slight disagreements outside the experimental uncertainties, the value in row *d* being somewhat too high, and the value in row *c* being too low. The latter value cannot be considered quite reliable because, although the large counter tray below the chamber was made as large as possible, making use of available counters, its size may yet have been somewhat too small to register all rays of interest. The significance of the discrepancies can be evaluated as follows. For the corresponding values of A_2/T_2 in columns 9 and 10 these discrepancies become quite considerable. First, comparing rows *a* and *c*, one sees that $A_{2\,\max}/T_2$, for instance, varies from a value of (63 ± 5) percent in row *a* to a value possibly as large as 100 percent in row *c*. The difference must be due to the fact that the lower energy limit $E_{\min}$ is considerably higher in row *c* than it is in row *a*. The mean electrical deflection for particles in the cut-off part of the energy spectrum ($0<E<4.5\times10^8$ ev) is $\geqq5°$, as follows from Williams' theory. Thus these particles of the lower energies contribute largely to electrical scattering through angles $>4.5°$, which is our lower limit here, and most of the scattering through $\alpha>4.5°$ observed for particles of energies higher than 4.5×10^8 ev is anomalous, in qualitative agreement with the results.

Next we compare the results for A_2/T_2 given in rows *a* and *d*. Here the energy limits for the particles observed in the cloud chamber are

identical. Yet a very large discrepancy is found. The latter is even more significant here than it was before because the uncertainties in row *d* are smaller than in row *c*. The only possible reason for the disagreement appears to be that the energy distributions in the two cases are not identical, but that under 88 cm of lead the number of mesotrons of low energy is reduced considerably. The absorber of 88 cm of lead was piled as an inverted truncated pyramid covering the solid angle of the counter system and the cloud chamber. Its average width measured along the cloud-chamber plane was about equal to its height, but measured along the direction of the axis of the cloud chamber its average width was $\frac{1}{3}$ of its height only. The lead above the chamber also scatters mesotrons. Some of the particles are scattered out of the lead at the four almost vertical sides and thus lost from observation, and a few entering these boundaries from the outside may be scattered into the solid angle under observation. An estimate of this effect shows that in a cylindrical absorber of rectangular cross section the fraction of particles lost in this way at two opposite boundaries is of the order of $z \approx 10^7 t^3/wE_M$, with w for the width and t for the thickness of the lead absorber. E_M can be taken as the geometric mean of the energies of the mesotrons at the top and at the bottom of the lead pile. The expression for z represents an approximation as long as $z<1$ and cannot be used when $z \geqq 1$, of course. With our values of $t=88$ cm, $w=30$ cm (average width of the truncated pyramid), and for particles sensitive to electrical scattering of, say, 3×10^8 ev (energy at the top of the lead pile $\sim 1.5\times10^9$ ev) one calculates that $z=40$ percent. For the truncated pyramid actually used the geometrical conditions are such that still more particles of these energies are prevented from entering the cloud chamber. Therefore, under a lead pile of $t>w$ we have to expect a very considerable reduction of particles sensitive to electrical scattering, and the high portion of anomalously scattered particles found in row *d* becomes understandable. It thus appears that above energies of $\sim 0.5\times10^9$ ev the anomalous scattering becomes all-important.

Substituting the values of A_2 from columns 7 and 8 into expression (9) of reference 2 one can calculate limits for an average cross section for the anomalous scattering through $4.5° \leqq \alpha \leqq 27°$. One finds

$$14\times10^{-28}\ \text{cm}^2 \pm 10\% < \sigma(4.5°, 27°) < 18 \times10^{-28}\ \text{cm}^2 \pm 8\% \quad (12)$$

per neutron or proton in lead, averaged over almost the whole energy spectrum of the mesotrons, or

$$18\times10^{-28}\ \text{cm}^2 \pm 12\% < \sigma(4.5°, 27°) < 22 \times10^{-28}\ \text{cm}^2 \pm 10\% \quad (13)$$

per neutron or proton in lead, averaged over the part of the energy spectrum lying above 5×10^8 ev.

Proceeding in exactly the same way for the data listed in Table II one finds corresponding values of

$$2\times10^{-28}\ \text{cm}^2 \pm 50\% < \sigma(9°, 27°) < 4 \times10^{-28}\ \text{cm}^2 \pm 20\% \quad (14)$$

for mesotrons of practically all energies of the energy spectrum, and

$$4\times10^{-28}\ \text{cm}^2 \pm 20\% < \sigma(9°, 27°) < 6 \times10^{-28}\ \text{cm}^2 \pm 15\% \quad (15)$$

for mesotrons of energies $>5\times10^8$ ev.

The observations of other investigators have been discussed in detail in reference 2.* Code's[4] results seem to be particularly well suited for a direct comparison with the present results. In 3.8 cm of tungsten (equivalent to $\sim$6 cm of lead) Code found 10 particles with energies greater than 6×10^8 ev scattered through angles larger than 9° where only 1 or 2 were expected if the scattering were purely Coulombian. This leads to a value of $A/T=(80\pm20)$ percent in qualitative agreement with our corresponding values listed in Table II, row *d*, columns 9 and 10, and also to a cross section of $\sigma(>9°)=5.7\times10^{-28}$ cm$^2\pm35$ percent in agreement with our expression (15) referring to similar ranges of energy and deflections. But our expression (13) for the anomalous scattering through angles between 4.5° and 27° is 3 or 4 times larger than any calculated from the observations of others. Unless some systematic error not yet accounted

* *Note added in proof:* Comparison with results published quite recently by M. S. Sinha [Phys. Rev. 68, 153 (1945)] has been made in a short article by the writer [Phys. Rev. 69, 128 (1946)].

[4] F. L. Code, Phys. Rev. 59, 229 (1941).

TABLE III. Mesotron showers.

Thickness of dense matter above cloud chamber		1 Number of mesotron pairs forming angles between 0°<2°	2 2°<4°	3 4°<6°	4 6°<8°	5 8°<10°	6 10°<20°	7 Total No. traversing ≧6 cm of lead	8 Pairs (0°–4°) originating from a point in the lead above cloud chamber	9 Showers of more than 2 mesotrons, originating in lead above cloud chamber
60 cm of concrete +15 cm of lead	*a* Cases	15	8	2	3	2	22	13400	3	1 (6 mesotrons)
	b Cases per 1000 traversals	1.1 ±0.3	0.6 ±0.2	0.15	0.22	0.15	1.6	1000	0.2±0.1	0.07
	c Random cases expected per 1000	0.28	0.28	0.28	0.28	0.28	1.4		0.03	
60 cm of concrete +88 cm of lead	*d* Cases	7	3	5	2	1	2	3100	5	1 (3 mesotrons)
	e Cases per 1000 traversals	2.3 ±0.9	0.9 ±0.5	1.4 ±0.6	0.6	0.3	0.6	1000	1.6±0.7	0.3
	f Random cases expected per 1000	0.28	0.28	0.28	0.28	0.28	1.4		0.18	

for has entered our own observations the most plausible among several possible explanations for the disagreement may be that all the observations of others have been made with only a single scattering plate while measuring the energy of the individual particles. Usually mesotrons of all energies were present, and the apparently considerable overlapping of the effects of Coulombian and anomalous scattering would then make detection of the latter more difficult than if the energies at which particles are sensitive to Coulomb scattering are cut off. Since the anomalous scattering as dependent on the energy of the mesotrons is of considerable theoretical interest it seems to this author that an experiment pertaining to this matter could be performed most efficiently by measuring the energy of the individual particles in the usual way, but carrying out the experiment under a lead pile geometrically similar to that employed here, a method which apparently eliminated a large number of mesotrons of energies sensitive to Coulomb scattering from observation in the cloud chamber.

Previously our results agreed with those following from a theory of nuclear scattering of mesotrons of a spin of $\frac{1}{2}$ as developed by Marshak and Weisskopf. By means of a more rigorous calculation Heitler and Peng[5] have shown more recently that a spin of 1 for the mesotron would also be in qualitative agreement with the experimental results obtained so far. These authors calculate that the scattering cross section should be of the order of 10^{-27} cm^2 for mesotrons of an energy of 8×10^8 ev.

Summarizing we can say that the anomalous scattering becomes of particular importance at energies $>5\times10^8$ ev, when the behavior of mesotrons becomes essentially relativistic and therefore spin forces are important, and that the distribution of the deflections extends down to and probably below angles of 4.5°. Removing the mesotrons of energies below 5×10^8 ev by some means lets the effect appear much more clearly since this procedure eliminates the particles sensitive to Coulomb scattering from observation.

3. MESOTRON SHOWERS

The existence of showers of mesotrons first was indicated by experiments conducted by Schmeiser and Bothe.[6] When measuring the number of cosmic-ray showers as a function of the thickness of dense material under which the observations were made ("Rossi Curve") these investigators

[5] W. Heitler and H. W. Peng, Phys. Rev. **62**, 81 (1942).
[6] K. Schmeiser and W. Bothe, Naturwiss. **25**, 669 (1937).

found a small "second maximum" where only one maximum was expected from the electron cascade theory. The matter has been studied further by several observers employing counter methods, work having been done at sea level as well as at high elevations.[7–9] The most extensive counter studies performed at sea level are due to Jánossy and Rochester.[10] Single cloud-chamber pictures of associated mesotrons have been obtained by many,[11–18] mostly at high elevations and with a frequency of one in 3000 or 4000 photographs of single tracks. A systematic study of the effect by means of the cloud-chamber method has been carried out more recently by Sinha.[19] Operated at sea level, Sinha's cloud chamber was controlled by an arrangement of counters such that only showers were recorded whose component rays formed small angles with respect to each other. The photographs include one case of 12 associated particles having a common point of origin in the lead block placed above the chamber and penetrating 2.2 cm of lead. The rays are not scattered appreciably and do not multiply in the lead, a fact which is commonly taken for sufficient evidence that actually mesotrons, and not electrons, are involved.

An analysis of the present data again confirms the existence of mesotron showers. The results are given in Table III. Only particles seen to penetrate at least 6 cm of lead inside the cloud chamber have been included in order to assure that no electrons are involved. All observations under 15 cm of lead have been combined in row *a* while those under 88 cm of lead are shown in row *d*. Rows *b* and *e* give the respective data reduced to a basis of 1000 traversals of single rays through the chamber. Standard errors are noted where they are of interest. Columns 1–8 concern showers of two mesotrons only. Two cases of showers of more than two mesotrons are listed in the ninth column. The projections of the angles between the pairs of tracks onto the cloud-chamber plane have been measured, and the results have been grouped into steps of 0° to, but not including 2° (expressed by $0°<2°$), 2° to, but not including 4° ($2°<4°$), etc., as indicated in columns 1–6. In these columns pairs diverging from a point above the cloud chamber have not been separated from those converging toward a point inside or below. It turns out that only small divergences are of interest, and two rays which originally may have appeared to diverge slightly may easily become convergent due to scattering. However, the pairs and multiple showers listed in columns 8 and 9, respectively, are only those which seem to diverge from a point in the lead above the chamber. Finally, column 7 gives the total number of mesotrons observed.

In these experiments a single mesotron was sufficient to trip the cloud-chamber mechanism. Thus any additional particle seen on a photograph either happens to be present at random or it is actually associated with the first one. To calculate the chance for random association of mesotrons in our arrangement we need the following quantities. Whether or not two mesotrons appear to be simultaneous in a cloud chamber depends on the relative width and luminous intensity of their tracks. From well-known theoretical and experimental investigations concerning the diffusion of ions in gases a "resolving time" of 1/20 sec. is found for this particular apparatus. The observations were made in a solid angle of 0.18. The counters covered an area of 40 sq. cm. With these values and a counting rate of 0.6 per minute per sq. cm per unit solid angle the expected number of chance coincidences of mesotrons has been calculated and tabulated in rows *c* and *f* of Table III.

Comparing within columns it is seen that the number of mesotron pairs is about as expected

[7] W. F. G. Swann, Rev. Mod. Phys. **11**, 250 (1939). W. F. G. Swann and W. E. Ramsey, Phys. Rev. **57**, 106 (1940). W. F. G. Swann, J. Frank. Inst. **230**, 323 (1940).
[8] M. Damy DeSouza Santos, P. A. Pompeia, and G. Wataghin, Phys. Rev. **59**, 902 (1941).
[9] J. F. Carlsson and M. Schein, Phys. Rev. **59**, 840 (1941). M. Schein, W. P. Jesse, and E. O. Wollan, Phys. Rev. **59**, 930 (1941).
[10] L. Jánossy, Proc. Roy. Soc. **A179**, 361 (1942). L. Jánossy, Phys. Rev. **64**, 345 (1943). L. Jánossy and G. D. Rochester, Proc. Roy. Soc. **A183**, 181 (1944).
[11] J. C. Street, J. Frank. Inst. **227**, 765 (1939).
[12] H. J. J. Braddick and G. S. Hensby, Nature **144**, 1012 (1939).
[13] G. Herzog and W. H. Bostick, Phys. Rev. **58**, 278 (1940).
[14] W. M. Powell, Phys. Rev. **60**, 413 (1941).
[15] D. J. Hughes, Phys. Rev. **60**, 414 (1940).
[16] E. O. Wollan, Phys. Rev. **60**, 532 (1941).
[17] L. Jánossy, C. B. McCusker, and G. D. Rochester, Nature **148**, 660 (1941).
[18] W. H. Bostick, Phys. Rev. **61**, 557 (1942).
[19] M. S. Sinha, Trans. Bose Res. Inst., Calcutta **15**, 191 (1942/43).

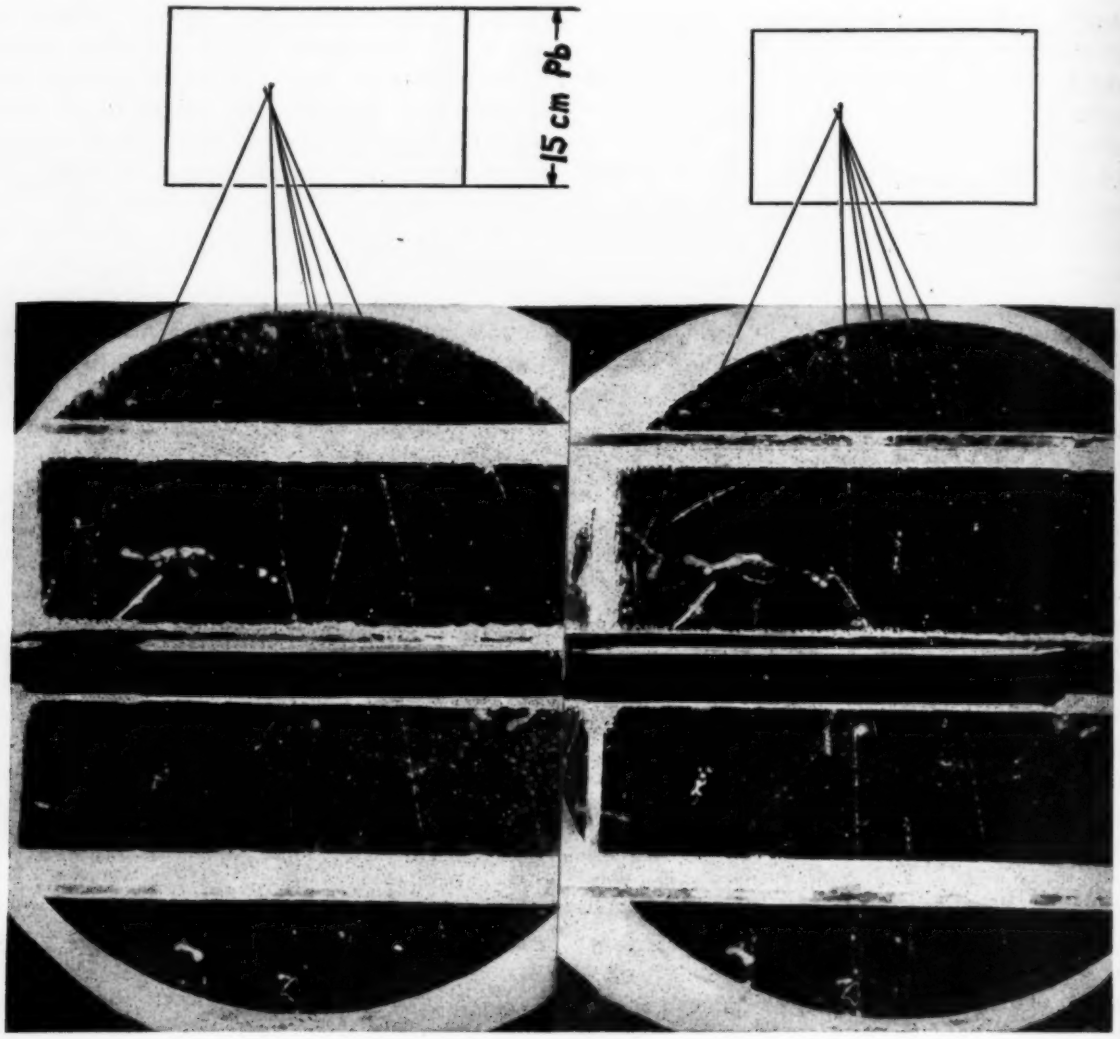

FIG. 1. A shower of 6 mesotrons produced near the center of a lead block 15 cm thick.

for random association for all angles larger than 6°. But for the smaller angles a discrepancy is present which is largest between 0° and 2°. This experiment thus confirms that there exist small angle showers of mesotrons whose angular spread ranges up to 6° or so.

Since most of the mesotrons occurring in the showers penetrate 6 cm of lead without any noticeable scattering effect, their energies must be of the order of 10^9 ev or more. This is in agreement with Jánossy's results.

For the rest of this section we shall be concerned only with the showers having their origin in the lead above the cloud chamber. From columns 7–9 of row *b* we have a rate of occurrence of about one mesotron shower for every 4000 single penetrating rays which is in agreement with previous rates observed in cloud chambers,[11–18] and also in qualitative agreement with a rate of one in 12,000 as reported by Jánossy.[10] In our arrangement 1000 traversals of single rays were observed in 5 hours. It follows that 5 mesotron showers were recorded in 100 hours which agrees with a value given by Sinha[19] for a similar experimental arrangement.

Sinha finds that the frequency of mesotron pairs is about equal to the frequency of showers containing more than two penetrating particles, while others, including ourselves (Table III, column 9), seem to have observed considerably

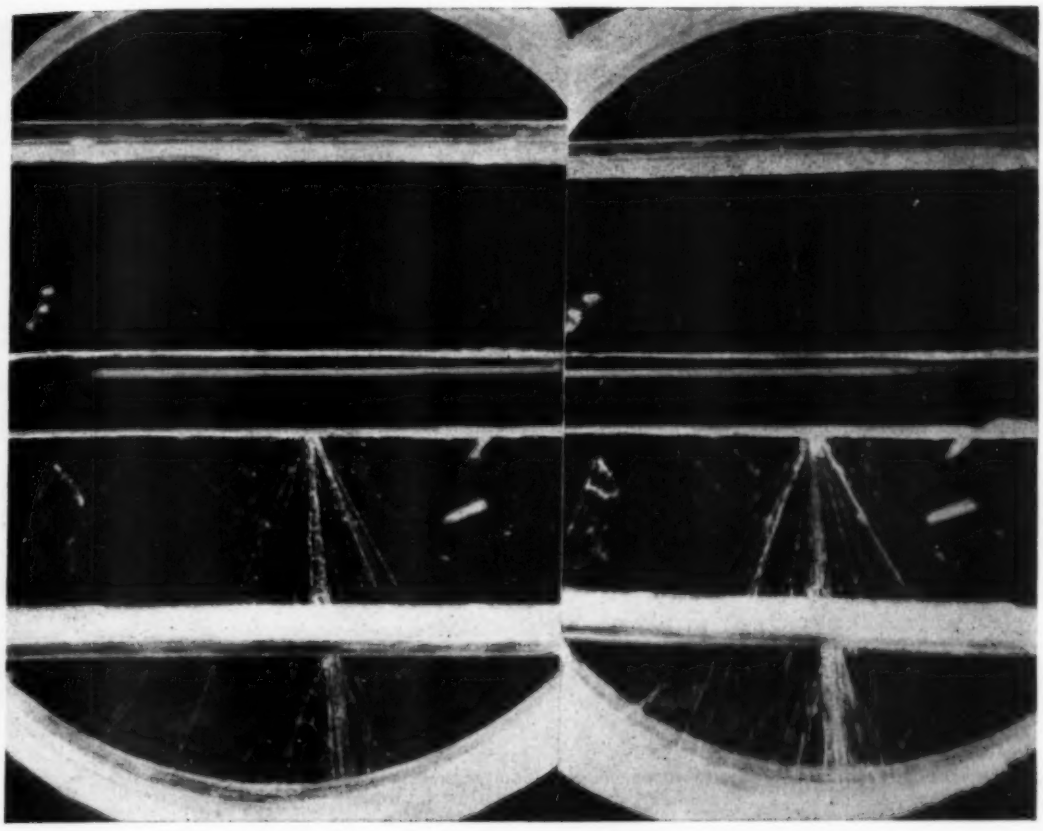

FIG. 2. A shower possibly containing as many as 11 mesotrons produced in 5 cm of lead.

less multiple showers than pairs. An explanation for this discrepancy may be found in the differences in geometry of the counters and cloud-chamber arrangements employed.

A serious discrepancy between these results and those of others appears in column 8, rows *b* and *e*. Both Jánossy and Sinha, observing under lead thicknesses ranging from 0 to ~20 cm, report saturation for the production of mesotron showers when the thickness of the lead absorber exceeds about 5 cm. Therefore we should expect to observe as many showers under 88 cm as were found under 15 cm. Instead we have 0.2 ± 0.1 cases for every 1000 traversals of mesotrons below 15 cm, and 1.6 ± 0.7 cases below 88 cm of lead. The ratio of these two values is 8 ± 5, while the ratio of the two lead thicknesses is 6. Thus indications are here that the number of mesotron showers is roughly proportional to the lead thickness traversed by the producing primary radiation, and that no saturation is reached up to thicknesses of 90 cm at least. However, it is felt that the large uncertainty resulting from the small number of cases observed here does not justify any further conclusions concerning this point at this time.

The most recent theory of the production of mesotrons by protons or neutrons is due to Hamilton, Heitler, and Peng,[20] and has been extended to cases of multiple showers by Jánossy.[10] In their treatment of the problem the existence of protons and neutrons of energies as high as 10^{12} ev is assumed, and reasonable agreement with Jánossy's and Sinha's experimental results is found, including the phenomenon of saturation which is not confirmed in the present article. If high energy protons or neutrons passing through or very close by nuclei of matter are responsible for the production of one or several mesotrons, a certain number of multiple mesotron showers might be expected to consist of particles which do not all have a common point of origin but

[20] J. Hamilton, W. Heitler, and H. W. Peng, Phys. Rev. 64, 78 (1943).

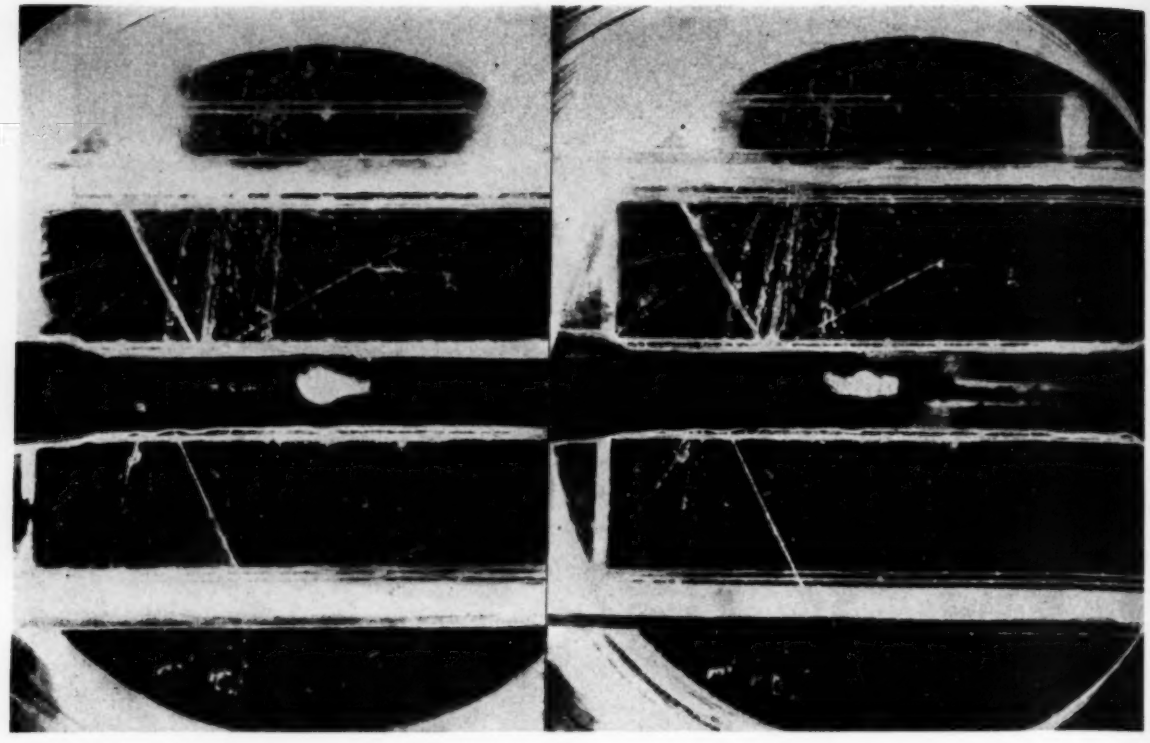

FIG. 3. A shower containing at least 4 mesotrons one of which ionizes heavily in the 3rd compartment. 3 heavily ionizing particles diverge backwards from a point near the top of the 5-cm lead plate.

were produced successively along the path of the primary. No definite case of this type has been observed so far. A process whereby protons of high energy may disintegrate spontaneously into several mesotrons in the presence of matter has been suggested by Swann.[21]

We shall now turn to a discussion of some photographs of special interest. In Fig. 1 a shower of at least 4, more probably 6, mesotrons is shown. The individual rays have been traced back to their origin, and it is seen that they intersect almost perfectly in one single point in both of the stereoscopic views. The particle at the extreme left has probably been scattered by the residual lead traversed after the production of the shower which explains the slight apparent deviation of this track from the common point of origin. Only 4 of the 6 rays definitely penetrate 6 cm of lead inside the cloud chamber while the remaining two rays are seen to traverse only one cm of lead which is not quite sufficient to ascertain that these particles are mesotrons, since it is not improbable that some electrons may penetrate one cm of lead without producing secondaries. However, the origin of the shower is found to lie near the center of the 15-cm lead block above the chamber. Thus all rays had had to traverse at least 7 cm of lead before entering the chamber. An electron of an energy sufficient to penetrate 7 cm of lead would produce a considerable number of secondaries, and in this process it would also very probably be deflected so that it could not be traced back to its origin. We therefore may identify all of the 6 particles as mesotrons produced in one single act. For the present experimental arrangement it is estimated that only one in 10^{20} photographs of this type may be expected to be due to random association of mesotrons.

During the course of these experiments one or two showers of mesotrons could have been expected to originate in the lead located inside the cloud chamber. One possible case of a mesotron shower produced in the 5-cm lead plate is shown in Fig. 2. The shower was produced by a proton or mesotron which had penetrated the 15 cm of

[21] W. F. G. Swann, Phys. Rev. 58, 200 (1940); Phys. Rev. 60, 470 (1941).

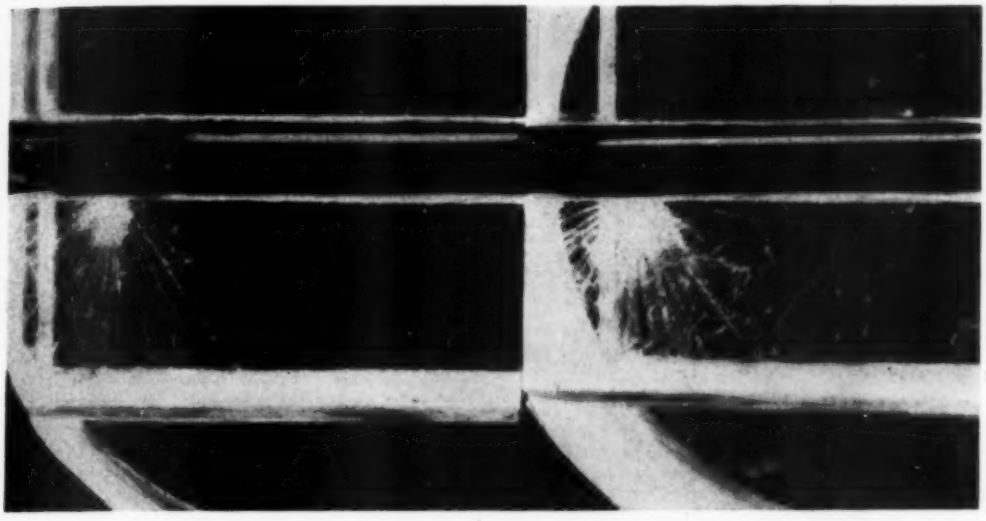

FIG. 4. A shower consisting of *ca.* 80 electrons of energies probably less than 15 Mev. No electrons of higher energies can be seen.

lead above the cloud chamber. The nature of the shower particles is doubtful because they are seen to penetrate only one cm of lead. Nevertheless indications are that some of the particles are mesotrons. One particle passing to the right ionizes 2 to 3 times as much as a fast particle and is found to stop in the one-cm lead plate. This particle is a mesotron because a proton ionizing that much could penetrate 3 or 4 cm of lead. Furthermore there are 3 rays passing through the plate without multiplication. These rays are not scattered appreciably which would usually be the case with an electron of an energy low enough to penetrate one cm of lead without multiplication. Finally the 7 particles forming the center "core" of the shower pass through the plate without being scattered. Some multiplication is present here, but most of these secondary electrons seem to be produced by one of the rays only. A calculation concerning the probability for the occurrence of a cascade shower of this structure is not possible because the energy of the individual particles is not known. But it is not impossible that this shower contains as many as 11 mesotrons produced in one single act.

TABLE IV. Particles stopping in lead.

Thickness of lead plate	Selected number of particles impinging on plate	Percent stopping
Upper, 1 cm	3100	0.3±0.1
Center, 5 cm	2700	1.8±0.2
Lower, 1 cm	2000	0.5±0.2
Upper and lower combined, 1 cm	5100	0.4±0.1

Mesotrons associated with large electron showers have been observed by Sinha.[19] In this experiment 18 large showers originating above the cloud chamber have been observed, at least 9 of which seem to contain one or more mesotrons. These showers were not further investigated since in most cases too many electrons were present to be sure of the number of mesotrons. One case containing only a moderate number of electrons is shown in Fig. 3. This shower originates at a point 14 cm inside the lead above the chamber. Associated with it are at least 4 mesotrons one of which ionizes heavily in the 3rd compartment and stops in the lower one-cm plate. If the shower reproduced in Fig. 2 were continued, it might have an appearance similar to that of the present one. The backward divergence of 3 heavily ionizing particles in the 2nd compartment is remarkable. Two of these particles are very probably protons of low energy. Showers with some slow rays passing backwards from a point in lead were observed previously by Street[11] and, of course, by several other investigators operating cloud chambers at high elevations. At the present time the most likely explanation is that a "nuclear evaporation" has been initiated by one of the shower particles.

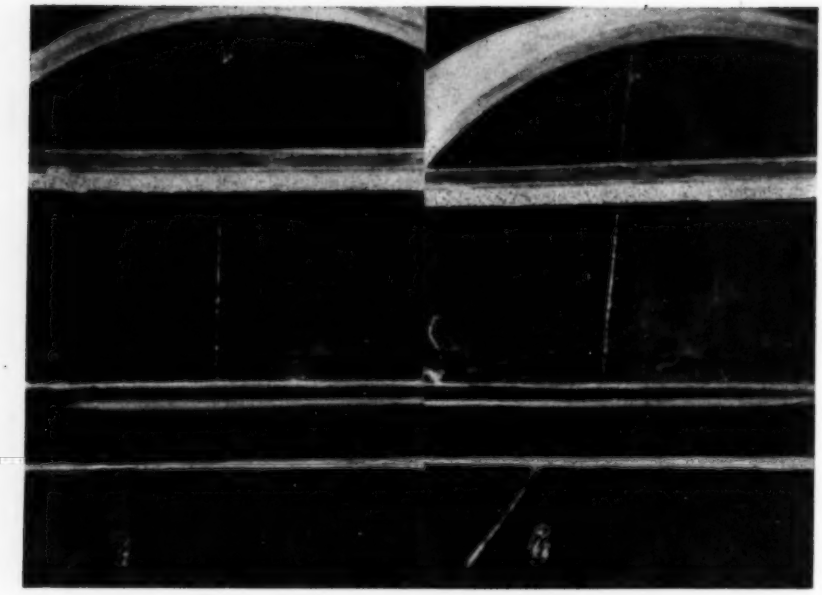

FIG. 5. A typical track of a slow proton ionizing heavily at both sides of a one-cm lead plate.

One of two observed cases of electron showers consisting of very many electrons of low energies is shown in Fig. 4. A similar picture was published by Street.[11] No ray is visible which could have been responsible for this shower. There are about 80 rays, 40 of which stop in the one-cm lead plate as can be ascertained when the picture is viewed stereoscopically, while the remaining rays pass out of view. The average direction of this shower is downward. It seems to the writer that a shower consisting of such a large number of electrons of relatively low energy (~15 Mev) with no high energy electrons at all visible would represent a very large fluctuation in terms of the cascade theory thus making the latter an improbable explanation of showers of this type. The possibility should not be excluded, therefore, that no cascade shower at all is involved.

4. Mesotrons of Low Energies

A study of slow mesotrons is of interest because of the possibility that such particles are removed from the energy spectrum by some hitherto unknown process such as capture by nuclei.

Investigating the relative stopping powers of lead and carbon for mesotrons Pomerantz and Johnson[22] found that, within the experimental uncertainties, no irregularity exists for mesotrons of energies as low as 40 Mev. The present data enable one to extend these studies to particles with energies below 20 Mev.

Table IV gives the percentages of particles stopped in the respective lead plates. The table has been compiled from a number of pictures selected with regard to clarity of the tracks and uniformity of background fog. From the photographs taken with the magnetic field of 1150 oersteds it is found that about 5 percent of the single particles stopped are electrons. This is negligible in view of the rather large probable errors.

Since the energy distribution of mesotrons at sea level has a maximum near 10^9 ev, which corresponds to a range of about 70 cm of lead, one would expect to find many more slow

TABLE V. Heavily ionizing particles.

Total number of tracks of penetrating particles in all compartments	Heavily ionized either above or below a 1-cm lead plate (Mesotron or proton)	Heavy above and below a 1-cm lead plate (Proton)
60,000	45	40

[22] M. A. Pomerantz and T. H. Johnson, Phys. Rev. 59, 143 (1941).

mesotrons under 88 cm of lead than are observed under 15 cm since mesotron decay can be neglected in dense materials. Actually the same number is present under both absorbers. It is believed that the missing particles have been deflected away from the cloud chamber by the lead absorber as was discussed in the first part of this article.

The ratio of the number of mesotrons stopped in the 5-cm plate to the number stopped in one cm should amount to approximately 5:1 if no abnormality is present. From the 3rd column of Table IV one actually obtains a ratio of $(1.8\pm0.2)/(0.4\pm0.1)=4.5\pm1.1$. The energy of a mesotron just stopped by 1 cm of lead is 30 Mev. Thus no irregularity is found for mesotrons below this energy. The value of $\sim$0.4 percent found here for the fraction of the total mesotron component stopped by one cm of lead agrees with a value obtained from the data of Pomerantz and Johnson, making use of their correction factor for scattering.

Mesotrons with energies below about 20 Mev produce considerably more ions along their path than mesotrons of higher energies. The heavily ionized tracks are easily recognized by direct inspection. In the following, an analysis of these tracks is given. Here the picture is complicated by the presence of slow, and therefore heavily ionizing, protons whose ranges are 9 times as long as that of a mesotron of a rest energy of 10^8 ev producing the same density of ionization.

The number of heavily ionized tracks found in the 4 compartments of the cloud chamber is given in Table V. Only single particles which could have passed through the counters above the chamber have been included. Every particle passing through all 4 compartments of the chamber contributes 4 to the grand total of 60,000 tracks of penetrating particles observed. A particle which ionizes heavily either above or below one of the one-cm lead plates is included in the total of 45 counted. Such a particle could either be a mesotron or a proton. A particle seen to ionize heavily at both sides of a one-cm plate must be a proton,[23] thus contributing 2 to the total of 40 given in the table. A typical photograph of a proton track is shown in Fig. 5.

[23] T. H. Johnson, J. G. Barry, and R. P. Shutt, Phys. Rev. 57, 1047L (1940).

Arranging the data in the described manner facilitates the following calculation. N_m shall stand for the number of tracks which could be due either to mesotrons or to protons, N_p is the number of tracks definitely due to protons. n_m is the actual number of slow mesotrons present in a compartment with ranges below a certain limit, while the number of protons with ranges below the same limit has been called n_p. The ratio of proton-mass/mesotron-mass is $\mu=9$. The energy loss by ionization of a slow particle does not depend on its mass. Therefore the chance for detection of a proton is μ times as large as that for detection of a mesotron, and we can put

$$n_m+\mu n_p=N_m+N_p. \tag{16}$$

The maximum residual ranges of protons and mesotrons included in Table V are $R_p(q)$ and $R_m(q)$, respectively, where q stands for the minimum density of ionization still identified as abnormally heavy. Assuming that the range distributions of the protons and mesotrons are constant within the narrow limits considered here, we can write

$$R_p(q)=\mu R_m(q). \tag{17}$$

In order to be recognized, a slow proton has to penetrate $t(=1)$ centimeters of lead. Therefore we can observe only $R_p(q)-t$ of the total range $R_p(q)$ through which a proton is heavily ionizing, and we have

$$n_p\mu\frac{R_p(q)-t}{R_p(q)}=N_p. \tag{18}$$

From Eqs. (16) to (18) it follows that

$$n_m=N_m-N_p\frac{t}{\mu R_m(q)-t} \tag{19}$$

and

$$n_p=N_p\frac{R_m(q)}{\mu R_m(q)-t}. \tag{20}$$

Thus n_m and n_p can be calculated if some feasible assumption for $R_m(q)$ can be made. If mesotrons did not exist, then $n_m=0$, and from Eq. (19) we would find $R_m(q)=0.21\pm0.03$ cm of lead, by using $N_m=45$, $N_p=40$, and $t=1$ cm. From the theory of ionization follows $q=(2.8\pm0.03)\times q_{\min}$, where $q_{\min}$ is the density of ionization of a fast particle producing minimum ionization. Thus, if q had the given value, our data would be consistent even if all the heavily ionized tracks

were due to protons. But there are indications that a lower value for q must be chosen. Figure 6 shows one out of several obtained photographs of a single, fast ray producing a collision electron in the 5-cm lead plate. It is seen that the track of the secondary coincides with that of the main ray in one of the stereoscopic photographs. The resulting double track shows that, under favorable conditions, a ray with a density of ionization of $q=2\times q_{\min}$ may still be recognized and thus be included among those listed in the table. In this case $R_m(q)$ becomes 0.5 cm of lead. But below $q\approx 3q_{\min}$ it is quite possible that some tracks may have been omitted and thus are not included in our results. Assuming that no tracks above $q=3q_{\min}$ have been omitted, and all below $q=2q_{\min}$, it has been estimated that the results for n_m and n_p calculated so far should be multiplied by a factor of 1.4. Furthermore n_m and n_p must be multiplied by estimated factors of 1.3 and 1.1, respectively, to correct for a certain number of particles scattered out of the field of view by the lead plates, an effect which is particularly serious at the low energies considered here. From (19) and (20), with $N_m=45\pm 7$, $N_p=40\pm 10$, $R_m(q)=0.5$ cm, $t=1$ cm, and the corrections given we obtain

$$n_m=62\pm 13 \tag{21}$$

and

$$n_p=9\pm 2, \tag{22}$$

or, if n_m is expressed as a fraction of the total number of penetrating rays observed,

$$n_m=(0.10\pm 0.02)\text{ percent}. \tag{23}$$

Now, the number of particles stopped by 1 cm of lead was (0.4 ± 0.1) percent as determined at the beginning of this section. Thus we should have expected a value of $n_m=(0.20\pm 0.05)$ percent which is in sufficient agreement with the value (23) found in view of the rather large estimated corrections, although there may be some slight evidence for a removal of mesotrons of low energies.

Next we shall compare the number of slow protons with that of the slow mesotrons of equal range. From (21) and (22) we find that $n_p/(n_m+n_p)=(12\pm 3)$ percent for a range of 0.5 cm of lead, and again making use of (20) one gets $n_p/(n_m+n_p)=(7\pm 2)$ percent for a range of 4.5 cm. Mesotrons of the latter range do not ionize heavily, of course, and the value of (0.4 ± 0.1) percent for the mesotrons stopped by one cm of lead again has been used. The two values of $n_p/(n_m+n_p)$ agree within the uncertainties. If we assume that slow protons are not removed by lead atoms, this agreement constitutes additional evidence that the number of slow mesotrons is about as large as expected, leaving only a slight indication that mesotrons with energies below 20 Mev are removed by some effect.

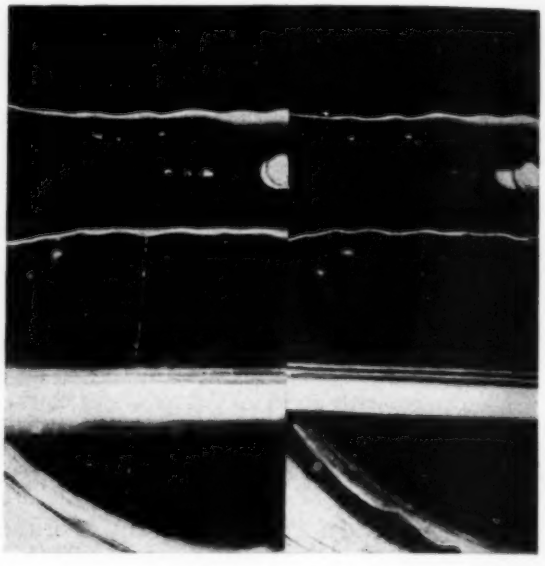

FIG. 6. The left picture shows a case of a track of a secondary electron superimposed upon the track of a fast primary particle, giving the impression of a doubly ionized track.

The number of protons of low energy found here is in agreement with the results of Montgomery *et al.*[24]

The author wishes to express his appreciation to Dr. T. H. Johnson whose never-tiring interest and advice have contributed greatly to this work. Thanks are also due to Drs. S. DeBenedetti and W. F. G. Swann for advice and enlightening conversations on some of the subjects covered in this article, and to Messrs. M. H. Hornstine and W. C. Sheppard for their assistance in operating the cloud chamber.

Most of the present work has been supported financially by the Carnegie Institution of Washington.

[24] C. G. Montgomery, D. D. Montgomery, W. E. Ramsey, and W. F. G. Swann, Phys. Rev. **50**, 403 (1936).

On the Inelastic Photo-Dissociation of the Deuteron

J. M. JAUCH
Palmer Physical Laboratory, Princeton University, Princeton, New Jersey
(Received January 21, 1946)

There exists the possibility of directly verifying the theoretical prediction of the existence of excited states of the nucleons at about 45 Mev above the ground state by an inelastic photo-electric dissociation process of the deuteron with γ-rays of energies larger than the excitation energy of these states. The cross section σ' for such processes is calculated in terms of the elastic cross section σ by using the simplest form of the strong coupling theory. The quantity σ'/σ has a maximum at about 87 Mev where it reaches the approximate value of 0.07. These processes should be experimentally detectable and would furnish valuable information about the properties of nuclei.

I. INTRODUCTION

At present there exist two different forms of the meson theory of nuclear forces which can claim some chance of success, the so-called strong coupling[1] and the weak coupling[2] theory. In both theories charged and neutral mesons are assumed to interact with the heavy nucleons (neutrons and protons) in a symmetrical way which guarantees the charge independence of the nuclear forces. Neither is completely satisfactory but the difficulties which remain may well be beyond the scope of the present status of the quantum theory of fields. On the basis of the generally available experimental results on atomic nuclei it seems impossible to make a definite choice between the two theories.

The two theories distinguish themselves primarily by the different kind of approximations which are considered for the calculation of the forces between two nucleons at sufficiently large separation from each other. In the strong coupling case the forces are obtained by a development into falling powers of the coupling parameter while the weak coupling theory uses a development in rising powers of this constant. But this is not the only distinction between the two theories. It is well known that in a relativistically invariant field theory with point sources the interaction term in the Hamiltonian leads in higher approximations to divergent results. In order to discuss the validity of an approximation it is necessary to compare the first-order term with the higher order terms in the expression for the nuclear forces. Thus some kind of a model of the nucleon is necessary which leads to convergent results. One possibility is to "smear" the nucleon over a finite region in space by introducing a source function $U(\mathbf{x})$. With this method the relativistic invariance of the procedure is destroyed but all the approximations are finite, and it is found that the weak coupling is inadmissible. With the source function one has introduced essentially a new parameter "a" which we may call the effective radius of the nucleon and which may be defined as

$$\frac{1}{a}=\int \frac{U(\mathbf{x})\,U(\mathbf{x}')}{|\mathbf{x}-\mathbf{x}'|}d^3x d^3x'.$$

This quantity is identical with the so-called spin inertia which enters in the classical theory of spinning particles.[3]

The model with the extended source is not the only possibility of a model which leads to a convergent theory. The other possibility is the so-called λ-limiting process of Wentzel and Dirac[4] which has the remarkable feature of leading to a convergent classical theory of particles interacting with a field without destroying the relativistic invariance of the theory. However in quantum mechanics some of the approximations are still divergent so that the λ-limiting process serves its

[1] G. Wentzel, Helv. Phys. Acta **13**, 269 (1940); **14**, 633 (1941); **15**, 685 (1942); **16**, 222 (1943); **16**, 551 (1943). J. R. Oppenheimer and J. Schwinger, Phys. Rev. **60**, 150 (1940). W. Pauli and S. M. Dancoff, Phys. Rev. **62**, 85 (1942). W. Pauli and S. Kusaka, Phys. Rev. **63**, 400 (1943). R. Serber and S. M. Dancoff, Phys. Rev. **63**, 143 (1943).

[2] W. Pauli, Phys. Rev. **64**, 332 (1943).

[3] H. J. Bhabha, Proc. Roy. Soc. **A178**, 314 (1941).

[4] G. Wentzel, Zeits. f. Physik **86**, 479, 635 (1933); **87**, 726 (1934). P. A. M. Dirac, Ann. de L'Inst. H. Poincaré **9**, 13 (1939).

purpose only if it is coupled with some other formalism which takes care of the remaining terms.[5] The condition for weak coupling is different from the condition in the case of the extended source, and it is found that the weak coupling condition can be fulfilled in this theory.[2]

In spite of the entirely different approach of the two methods the result for the nuclear force between two nucleons is strikingly similar in the two cases. The essential difference between the two theories is to be found in the prediction of the existence of excited states of the system "nucleons plus meson field" in the case of strong coupling. The excitation energy of these states is in the case of pseudo-scalar meson field

$$\Delta E=\epsilon\{s(s+1)-\tfrac{3}{4}\},$$

where s is a quantum number which may assume all half-integer values, $\frac{1}{2}, \frac{3}{2}, \cdots$. The parameter ϵ is related to the coupling constant f of the dimension of length and the nuclear size "a" by the formula[1]

$$\epsilon=a\hbar c/4f^2.$$

The first excited state will then be 3ϵ above the ground state of the nucleons. The ground state of the nucleon is doubly degenerate corresponding to the two states "proton" and "neutron" of the nucleon while the excited states allow higher values for the charge as well as the spin. Thus the first excited state for instance has total spin $\frac{3}{2}$ and the charge number may assume all integer values from -1 to $+2$.

For the discussion of the physical consequences of this theory the magnitude of ϵ is the decisive factor. If ϵ is large compared to the energy of a two-nucleon problem, then the force which derives from the strong coupling theory is identical with the weak coupling case apart from a numerical factor.[6] If ϵ is comparable or even smaller than the total energy in question, then the nuclear force exhibits entirely new features.

For a discussion of the nuclear forces, scattering experiments with high energies will therefore be of particular interest. Such experiments were carried out by Amaldi[7] and co-workers and by Champion and Powell.[8] It is the angular dependence of the N–P scattering which was measured by these authors up to energies as high as 14 Mev. The results show a marked preference of the scattering in the forward direction. It is interesting that the weak coupling theory in any of the symmetrical forms is at variance with this result.[9] This feature is directly related to the exchange character of the nuclear forces which causes a reversal of the sign of the potential in P-states and thus a strong backwards scattering.

On the other hand the strong coupling theory leads to the correct angular distribution for an isobar-energy $\epsilon=15$ Mev.[10] This seems to be an indication that the strong coupling variety of the meson theory with its prediction of the isobaric states of nucleus corresponds to reality.

In view of this conclusion it seems of considerable interest to look for other experimental phenomena which would give even more direct evidence for the existence of the excited states of the nucleons. Thus for instance if scattering experiments with nucleons were carried out with an initial energy of the scattered particles larger than $2\Delta E=6\epsilon$ in the laboratory system, the scattering will contain an inelastic part where one of the nucleons is excited. Calculations indicate that the ratio of the inelastic to the elastic cross section will be of the order 0.03 for an initial energy of the scattered nucleons of $\sim$100 Mev in the laboratory system.[11]

This paper treats the theory of another possible process which could be observed and which would furnish a clear cut and simple proof of the existence of excited states of the nucleons, the inelastic photo-effect of the deuteron. If the deuteron is irradiated with 100 Mev γ-rays which can now be produced with the betatron or similar devices for accelerating electrons, then one would

[5] P. A. M. Dirac, Proc. Roy. Soc. **A180**, 1 (1942). W. Pauli, Rev. Mod. Phys. **15**, 175 (1943).

[6] W. Pauli and S. Kusaka, Phys. Rev. **63**, 400 (1943). M. Fierz and G. Wentzel, Helv. Phys. Acta **17**, 215 (1944). G. Wentzel, Helv. Phys. Acta **17**, 252 (1944).

[7] E. Amaldi, D. Bocciarelli, B. Ferretti, G. G. Trabachi, Naturwiss. **30**, 582 (1942).

[8] F. C. Champion and C. F. Powell, Proc. Roy. Soc. **183**, 64 (1944).

[9] L. Hulthén, Arkiv. f. Mat. Astron. Fys. **29**, No. 33 (1943). B. Ferretti, Nuovo Cimento **21**, No. 1, 25 (1943). J. M. Jauch, Phys. Rev. **67**, 125 (1945).

[10] G. Wentzel, Helv. Phys. Acta **18**, 430 (1945). According to a private communication of Professor Wentzel, it seems however impossible to reconcile such a low value of ϵ with the instability of the ^1S-state of the deuteron. This question needs therefore further investigation and more accurate experiments should be performed.

[11] J. L. Lopes, Ph.D. Thesis, Princeton University.

observe in addition to the normal photo-dissociation a certain fraction of dissociations with excitations of one of the nuclear particles. Because of the change in velocity, such dissociation protons would produce a considerably stronger ionization in a Wilson chamber and could therefore be in principle detected.

The excited states of the nucleon have a very short lifetime because of the emission of a magnetic dipole radiation. The electric dipole and the electric quadrupole radiation are zero in the strong coupling approximation.* The transition probability is easily calculated from the well-known formula

$$P=\frac{64}{3}\frac{\pi^4}{hc^3}\nu^3|M_{mn}|^2,$$

where ν is the frequency of the emitted radiation and M_{mn} is the matrix element of the magnetic dipole moment operator which was calculated by Pauli and Dancoff.† One obtains in this way for the lifetime

$$\tau=1/P=1.15\times10^{-18}\text{ sec.}$$

The decay radiation carries within the average the excitation energy of the nucleon. Because of the Doppler effect it may fluctuate around this value by as much as 30 percent. This fact may make the identification of an excited proton difficult. However if the neutron is excited by this process this difficulty does not appear.

2. NOTATIONS AND FORMULATION OF THE PROBLEM

We consider in the following the two-nucleon problem with the interaction operator which follows from the charge symmetrical theory with a mixed pseudoscalar and vector field. The two coupling constants and the two values of the masses shall be taken as equal in magnitude. We obtain in this way the strong coupling form of the theory which was originally proposed by Møller and Rosenfeld.[12] In the static approximation of the interaction operator (nucleons at rest) no tensor force is obtained in this theory. It is very likely that the correct nuclear interaction should contain a tensor force already in the static approximation but we disregard this force for the problem which we want to discuss here. The total value for the cross section is probably not appreciably influenced by this approximation although for some of the finer features of the photo-dissociation, as for instance the angular dependence of the emitted protons, the tensor force would be essential.[13] The approximation introduces a considerable simplification in the calculation.

In this theory a nucleon is described by the following commuting variables: the position vector $\mathbf{z}$, the spin vector $\mathbf{s}$, and the isotopic spin vector $\mathbf{t}$.[14] The commutation rules of angular momenta apply for $\mathbf{s}$ and $\mathbf{t}$. The magnitudes of these vectors together with their third component form a complete set of commuting quantities with respect to the internal degrees of freedom. In a representation in which these quantities are diagonal we have

$$\mathbf{s}^2=\mathbf{t}^2=s(s+1),\quad (s=\tfrac{1}{2},\tfrac{3}{2},\cdots),\quad s_3=m,\quad t_3=n,$$
$$-s\leqslant n,\ m\leqslant s,\quad (m,n=\pm\tfrac{1}{2},\pm\tfrac{3}{2},\cdots).$$

The physical significance of $\mathbf{s}$ is the spin while for $\mathbf{t}$ only the component t_3 has a simple physical interpretation. The charge quantum number of the nucleon is $t_3+\frac{1}{2}=n+\frac{1}{2}$. For the ground state we have $s=\frac{1}{2}$, $n=\pm\frac{1}{2}$. Thus the charge is restricted to the two values 0 (neutron) and 1 (proton).

We distinguish the two sets of variables for the two nucleon problems with indices: $\mathbf{z}_1\mathbf{s}_1,\mathbf{t}_1;\mathbf{z}_2\mathbf{s}_2,\mathbf{t}_2$. The quantum numbers $s_1, m_1, n_1; s_2, m_2, n_2$ may be used to label the internal states of the two-nucleon problem. The interaction operator between two nucleons may be written

$$V=(f\mu)^2\frac{\exp[-\mu r]}{r}\Gamma,$$

where μ is the mass of the meson, $r=|\mathbf{z}_1-\mathbf{z}_2|$ and Γ is a certain operator, operating only on the internal degrees of freedom. Γ is the generalization of the operator $(\boldsymbol{\tau}_1\cdot\boldsymbol{\tau}_2)(\boldsymbol{\sigma}_1\cdot\boldsymbol{\sigma}_2)$ of the weak

* I am indebted to Professor W. Pauli for discussion on this point.

† Reference 1, page 106.

[12] C. Møller and L. Rosenfeld, Kgl. Danske Vid. Sels. **17**, 8 (1940).

[13] Cf. for instance, W. Rarita and J. Schwinger, Phys. Rev. **59**, 556 (1941).

[14] We use in the following the notation of W. Pauli and S. Kusaka (see footnote 1). The units are atomic units $\hbar, c$, and 1 cm.

coupling theory, where σ and τ denote the ordinary and isotopic spin matrices. In case ϵ is large compared to the average energy we can disregard the matrix elements which connect the ground state of the nucleons with its excited states. For the remaining matrix elements we have then[14]

$$\Gamma \rightarrow \tfrac{1}{9}(\tau_1 \cdot \tau_2)(\sigma_1 \cdot \sigma_2).$$

The total energy of the two-nucleon system in the absence of any external perturbation will then be

$$H_{\text{nucl}} = \frac{1}{2M} p_1^2 + \frac{1}{2M} p_2^2 + \epsilon\{(s_1+\tfrac{1}{2})^2 + (s_2+\tfrac{1}{2})^2 - 2\} + (f\mu)^2 \frac{\exp[-\mu r]}{r} \Gamma.$$

The first two terms represent the kinetic energy of the two nucleons, their masses being taken as equal. The third term is the isobar energy, and the fourth term is the interaction energy.

We consider now these two nucleons under the influence of a radiation field described by the operator of the vector potential

$$\mathbf{A}(\mathbf{x}) = \frac{1}{\sqrt{V}} \sum_k \frac{1}{(2k^0)^{\frac{1}{2}}} \times \{\mathbf{a}(\mathbf{k}) \exp[i\mathbf{k}\cdot\mathbf{x}] + \mathbf{a}^*(\mathbf{k}) \exp[-i\mathbf{k}\mathbf{x}]\}.$$

To simplify the calculations we have adopted the usual procedure of describing the field in a cubical box of volume $V = L^3$. If we impose periodic boundary conditions, the vectors $\mathbf{k}$ are restricted to the values $k_i = 2\pi n_i / L$ with integer numbers n_i. Since we are dealing with a pure radiation field the vector $\mathbf{A}(\mathbf{x})$ satisfies the condition $\nabla \mathbf{A} = 0$, which implies for the operators $\mathbf{a}(\mathbf{k})$

$$\mathbf{k} \cdot \mathbf{a}(\mathbf{k}) = 0. \tag{1}$$

The interaction of a charged particle of charge e with an external electromagnetic field is obtained by replacing in the force free Hamiltonian the momenta $\mathbf{p}$ by $\mathbf{p} - e\mathbf{A}$ where $\mathbf{A}$ is to be taken at the position $\mathbf{z}$ of the particle. This leads to terms in the Hamiltonian which are linear and quadratic in $\mathbf{A}$. The quadratic terms do not contribute anything to the photo-dissociation of the deuteron. They lead rather to scattering of photons, processes which are not considered in this paper. In the following we disregard, therefore, the quadratic terms. Since the charge of the elementary particles may be any positive or negative integer in this theory corresponding to the state of the internal degrees of freedom, we must replace the scalar quantity e by the more general charge operator defined above: $e(t_3+\frac{1}{2})$. We obtain in this way the operator for the interaction of the electromagnetic field with the nucleons the expression

$$H_{\text{int}} = -\frac{e}{M}\{(t_3^{(1)}+\tfrac{1}{2})\mathbf{p}_1 \cdot \mathbf{A}(\mathbf{z}_1) + (t_3^{(2)}+\tfrac{1}{2})\mathbf{p}_2 \cdot \mathbf{A}(\mathbf{z}_2)\}$$

$$= -\frac{e}{M}\frac{1}{\sqrt{V}} \sum_k \frac{1}{(2k^0)^{\frac{1}{2}}}\{(t_3^{(1)}+\tfrac{1}{2})\mathbf{p}_1 \cdot \mathbf{a}(\mathbf{k}) \exp[i\mathbf{k}\mathbf{z}_1] + (t_3^{(2)}+\tfrac{1}{2})\mathbf{p}_2 \cdot \mathbf{a}(\mathbf{k}) \exp[i\mathbf{k}\mathbf{z}_2] + \text{conj.}\},$$

where here and in the following we use the abbreviation "conj." to denote the Hermitian conjugate of the preceding expression. We remark that by virtue of (1) the order of the factors $\mathbf{p}$ and $\mathbf{A}$ is not important. For the field energy alone we have from electromagnetic theory

$$H_{\text{field}} = \sum k^0 \mathbf{a}^*(\mathbf{k}) \mathbf{a}(\mathbf{k}).$$

Since the field operators a, a^* satisfy the commutation rules

$$[a_r(k), a_s^*(k')] = \delta_{rs}\delta_{kk'},$$

the above expression for the field energy may also be written as

$$H_{\text{field}} = \sum k^0 n(\mathbf{k}, \lambda),$$

where $n(\mathbf{k}, \lambda)$ denotes the number of photons with propagation vector $\mathbf{k}$ and polarization λ. In our problem the unperturbed state of the field will be described by one of the n's of a given $\mathbf{k}$ and λ being equal to 1 while all the others are equal to zero. Thus H_{field} simply reduces to $H_{\text{field}} = k^0$.

The total Hamiltonian for the problem of the photo-dissociation may now be written as follows

$$H = H_{\text{nucl}} + H_{\text{field}} + H_{\text{int}}. \tag{2}$$

We have disregarded in this expression for H the interaction of the field with the magnetic moment and the meson field directly. As Pais has shown, both these effects give a negligible contribution to the cross section in the energy region which we are going to consider.[15]

A considerable simplification of the problem is obtained if we transform to a new set of variables of which some are constants of motion. Now it is easily seen that $\mathbf{S}=\mathbf{s}_1+\mathbf{s}_2$ and $\mathbf{T}=\mathbf{t}_1+\mathbf{t}_2$ commute with the Hamiltonian (2) and hence are constants of motion.[16] A commuting set of integrals is obtained from these if we consider

$$\mathbf{S}^2=S(S+1);$$

$$\mathbf{T}^2=T(T+1);$$

$$S_3=M;$$

$$T_3=N.$$

S and T are integers and represent the values of the total spin and isotopic spin which for a given set of s_1, s_2 are subject to the conditions of the vector model

$$|s_1-s_2|\leqslant S,\ T\leqslant s_1+s_2. \tag{3}$$

M and N, which represent the third component of the spin and isotopic spin are restricted by

$$-S\leqslant M\leqslant S,$$

$$-T\leqslant N\leqslant T.$$

The quantum numbers S, T, M, N, s_1s_2 form again a complete set of numbers for labeling the states of the internal degrees of freedom of the nucleons. The advantage of this set is however that the operator Γ is diagonal with respect to S, T, M, N and decomposes for each set of these numbers into submatrices with respect to s_1 and s_2. The transformation of the operator Γ to this representation was carried out by Fierz.[17] It will not be necessary to write down here the complete expression for these matrix elements since we are going to use them only for a very special case.

For the following it will be convenient to introduce the coordinates of the center of mass and the relative coordinates for which we write

$$\mathbf{Z}=\tfrac{1}{2}(\mathbf{z}_1+\mathbf{z}_2),$$

$$\mathbf{z}=\mathbf{z}_1-\mathbf{z}_2.$$

The corresponding transformation of the momentum is

$$\mathbf{P}=\mathbf{p}_1+\mathbf{p}_2,\quad \mathbf{p}=\tfrac{1}{2}(\mathbf{p}_1-\mathbf{p}_2),$$

with the solutions

$$\mathbf{z}_1=\mathbf{Z}+\tfrac{1}{2}\mathbf{z},\quad \mathbf{p}_1=\tfrac{1}{2}\mathbf{P}+\mathbf{p},$$

$$\mathbf{z}_2=\mathbf{Z}-\tfrac{1}{2}\mathbf{z},\quad \mathbf{p}_2=\tfrac{1}{2}\mathbf{P}-\mathbf{p}.$$

3. PERTURBATION THEORY

The problem which we want to treat here is the interaction of electromagnetic radiation with the deuteron. It is of course necessary to make a perturbation calculation where we consider the interaction energy of radiation with the deuteron as small compared to the energy of the deuteron and the radiation alone. Such a procedure involves the exact knowledge of the unperturbed wave function, in this case the wave function of the deuteron in the ground state and in the dissociated state.

The deuteron problem in the strong coupling approximation leads to a very complicated eigenvalue problem since the operator Γ has matrix elements which connect the ground state $s_1=s_2=\frac{1}{2}$ with an infinite series of excited states.[18] Fortunately it is possible to show that for sufficiently high values of the excitation energy ΔE the influence of the states with $s_1\neq\frac{1}{2}$ or $s_2\neq\frac{1}{2}$ are negligible. The condition for this to hold was shown by Pauli and Kusaka[1] to be that $|E_D|\ll\Delta E$, where E_D is the binding energy of the deuteron. This condition is well satisfied for $\Delta E\sim 45$ Mev since $|E_D|=2.17$ Mev. We decompose therefore the operator Γ into two parts $\Gamma=\Gamma_0+\Gamma_1$, where Γ_0 contains only the diagonal elements of Γ and Γ_1 contains the off diagonal elements. These latter will be important for the calculation of the inelastic photo-effect but they are unimportant for the calculation of the unperturbed wave functions of the deuteron. The Hamiltonian of the problem may then be written in the form

$$H=H_0+H',$$

[15] A. Pais, Kgl. Danske Vid. Sels. Mat.-Fys. Medd. **20**, No. 17 (1943).
[16] See W. Pauli and S. Kusaka, reference 1, page 407.
[17] M. Fierz, Helv. Phys. Acta **17**, 181 (1944).
[18] M. Fierz and G. Wentzel, Helv. Phys. Acta **17**, 215 (1944); G. Wentzel, Helv. Phys. Acta **17**, 252 (1944).

where

$$H_0=\frac{1}{4M}P^2+\frac{1}{M}p^2+\epsilon\{(s_1+\tfrac{1}{2})^2+(s_2+\tfrac{1}{2})^2-2\}+(f\mu)^2\frac{e^{-\mu r}}{r}\Gamma_0+k^0, \quad (4)$$

$$H'=(f\mu)^2\frac{e^{-\mu r}}{r}\Gamma_1-\frac{e}{M}\{(t_3^{(1)}+\tfrac{1}{2})(\tfrac{1}{2}\mathbf{P}+\mathbf{p})\cdot\mathbf{A}(\mathbf{z}_1)+(t_3^{(2)}+\tfrac{1}{2})(\tfrac{1}{2}\mathbf{P}-\mathbf{p})\cdot\mathbf{A}(\mathbf{z}_2)\}.$$

with $\mathbf{A}(\mathbf{z}_i)$ given by

$$\mathbf{A}(\mathbf{z}_i)=\frac{1}{\sqrt{V}}\sum_k\frac{1}{(2k^0)^{\frac{1}{2}}}\{a(\mathbf{k},\lambda)\mathbf{e}_\lambda\times\exp[i\mathbf{k}\mathbf{z}_i]+\text{conj.}\}\quad(i=1,2), \quad (5)$$

H' is the perturbation term in our problem. The differential cross section for the photoelectric effect is given by perturbation theory to[19]

$$d\sigma=2\pi V|\mathfrak{M}|^2d\rho_E, \quad (6)$$

where $d\rho_E$ represents the density of final states per unit energy range for the initial energy E. $\mathfrak{M}$ stands here for the matrix elements of the perturbation energy which connect the initial with the final states. It is equal to

$$\mathfrak{M}=H_{IF}'=\int\Psi_IH'\Psi_Fd\tau \quad (7)$$

for the direct transitions and

$$\mathfrak{M}=\sum_{II}\frac{H_{I\,II}'H_{II\,F}'}{E_I-E_{II}} \quad (8)$$

for the indirect transitions. In the first case we obtain the first-order effect of the elastic cross section whereas the second case describes inelastic processes with excitation of the isobaric states. This latter case also contains a second-order correction to the elastic photo-effect which is however negligible and is disregarded here. There exists no direct (first-order) transitions which would excite the isobaric states. This is caused by the fact that the perturbation energy H' is a sum of two operators, the first of which gives only rise to transitions of the internal states of the nucleon whereas the second changes one of the numbers of the photons in the radiation field. A simultaneous change of both kinds is therefore only possible through a second-order transition of the type (8).

For the wave functions Ψ_I, Ψ_{II}, Ψ_F which describe the initial, intermediate, and final states we have the following expression

$$\Psi_I=\Phi(1_{\mathbf{k},\lambda})\psi_D(\mathbf{z})\delta_{s_11/2}\delta_{s_21/2}\delta_{T,0}\delta_{S,1}\times\delta_{M,M_0}\delta_{N,0}1/\sqrt{V}\exp[i\mathbf{K}\mathbf{Z}]. \quad (9)$$

Here $\phi(1_{\mathbf{k},\lambda})$ denotes the wave function of the radiation field with one photon present of momentum $\mathbf{k}$ and polarization in the direction $\mathbf{e}_\lambda$. $\psi_D(\mathbf{z})$ is the wave function of the deuteron which in the ground state is a spin triplet ($S=1$) and an isotopic spin singlet ($T=0$). The total charge is $N+1=1$ so that $N=0$, while M, the spin component in the x_3-direction may assume the three values $M_0=0,\pm1$. Since the interaction operator is diagonal with respect to M it follows that the cross section is independent of M_0 and we may take for the initial state an arbitrary value of M_0 and calculate with it the total cross section without any further averaging. The last factor in (9) represents the wave function of the motion of the center of mass with momentum vector $\mathbf{K}$. The wave function is antisymmetrical with respect to interchange of the two particles as it is required by the exclusion principle, since the symmetry character of the spin-isotopic spin function is $(-1)^{S+T}$ and $\psi_D(-\mathbf{z})=\psi_D(\mathbf{z})$.

For the intermediate states II which in the elastic case (7) are the final states, we have two possibilities since the transition may occur to states with $T=1$ as well as $T=0$. Since the Hamiltonian (4) is symmetrical in the two particles these states will again be antisymmetrical as the initial states I. If the energy of the ejected particles is sufficiently high we may treat them as free, a procedure which is characteristic for the Born approximation. We write therefore

$$\Psi_{II,1,2}=\Phi(0)\left(\frac{2}{V}\right)^{\frac{1}{2}}\begin{Bmatrix}\sin\varkappa\mathbf{z}\delta_{T,1}\\ \cos\varkappa\mathbf{z}\delta_{T,0}\end{Bmatrix}\times\delta_{S,1}\delta_{M,M_0}\delta_{N,0}\delta_{s_11/2}\delta_{s_21/2}\frac{1}{\sqrt{V}}\exp[i\mathbf{K}'\mathbf{Z}]. \quad (10)$$

[19] Cf. W. Heitler, *The Quantum Theory of Radiation* (Oxford University Press, New York, 1936), first edition, p. 121.

Here $\varkappa$ denotes the value of the relative momentum of the two particles and $\mathbf{K}'$ is the momentum of the center of mass.

The final states F have one of the quantum numbers $s=\frac{3}{2}$. Since the operator Γ is symmetrical in $s_1 s_2$ and the initial state is $s_1=s_2=\frac{1}{2}$, it is only the symmetrical combination of these two states which can occur as final state. The inequality (3) forbids any final states with $T=0$, thus only one final state is possible described by the wave function

$$\Psi_F=\Phi(0)\left(\frac{2}{V}\right)^{\frac{1}{2}}\sin\varkappa'\mathbf{z}\,\delta_{T,1}\delta_{S,1}\delta_{M,M_0}\delta_{N,0}\frac{1}{\sqrt{2}}$$

$$\times\{\delta_{s_1 1/2}\delta_{s_2 3/2}+\delta_{s_1 3/2}\delta_{s_2 1/2}\}\frac{1}{\sqrt{V}}\exp[i\mathbf{K}'\mathbf{Z}]. \quad (11)$$

The energy of the unperturbed system which belongs to these states is

$$\left.\begin{aligned} E=E_{\mathrm{I}}&=\frac{1}{4M}K^2+E_D+k^0,\\ E_{\mathrm{II}}&=\frac{1}{4M}K'^2+\frac{1}{M}\varkappa^2,\\ E_F&=\frac{1}{4M}K'^2+\frac{1}{M}\varkappa'^2+3\epsilon. \end{aligned}\right\} \quad (12)$$

From the conservation of energy we have

$$\frac{1}{4M}K^2+E_D+k^0=\frac{1}{4M}K'^2+\frac{1}{M}\varkappa'^2+3\epsilon. \quad (12')$$

For our special choice of the initial state of the radiation field we have for the matrix element of the field operators

$$\Phi(1_{\mathbf{k}\lambda})a^*(\mathbf{k}'\lambda')\Phi(0)=\delta_{\lambda\lambda'}\delta_{\mathbf{k}\mathbf{k}'} \quad (13)$$

$$\Phi(1_{\mathbf{k}\lambda})a(\mathbf{k}'\lambda')\Phi(0)=0. \quad (14)$$

From (5), (7), (9), (10), and (11) we find for the different matrix elements[20]

$$H_{\mathrm{I}\,\mathrm{II}_1'}=\frac{e}{M}\frac{i}{\sqrt{k^0 V}}(\boldsymbol{\varkappa}\cdot\mathbf{e}_\lambda)\delta_{\mathbf{K}+\mathbf{k}-\mathbf{K}'}$$

$$\times\int\psi_D^*(\mathbf{z})\exp\left[-\frac{i}{2}\mathbf{k}\cdot\mathbf{z}\right]\cos\varkappa\mathbf{z}\,d^3z, \quad (15)$$

$$H_{\mathrm{I}\,\mathrm{II}_2'}=-\frac{e}{M}\frac{i}{\sqrt{k^0 V}}(\boldsymbol{\varkappa}\cdot\mathbf{e}_\lambda)\delta_{\mathbf{K}+\mathbf{k}-\mathbf{K}'}$$

$$\times\int\psi_D^*(\mathbf{z})\exp\left[-\frac{i}{2}\mathbf{k}\mathbf{z}\right]\sin\varkappa\mathbf{z}\,d^3z, \quad (16)$$

$$H_{\mathrm{II}F'}=\frac{16}{9}\frac{(f\mu)^2}{V}$$

$$\times\int\frac{\exp[-\mu r]}{r}\sin\varkappa\mathbf{z}\sin\varkappa'\mathbf{z}\,d^3z. \quad (17)$$

The δ-function in the first two equations expresses the conservation of momentum

$$\mathbf{K}+\mathbf{k}-\mathbf{K}'=0. \quad (18)$$

The relations (12′) and (18) which are four equations with six variables determine the energy of the ejected particles as a function of their direction. This dependence is useful if one has to distinguish experimentally between protons which are emitted in the elastic or the inelastic process. We have for the velocity v_P of the proton which is emitted in the direction θ with the incident γ-ray if the deuteron was initially at rest ($K=0$)

$$v_P=\frac{k}{2M}\left\{\cos\theta\pm\left(4\frac{|\varkappa|^2}{|k|^2}-\sin^2\theta\right)^{\frac{1}{2}}\right\}, \quad (19)$$

where $|\varkappa|^2$ has to be taken from the energy Eq. (12′) without or with the last term 3ϵ according to whether the process is elastic or inelastic.

4. EVALUATION OF THE CROSS SECTION

For the evaluation of the integrals in (15), (16) we assume for the wave function of the deuteron in the ground state

$$\psi_D(\mathbf{z})=(\beta/2\pi)^{\frac{1}{2}}(1/r)e^{-\beta r}\quad\text{with}\quad\beta=(M|E_D|)^{\frac{1}{2}}.$$

[20] The numerical factor in $H_{\mathrm{II},F'}$ is obtained from Fierz' expression of the matrix elements for Γ (cf. reference 17).

With this function the integrals may readily be evaluated and we have

$$\int \psi_D^*(\mathbf{z}) \exp\left[-\frac{i}{2}\mathbf{k}\cdot\mathbf{z}\right] \cos \boldsymbol{\kappa}\mathbf{z} = (8\pi\beta)^{\frac{1}{2}} \frac{\beta^2+\kappa^2+\frac{1}{4}k^2}{(\beta^2+(\boldsymbol{\kappa}+\frac{1}{2}\mathbf{k})^2)(\beta^2+(\boldsymbol{\kappa}-\frac{1}{2}\mathbf{k})^2)}, \tag{20}$$

$$\int \psi_D^*(\mathbf{z}) \exp\left[-\frac{i}{2}\mathbf{k}\cdot\mathbf{z}\right] \sin \boldsymbol{\kappa}\mathbf{z} = -i(8\pi\beta)^{\frac{1}{2}} \frac{\boldsymbol{\kappa}\cdot\mathbf{k}}{(\beta^2+(\boldsymbol{\kappa}+\frac{1}{2}\mathbf{k})^2)(\beta^2+(\boldsymbol{\kappa}-\frac{1}{2}\mathbf{k})^2)}, \tag{21}$$

$$\int \frac{\exp[-\mu r]}{r} \sin \boldsymbol{\kappa}\mathbf{z} \sin \boldsymbol{\kappa}'\mathbf{z} = \frac{8\pi\boldsymbol{\kappa}\cdot\boldsymbol{\kappa}'}{(\mu^2+(\boldsymbol{\kappa}-\boldsymbol{\kappa}')^2)(\mu^2+(\boldsymbol{\kappa}+\boldsymbol{\kappa}')^2)}. \tag{22}$$

The density function $d\rho_E$ for the final states with propagation vector $\boldsymbol{\kappa}$ situated within a solid angle $d\omega$ around a fixed direction (ϑ, φ) is given by

$$d\rho_E = \frac{1}{2}\frac{V}{(2\pi)^3}\kappa^2\frac{d\kappa}{dE}d\omega = \frac{V}{32\pi^3}M\kappa d\omega. \tag{23}$$

For the differential cross section of the elastic photoelectric effect we obtain from (6), (20), (21), and (23) for an incident radiation with momentum $\mathbf{k}$ and polarization direction $\mathbf{e}_\lambda$

$$d\sigma = \frac{1}{2\pi}\frac{e^2}{Mk^0}\beta\kappa(\mathbf{e}_\lambda\cdot\boldsymbol{\kappa})^2\left\{\frac{(\beta^2+\kappa^2+\frac{1}{4}k^2)^2+(\boldsymbol{\kappa}\cdot\mathbf{k})^2}{(\beta^2+\kappa^2+\frac{1}{4}k^2)^2-(\boldsymbol{\kappa}\cdot\mathbf{k})^2}\right\}.$$

If we average over all directions of the polarization of the incident light we obtain for

$$(\mathbf{e}_\lambda\cdot\boldsymbol{\kappa})_{\text{Av}}^2 = \kappa^2\sin^2\vartheta\frac{1}{2\pi}\int_0^{2\pi}\cos^2\varphi d\varphi = \tfrac{1}{2}\kappa^2\sin^2\vartheta.$$

For the total cross section we obtain then by integrating over all the directions of κ the formula:

$$\sigma = \frac{e^2}{Mk^3}\beta\kappa\left\{\frac{\beta^2+\kappa^2+\frac{1}{4}k^2}{\kappa k}\ln\frac{\beta^2+\kappa^2+\frac{1}{4}k^2+\kappa k}{\beta^2+\kappa^2+\frac{1}{4}k^2-\kappa k}-2\right\}. \tag{24}$$

For $\kappa k \ll \beta^2+\kappa^2+\frac{1}{4}k^2$ this expression goes over into the formula of Bethe and Peierls,[21]

$$\sigma = \frac{2}{3}\frac{e^2}{Mk}\frac{\beta\kappa^3}{(\beta^2+\kappa^2+\frac{1}{4}k^2)^2}. \tag{25}$$

These two expressions (24) and (25) are only then appreciably different from each other if $k/M\sim 1$ for 100-Mev γ-rays $k/M\sim\frac{1}{9}$. For these energies the error due to the simplified wave function of the deuteron is probably still larger. It must be remarked also that for $k\sim M$ the relativistic effects which we did not consider here become important. The inelastic cross section is obtained from (6) and (8).

[21] H. A. Bethe and R. Peierls, Proc. Roy. Soc. **A148**, 146 (1945). In comparing our formula with theirs, one has to remember that the unit of charge is so chosen that $e^2=4\pi/137$.

For $\mathfrak{M}$ we obtain with the help of (20) and (22)

$$\mathfrak{M}=\frac{16}{9}(f\mu)^2\frac{(8\pi)^{\frac{1}{2}}}{(k^0)^{\frac{1}{2}}V}i\sqrt{\beta}\int(\boldsymbol{\kappa}\cdot\mathbf{e}_\lambda)\frac{\beta^2+\kappa^2+\frac{1}{4}k^2}{(\beta^2+\kappa^2+\frac{1}{4}k^2)^2-(\boldsymbol{\kappa}\cdot\mathbf{k})^2}$$

$$\times\frac{\boldsymbol{\kappa}\cdot\boldsymbol{\kappa}'}{(\mu^2+\kappa^2+\kappa'^2)^2-4\boldsymbol{\kappa}\cdot\boldsymbol{\kappa}'}\frac{1}{E_D+k^0-\frac{1}{4M}k^2-\frac{1}{M}\kappa^2}d^3\kappa. \quad (26)$$

The integration must be carried out over all values of the wave vector for the intermediate states. The last factor has a pole for

$$\kappa=(Mk^0-\beta^2-\tfrac{1}{4}k^2)^{\frac{1}{2}}.$$

The value of the integral would thus become undetermined unless some boundary conditions for the wave functions are introduced. The condition which is here necessary requires that in the intermediate states for large distances from the scatterer only out-going spherical waves shall exist. As is shown in the appendix this condition leads for the integration over the magnitude of κ to the rule that the pole must be avoided by displacing the path of integration around the pole into the lower half of the complex κ-plane.

We carry out first the integration over the angles. Here a simplification is possible if the energy of the γ-radiation is not too large; more precisely, if

$$\kappa k/(\beta^2+\kappa^2+\tfrac{1}{4}k^2)\ll 1. \quad (27)$$

This is the same condition which allowed us to replace (24) by (25).[22] In this case we may neglect the variation of the denominators and we obtain for $\mathfrak{M}$ the simplified expression:

$$\mathfrak{M}=\frac{16}{9}(f\mu)^2\frac{e}{V}\left(\frac{\beta}{k}\right)^{\frac{1}{2}}\frac{(8\pi)^{\frac{1}{2}}}{(2\pi)^3}i\int d^3\kappa\frac{(\mathbf{e}_\lambda\cdot\boldsymbol{\kappa})(\boldsymbol{\kappa}\cdot\boldsymbol{\kappa}')}{(\beta^2+\kappa^2+\frac{1}{4}k^2)(\mu^2+\kappa^2+\kappa'^2)^2(kM-\beta^2-\frac{1}{4}k^2-\kappa^2)}.$$

The integration over the angles is now easily carried out and the result is

$$\mathfrak{M}=\frac{16}{9}(f\mu)^2\frac{e}{V}\left(\frac{\beta}{k}\right)^{\frac{1}{2}}\frac{(8\pi)^{\frac{1}{2}}}{(2\pi)^3}i(\boldsymbol{\kappa}'\mathbf{e}_\lambda)I,$$

with

$$I=\int_0^\infty\frac{\kappa^4d\kappa}{(A^2+\kappa^2)(B^2+\kappa^2)^2(C^2-\kappa^2)},$$

$$A^2=\beta^2+\tfrac{1}{4}k^2,$$

$$B^2=\mu^2+\kappa'^2,$$

$$C^2=kM-\beta^2-\tfrac{1}{4}k^2.$$

Since the integrand is an even function in κ, we may extend the path of integration from $-\infty$ to $+\infty$. The pole $\kappa=-C$ on the negative real axis will then be avoided by displacing the path of integration into the positive imaginary half-plane. Since the integrand goes to zero like κ^{-4} for large κ we can complete the path of integration by a large half-circle in the positive imaginary half-plane to a closed path and then use the theorem of the residues. With this method we obtain

$$I=i\pi\{\text{Res}\,(iA)+\text{Res}\,(iB)+\text{Res}\,(C)\}.$$

[22] This approximation corresponds to the neglection of multipole transitions. For 100-Mev γ-rays the error due to this approximation is about 20 percent. Neglecting the tensor force introduces an uncertainty which is probably larger than this error.

A detailed numerical discussion shows that the first two terms may be neglected for γ-rays with energies ~ 100 Mev.[23] We find thus for the integral the approximate value

$$I=i\frac{\pi}{2}\frac{C^3}{(A^2+C^2)(B^2+C^2)^2}.$$

The cross section for the inelastic photo-effect becomes then

$$\sigma'=0.053(f\mu)^4e^2\frac{\beta}{k^3}\frac{\kappa'^3}{M}\frac{(kM-\beta^2-\frac{1}{4}k^2)^3}{(\mu^2+\kappa'^2+kM-\beta^2-\frac{1}{4}k^2)^4}.$$

The ratio of the inelastic to the elastic cross section is

$$\frac{\sigma'}{\sigma}=0.08(f\mu)^4M^2\frac{(Mk-\beta^2-\frac{1}{4}k^2)^{\frac{1}{2}}(Mk-\beta^2-\frac{1}{4}k^2-3\epsilon M)^{\frac{1}{2}}}{(\mu^2+2Mk-2\beta^2-\frac{1}{2}k^2-3\epsilon M)^4}.$$

For $k\sim 100$ Mev we may neglect the term $\frac{1}{4}k^2$ in all these brackets and we have, writing $x=Mk-\beta^2-3\epsilon M$,

$$\sigma'/\sigma=0.08(f\mu)^4M^2F(x),$$

$$F(x)=\frac{x^{\frac{1}{2}}(x+3\epsilon M)^{\frac{1}{2}}}{(\mu^2+3\epsilon M+2x)^4}.$$

F has a maximum at $x=\frac{1}{2}\{3\mu^2-6\epsilon M+[(3\mu^2-6\epsilon M)^2+18\epsilon M(\mu^2+3\epsilon M)]^{\frac{1}{2}}\}$ which corresponds to an energy of the incident γ-rays of 87 Mev. For this value of the energy we have

$$\sigma'/\sigma\sim 0.125\times(f\mu)^4.$$

For $(f\mu)^4$ Pauli and Kusaka[6] find the value 0.14 while Hulthen[24] obtains ~ 0.58. Hulthen's value is calculated without the tensor force which furnishes additional attractive potential in the ground state of the deuteron. This is the reason for the somewhat higher value. Since we have calculated without the tensor force throughout, Hulthen's value is probably the better. The correct value would probably be somewhere between these two. With Hulthen's value we find for σ'/σ near the maximum:

$$\sigma'/\sigma=7.2 \text{ percent.} \tag{28}$$

5. CONCLUSION

It is seen from (28) that the ratio of the number of inelastic to the number of elastic photoelectric dissociations of the deuteron is near the maximum about 7 percent. The maximum is reached for an initial energy of the γ-rays of 87 Mev if we assume the first excited states of the nucleons at 45 Mev. It is conceivable that a systematic search for the inelastic dissociation process might lead to the discovery of the excited states of the nucleons.

APPENDIX

We use the stationary state method of perturbation theory and write for the problem

$$(H+H')\psi=E\psi.$$

E is the total energy, H is the unperturbed Hamiltonian given by (ψ), and H' is the perturbation energy. The states are labeled by k, κ, s where k stands for the state of the radiation field, κ describes the relative motion of the nucleons, and s contains the quantum numbers for the internal states of the nucleons. We write then for the wave function the development

$$\psi=\psi_0+\psi_1+\psi_2+\cdots,$$

where the terms are arranged in rising order of smallness. For these wave functions we obtain then the following set of equations:

$$H\psi_0=E\psi_0,$$
$$H'\psi_1=(E-H)\psi_0,$$
$$H'\psi_2=(E-H)\psi_1,\ \cdots.$$

Let the state of the unperturbed system be denoted by $\psi_0(k_0\kappa_0 s_0)$. Since H is diagonal in the variables $k_0\kappa_0 s_0$, this function will be a δ-function in these variables representing a photon with momentum and polarization, characterized by the letter k_0, a deuteron in the ground state with center of gravity at rest (κ_0) and the internal degrees of freedom s_0 of two nucleons in the ground state.

[23] I am indebted to Mr. E. Gross for some help with the evaluation of these integrals.

[24] L. Hulthen, Arkiv för mat. astr. och fysik **A28**, No. 5 (1942).

From the second equation we obtain then

$$\psi_1(k'\kappa's')=(k'\kappa's'|H'|k_0\kappa_0s_0)\left\{\frac{1}{E-E_I}-i\pi\delta(E-E_I)\right\},$$

where E_I is the energy which belongs to the state $(k'\kappa's')$. The second term is so chosen that this solution when transformed to X-space represents only outgoing spherical waves provided that we define an integration over the pole $E=E_I$ always by its principle value.[25] The second-order solution which is of interest in our problem becomes then

$$\psi_2(k,\kappa,s)=\frac{1}{E-E_F}\sum_{k'\kappa's'}(k,\kappa,s|H'|k'\kappa's')(k'\kappa's'|H'|k_0\kappa_0s_0)\times\left\{\frac{1}{E-E_I}-i\pi\delta(E-E_I)\right\}.$$

The summation on the right-hand side is equivalent with an integration without δ-term in such a way that the path of integration is displaced in the complex κ-plane around the pole in the negative imaginary half-plane. This was the procedure used in the text.

[25] Compare P. A. M. Dirac, The Principles of Quantum Mechanics, Clarendon Press, Oxford, second ed., p. 195ff.

PHYSICAL REVIEW VOLUME 69, NUMBERS 7 AND 8 APRIL 1 AND 15, 1946

On the Heavy-Electron Pair Theory in the Limit of Strong Coupling

JOHN M. BLATT
Princeton University, Princeton, New Jersey*

(Received January 21, 1946)

The pair theory of Marshak and Weisskopf was investigated assuming strong coupling. The strong coupling criterion is $A=(Nf/\mu)>5$ where f=coupling constant, μ=heavy electron mass, $N=\int U^2(x)d^3x$, $U(x)$=source function of the nucleon. $N\cong 1/\pi a^3$, where a=source radius (all in units where $\hbar=c=1$). With this condition, the magnetic moment turns out to be of order A^{-1}, and of magnitude too small to account for the observed anomalies. The leading term in the potential of the force between two nucleons (for $r_{AB}>2a$) is independent of the spin orientations, of the coupling constants, and of the type of coupling (as long as no derivatives of the heavy-electron field quantities occur in the coupling term). This potential is identical with the one calculated by Jauch and Houriet, but was not considered by Nelson and Oppenheimer. The next term in the potential is of order A^{-3}. It corresponds to a superposition of a $(\Sigma_A\cdot\Sigma_B)$ term, a tensor force term, and an ordinary force. Being of order A^{-3} it is too small, however, to fit the experimental results.

1. INTRODUCTION

THIS paper deals with the strong coupling version of the meson theory proposed by Marshak and Weisskopf.[1] In this theory the meson field quantity is assumed to be a complex spinor. The associated quanta (mesons) are then heavy electrons in all respects. They satisfy Dirac's equation in the absence of interactions with nucleons. The negative energy states are taken into account by the usual hole-theory approach. The interaction term with the nucleon is assumed to be quadratic in the meson field quantities. This identifies the theory as a "pair theory." The name refers to the fact that in the weak coupling approximation the mesons are emitted and reabsorbed by the nucleons in pairs. The particular interaction term proposed by Marshak and Weisskopf is of the form

$$\bar{H}_i=f\psi^+(z)P_s\psi(z). \qquad (1.1)$$

Here $\bar{H}_i$ is the interaction term in the Hamiltonian, f is a coupling constant, ψ is the meson field quantity (an operator), a cross denotes its Hermitean conjugate, z is the position of the nucleon in question, and P_s is one of several operators which are possible if we want the theory to be relativistically invariant. Marshak points out that it is possible, in a weak coupling theory, to eliminate all but one of them by a consideration of the deuteron problem.

It is true, however, that a weak coupling theory based on an interaction term of the form (1.1) can never explain the anomalous magnetic moments of the proton and neutron. Since $\bar{H}_i$ contains both ψ^+ and ψ, the isotopic spin of the

* Now with RCA Laboratories, Princeton, New Jersey.
[1] R. E. Marshak, Phys. Rev. 57, 1101 (1940); R. E. Marshak and V. F. Weisskopf, Phys. Rev. 59, 130 (1941).

nucleon is an exact constant of motion. The operator P_s cannot contain the operators transforming a neutron into a proton or *vice versa* because that would destroy the conservation of charge in an elementary process. The only way in which the isotopic spin degree of freedom can enter the problem at all is through a choice of the coupling constant f. But it is easy to see that it is impossible to make a satisfactory choice, provided we limit ourselves to a weak coupling theory. If the magnetic moment arises in a perturbation of even order, there is no possibility at all to fit the opposite signs of the anomalies for the proton and neutron. If the magnetic moment arises in an odd-order perturbation, we might try to pick coupling constants of opposite sign for the two heavy particles. But the nuclear force between particles A and B will contain the factor $f_A f_B$ for every operator P_s considered by Marshak. Our tentative choice of coupling constants would, therefore, lead to opposite signs for like and unlike particle forces, and this is unacceptable. It may be remarked that all meson pair theories proposed so far suffer from this same defect.

For this reason, and because a rough estimate seems to show that it is not possible to choose the coupling constants big enough to give the correct binding energy of the deuteron without violating the weak coupling criterion, it was considered advisable to investigate the strong coupling limit of this theory. The results are:

(1) The strong coupling condition is $A = Nf/\mu \gg 5$ where N is the reciprocal of the volume of the source, and μ is the meson mass.

(2) The magnetic moment changes sign when f changes sign, but it is much too small to give the observed anomalies as long as (1) is satisfied and $\mu a \ll 1$, where a is the radius of the source.

(3) The leading term in the potential of the force between two nucleons (for $r_{AB} > 2a$) is independent of the spin orientations, of the coupling constants, and of the type of coupling, i.e., of the choice of operator P_s in Eq. (1.1). This potential is identical with the one calculated by Jauch and Houriet,[2] but was not considered by Nelson and Oppenheimer.[3]

(4) The spin-dependent part of the force arises in order A^{-2}. It then gives a superposition of a term of type $\mathbf{S}_A \cdot \mathbf{S}_B$ and a tensor force term. Since $A \gg 5$ by assumption, this force is very small.

[2] J. M. Jauch, Helv. Phys. Acta **15**, 175 (1942); A. Houriet, Helv. Phys. Acta **16**, 529 (1943).

[3] E. Nelson and J. R. Oppenheimer, Phys. Rev. **61**, 202 (1942).

The theory is, therefore, unsatisfactory both in the weak coupling and the strong coupling limits. The only remaining possibility is an intermediate coupling strength (A of order unity). The present treatment is not applicable to this case.

2. THE ONE-BODY PROBLEM

In any strong coupling theory it is necessary to use a source function convergence method. This means that we replace $\psi(z)$ in Eq. (1.1) by

$$\bar{\psi} = \int \psi(\mathbf{x}) U(\mathbf{x}-\mathbf{z}) d^3x, \tag{2.1}$$

where the source function U is chosen so that its integral over all of space is unity; usually it is chosen spherically symmetrical, and so that it is very small beyond a certain distance from the nucleon. It is common to define an effective radius of the source by

$$(a)^{-1} = \int\int \frac{U(x)\,U(x')}{|\mathbf{x}-\mathbf{x}'|} d^3x d^3x'. \tag{2.2}$$

It then turns out that for most reasonable choices of the source function, the nuclear forces do not depend very much on $U(x)$ as long as the internuclear distance is much larger than the source diameter $2a$. It must be realized that this formalism is only a preliminary convergence device necessitated by the lack of a consistent quantum theory of the interaction of fields and point sources. Therefore the restriction to distances greater than the source diameter is not really a loss in generality. We would not be willing to trust the theory at shorter distances, anyway.

In the strong coupling case, the starting state of a valid perturbation treatment will be obtained by splitting the meson field into two parts: a static field attached to the nucleon and a wave field largely independent of it. *We then consider the complex "nucleon+static meson field" as one unit, which we shall call the stat-nucleon, and we assume that it is this unit which is observed experimentally.* Because of the various possible states of the static meson field, the stat-nucleon has many more states than the original nucleon. The excited states of the stat-nucleon are referred to as isobaric states. It is clear that the existence of

isobaric states leads to two requirements for a reasonable theory. First, the ground state of the stat-nucleon must have spin one-half. Second, the excitation energy of the lowest isobar state must be high enough to account for the fact that these states have not been observed as yet.

The Hamiltonian of our problem is

$$\bar{H}=\bar{H}_f+\bar{H}_i=\int\psi^+(\mathbf{x})(\boldsymbol{\alpha}\cdot\mathbf{p}+\mu\beta)\psi(\mathbf{x})d^3x + f\bar{\psi}^+\beta\boldsymbol{\sigma}\cdot\boldsymbol{\Sigma}\bar{\psi}. \quad (2.3)$$

Here $\bar{H}_f$ is the free meson field Hamiltonian, $\bar{H}_i$ the interaction term with the nucleon; $\boldsymbol{\alpha}$ and β are the usual Dirac matrices (it must be remembered that ψ is a spinor), $\mathbf{p}$ is $(-i)$ times the gradient operator, and μ is the meson mass. The units are chosen so that $\hbar=c=1$, and lengths are measured in cm. In $\bar{H}_i$ we have chosen the operator P_s proposed by Marshak and Weisskopf; $\boldsymbol{\sigma}$ is the spin operator of the mesons (i.e., $\sigma_z=-i\alpha_x\alpha_y$) and $\boldsymbol{\Sigma}$ is the spin operator of the heavy particle. $\boldsymbol{\Sigma}$ can be represented by the usual Pauli 2-by-2 matrices.

Notice that $\bar{H}_i$ contains ψ^+, ψ, and Σ. The equations of motion will contain products of two of these operators, and will therefore be *non-linear*. The non-linearity of this theory distinguishes it from the case treated by Jauch and Houriet.[2] They use $P_s=\beta$ which leads to *linear* equations of motion. This point is discussed further in Section 4.

The meson field is quantized in accordance with the exclusion principle, so ψ has to satisfy the usual anti-commutation rules

$$\psi_\gamma^+(\mathbf{x})\psi_{\gamma'}(\mathbf{x}')+\psi_{\gamma'}(\mathbf{x}')\psi_\gamma^+(\mathbf{x})=\delta_{\gamma\gamma'}\delta(\mathbf{x}-\mathbf{x}'), \quad (2.4)$$

while the other anti-commutators vanish. The index γ denotes the spinor components of ψ and runs from 1 to 4.

We now split the field into a static field and a wave field. To do this we define the integral $N=\int U^2(\mathbf{x})d^3x$ and the function $u(\mathbf{x})=N^{-\frac{1}{2}}U(\mathbf{x})$. Then we put

$$\psi(\mathbf{x})=Qu(\mathbf{x})+\psi'(\mathbf{x}) \quad (2.5)$$

with an analogous formula for $\psi^+(\mathbf{x})$. We further postulate the orthogonality condition

$$\int u(\mathbf{x})\psi'(\mathbf{x})d^3x=0. \quad (2.6)$$

From (2.5) and (2.6) it follows that

$$Q=\int u(x)\psi(x)d^3x.$$

Assuming a spherically symmetric source function, it is easily seen that

$$\bar{H}=\bar{H}_0+\bar{H}'+\Omega, \quad (2.7)$$

where

$$\bar{H}_0=Q^+(\mu\beta+Nf\beta\boldsymbol{\sigma}\cdot\boldsymbol{\Sigma})Q, \quad (2.8)$$

$$\bar{H}'=\int\psi'^+(\mathbf{x})(\boldsymbol{\alpha}\cdot\mathbf{p}+\mu\beta)\psi'(\mathbf{x})d^3x, \quad (2.9)$$

$$\Omega=Q^+\int u(\mathbf{x})(\boldsymbol{\alpha}\cdot\mathbf{p}+\mu\beta)\psi'(\mathbf{x})d^3x + \int\psi'^+(\mathbf{x})(\boldsymbol{\alpha}\cdot\mathbf{p}+\mu\beta)u(\mathbf{x})d^3x\,Q. \quad (2.10)$$

The anti-commutation relations are to be derived from (2.4), (2.5), and (2.6). They turn out to be

$$Q_\gamma^+Q_{\gamma'}+Q_{\gamma'}Q_\gamma^+=\delta_{\gamma\gamma'}, \quad (2.11)$$

$$\psi_\gamma'^+(\mathbf{x})\psi_{\gamma'}'(\mathbf{x}')+\psi_{\gamma'}'(\mathbf{x}')\psi_\gamma'^+(\mathbf{x}) =\delta_{\gamma\gamma'}[\delta(\mathbf{x}-\mathbf{x}')-u(\mathbf{x})u(\mathbf{x}')] \quad (2.12)$$

while the other anti-commutators vanish.

The decomposition of the Hamiltonian (2.7) has the significance that $\bar{H}_0$ describes the stat-nucleon, $\bar{H}'$ describes the wave-field, and Ω is the interaction between them. The strong coupling condition will be the condition of validity for a perturbation treatment on Ω.

We first discuss the $\bar{H}_0$ problem. The operators Q have to satisfy the conditions (2.11). They can then be represented as 16-by-16 matrices. The occurrence of $\boldsymbol{\Sigma}$ in the Hamiltonian requires a doubling of those matrices so that they become 32-by-32. It is easily seen that $B_+=Q_1^+Q_1+Q_2^+Q_2$ and $B_-=Q_3^+Q_3+Q_4^+Q_4$ as well as the stat-nucleon spin operator $\mathbf{s}=(1/2)(Q^+\boldsymbol{\sigma}Q+\boldsymbol{\Sigma})$ are constants of motion. Starting with a representation which is diagonal in B_+, B_- and the z component of $\mathbf{s}$, it is easy to find the simultaneous eigenstates of these three operators and $\bar{H}_0$. It turns out that we get two doublet and one quadruplet states with energy 0; the remaining states occur in pairs of positive and negative energy. Listing only one of each pair, we have singlets with energies $\mu+3Nf$ and $\mu-3Nf$, doublets with energies 2μ and $2(3)^{\frac{1}{2}}Nf$, and

triplets with energies $\mu+Nf$ and $\mu-Nf$, giving thirty-two states in all. For large values of f the ground state will be the doublet state of energy $-2(3)^{\frac{1}{2}}Nf$. The first excited state will be the singlet state of energy $-(\mu+3Nf)$. Closer investigation shows that the *strong coupling condition* is obtained by requiring the *excitation energy of this first isobar state* to be *much larger than the rest energy μ of the meson*. This is the condition quoted in the introduction. Notice that the energies above *cannot* be written in the form $\sum_{\gamma=1}^{4} N_\gamma E_\gamma$ where $N_\gamma=0$ or 1, and the E_γ are constants. This is due to the non-linearity of the $\bar{H}_0$-problem.

We now turn our attention to the wave-field problem. The Hamiltonian $\bar{H}'$ looks just like the free-field Hamiltonian $\bar{H}_f$. There is, however, a significant difference between the two caused by the auxiliary condition (2.6) and the corresponding anti-commutation rules (2.12). Following Pauli and Hu[4] we shall treat this problem by the method of Lagrange multipliers. We are looking for a system of c-number spinor functions $\phi_\rho(\mathbf{x})$ which fulfill (2.6) and diagonalize the expression (2.9) with ϕ substituted for ψ'. Having found such a system, we can put

$$\psi'(\mathbf{x})=\sum_\rho a_\rho\phi_\rho(\mathbf{x}), \tag{2.13}$$

where the a_ρ are scalar operators satisfying the usual anti-commutation rules. The Hamiltonian $\bar{H}'$ then assumes the simple form

$$\bar{H}'=\sum_\rho a_\rho^+ a_\rho E_\rho, \tag{2.14}$$

where the E_ρ are the values of (2.9) obtained by substituting $\phi_\rho(\mathbf{x})$ for $\psi'(\mathbf{x})$.

We now observe that the problem of finding the functions $\phi(\mathbf{x})$ is equivalent to the variation problem: to extremize the integral

$$I=\int\phi^*(\mathbf{x})(\boldsymbol{\alpha}\cdot\mathbf{p}+\mu\beta)\phi(\mathbf{x})d^3x \tag{2.15}$$

subject to the conditions

$$\int\phi^*(\mathbf{x})\phi(\mathbf{x})d^3x=1, \tag{2.16}$$

$$\int\phi^*(\mathbf{x})u(\mathbf{x})d^3x=\int\phi(\mathbf{x})u(\mathbf{x})d^3x=0. \tag{2.6}'$$

[4] W. Pauli and Ning Hu, Rev. Mod. Phys. **17**, 267 (1945).

Since the wave-field problem is one of infinitely many degrees of freedom, it is not convenient to take the volume integrals over all of x space. We shall need the spherical symmetry of the one-body problem later on in the calculation of the anomalous magnetic moment. Therefore we will pick a sphere of radius R as our volume of integration, and we shall let R become infinitely large at the end. We now use the method of Lagrange multipliers on the variation problem just outlined. We multiply (2.16) by the scalar $-E$ and pre-multiply (2.6)′ by the spinors $-\lambda^*$ and $-\lambda$, respectively; we then add the resulting equations to (2.15) and vary $\phi^*(\mathbf{x})$. Setting the variation equal to zero we obtain

$$(\boldsymbol{\alpha}\cdot\mathbf{p}+\mu\beta-E)\phi(\mathbf{x})=\lambda u(\mathbf{x}). \tag{2.17}$$

This equation clearly indicates that the eigenwaves of the wave-field problem split into two distinct groups: those with $\lambda=0$ and those with $\lambda\neq0$. If $\lambda=0$, $\phi(\mathbf{x})$ satisfies the ordinary Dirac equation. So this class is just the *class of all eigenstates of the free meson field (before introduction of the nucleon) which are already orthogonal to the source function.* It will turn out that all our results will be independent of these eigenstates of the wave-field problem.

The other class, with $\lambda\neq0$, has to be investigated more closely. We pre-multiply (2.17) by $(\boldsymbol{\alpha}\cdot\mathbf{p}+\mu\beta+E)$ to get

$$(p^2+\mu^2-E^2)\phi(\mathbf{x})=(\boldsymbol{\alpha}\cdot\mathbf{p}+\mu\beta+E)\lambda u(\mathbf{x}).$$

This implies that we can put

$$\phi(\mathbf{x})=(\boldsymbol{\alpha}\cdot\mathbf{p}+\mu\beta+E)\lambda v(\mathbf{x}), \tag{2.18}$$

where the scalar function $v(\mathbf{x})$ satisfies

$$(p^2+\mu^2-E^2)v(\mathbf{x})=u(\mathbf{x}) \tag{2.19}$$

and (2.6) with ψ' replaced by $v(\mathbf{x})$. A closer investigation shows that we are free to pick convenient boundary conditions for v on the surface of the large sphere, and we shall require v to be zero on that surface. To simplify calculations we shall pick as source function $U(r)=(\alpha^2/4\pi r)\exp(-\alpha r)$ with the corresponding $u(r)=(\alpha/2\pi)^{\frac{1}{2}}1/r\exp(-\alpha r)$. The solutions of (2.19) which are square integrable and have a square integrable gradient are of type $v(r)=w(r)/r$

where w is given by

$$w(r)=-[\alpha/2\pi]^{\frac{1}{2}}[\alpha^2+k^2]^{-1}[\exp(-\alpha r) -\cos(kr)+B\sin(kr)].$$

Here $k^2=E^2-\mu^2$ and B is a constant to be determined. The orthogonality to the source function leads to the condition $B=(\alpha^2-k^2)/2\alpha k$. The boundary condition at the surface of the large sphere leads to $B^{-1}=\tan(kR)$. These two conditions combined give the equation which determines the allowed values of k and therefore of E. It should be noticed that these eigenvalues are not identical with the ones obtained without the auxiliary condition. This is the reason why the $\bar{H}'$ problem leads to forces in the two-body problem.

The *operator* Ω defined by (2.10) will be treated as a perturbation. We can use the result (2.17) to simplify its form considerably:

$$(\boldsymbol{\alpha}\cdot\mathbf{p}+\mu\beta)\psi'(\mathbf{x})=(\boldsymbol{\alpha}\cdot\mathbf{p}+\mu\beta)\sum_\rho a_\rho\phi_\rho(\mathbf{x}) =\sum_\rho a_\rho(E_\rho\phi_\rho(\mathbf{x})+\lambda_\rho u(x)).$$

Because of (2.6)′ Ω becomes

$$\Omega=Q^+\sum_\rho a_\rho\lambda_\rho+\sum_\rho a_\rho^+\lambda_\rho^*Q. \qquad (2.20)$$

This shows immediately why the states with $\lambda=0$ are not important for our problem. They are not contained in the perturbing Hamiltonian and are therefore exact eigenwaves of the complete Hamiltonian. In particular, if the occupation numbers are 0 for those states in zero-order approximation they will be zero in all orders of a perturbation calculation.

It is easy to see that the problem admits an *angular momentum integral of motion*. This follows immediately from the invariance under rotations about the heavy particle. The integral in question is the operator

$$\mathbf{J}=\int\psi^+(\mathbf{x})[\mathbf{x}\times\mathbf{p}+\tfrac{1}{2}\boldsymbol{\sigma}]\psi(\mathbf{x})d^3x+\tfrac{1}{2}\boldsymbol{\Sigma}. \qquad (2.21)$$

The remarkable thing about this expression is that it commutes with $\bar{H}_0+\bar{H}'$ and Ω separately. This can be shown by introducing (2.5) and noticing that there are no cross terms between the static and wave fields; it also follows from the fact that both the stat-nucleon and the wave-field problem are invariant under rotations about the heavy particle. This fact is not important for the study of the one-body case, but will prove very important for the two-body problem.

3. THE MAGNETIC MOMENT

To find the contribution of the meson field to the magnetic moment of the stat-nucleon, we calculate the expectation value of the magnetic moment operator in the ground state. This operator is determined in the usual way. We assume a magnetic field $\mathfrak{C}$ in the z direction. A vector potential corresponding to this is given by $A_x=-\frac{1}{2}\mathfrak{C}y$, $A_y=\frac{1}{2}\mathfrak{C}x$, and $A_z=0$. We then replace $\mathbf{p}$ by $\mathbf{p}+\epsilon\mathbf{A}$ in the Hamiltonian (2.3). Since we assume no static electric field, there are no changes in the definition of the canonical conjugate $\pi(x)=i\psi^+(x)$ of the operator ψ. The Hamiltonian will then contain an additional term proportional to the magnetic field strength, and the magnetic moment operator is defined as the derivative of this new term with respect to the magnetic field. It is easily seen that the magnetic moment operator for our problem is

$$\mathbf{M}=\frac{\epsilon}{2}\int\psi^+(\mathbf{x})[\mathbf{x}\times\boldsymbol{\alpha}]\psi(\mathbf{x})d^3x. \qquad (3.1)$$

Upon introduction of (2.5) it is seen that the term quadratic in Q becomes identically zero. This means that the $\bar{H}_0$ problem by itself does not lead to a magnetic moment. There remain two terms, one quadratic in ψ' and the other bi-linear in ψ' and Q. It can be shown without difficulty that the expectation value of the term quadratic in ψ' is zero in the state for which the occupation numbers $N_\rho=a_\rho^+a_\rho$ for positive values of E_ρ and $N_\rho=a_\rho a_\rho^+$ for negative values of E_ρ are all zero. The contributions of this term will come in even orders of a perturbation treatment.

The cross term is given by

$$\mathbf{M}''=\tfrac{1}{2}\epsilon Q^+\int u(\mathbf{x})[\mathbf{x}\times\boldsymbol{\alpha}]\psi'(\mathbf{x})d^3x +\text{complex conjugate.} \qquad (3.2)$$

Upon introduction of (2.13) this expression simplifies to

$$M_z''=-(\epsilon/6)\sum_\rho s_\rho K_\rho(a_\rho^+\lambda_\rho^*Q+Q^+\lambda_\rho a_\rho). \qquad (3.3)$$

Here we have picked the Lagrange multipliers λ_ρ as spinors with all but one component equal to zero, and that component real. The operator s_ρ is defined to be $+1$ if this non-zero component is the first or third, -1 otherwise. It is easily seen, by the way, that it is related to the angular momentum integral for the $\bar{H}'$ problem through

$$J_z' = \tfrac{1}{2}\sum_\rho s_\rho a_\rho^+ a_\rho + \text{contribution of modes with } \lambda = 0. \quad (3.4)$$

The expression K_ρ in (3.3) is given by

$$K_\rho = \int u(\mathbf{x})\mathbf{x}\cdot\text{grad } v(\mathbf{x}) d^3x$$

and is seen to be $-[2(\alpha^2+k^2)]^{-1}$.

The operator M_z'' contributes in the first order of a perturbation treatment, and it is this contribution which we are going to calculate. The method is the usual one. We expand the wave-functional Φ of the ground state in powers of the parameter $A = [Nf/\mu]^{-1}$

$$\Phi = \Phi_0 + \Phi_1 + \Phi_2 + .$$

We then obtain the equations

$$(\bar{H}_0 + \bar{H}')\Phi_1 + \Omega\Phi_0 = i(d\Phi_1/dx_0),$$

$$(\bar{H}_0 + \bar{H}')\Phi_2 + \Omega\Phi_1 = i(d\Phi_2/dx_0),$$

and so on. We can find Φ_1 by an expansion in terms of eigenfunctionals X of $(\bar{H}_0 + \bar{H}')$. The expression we are looking for is $2\Phi_0^* M_z''\Phi_1$. If we start from the unperturbed state in which the eigenvalue of $\bar{H}_0$ is $-2(3)^{\frac{1}{2}}Nf$ and the occupation numbers N_ρ are zero, and go to the limit as the large sphere becomes very big, we obtain

$$\Phi_0^* M_z''\Phi_1 = -\frac{\epsilon\alpha}{6\pi}\sum_{r=1}^{32}\sum_{\gamma=1}^{4}\left\{ s_\gamma (r|Q_\gamma|1)^2 \int_0^\infty dk \frac{k^2}{(\alpha^2+k^2)\epsilon_k(\epsilon_k+\mu\beta_\gamma)(\epsilon_k+E^{(r)}-E^{(1)})} \right.$$

$$\left. + s_\gamma (r|Q_\gamma^+|1)^2 \int_0^\infty dk \frac{k^2}{(\alpha^2+k^2)\epsilon_k(\epsilon_k-\mu\beta_\gamma)(\epsilon_k+E^{(r)}-E^{(1)})} \right\}. \quad (3.5)$$

The notation of (3.5) is as follows: The first sum is taken over all eigenstates of $\bar{H}_0$, the second sum over the four components of the spinor Q. The quantity s_γ is defined to be $+1$ for $\gamma = 1$ and 3, -1 for $\gamma = 2$ and 4; the quantity β_γ is $+1$ for $\gamma = 1$ and 2, -1 for $\gamma = 3$ and 4. The matrix element $(r|Q_\gamma|1)$ connects the arbitrary state r of the stat-nucleon problem to the starting state 1 (of energy $-2(3)^{\frac{1}{2}}Nf$) and similarly for the matrix elements of Q_γ^+. $E^{(r)}$ is the energy of eigenstate r of the H_0 problem, while $E^{(1)} = -2(3)^{\frac{1}{2}}Nf$. Finally ϵ_k is the absolute value of E_ρ, that is $\epsilon_k = +(k^2+\mu^2)^{\frac{1}{2}}$.

We are clearly led to the integrals

$$I_1 = \int_1^\infty \frac{(x^2-1)^{\frac{1}{2}}dx}{(x-1)(x+\eta)(x^2+\zeta^2)},$$

$$I_2 = \int_1^\infty \frac{(x^2-1)^{\frac{1}{2}}dx}{(x+1)(x+\eta)(x^2+\zeta^2)},$$

where the strong coupling condition assures us that $\eta > 1$ for all intermediate states r. These integrals can be evaluated by trigonometric substitution and introduction of the half angle. The result is

$$I = (\eta^2+\zeta^2)^{-1}[A(\zeta)\eta - f(\eta) + B(\zeta)],$$

where

$$A_{1,2}(\zeta) = (\zeta^2+1)^{-\frac{1}{2}}\left[\frac{\pi}{2} \pm (\zeta)^{-1}\log[(\zeta+1)^{\frac{1}{2}}+\zeta]\right],$$

$$B_{1,2}(\zeta) = (\zeta^2+1)^{-\frac{1}{2}}\left[\zeta\log[(\zeta^2+1)^{\frac{1}{2}}+\zeta] \mp \frac{\pi}{2}\right],$$

$$f_{1,2}(\eta) = (\eta\mp 1)^{\frac{1}{2}}(\eta\pm 1)^{-\frac{1}{2}}\log[(\eta^2-1)^{\frac{1}{2}}+\eta].$$

The calculations were carried out explicitly for $\alpha/\mu = 10$ and $Nf/\mu = 5$. Larger values of the latter will make the magnetic moment even smaller. We obtain $2\Phi_0^* M_z''\Phi_1 = -0.00354(\epsilon/\mu)$. This has to be compared with the magnetic moment of the proton according to the usual Dirac theory, that is ϵ/μ_P (μ_P = proton mass). For a mass ratio of order 10, we get the result that the contribution of the meson field is less than one-tenth the intrinsic magnetic moment of the proton. This is much too small to explain the experimental value of about 1.85. It might be objected that this is only the result of a first-order treatment and that

higher terms might increase the magnetic moment considerably. Although this is not impossible for relatively small coupling constants, it is very unlikely if $Nf/\mu \gg 5$.

It is verified without difficulty that M changes sign when we start from the state in which the spin of the stat-nucleon is oppositely directed. It can also be shown that this first-order contribution to the magnetic moment changes sign when f changes sign. (This implies using the state for which $\bar{H}_0 = +2(3)^{\frac{1}{2}}Nf$ as the starting state.) So we could assign $f>0$ to the proton and $f<0$ to the neutron to fit the opposite anomalies for the two particles. It will turn out that the nuclear force is largely independent of f so that the objection made against this procedure in the weak coupling case is not valid. However, the magnitude of the magnetic moment is too small, and the force, while largely independent of f, is otherwise unacceptable

It is interesting to point out the fact that this pair theory is not quite symmetrical in the positive and negative energy states. If it were, the magnetic moment would have to vanish. The sign of the magnetic moment is determined from the sign of ϵ, and ϵ is the charge of the field-quantum (meson) of a positive energy state, while the "holes" correspond to mesons of charge $-\epsilon$.

4. THE POTENTIAL OF NUCLEAR FORCES

We shall first give a treatment of the many-body problem, using the Fourier transforms of the wave functions. Then we shall specialize to the two-body problem.

The Hamiltonian for the many-body problem is

$$\bar{H} = \int d^3x \psi^+(x)(\boldsymbol{\alpha}\cdot\mathbf{p}+\mu\beta)\psi(x) + \sum_{A=1}^{Z} f_A \bar{\psi}_A^+ (\beta\boldsymbol{\sigma}\cdot\boldsymbol{\Sigma})\bar{\psi}_A. \quad (4.1)$$

Here A is an index distinguishing the nucleons, at positions $\mathbf{z}_A$. We have allowed for the possibility that the coupling constants may be different for neutrons and protons. Furthermore,

$$\bar{\psi}_A = \int d^3x U(\mathbf{x}-\mathbf{z}_A)\psi(x). \quad (4.2)$$

The commutation rules (2.4) are unchanged.

We shall now introduce a Fourier transform through

$$\psi(\mathbf{x}) = [1/(V)^{\frac{1}{2}}] \sum_k q_k \exp[i\mathbf{k}\cdot\mathbf{x}]. \quad (4.3)$$

The sum is taken only over those vectors $\mathbf{k}$ whose components are integral multiples of $2\pi/L$, and $V=L^3$. This means that we have introduced the *periodicity condition*

$$\psi(\mathbf{x}+\mathbf{a}) = \psi(\mathbf{x}) \quad (4.3a)$$

for all vectors $\mathbf{a}$ whose components are integer multiples of L. Later on we shall go to the limit $L\to\infty$.

The treatment of Section 2 was particularly suited to the one-body problem, since it allowed us to use the rotational symmetry of the problem directly. In the general many-body problem there is no rotational symmetry, and it is then advantageous to transform from differential equations to algebraic equations. This is the reason for the use of the Fourier transform.

Later on we will use the invariance of the two-body problem with respect to rotations about the axis connecting the two nucleons. It will then be necessary to transform back to x space to avoid the periodicity condition, which is not invariant with respect to this operation.

We now put $N=\int d^3x U^2(x)$, as before, and define $Q_A=[1/(N)^{\frac{1}{2}}]\bar{\psi}_A$ in analogy with the one-body problem. To find the commutation rules for the Q's, we substitute (2.4). This gives

$$[Q_{A\gamma}, Q_{A'\gamma'}]_+ = \delta_{AA'}\delta_{\gamma\gamma'}, \quad (4.4)$$

provided $|\mathbf{z}_A-\mathbf{z}_{A'}|$ *is large enough that the overlap integral*

$$\int U(\mathbf{x}-\mathbf{z}_A)U(\mathbf{x}-\mathbf{z}_{A'})d^3x$$

can be neglected. From now on we shall *assume this condition to hold.* This implies that all our results for the nuclear forces will be valid only when the *internuclear separation exceeds the source diameter* $2a$.

It is reasonable to investigate this case only, since a force resulting from an overlap of the source distributions cannot properly be called a *field* force. For $r<2a$ the type of source function used will essentially determine the result. Since the source function is only a preliminary con-

vergence device, we would not feel justified in placing any confidence in expressions which depend upon it greatly.

The Hamiltonian becomes

$$\bar{H}=\sum_k q_k^+(\alpha\cdot\mathbf{k}+\mu\beta)q_k + N\sum_A f_A Q_A^+(\beta\sigma\cdot\mathbf{\Sigma}_A)Q_A. \quad (4.5)$$

The potential energy of the system of Z nucleons placed at positions $\mathbf{z}_1\cdots\mathbf{z}_Z$ is calculated as follows: We first diagonalize the operator $\bar{H}$. It will have positive and negative eigenvalues, corresponding to positive and negative energy states of the complete system. *The ground state (vacuum) is by definition the state with the most negative energy.* Because of the infinite number of degrees of freedom of the field, this eigenvalue will diverge.

We then diagonalize $\bar{H}$ with $f_A\equiv 0$, i.e., the free meson field Hamiltonian which we will call $\bar{H}_f$. Its eigenvalues will again be of both signs, and the ground state is again defined as the state of most negative energy. Since the $\bar{H}_f$-problem is linear, the diagonalized free-field Hamiltonian can be written as a sum of terms

$$\bar{H}_f=\sum_s E_s a_s^+ a_s, \quad (4.6)$$

where the operators a_s satisfy the anti-commutation relations (2.11). The most negative state is then the one in which the eigenvalues of $(a_s^+\cdot a_s)$ are $=1$ if $E_s<0$ and $=0$ if $E_s>0$. It is this state of affairs which is referred to when one speaks of "filling up all the negative energy states." It may be worth while to point out here that for $f_A\neq 0$ the problem is not linear. That is, $\bar{H}$ can be diagonalized, but it cannot be represented by the simple form (4.6); the energy of a state corresponding to two "simple" states of the field in superposition is *not* necessarily the sum of the energies of the separate states. It is therefore impossible to speak of "filling up all the negative energy states." The definition of the groundstate of $\bar{H}$ as the state of most negative energy remains meaningful, however; it is the natural generalization of the hole-theory approach to non-linear problems.

The difference between the energy of the ground state of $\bar{H}$ and that of $\bar{H}_f$ is defined to be the potential energy W_Z of the system of Z nucleous at positions $z_1\cdots z_Z$. W_Z will of course be a function of these position variables. It is usual to subtract from W_Z the contribution of the self-energies. That is, we define the potential $V_Z\equiv W_Z-Z\cdot W_1$. Since W_1 is independent of the positions of the nucleons in question, this amounts only to a subtraction of a constant term and is therefore not an essential step. It is useful sometimes for mathematical convenience.

So far the definition of W_Z is ambiguous. The two energy-values whose difference we are to take are both infinite. To make the procedure definite, we have to specify a method of doing the subtraction. The method which suggests itself is based on the principle of adiabatic invariance. This says that a continuous change in the coupling parameters $f_1\cdots f_s$ will induce a continuous change in the eigenvalues of the operator $\bar{H}$. Now, *if the $\bar{H}$-problem is linear*, then $\bar{H}$ can be written:

$$\bar{H}=\sum_s E_s' a_s'^+ a_s'. \quad (4.7)$$

The principle of adiabatic invariance now allows us to make a *unique correspondence* between the eigenvalues E_s of $\bar{H}_f$ and E_s' of $\bar{H}$. Having made this correspondence, we define

$$W_Z\equiv\sum_s (E_s'-E_s), \qquad E_s, E_s'<0. \quad (4.8)$$

(4.8) is the definition used by Wentzel and others.[5] It assumes implicitly that no negative eigenvalue becomes positive as the f_A are increased from zero. The modifications in case this occurs are straight-forward, however.

A more difficult question presents itself when (as in our case) the $\bar{H}$ problem is *not linear*, so that $\bar{H}$ cannot be written in the form (4.7). In our case we shall avoid the difficulty by using an expansion of the eigenvalues of the $\bar{H}$ problem according to the usual perturbation procedure. It will turn out that in zero order in Nf/μ the eigenvalues of $\bar{H}$ can be represented in the form

$$\sum_{A=1}^{Z}(E_r)_A+\sum_\rho E_\rho N_\rho, \quad (4.9)$$

[5] G. Wentzel, Zeits. f. Physik **104**, 36 (1936); Helv. Phys. Acta **10**, 107 (1937); Zeits. f. Physik **118**, 277 (1941). G. Gamow and E. Teller, Phys. Rev. **51**, 289 (1937). C. Critchfield and E. Teller, Phys. Rev. **53**, 812 (1938). E. P. Wigner, C. Critchfield, and E. Teller, Phys. Rev. **56**, 531 (1939). C. Critchfield and W. Lamb, Phys. Rev. **58**, 46 (1940). C. Critchfield, Phys. Rev. **56**, 540 (1939).

where each $(E_\tau)_A$ is one of the thirty-two eigenvalues of the problem of a single stat-nucleon, the E_ρ are the energies of the eigenwaves of the wave-field problem, and the N_ρ are occupation numbers which can assume the values 0 and 1. It is then possible to correlate the E_ρ with unique E_s of (4.6). It is not necessary to make such correlations for the E_τ, since only Z terms are concerned, and a finite number of terms does not cause any difficulty.

We now define the 0-order potential energy

$$W_Z^{(0)} \equiv \sum_{\substack{E_s<0 \\ E_\rho<0}} (E_\rho - E_s), \tag{4.10}$$

where we have to take differences of corresponding terms, the correspondence to be determined by the principle of adiabatic invariance.

It may be remarked that some states of the $\bar{H}_f$ problem are not subtracted, since they do not correspond to any E_ρ, but correspond to $\sum_{A=1}^{Z}(E_\tau)_A$. This does not matter since it means only an addition of a finite constant to $W_Z^{(0)}$. Similarly, the omission of $\sum_{A=1}^{Z}(E_\tau)_A$ itself does not do any harm because this sum is finite and does not depend upon the positions of the nucleons. (This is true only if there is no source-overlap. Otherwise the corresponding term would have to be included. It would then not be just a sum of contributions of separate stat-nucleons.)

To find higher approximations to the potential energy, we simply have to add the corrections to the energy of the ground-state of the $\bar{H}$-problem to $W_Z^{(0)}$. No more subtraction need be done. The corrections in question are found by standard perturbation procedure.

It is clear from the preceding remarks that our perturbation approach has enabled us to avoid defining W_Z uniquely for the general case of non-linear $\bar{H}$. To the best of our knowledge, no such general definition has yet been proposed.

We now proceed to prove (4.9). To do this, we first define

$$g_k = [1/(V)^{\frac{1}{2}}] \int d^3x\, u(x) \exp[-i\mathbf{k}\cdot\mathbf{x}],$$

with $u(x) = [1/(N)^{\frac{1}{2}}]U(x)$, as before. This definition implies

$$\sum_k |g_k|^2 = 1,$$

and

$$Q_A = \sum_k q_k g_k \exp[i\mathbf{k}\cdot\mathbf{z}_A].$$

We then decompose the field into a static field and a wave field (similar to 2.5).

$$q_k = \sum_A Q_A g_k \exp[-i\mathbf{k}\cdot\mathbf{z}_A] + q_k', \tag{4.11}$$

$$\sum q_k' g_k \exp[i\mathbf{k}\cdot\mathbf{z}_A] = 0. \tag{4.12}$$

The Hamiltonian (4.5) becomes $\bar{H} = \bar{H}_0 + \bar{H}' + \Omega$ where

$$\bar{H}_0 = \sum_A Q_A^+ (\mu\beta + N f_A \beta\boldsymbol{\sigma}\cdot\boldsymbol{\Sigma}_A) Q_A, \tag{4.13}$$

$$\bar{H}' = \sum_k q_k' (\boldsymbol{\alpha}\cdot\mathbf{k} + \mu\beta) q_k', \tag{4.14}$$

$$\Omega = \sum_A \sum_k Q_A^+ g_k \exp[i\mathbf{k}\cdot\mathbf{z}_A](\boldsymbol{\alpha}\cdot\mathbf{k} + \mu\beta) q_k' + \text{complex conjugate}. \tag{4.15}$$

Provided that a perturbation treatment based on eigenstates of $\bar{H}_0 + \bar{H}'$ is valid (i.e., the strong coupling condition is satisfied), it follows immediately that (4.9) is correct. The E_ρ are energies of eigenwaves of the $\bar{H}'$-problem. We can now draw some conclusions with very little effort. Together with one more result (whose proof will be left for later) they form the *main statements* of this paper.

(1) As was remarked before, the contribution of $\bar{H}_0$ to the energy of the ground state of $\bar{H}$ (in zero-order perturbation) is a sum of terms $\sum_A (E_\tau)_A$, each of which refers to a single stat-nucleon. Furthermore, these terms are independent of the positions of the nucleons. Both statements follow from (4.13) immediately. Therefore the $\bar{H}_0$ problem does not lead to nuclear forces. It may be well to keep in mind the fact that (4.13) is the correct expression for the term quadratic in Q only if the internuclear distances exceed $2a$.

(2) The E_ρ entering (4.10) are eigenvalues corresponding to eigenwaves of the $\bar{H}'$-problem. Now this problem is defined by (4.12) and (4.14). Neither one of them contains the coupling parameters f_A or the nucleon spin operators $\boldsymbol{\Sigma}_A$. The only way in which the nucleons enter into the problem at all is through the *geometrical* conditions (4.12) which involve only the positions $\mathbf{z}_A$ of the nucleons and their source functions. Therefore the 0-order potential $W_Z^{(0)}$ will be independent of the coupling constant f_A and the spin variables of the nucleons (or, more properly, of the stat-nucleons). Even more can be said. The only way in which the type of coupling (i.e., the

operator P_s of (1.1) enters into the $\bar{H}'$-problem is the fact that it necessitates the particular splitting (4.11) of the meson field. This same splitting will be indicated whenever P_s does not involve a differential operator acting on the meson field quantity.

This proves that $W_Z^{(0)}$ is even independent of the type of coupling provided no meson field derivatives occur in the coupling term. Indeed, it will be shown in the next section that $W_2^{(0)}$ is identical with the potential already calculated by Jauch and Houriet[2] who assumed a different coupling term.

(3) The third significant result cannot be seen immediately. Nevertheless, it will be stated here, with the proof reserved for a later section. It turns out that a perturbation treatment on Ω gives 0 in all odd-order perturbations. Furthermore, for the two-body problem the second-order perturbation does not lead to a spin-dependent force. Therefore the spin-dependent part of the force between two nucleons is of order $(Nf/\mu)^{-3}$ which is by assumption a very small quantity.

These results allow us to reject the heavy-electron pair theory in the limit of *strong coupling*. In the introduction we mentioned that all *weak coupling* pair theories are unacceptable because the results for the anomalous magnetic moments cannot be reconciled with the equality of like and unlike particle forces. There remains only the possibility of an *intermediate coupling*, i.e., $Nf/\mu \sim 1$. The present treatment gives no information about that case.

5. THE ZERO-ORDER POTENTIAL

We treat the $\bar{H}'$-problem in almost exactly the same manner as before (Section 2). The differences are that (1) the differential equations are now algebraic equations; (2) the boundary conditions at the surface of a sphere of radius R are replaced by the periodicity condition (4.3a).

Consider the auxiliary problem: it is required to extremize the quadratic form

$$\sum_k x_k^*(\boldsymbol{\alpha}\cdot\mathbf{k}+\mu\beta)x_k \tag{5.1}$$

subject to the conditions

$$\sum_k x_k^* x_k = 1, \tag{5.2}$$

$$\sum_k x_k g_k \exp[i\mathbf{k}\cdot\mathbf{z}_A] = \sum_k x_k^* g_k \exp[-i\mathbf{k}\cdot\mathbf{z}_A] = 0. \tag{5.3}$$

The x_k are c-number spinors, and (5.3) is intended to hold for all values of A.

Multiply (5.2) by the scalar Lagrange factor $(-E)$ and premultiply (5.3) by the spinor $(-\lambda_A)$ for every value of A. Then add the equations to (5.1) and differentiate with respect to each spinor component of x_k^*. Equating the result to zero (in order to get an extremum) yields

$$(\boldsymbol{\alpha}\cdot\mathbf{k}+\mu\beta-E)x_k = \sum_A \lambda_A g_k \exp[-i\mathbf{k}\cdot\mathbf{z}_A]. \tag{5.4}$$

This is the determining equation for the x_k. To treat it, premultiply by $(\boldsymbol{\alpha}\cdot\mathbf{k}+\mu\beta+E)$ on both sides. This gives

$$(k^2+\mu^2-E^2)x_k = \sum_A g_k \exp[-i\mathbf{k}\cdot\mathbf{z}_A](\boldsymbol{\alpha}\cdot\mathbf{k}+\mu\beta+E)\lambda_A. \tag{5.5}$$

There are two types of solutions to (5.5), depending upon whether $\lambda_A = 0$ (all A) or not. If $\lambda_A = 0$, then

$$E^2 = \mu^2 + k^2$$

for some value of k^2 allowed by the periodicity condition, and $x_k = 0$ unless $k^2 = E^2 - \mu^2$. We therefore have a linear combination of plane-wave solutions of the Dirac equation with the same energy, chosen so as to be orthogonal to the source function. (With our choice of the source-functions, none of the original plane-wave solutions of Dirac's equation are orthogonal to all the $u(\mathbf{x}-\mathbf{z}_A)$.) There is clearly no energy shift involved in those solutions, and, as has been pointed out already in Section 2, the perturbation Hamiltonian is also independent of them.

The solutions for which $\lambda \neq 0$ are possible only if $k^2+\mu^2-E^2 \neq 0$ for every value of k^2 which belongs to a lattice point. We can then divide (5.5) by $k^2+\mu^2-E^2$ to get

$$x_k = \sum_A \frac{g_k \exp[-i\mathbf{k}\cdot\mathbf{z}_A]}{k^2+\mu^2-E^2}(\boldsymbol{\alpha}\cdot\mathbf{k}+\mu\beta+E)\lambda_A. \tag{5.6}$$

We substitute this into (5.3) to get

$$\sum_k \sum_A \frac{g_k^2 \exp[i\mathbf{k}\cdot(\mathbf{z}_A-\mathbf{z}_{A'})]}{k^2+\mu^2-E^2} \times(\boldsymbol{\alpha}\cdot\mathbf{k}+\mu\beta+E)\lambda_A = 0. \tag{5.7}$$

This is a set of equations, four for each value of A'. We have $4Z$ homogeneous linear equations

in the $4Z$ independent components of the spinors $\lambda_1 \cdots \lambda_Z$. They can be satisfied only if the determinant of the system vanishes. *This determines the allowed values of* E. To solve the problem completely, we would have to substitute (5.6) with these values of E into (5.2) in order to normalize the λ_A. It will not be necessary to do so for our purposes. We would have sets $x_{\rho,k}$ of spinors and (normalized) spinors $\lambda_{\rho,A}$ for each allowed value E_ρ. We could then put

$$q_k' = \sum_\rho a_\rho x_{\rho,k}, \tag{5.8}$$

and the Hamiltonian of the wave-field problem would become

$$\bar{H}' = \sum_\rho E_\rho a_\rho^+ a_\rho. \tag{5.9}$$

It is easily verified that the a_ρ obey the commutation rules (2.11).

We shall now write down the determinants involved for the one- and two-body problems. For the one-body problem, we put $\mathbf{z}_A = 0$ and get

$$D_1 = det\left\{\sum_k \frac{g_k^2}{k^2+\mu^2-E^2}(\boldsymbol{\alpha}\cdot\mathbf{k}+\mu\beta+E)\right\}, \tag{5.10}$$

$$D_1 = (E^2-\mu^2)^2[S(E^2)]^4 = 0,$$

where

$$S(E^2) = \sum_k \frac{g_k^2}{k^2+\mu^2-E^2}. \tag{5.11}$$

The condition involved is then simply $S(E^2)=0$ since the solutions of $(E^2-\mu^2)^2=0$ do not yield any energy-shifts from the free-field case.

It is worth while here to notice that this checks against Houriet's[5] calculations. Houriet finds as the equation determining the positions of the shifted energy levels $\phi_1^2(E^2)=0$ where

$$\phi_1(E^2) = \left\{1+f\sum_k g_k^2\left(\frac{\mu+E}{k^2+\mu^2-E^2}\right)\right\} \cdot \left\{1+f\sum_k g_k^2\left(\frac{\mu-E}{k^2+\mu^2-E^2}\right)\right\}. \tag{5.12}$$

In the limit $f\to\infty$ this reduces to (5.10).

For the two-body problem, we first define the sums

$$T(E^2, r) = \sum_k g_k^2 \frac{\exp[-i\mathbf{k}\cdot\mathbf{r}]}{k^2+\mu^2-E^2}, \tag{5.13}$$

$$iP(E^2, r) = \sum_k g_k^2 \frac{k_z \exp[-i\mathbf{k}\cdot\mathbf{r}]}{k^2+\mu^2-E^2}, \tag{5.14}$$

where $\mathbf{r}=\mathbf{z}_{II}-\mathbf{z}_I$ was used to define the z axis of our coordinate system.

With these definitions, (5.7) becomes

$$\left.\begin{aligned}(E+\mu\beta)S\lambda_I+\{(E+\mu\beta)T+i\alpha_z P\}\lambda_{II}=0\\ \{(E+\mu\beta)T-i\alpha_z P\}\lambda_I+(E+\mu\beta)S\lambda_{II}=0\end{aligned}\right\}. \tag{5.15}$$

The determinant of this system is

$$D_2(E^2, r) = [(E^2-\mu^2)(S^2-T^2)-P^2]^4 = 0. \tag{5.16}$$

We can again check this against Houriet. He gets for the equation determining the shifted energy values

$$[\phi_{21}(E^2)\cdot\phi_{22}(E^2)]^2 = 0,$$

where

$$\phi_{2;1,2}(E^2) = 1+2f(\mu S \pm ET) + f^2(\mu^2-E^2)(S^2-T^2)+f^2P^2.$$

Here we have used the quantities S, T, P defined in (5.11), (5.13), (5.14). They are related to Houriet's D, F, E, as follows:

$$D = S+T, \quad F = S-T, \quad E = -P.$$

It is seen that this reduces to (5.14) if we keep only the terms in f^2.

This check is, of course, no accident. It was pointed out in Section 4 that the H'-problem is independent of the coupling type, and that it determines the potential [except for terms of higher order in $(Nf/\mu)^{-1}$] provided the strong coupling approximation is valid. Therefore, we *had* to get the same result as Houriet (in the limit $f\to\infty$), in spite of the fact that we used a different interaction term.

Since Houriet has already calculated this potential, the calculation will not be given here. The very elegant method is due to Wentzel,[6] and reference should be made to these two papers.

6. THE HIGHER ORDER POTENTIAL IN THE TWO-BODY PROBLEM

In the definition of the potential energy W_2 of a system of two nucleons

$$W_2 = (\text{energy of ground state of } \bar{H}) - (\text{energy of ground state of } \bar{H}_f), \tag{6.1}$$

we have so far evaluated the first term only to zero-order in $A = Nf/\mu$. To get the higher ap-

[6] G. Wentzel, Helv. Phys. Acta **15**, 111 (1942).

proximations to W_2 we write

$$W_2 = W_2^{(0)} + W_2^{(1)} + W_2^{(2)} + , \qquad (6.2)$$

where $W_2^{(0)}$ is given by (4.10) with $Z=2$.

It is clear that the correction terms are corrections to the energy of the ground state of $\bar{H}$. These corrections will be found by means of customary perturbation procedure. This will give an expansion in inverse powers of A. The superscripts in (6.2) will indicate the power of A^{-1} involved.

The state whose energy we have to find by the perturbation method is a degenerate state. There are four states of the two-body problem, of equal (lowest) energy in zero order in A. They are described by

$$\begin{aligned} X(1;1;0,0,0,\cdots) &\equiv X_1, \\ X(2;1;0,0,0,\cdots) &\equiv X_2, \\ X(1;2;0,0,0,\cdots) &\equiv X_3, \\ X(2;2;0,0,0,\cdots) &\equiv X_4. \end{aligned} \qquad (6.3)$$

Here the first index refers to the eigenstate of the first stat-nucleon, the second to the eigenstate of the second stat-nucleon, and the remaining indices denote the eigenvalues of the operators N_ρ defined in Section 3.

The general procedure for finding the energy perturbation of a state degenerate in zero-order is the following: We calculate matrix elements $H_{mm'}^{(n)}$:

$$H_{mm'}^{(1)} = (m|\Omega|m'), \qquad (6.4\text{-}1)$$

$$H_{mm'}^{(2)} = \sum_{m''}{}' \frac{(m|\Omega|m'')(m''|\Omega|m')}{E(m)-E(m'')}, \qquad (6.4\text{-}2)$$

$$H_{mm'}^{(3)} = \sum_{m''m'''}{}' \frac{(m|\Omega|m'')(m''|\Omega|m''')(m'''|\Omega|m')}{[E(m)-E(m'')][E(m)-E(m''')]}, \qquad (6.4\text{-}3)$$

and similarly for higher values of n. We use here one index m to denote the ensemble of indices necessary to define the simultaneous eigenstates of $\bar{H}_0$ and $\bar{H}'$. The eigenfunctionals for $m=1,2,3,4$ are defined in (6.3). In $H_{mm'}^{(n)}$ m and m' assume the values 1, 2, 3, 4 only, while m'', m''', etc., run over all possible values. However, the prime on the sums indicates that $m''m'''$, etc., do *not* assume the values 1, 2, 3, 4.

Let us consider the first non-zero matrix $H_{mm'}^{(n)}$. It will be non-diagonal in general. We determine its eigenvectors $Y_1 \cdots Y_4$ and the corresponding eigenvalues. The eigenvectors Y are then the linear combinations of the X "appropriate" to the problem, and their eigenvalues are the lowest (nth) order corrections to the energy of the ground state of $\bar{H}$ corresponding to the "appropriate" zero-order states Y. These corrections will be different for different Y, in general, and $W_2^{(n)}$ will, therefore, depend upon the zero-order state chosen for the system of two stat-nucleons plus wave-field. It will be shown later that the states X are eigenstates of the z component of the angular momentum, with eigenvalues $+1$, 0, 0, -1, respectively. The "appropriate" zero-order states Y will just be the usual singlet and triplet eigenvectors. The treatment will thus yield a potential $W_2^{(n)}$ which depends upon the spin-directions of the stat-nucleons.

It turns out in our case that the first non-zero matrix, $H_{mm'}^{(2)}$, is already diagonal, with the diagonal elements equal to each other. The potential $W_2^{(2)}$ is therefore spin-independent, and the spin-dependent forces will arise in the next non-zero perturbation. It will be shown later that all odd-order perturbations give zero. Therefore the spin-dependent forces are contained in $W_2^{(4)}$. A simple calculation shows that the matrix to be diagonalized is

$$G_{mm'}^{(4)} = H_{mm'}^{(4)} - W_2^{(2)} \sum_{m''}{}' \frac{(m|\Omega|m'')(m''|\Omega|m')}{[E(m)-E(m'')]^2}. \qquad (6.5)$$

The matrix elements $(m|\Omega|m')$ entering in these formulas are independent of f (since (4.15) does not involve f). The matrix (6.5) is therefore of order A^{-3}, and this will be the order of the spin-dependent forces.

In view of the fact that $W_2^{(2)}$ is only an ordinary force superposed on $W_2^{(0)}$, and that the spin-dependent forces are of the third order in A^{-1},

neither of them was calculated explicitly. It is possible to show, however, that $W_2^{(4)}$ can be written as a superposition of a spin-independent term, a $(\mathbf{S}_I \cdot \mathbf{S}_{II})$ term, and a tensor force term, provided that $f_I = f_{II}$.

In order to complete the argument, it remains to show that (a) $H_{mm'}{}^{(n)}$ is zero for odd n, (b) $H_{mm'}{}^{(2)}$ is a multiple of the (4 by 4) unit matrix.

(a) is obvious from (6.4) and the fact that Ω connects only states with occupation numbers N, N' such that

$$\sum_\rho N_\rho = (\sum_\rho N_\rho') \pm 1;$$

so, in order to get back to one of the states X_m, all of which have $\sum N_\rho = 0$, an even number of steps is necessary.

(b) will be proved in 3 steps. *First*, we shall show that all but two of the off-diagonal elements of $H_{mm'}{}^{(n)}$ are zero in all orders n. This will follow from the conservation of angular momentum around the z axis. *Second*, we shall show that the two remaining off-diagonal elements are zero in second order. *Third*, it will be proved that the diagonal elements $H_{mm}{}^{(2)}$ are independent of m.

It is easily seen that the z component of the angular momentum operator

$$J_z = \int \psi^+(x)[(\mathbf{x}\times\mathbf{p})_z + \tfrac{1}{2}\sigma_z]\psi(x)d^3x + \tfrac{1}{2}(\sum_I)_z + \tfrac{1}{2}(\sum_{II})_z \quad (6.6)$$

commutes with the Hamiltonian $\bar{H}$, (4.1).

Here we assume the two nucleons to be situated somewhere along the z axis of our coordinate system.

The splitting of the field (4.11) becomes in x space:

$$\psi(x) = \sum_A Q_A u(\mathbf{x}-\mathbf{z}_A) + \psi'(x), \quad (6.7)$$

$$\int \psi'(x) u(\mathbf{x}-\mathbf{z}_A) d^3x = 0. \quad (6.8)$$

Using these formulas together with the fact that $u(\mathbf{x}) = u(|\mathbf{x}|)$ only, it is easily seen that

$$J_z = (J_z)_0 + (J_z)', \quad (6.9)$$

where

$$(J_z)_0 = \tfrac{1}{2}\sum_{A=1,2}(Q_A^+\sigma_z Q_A) + \tfrac{1}{2}(\sum_A)_z, \quad (6.10)$$

$$(J_z)' = \int \psi'^+(x)[(\mathbf{x}\times\mathbf{p})_z + \tfrac{1}{2}\sigma_z]\psi'(x). \quad (6.11)$$

The expression (6.10) is valid only as long as the overlap integral is zero.

The important point here is that J_z commutes not only with $\bar{H} = \bar{H}_0 + \bar{H}' + \Omega$, but also with $\bar{H}_0 + \bar{H}'$ and Ω, separately. It is easily seen that the states (6.3) correspond to $(J_z)' = 0$ and $(J_z)_0 = +1, 0, 0, -1$, respectively. Now, since Ω commutes with J_z, there cannot be any non-zero matrix elements of Ω between states with different values of J_z. *This proves that the only non-zero off-diagonal elements of the matrices $H_{mm'}{}^{(n)}$ can be $H_{23}{}^{(n)}$ and its complex conjugate $H_{32}{}^{(n)}$.*

The perturbing Hamiltonian Ω is, according to (4.15) and (5.4),

$$\Omega = \sum_{A=1,2}\sum_\rho (Q_A^+\lambda_A a_\rho + a_\rho^+\lambda_{A,\rho}Q). \quad (6.12)$$

Now the matrix elements $(1|Q|2)$ and $(1|Q^+|2)$ are zero. Therefore one needs at least *four steps* to go from X_2 to X_3. *This proves that* $H_{23}{}^{(2)} = H_{32}{}^{(2)} = 0$.

The proof that the diagonal elements $H_{mm}{}^{(2)}$ are equal to each other depends upon special properties of the matrix elements $(r|Q|1)$, etc., and of the system (5.15). It is simple and will not be given here. Reference may be made to the thesis submitted to Princeton University by the author.

These arguments complete the proof that the spin-dependent forces in the two-body problem arise in order A^{-2}.

ACKNOWLEDGMENT

The author wishes to express his sincere thanks to Dr. J. M. Jauch, of Princeton University, and Dr. W. Pauli, of the Institute for Advanced Study, for the suggestion of the problem and many interesting and helpful discussions.

Cascade Showers and Mesotron-Produced Secondaries in Lead

SALWA NASSAR* AND W. E. HAZEN
Department of Physics, University of California, Berkeley, California
(Received October 17, 1945)

A study has been made of cascade showers in lead and also of electron secondaries accompanying mesotrons in lead. The cloud chamber that was used for the observations contained four lead plates and was placed in an 1100-gauss magnetic field. In the case of showers, comparison with theory was made in terms of: (a) the average shower curve for 11 showers with initiating energies of about 200 Mev; (b) the energy distribution near the shower maximum of 17 showers; (c) the ratio of height to area of the shower curve of 44 showers; and (d) the fluctuation in number of particles in the showers of (a). The theory agrees with the experiment for (b) and (d) but not for (a) and (c). It is likely that errors arising from known physical approximations in the theory account for the discrepancies. In the case of electron secondaries accompanying mesotrons, a study was made of the number of electrons with energy greater than E relative to the number of mesotrons. For small values of E, the theoretical values are too large by a factor of two, but as E increases the discrepancy becomes smaller.

I. CASCADE SHOWERS

COSMIC-RAY experiments have demonstrated the general validity of the Bethe-Heitler radiation and pair-production cross sections for electrons and photons of energies up to at least 10^9–10^{11} ev. These experiments, however, have been quite general in character and chiefly have demonstrated that there is not a complete breakdown in the theory at high energies. The multiplication cross sections have been used in the development of equations describing the course of cascade showers and hence the penetrating power of electrons and photons. The calculations involve physical and mathematical approximations that, until recently, have limited the accuracy of the results to somewhat better than order of magnitude. Nevertheless, the rough theory has sufficed for the interpretation of cosmic-ray phenomena in a qualitative way. It is now important to obtain experimental data that will allow a quantitative verification of shower theory in order that there be no limitation in its usefulness as a tool in unraveling more complex interrelations between cosmic rays. For example, the studies of bursts, of the origin of the soft component, of Auger showers, etc., all involve shower theory.

Problems such as Auger showers and the development of the soft component in the atmosphere involve cascade showers in air. Since it is relatively difficult to make a detailed study of showers in elements of low atomic number, we must depend on measurements in substances such as lead. The energies involved in some problems of air showers are much greater than in the showers studied in lead, but, since the critical energy in air is 15 times as great as in lead, the results in lead correspond to energies 15 times greater in air, i.e., energies up to 10^{10} ev in the case of the present results. As mentioned in an earlier article,[1] there are no good experimental results that allow a really detailed verification of shower theory. On the other hand, the theoretical calculations have recently been improved[2,3] to the extent that the predictions are probably accurate to 20–30 percent, even in the case of moderately low energies in lead. The present experiment is an improvement over the earlier experiment[1] in that electron energies have been measured, and the showers occurred under more carefully controlled conditions. More extensive comparisons with theory have thus been made possible. The initiating energies were still not determined directly.

Experimental Procedure

Four lead plates, each 0.7 cm thick, were placed in a cloud chamber that was 30 cm in

* Now at the American University of Beirut, Lebanon.

[1] W. E. Hazen, Phys. Rev. 66, 254 (1944).
[2] H. J. Bhabha and S. K. Chakrabarty, Proc. Ind. Acad. Sci. A15, 464 (1942).
[3] H. J. Bhabha and S. K. Chakrabarty, Proc. Roy. Soc. A181, 267 (1943).

diameter and 45 cm in depth. The plates, which were separated by 5.3 cm, were tilted so that the camera viewed them nearly edge on. For aid in illumination, the lead plates were covered with thin aluminum foil. The chamber was placed in a magnetic field of 1100 gauss, which was produced by a pair of coils. In the photographed region the field was uniform to within 15 percent. The cloud-chamber expansion was controlled by a three-counter telescope placed above the chamber. The glass counter cylinders were painted with an "Aquadag" cathode in order to reduce their absorbing power and thus to minimize the possibility of starting a shower in the immediate vicinity of the chamber. During most of the investigation, there was a thin sheet-iron roof over the apparatus, and during a small portion of the investigation a thin sheet of lead was placed above the top counter with the hope that some of the photons would materialize into shower-producing particles.

For illumination two pairs of discharge tubes were used, one on each side. The beams of light were directed forward at an angle of 45°. Each pair of tubes was connected across a bank of condensers of 150 μf charged to 2200 volts. Later it was found more advantageous to use 150 μf across each discharge tube; longer service was thus obtained, and the capillaries were kept free of dark deposits. A stereoscopic camera was used for the photography.

It was desirable to obtain narrow tracks in order to minimize the uncertainty in measuring their curvatures. A very deep chamber requires additional precautions in order to obtain narrow tracks. For example, the diaphragm has a large distance to travel and therefore requires a larger driving force than a shallow chamber. The track width finally obtained was 0.14 cm in the chamber. From comparisons with other chambers, it was concluded that the limitation on the expansion speed, as the chamber was finally operated, was the rate of air flow through the black velvet. The curvature of the high energy tracks was determined from plots of coordinates that were obtained from traveling microscope readings.[4]

[4] C. D. Anderson, Phys. Rev. **44**, 406 (1933).

Results

A particular shower is completely described when the initiating energy is given and when the numbers of positrons, electrons, and photons and their energy distributions are stated as a function of depth of absorber. In practice, theoretical results have been obtained for (1) the *average* number of electrons (plus and minus) and the average number of photons as a function of initiating energy and depth, (2) the energy distributions at various depths for the "average" shower, and (3) the expected mean square deviation from the average. Previous experimental results that can be compared with any of the above theoretical predictions are almost completely lacking.

The present results consist in a comparison with the theory of (a) the average number of particles (from eleven showers with approximately the same total number of particles) as a function of depth, (b) the energy distribution of the particles near the maximum for 17 of the larger showers, (c) the number of particles at the maximum *versus* the total number in four or five shower units, and (d) the mean square deviations for the showers of (a). Where no ambiguity is likely to result, (a) will be called a "shower curve," (b) the "energy distribution," (c) the "shape of the shower curve," and (d) the "fluctuation."

The following notation will be used in the discussion of the cascade showers:

E_0 = energy of initiating particle,
t = depth in showers units (=0.52 cm in lead),

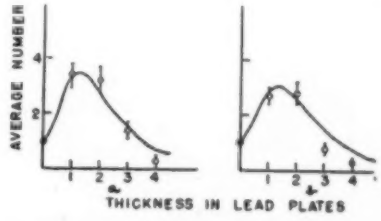

FIG. 1. Shower curves for a small initiating energy. The experimental points were obtained as the averages of eleven showers that contained a total of eight to ten particles. (a) (Left) $N(E_0, 0, t)$ *versus* depth. The curve is for E_0=140 Mev (see Fig. 7), according to the results of B–C. (b) $N(E_0, \beta/2, t)$ *versus* depth. The curve is for E_0=230 Mev (see Fig. 7), according to the equations of B–C. The curve of (a) gives a false impression of agreement with the data. A curve for larger E_0 (say 230 Mev) should be used but B–C do not give figures for this initiating energy.

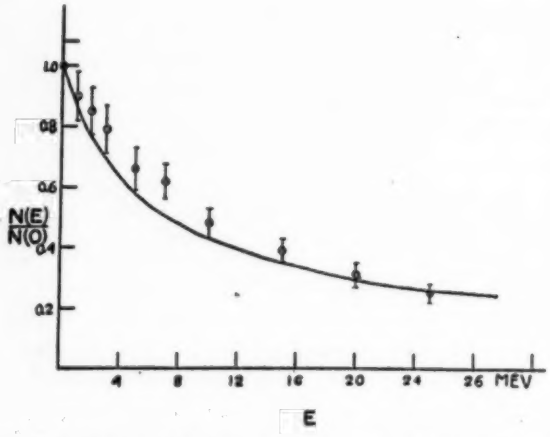

FIG. 2. Energy distribution among the electrons at the observed maxima of 17 showers with initiating energies of 200–1000 Mev. $N(E)/N(0)$ is the relative number of electrons with energy greater than E. The curve was obtained from equations of B–C.

E = energy of shower particle,
β = critical energy (=6.9 Mev in lead) (following reference 3),
$N(E_0, E, t)$ = average number of particles with energy $>E$ at a depth t in a shower initiated by a particle of energy E_0.

(a) *Shower Curve*

Among 1500 photographs, there were 53 with cascade showers. Eleven of the 53 showers contained a total of eight to ten particles and therefore were judged to have been initiated by electrons of approximately the same energy. This particular group was chosen because it was in the most densely populated region of the size distribution. Four of the eleven showers had a total of eight particles each, one had nine, and the remainder had ten each. An average shower, compounded from the above group of eleven actual showers, is indicated in Fig. 1. The points represent simply the average number of particles under each of the lead plates, and the vertical lines indicate the standard probable errors. The plot (Fig. 1b) for $N(E_0, \beta/2, t)$ was made in order to eliminate uncertainties deriving from approximations in the theory that are very poor at the lowest energies.

The curve of Fig. 1a was obtained from the equations of Bhabha and Chakrabarty[2] (hereinafter referred to as B–C). Saddle points were determined from Eq. (26) and the values of $N(E_0, \beta/2, t)$ from Eq. (27) of reference 2. Many of the functions of the introduced variable s that enter into the calculations are given in the tables of Rossi and Greisen[5] with somewhat different notation, e.g., s in reference 2 becomes $s+1$ in reference 5. The value of N thus obtained is actually the first term of a series, but the second term is quite small except for large values of t, values that are not considered here. The curve of Fig. 1a was obtained from the tables of values for N and from the equations for position and height of the maximum given by B–C.

As a result of the following considerations, showers with the same total number of particles are considered to have approximately the same initiating energies. The entire original energy is ultimately dissipated by particles in collision losses and hence

$$E_0 = \int_0^\infty N(E_0, 0, t)(dE'/dt)dt, \qquad (1)$$

where the rate of energy loss by particles $(dE'/dt) \simeq \text{constant} = \beta$. The area A under a

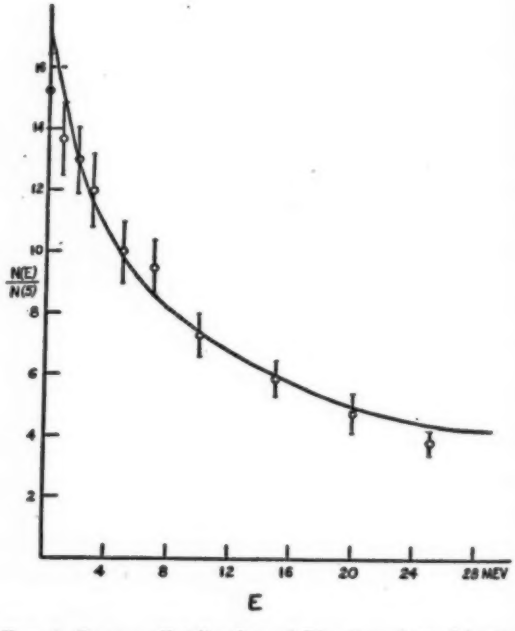

FIG. 3. Energy distribution of Fig. 2 replotted in terms of the number of electrons with energy greater than E relative to the number with energy greater than 5 Mev. Thus the effects of approximations in the theory that are poor at low energies are eliminated.

[5] B. Rossi and K. Greisen, Rev. Mod. Phys. **13**, 240 (1941).

shower curve is found to be approximately

$$A \simeq E_0/\beta \simeq \int_0^\infty N(E_0, 0, t)dt. \qquad (2)$$

Thus the total number of observed particles, which is a summation and approximates the integral (2), is a reasonably satisfactory way of determining the initiating energy. In the experiment, the summation extended to only the fourth or fifth radiation unit, but contributions at greater depths would be small and their variations still smaller.

(b) *Energy Distribution*

Among the 53 showers, 17 were found suitable for a study of the energy distribution near the shower maximum. Each of the 17 showers contained 6 to 20 particles at the observed maximum and thus was probably initiated by an electron with energy 200 to 1000 Mev. The observed energy distribution is given in the form of an integral spectrum in Fig. 2. The vertical lines, which represent probable errors, do not include uncertainty in energy determinations but simply indicate the statistical uncertainty. Since approximations in the theory are very poor at extremely low energies, the data have been replotted in Fig. 3 in units of number of particles with energy greater than 5 Mev.

The theoretical curves were obtained from the equations of B–C.[2] The calculations were made by the method employed by B–C in obtaining their Eq. (33). Since the spectral distributions for energies up to 30 Mev are nearly the same for initiating energies of 380 to 1000 Mev, the procedure of including showers within a wide range of energies is justified.

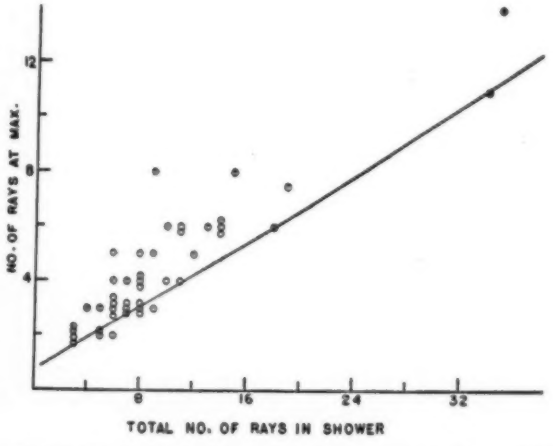

FIG. 4. Shapes of the shower curves. Number of particles at the observed maxima *versus* the total number of rays in the shower for *four* lead plates.

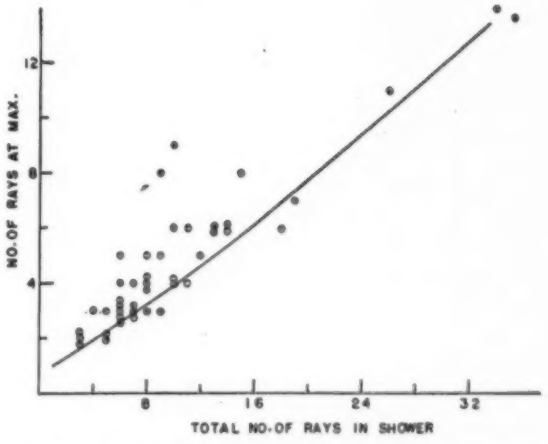

FIG. 5. Shapes of the shower curves. The total number is for *three* lead plates.

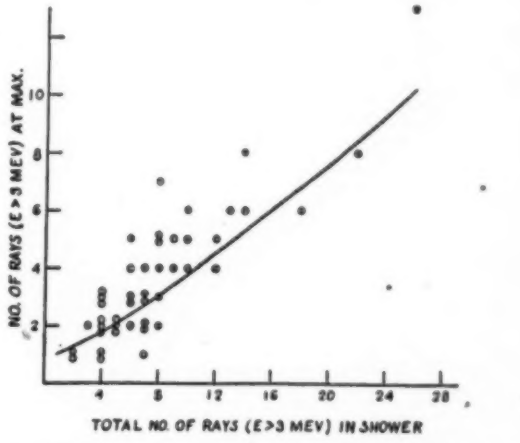

FIG. 6. Shapes of the shower curves with particles of $E>3.5$ Mev excluded. The total number is for three lead plates.

(c) *Shape of the Shower Curves*

The method of analysis that includes the greatest number of showers is that of comparing the number of rays at the maximum with the total number of rays in the shower. There were 44 showers that are suitable for this type of analysis. Since the illumination in the bottom section of the chamber, below the fourth lead plate, was not always as intense as in other regions of the chamber, the data are plotted both for three and

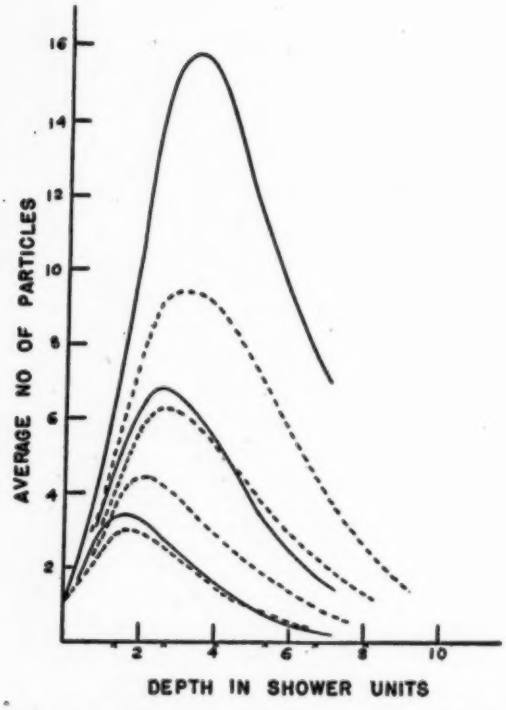

FIG. 7. Theoretical shower curves for electron initiated showers. The arrows on the scale of abscissae indicate depths in number of lead plates. The solid curves are from figures given by B–C for number of particles of all energies and are for initiating energies of 1000, 380, and 140 Mev. The dotted curves were obtained from equations of B–C and are for number of particles with $E>3.5$ Mev. The initiating energies are 1000, 620, 380, and 230 Mev.

also for four lead plates. As in (a) and (b), the results are also given with particles of low energy ($E<\beta/2$) excluded. The experimental results are represented by the circles in Figs. 4–6.

The theoretical curves were obtained from the shower curves of Fig. 7. The shower curves were calculated from the equations of B–C in the manner described under (a). The ordinates of the curves in Figs. 4–6 are simply the heights of the curves of Fig. 7, and the abscissae are the sums of the number of particles at depths of 0, 1, 2, 3, and 4 lead plates (Fig. 4) or 0, 1, 2, and 3 lead plates (Figs. 5 and 6). Since the abscissae of Figs. 4–6 represent the area under a shower curve and the ordinates the height, the plots are simply a measure of the shape of the shower curves.

(d) *Fluctuations*

The eleven showers of (a), each of which probably represents roughly the same initiating energy, were analyzed for magnitude of fluctuations at depths of 1 and 2 lead plates. The magnitude of the fluctuations, as usual, is measured by $\langle(N-\bar{N})^2\rangle_{Av}$. The experimental results are presented in tabular form in Table I.

If the shower particles were completely independent, we should expect a distribution in observed values of N that approached a Poisson distribution for a large number of observations and consequently $\langle(N-\bar{N})^2\rangle_{Av}=\bar{N}$. But since the particles are in fact related, we certainly expect larger fluctuations. The simplest model (Furry model) that takes this fact into account predicts $\langle(N-\bar{N})^2\rangle_{Av}=\bar{N}(\bar{N}-1)$. Scott and Uhlenbeck[6] have included ionization loss in the theory of fluctuations and obtain results that indicate an expected root mean square deviation a few times $\bar{N}$. The values of $\bar{N}$ and $\bar{N}(\bar{N}-1)$ are included in Table I for the sake of comparison.

Comparisons of theory and experiment lead to the conclusions stated in the following paragraphs.

(a) The shower curves agree moderately well with experimental data (Fig. 1), but there is an indication that the theoretical curve does not decrease with sufficient rapidity after the maximum. Exclusion of low-energy electrons does not result in better agreement (Fig. 1b).

(b) The energy distribution (Fig. 2) differs significantly from the experimental results, but in this case exclusion of low energy particles (Fig. 3) does result in satisfactory agreement.

(c) The results show that the ratio of height to area given by the theory is too small (Figs. 4 and 5). When low energy electrons are omitted (Fig. 6), there is less discrepancy, but the discrepancy still exists.

(d) The observed fluctuations are such that the mean square deviation is roughly 1½ times the

TABLE I. Distribution in size, at two depths, for eleven showers initiated by approximately the same energy.

		Below 1st plate	Below 2nd plate
(a)	$\bar{N}$	3.4	3.2
(b)	$\bar{N}(\bar{N}-1)$	8.2	7.0
(c)	$\langle(N-\bar{N})^2\rangle_{Av}$	4.3	5.2

(a) The observed average number of particles ($\bar{N}$) and hence the expected value of $\langle(N-\bar{N})^2\rangle_{Av}$ according to Poisson distribution.
(b) Expected value for $\langle(N-\bar{N})^2\rangle_{Av}$ according to the Furry model.
(c) Observed value for $\langle(N-\bar{N})^2\rangle_{Av}$.

[6] W. T. Scott and G. E. Uhlenbeck, Phys. Rev. 62, 497 (1942).

Poisson value, whereas Scott and Uhlenbeck[6] have predicted a mean square deviation 2 to 3 times the Poisson value for somewhat larger showers. The disagreement probably need not be considered as significant in view of the approximations in the calculations, the smallness of the sample of showers, and the small size of the showers.

Discussion

The main experimental uncertainty is in the determination of energies and results from uncertainties in the measurement of the curvature and of the angle of the particle with the magnetic field. The uncertainty in curvature increases with energy and is such that the error is of the same magnitude as the curvature itself for energies of 35 Mev in the case of the best tracks. The angle of inclination of the high energy rays in a shower is generally so small that errors in its measurement are unimportant. Aside from the study of the energy distribution (b), there is no particular interest in the energy of particles except near 3.5 Mev. At low energies there is little uncertainty in the curvature measurements, but the angle with H is frequently large and uncertainties in the angle become more important. The estimated error for low energies is 15 percent.

The inaccuracies of the theoretical calculations originate in mathematical and physical approximations. In the work of B–C, errors due to the former are probably unimportant insofar as comparison with the present experimental results is concerned. The important physical approximations are the assumptions that (1) the collision loss by particles is independent of energy, (2) the shower is one-dimensional, (3) the multiplication cross sections are those for complete screening, and (4) the Compton effect is negligible.

(1) In reality, the collision loss increases rapidly for electrons with $E<1$ Mev and increases slowly (roughly as log E) for $E>10$ Mev. (2) The lateral spread of the shower is determined almost entirely by scattering of the electrons.[5] In the case of lead, scattering becomes important at 3 Mev and serious at 1 Mev. The result is a decrease in the actual penetration of the electrons in the direction of shower propagation. (3) When incomplete screening is taken into account, the pair production cross sections are reduced significantly at lower energies (10–200 Mev for lead).[7] (4) In lead, the Compton cross section becomes equal to the pair production cross section for a photon energy of about 5 Mev. At the energies involved in our shower studies, the Compton effect results in the production of low energy electrons and the consequent dissipation of the energy of the photon at the rate of 1–2 Mev per cm in the case of lead.[3]

The principal conclusion that can be made is that the shape of the theoretical curves is wrong. From (c) we can conclude that the theoretical curves should be more sharply peaked for all initiating energies up to 1000 Mev, and from (a) we can add that the error is probably on the side of the peak toward greater thicknesses.

The most important experimental uncertainty, energy measurement, can have no effect on the results when particles of all energies are included. The most useful comparison with theory is made, however, by excluding the particles of low energy, because the effect of certain approximations in the theory can thus be eliminated: namely, the neglect of scattering (2) and increased collision loss (1) at low energies, which, if not neglected, virtually eliminate the contribution of electrons to a shower when their energies fall below one Mev. When we consider the cases in which low energy electrons are excluded, the experimental uncertainty in energy measurement would tend to increase the included number of electrons since the population is greater at the lower energies. The effect is smaller at the maximum of the shower curve, where the average energy is high, than at greater depths, where the average energy decreases. The predicted consequence of the experimental uncertainties would therefore be a broadening of the shower curves when low energy particles are excluded. Thus a correction would result in a *greater* discrepancy.

Let us consider the qualitative effect of the other physical approximations used in the theory. If we take into account increased collision loss at higher energies (1), the value of dE'/dt becomes larger for larger energies. The area under

[7] H. C. Corben, Phys. Rev. **60**, 435 (1941).

a given portion of the shower curve,

$$A = E_0/(dE'/dt)_{t_1} = \int_{t_1}^{t_2} N(E_0, 0, t)dt,$$

is decreased more for small t than for large t because the average energy of the particles and consequently $(dE'/dt)_{t_1}$ are greater for small t. Thus a correction would lead to a broader shower curve and greater divergence from the experimental results.

When we take incomplete screening into account (3), the multiplication cross sections are smaller, particularly the pair-production cross section at lower energies. The result is a decrease in the number of particles for thickness $t<3t_{\max}$[7] and, from conservation of energy, an increase in the number of particles for greater thicknesses. Corben[7] has shown that the maximum of a shower with $E_0=1000$ Mev is only 13.5 particles as contrasted with 16 particles[2] when complete screening is assumed. Thus the theoretical curve is again broadened when the theory is improved. On the other hand, when only electrons with $E>\beta/2$ are considered, there is a partially compensating effect which may be seen from the following consideration. The area under a shower curve ($N(E_0, \beta/2, t)$ *versus* t) is

$$\int N(E_0, \beta/2, t)dt = E_0/\beta - \int [N(E_0, 0, t) - N(E_0, \beta/2, t)]dt, \quad (3)$$

where the latter integral is the track length generated by electrons with $0<E<\beta/2$.

The latter integral represents the track length generated by all particles while their energies are less than $\beta/2$. When incomplete screening is taken into account, the number of individual particles is reduced and hence the latter integral is reduced. Since E_0/β is unchanged, the former integral is increased. Thus the area under a shower curve in which low energy electrons are excluded is increased, and, since the number of electrons that fall below the energy limit $\beta/2$ is greater where the average energy is smaller, we should expect the increase in area to occur predominately in the early stages, i.e., near the maximum.

Finally, the neglect of the Compton effect ascribes a significantly greater penetrability to the lower energy photons, since the photons actually dissipate a portion of their energy in the production of low energy Compton recoils. The result is an increase in the height to area ratio of a shower curve. When low energy electrons are excluded, the effect is enhanced: the second integral in Eq. (3) is increased, since inclusion of the Compton effect predicts more particles, and the area under the shower curve is decreased, the main decrease occurring at greater depths because the average energy is less.

It is difficult to estimate the magnitude of the changes that would be produced by the modifications discussed in the above paragraphs. It seems likely, however, that improvements in the physical approximations of the theory might result in satisfactory agreement with the experimental results. At present, it is only possible to say that the theoretical multiplication cross sections have been approximately verified for energies up to 10^9 ev. The methods herein employed amount to a comparison between multiplication processes and collision losses. The latter have been confirmed experimentally and hence a satisfactory verification of the shower theory would constitute a confirmation of the multiplication cross sections.

II. MESOTRON-PRODUCED SECONDARIES

The electron component of cosmic rays in air apparently originates almost entirely as a secondary effect of mesotrons,[8] a secondary effect that occurs in the lower regions of the atmosphere insofar as the majority of the electron secondaries observed at sea level are concerned. Since both mesotron decay and close electron collisions play important roles in the production of secondaries, it is of importance to study one or the other individually in order to separate the two effects. Decay electrons can be practically eliminated by observing the secondaries under dense materials. Cloud-chamber observations alone have given unambiguous results, but there is poor agreement among many of the findings.[9] Likely explanations for the discrepancies are given in reference 9. In order adequately to compare results with the theory, it is necessary to know at least the

[8] K. Greisen, Phys. Rev. **63**, 323 (1943); B. Lombardo and W. E. Hazen, Phys. Rev. **68**, 74 (1945).
[9] W. E. Hazen, Phys. Rev. **64**, 7 (1943).

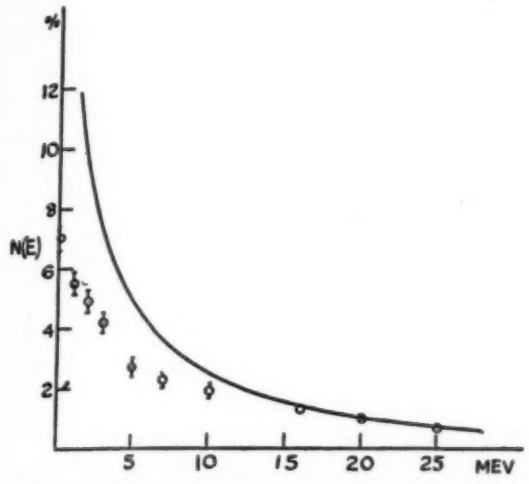

FIG. 8. Number of secondary electrons in equilibrium with mesotrons in lead. $N(E)$ is the number of electrons with energy greater than E. The curve is from equations of Tamm and Belenky.

distribution in energy of the secondaries at the lower energies. Wilson and Neddermeyer and Anderson[10] have previously studied secondary production with a magnetic field. Neddermeyer and Anderson used their data individually as arguments against the possibility of protons as the main constituent of the hard component. Wilson used his data statistically as an indication of a mesotron mass of a few hundred electron masses.

In the present work the same group of pictures that was used in the study of showers was analyzed for number and energy distribution of electron secondaries accompanying the mesotrons in lead.

Results and Discussion

Only those pictures that showed counter-controlled mesotron tracks with the three center segments clearly defined were chosen. There was thus considerable assurance that very few secondaries would escape observation. The observed number of secondaries for various lower energy limits are indicated in the integral spectrum plotted in Fig. 8. The total number of mesotron traversals of a lead plate was 1674. Tamm and Belenky[11] have obtained an expression for the number of secondaries to be expected in lead. In making a numerical evaluation, T–B used a mesotron energy spectrum that was appropriate for determining the number of secondaries in air, and they used a mesotron mass of $160m_e$. In the present experiment, the observed secondaries are all produced within the apparatus, and hence it is the sea-level mesotron spectrum that should be used for the calculations. In addition, present experimental evidence favors a mesotron mass somewhat greater than $160m_e$. Consequently the theoretical curve of Fig. 8 has been obtained from Eq. (6.1) of T–B, but with a value of $\bar{E}_m$ (the maximum transferable energy averaged over the mesotron spectrum) determined with the use of Blackett's sea level spectrum[12] and a mesotron mass of $200m_e$. Williams[13] has calculated the relative number of electron secondaries to be expected in lead with a result of 8 to 13 percent with energy greater than 3 Mev. The lower limit of 8 percent is slightly above the curve obtained from T–B.

The theoretical curve is in marked disagreement with the data even at moderately high energies, energies where scattering is not serious. Wilson, on the other hand, observed a value of 4.8 percent for the number of electrons with $E>10$ Mev in equilibrium with mesotrons in gold. When the theory of T–B is used in order to change 4.8 percent to a corresponding value for lead, the result is 5.0 percent. This point would lie above the curve of Fig. 8. Wilson does not mention the type of counter control that was employed, but it is likely that it consisted of counters both above and below the chamber. Evidence for this conclusion is given by the fact that his data indicate an extremely high proportion of events with high energy secondaries and with two or more secondaries. A counter below the chamber would result in a selectivity in favor of mesotrons accompanied by high energy secondaries. Unless this fact were taken into account in selecting the photographs to be studied, it might result in an apparent increase by a factor as large as two, depending on the magnetic field strength, for secondaries with $E>3\times10^7$ ev.

The accuracy of the theoretical curve is not

[10] J. G. Wilson, Nature **142**, 73 (1938); S. H. Neddermeyer and C. D. Anderson, Rev. Mod. Phys. **11**, 191 (1939).

[11] Ig. Tamm and S. Belenky, J. Phys. Acad. U. S. S. R. **1**, 177 (1939).

[12] P. M. S. Blackett, Proc. Roy. Soc. **A159**, 1 (1937).

[13] E. J. Williams, Proc. Camb. Phil. Soc. **36**, 183 (1940).

known and is difficult to estimate since it involves shower theory. Williams' calculations indicate an uncertainty of about 30 percent for his results but unfortunately the suggested range of possible values extends upward from the curve. His calculations would agree moderately well with those of T–B if the more exact cross section for production of knock-on electrons were used.

Large changes in mesotron mass would be required in order to remove the discrepancy, e.g., an increase in mesotron mass from 200 to $250m_e$ results in only a 12 percent decrease in the predicted number of secondaries. Large changes in the mesotron spectrum also produce only small alterations in the expected number of secondaries.

We have greatly appreciated instructive conversations with Dr. David Bohm concerning the shower theory.

PHYSICAL REVIEW VOLUME 69, NUMBERS 7 AND 8 APRIL 1 AND 15, 1946

Disintegration Schemes of Radioactive Substances IX. Mn^{52} and V^{48}

WENDELL C. PEACOCK AND MARTIN DEUTSCH
Massachusetts Institute of Technology, Cambridge, Massachusetts

(Received December 29, 1945)

The radiations emitted in the decay of $_{25}Mn^{52}$ (6.5 day) and of $_{23}V^{48}$ have been investigated by spectrometer and coincidence methods. Mn^{52} decays with the emission of positrons of maximum energy 0.582 ± 0.015 Mev, followed by three gamma-rays in cascade, of energies 0.734 ± 0.015 Mev, 0.940 ± 0.02 Mev, and 1.46 ± 0.03 Mev, respectively. These energies are the multiples 3, 4, and 6 of 0.240 Mev, within the experimental errors. The orbital electron capture by Mn^{52} leads to the same excited state of Cr^{52} as the positron emission with which it competes. The positrons of V^{48} are emitted with a maximum energy of 0.716 ± 0.015 Mev, with successive emission of two gamma-rays of 1.33 ± 0.03 Mev and 0.980 ± 0.02 Mev energy. These gamma-ray energies are in the ratio 4:3. From the disintegration schemes one finds the mass differences between neutral atoms: $Mn^{52}-Cr^{52}=5.10\pm0.15\times10^{-3}$ a.m.u. and $V^{48}-Ti^{48}=4.37\pm0.12\times10^{-3}$ a.m.u. Some evidence is also presented concerning the disintegration of V^{52} and of Sc^{49}. The energy levels of Cr^{52} and Ti^{48} identified in the radioactive processes are compared with those found by other methods. The disintegration energies of several nuclei studied are examined with a view to their dependence on atomic weight. It is shown that beta-ray theory explains consistently the lifetimes, the shapes of the positron spectra, and the ratio of electron capture to positron emission if one assumes tensor interaction, angular momentum change $\Delta I=0$ or $\Delta I=\pm1$ (not $0\rightarrow0$) without parity change in the case of Mn^{52} and with parity change in the case of V^{48}.

INTRODUCTION

IN paper VII of this series[1] we called attention to some apparent similarities between the energy levels of certain nuclei in the same region of the periodic table. It seems desirable to study the excited states of several nuclei which might be expected to differ in some regular fashion in their internal structure. The most desirable method for such a study would be—in many respects—the measurement of the energies of secondary heavy particles from transmutation or inelastic scattering processes. When this method is developed to the ultimate precision of which it is capable, it should prove to be as powerful a tool for the analysis of energy levels in light nuclei as the study of spontaneously emitted alpha-particles has been for the levels of very heavy nuclei. However, the contemporary techniques are such that the resolution obtained is less than some known level spacings, even in rather light nuclei, such as Fe^{56} (paper VI). Therefore a study of the radiations emitted in radioactive disintegrations appears to be the most hopeful approach at present. This method has yielded reliable and rather precise information concerning the energy levels of a number of nuclei, but its extension to the study of any selected sequence or group of nuclei presents certain inherent difficulties. Each of the nuclei to be investigated must be the product of one or, preferably, two or three radioactive processes of sufficiently long period to permit thorough study, and involving several excited states. Furthermore there must be some practical method to produce the radioactive species in-

[1] Reference to the first five papers will be found in paper VI: Phys. Rev. **64**, 321 (1943); papers VII and VIII appeared in Phys. Rev. **65**, 211 (1944) and **68**, 193 (1945).

volved either free from other activities of the same element or at least free from such activities as might interfere with the unambiguous assignment of the radiations. Few groups of nuclei which might exhibit structural similarities satisfy these conditions with the techniques available.

The group of stable nuclear species of even atomic number and isotopic number four which extends from S^{36} to Zn^{64} is one of the few available for our purpose. The members of this group may be thought of as built up from S^{36} by the addition of from one to seven alpha-particles. While there is no definite evidence that such a group could be considered a sequence of nuclear homologues, it appeared at least as a possible starting point, in view of our slight knowledge of the structure of any but the lightest nuclei. Two members of the group, Fe^{56} and Ni^{60}, have been discussed in papers VI and VIII of this series[1] while some evidence concerning other members has been reported by other authors. In this paper we present results concerning Cr^{52} and Ti^{48} in the light of the radioactive decay of their neighbors. The results are not as complete as might be desired because of the pressure of more urgent work. The beta- and gamma-ray spectrometer[2] and coincidence techniques have been described in earlier papers.[1]

A. Mn^{52}

The species of manganese with 6.5 day half-life has been assigned to mass number 52 by Livingood and Seaborg.[3] It appears to be isomeric with the 21-minute activity assigned to the same mass number. Hemmendinger[4] studied Mn^{52} and reported that the maximum energy of the positrons emitted by the 6.5-day species is 0.77 Mev. He also reported finding gamma-rays of 1-Mev and 2-Mev quantum energy and estimated that 95 percent of the disintegrations proceed by orbital electron capture.

PREPARATION OF SOURCES OF Mn^{52}

Mn^{52} was produced for our experiments by the reaction $Cr^{52}(d, 2n)Mn^{52}$. A water-cooled "probe" of the Massachusetts Institute of Technology cyclotron was chromium-plated and bombarded for two hours with an average current of 0.5 milliamperes of 13.5-Mev deuterons. The bombardment was concentrated on an area of about 0.5 cm^2 as indicated by a slight discoloration of the bright chromium plate. The plating was dissolved from this area in hydrochloric acid and 2 mg of Mn, 5 mg of V, and 5 mg of Cu were added to this solution as chlorides. Manganese and copper were precipitated with sodium peroxide; the precipitate was redissolved and the copper removed with H_2S. Finally MnO_2 was precipitated from concentrated HNO_3.

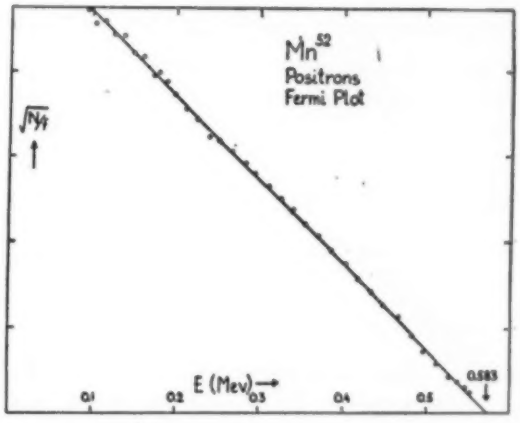

FIG. 1. Positron spectrum of Mn^{52} (6.5 day).

Sources for the study of the beta-rays were prepared as follows. A drop of a dilute solution of active $MnCl_2$ was deposited on a thin (about 0.25 mg/cm^2) aluminum leaf, mounted on a brass frame. This was then covered with an inverted watch glass on which a few drops of concentrated ammonium hydroxide had been deposited. This produced a hydroxide precipitate which, upon gentle warming, formed a very uniform and adherent film, probably with partial conversion to oxide. The thickness of this deposit was less than that of the supporting aluminum. Gamma-ray sources were prepared by sealing a small amount of the active oxide into a suitable copper capsule.

The intensity of the radiations due to the long-lived Mn^{54} (paper VII) was quite negligible during the first few weeks after bombardment. The 21-minute isomer of Mn^{52} had completely decayed before the measurements were begun.

[2] M. Deutsch, L. G. Elliott, and R. D. Evans, Rev. Sci. Inst. **15**, 178 (1944).
[3] J. J. Livingood and G. T. Seaborg, Phys. Rev. **54**, 391 (1938).
[4] A. Hemmendinger, Phys. Rev. **58**, 929 (1940).

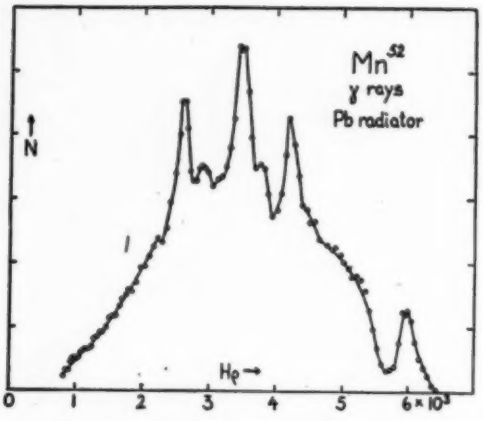

FIG. 2. Photoelectrons and Compton recoil electrons due to the gamma-rays of Mn^{52}.

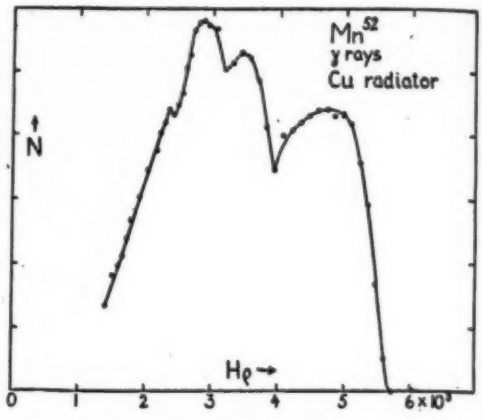

FIG. 3. Compton recoil electrons due to the gamma-rays of Mn^{52}.

THE POSITRON SPECTRUM OF Mn^{52}

Figure 1 shows a Fermi plot of the beta-ray spectrum of Mn^{52} obtained with the magnetic lens spectrometer.[2] The maximum energy, as found from the intercept on the axis, is 0.582 $\pm$0.03 Mev. The fact that the plot is a straight line indicates that the distribution agrees with that predicted by the Fermi theory for an allowed transition, within the experimental error. Below about 0.20 Mev the experimental points may be slightly shifted by instrumental effects. The shape of the upper two-thirds of the energy range should, however, be reliable. There can be no doubt that the spectrum is simple, i.e., there is only one mode of beta-decay, and there are no pronounced internal conversion lines, at least above 0.1 Mev.

THE GAMMA RAYS OF Mn^{52}

Figure 2 shows a typical secondary electron spectrum produced by the gamma-rays of Mn^{52} in a lead foil of 36 mg/cm^2-thickness and in the copper capsule containing the source, and observed in the magnetic lens spectrometer. There are pronounced photoelectron peaks due to four gamma-rays of energies 0.510$\pm$0.01 Mev, 0.734 $\pm$0.015 Mev, 0.940$\pm$0.02 Mev, and 1.46$\pm$0.03 Mev. Figure 3 shows the spectrum of Compton recoil electrons produced in a copper radiator, indicating the same four gamma-rays. The lowest energy gamma-ray is certainly due to annihilation radiation. The particular radiators and resolution used are not well suited for an estimate of the relative intensities of the gamma-rays.[2] It would seem, however, that all of the rays, including the annihilation radiation are of approximately equal intensity.

COINCIDENCE MEASUREMENTS OF Mn^{52}

Coincidences between positrons and gamma rays were studied in the standard arrangement (paper V). The number of such coincidences per recorded positron was $4.18\pm0.12\times10^{-3}$. This number did not change when some aluminum absorber was placed between source and beta-ray counter, indicating that the positron spectrum is simple, in agreement with the shape of the Fermi plot (Fig. 1). From the known efficiency curve for the gamma-ray counter in the geometry used (very similar to Fig. 6, paper V), we find that the efficiencies for detecting each of the three nuclear gamma-rays identified in the secondary electron spectrum (Fig. 2) are, respectively, 1.10×10^{-3}, 1.25×10^{-3}, and 1.80×10^{-3}, in order of increasing energy. It is seen that the sum of these three is just equal to the observed coincidence rate, within the experimental error. Since the positron spectrum has but a single component, we may conclude that the emission of a positron by Mn^{52} is always followed by three gamma-rays in cascade.

Coincidences between x-rays, emitted in the orbital electron capture process, and gamma-rays were also measured, by replacing the beta-ray counter in the standard geometry with an x-ray counter (paper VII). The number of x-ray-gamma-coincidences per recorded x-ray was the same as the number of coincidences per recorded

positron. This indicates that the K-electron capture process leads to the same level as the positron emission. Gamma-gamma-coincidences were not studied in the standard arrangement because the presence of the annihilation radiation makes the interpretation of such an experiment difficult.

DISINTEGRATION SCHEME OF Mn^{52}

In the light of the results reported in the preceding sections, it may be concluded that most, if not all, of the disintegrations of Mn^{52} (6.5 day) proceed according to the scheme shown in Fig. 4. Our experiments throw no light on the order of emission of the three gamma-rays, and the particular arrangement of the levels shown is rather arbitrary. Some indirect evidence supporting the assignment of an excitation energy of 1.46 Mev to the lowest level involved is presented in the next section. The relative probabilities of positron emission and orbital electron capture has been determined in this laboratory by W. M. Good[5] using a modification of the coincidence technique. He found $\lambda_+/\lambda_{cap.}=0.54\pm0.05$.

DISINTEGRATION SCHEME OF V^{52}

The negatron decay of V^{52} (3.9 min.) leads to the same product nucleus—Cr^{52}—as the decay of Mn^{52}. Martelly[6] reports as a result of very careful absorption experiments that the gamma-rays emitted by V^{52} consist of a single group of 1.47-Mev quantum energy. Preliminary observations of beta-gamma-coincidences carried out by us are consistent with the assumption that the beta-ray spectrum is simple, and that each beta-ray is accompanied by a single gamma-ray of about 1.5 Mev. Using the value 2.05 Mev for the maximum energy of the beta-rays, given by Davidson,[7] we have drawn a tentative decay scheme indicated by dotted lines in Fig. 4.

B. V^{48}

The species of vanadium with 16 day half-life has been assigned to mass number 48 by Walke.[8] He reported that it decays by positron emission and by orbital electron capture and gave a value of 1 Mev for the maximum energy of the positrons as observed in the cloud chamber. Richardson[9] by observation of recoil electrons in a cloud chamber found a gamma-ray of 1.05-Mev quantum energy. Recently, Hibdon, Pool, and Kurbatov[10] also investigated the decay of V^{48} and reported a maximum positron energy of 0.58 Mev, a gamma-ray of 1.50 Mev, and a relative probability of orbital electron capture eighteen times as great as that for positron emission.

PREPARATION OF SOURCES OF V^{48}

Vanadium was separated by precipitation with cupferron from the chromium targets used to prepare Mn^{52}. The cupferron precipitate was dissolved, freed of the hydrogen sulphide group and of elements precipitated by sodium peroxide. Finally the vanadium was re-precipitated with cupferron, and the precipitate ignited to the oxide.

Sources for beta-ray measurements were made by evaporating the oxide in vacuum from a platinum filament onto aluminum of 0.25 mg/cm² thickness. Gamma-ray sources were made by sealing the active oxide into a brass capsule. The shorter-lived activities of V^{50} and V^{51} were allowed to decay completely before measurements were started.

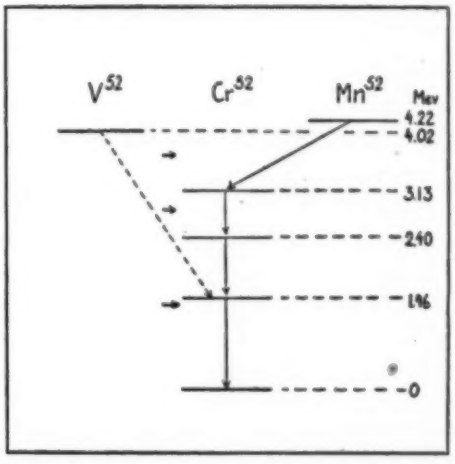

FIG. 4. Disintegration scheme of Mn^{52} (6.5 day). 35 percent of the disintegrations are by positron emission, the rest by orbital electron capture. Dotted line indicates a tentative decay scheme for V^{52}. Short arrows locate energy levels of Cr^{52} found by inelastic scattering of protons.

[5] W. M. Good, D. Peaslee, M. Deutsch, Phys. Rev. **69**, 313 (1946).
[6] J. Martelly, Comptes rendus **216**, 838 (1944).
[7] Quoted by G. T. Seaborg, Rev. Mod. Phys. **16**, 1 (1944).
[8] H. J. Walke, Phys. Rev. **52**, 669, 777 (1937); Proc. Roy. Soc. **171**, 360 (1939).
[9] J. R. Richardson, Phys. Rev. **53**, 124 (1938).
[10] C. T. Hibdon, M. L. Pool, and J. D. Kurbatov, Phys. Rev. **65**, 351 (1944).

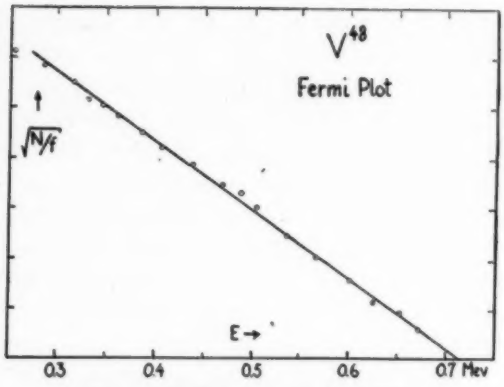

FIG. 5. Positron spectrum of V^{48}.

THE POSITRON SPECTRUM OF V^{48}

Figure 5 shows a Fermi plot of the positron spectrum of V^{48}. The fact that the points fall nearly on a straight line indicates that the spectrum is simple above 0.25 Mev. The deviation from the theoretical distribution for an allowed transition is small and could be due to instrumental effects. The intercept on the axis yields a value 0.716 ± 0.015 Mev for the maximum energy of the spectrum. The energy range between 0.18 Mev and 0.25 Mev also showed no unusual features. The relatively low specific activity of the material made it impossible to prepare sources which were sufficiently thin and at the same time small enough to permit the use of a very thin window. Therefore the data below 0.25 Mev were definitely distorted by instrumental effects and are not included in Fig. 5.

THE GAMMA RAYS OF V^{48}

The secondary electron spectrum from a 36 mg/cm²-lead radiator shown in Fig. 6 indicates photoelectron peaks and Compton recoil groups due to three gamma-rays. The one of lowest energy, 0.51 Mev, is again undoubtedly annihilation radiation while the other two are nuclear gamma-rays of quantum energies 0.980 ± 0.02 Mev and 1.33 ± 0.03 Mev, respectively. As in the case of Mn^{52} only a rough estimate of the relative intensities can be made. The three gamma-rays seem to be of approximately equal abundance.

COINCIDENCE MEASUREMENTS OF V^{48}

Coincidences between the positrons and nuclear gamma-rays emitted in the decay of V^{48} were observed in the standard arrangement (paper V). $2.93\pm0.09\times10^{-3}$ beta-gamma-coincidences per recorded positron were observed. The known efficiency curve of the gamma-ray counter indicates that the sum of its efficiencies for a gamma-ray of 0.98 Mev and one of 1.33 Mev is $3.04\pm0.08\times10^{-3}$. This agreement with the observed coincidence rate shows that each positron is accompanied by the emission of two gamma-rays in cascade. Introduction of a thin (30 mg/cm²)-aluminum absorber between source and beta-ray counter did not affect the coincidence rate per recorded particle. This shows that the positron spectrum is simple also at low energies. As in the case of Mn^{52}, gamma-gamma-coincidences were not studied because of the presence of annihilation radiation.

Unfortunately the x-rays of titanium, emitted in the orbital electron capture process, are so soft that they are almost completely absorbed in a beryllium absorber thick enough to eliminate the positrons when one wishes to observe x-ray-gamma-coincidences. Absorbers of lithium metal, which should make the experiment possible, are rather inconvenient to handle and were not available at the time this study was made. Therefore no direct evidence concerning the excited states involved in orbital electron capture by V^{48} was obtained.

DISINTEGRATION SCHEME OF V^{48}

The evidence presented in the preceding sections leaves little doubt that the positron emission by V^{48} is followed by the successive emission of two gamma-rays of 0.98 Mev and 1.33 Mev,

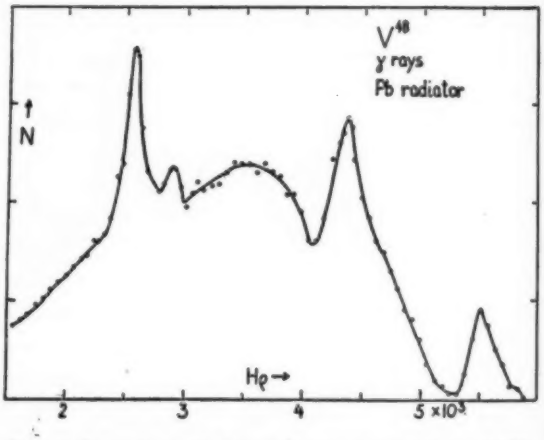

FIG. 6. Secondary electrons due to gamma-rays of V^{48}.

respectively, as shown in Fig. 7. The order of emission of the two gamma-rays is unknown.

No direct evidence is available concerning the levels involved in the orbital electron capture process. As in the case of Co^{56} (paper VI), some rather plausible considerations may be applied to this question. Although the theory of beta-decay is probably not in its final form, the main features of the process seem to be sufficiently well understood to make it very unlikely that abundant capture transitions could take place to the ground state or a low excited state without observable emission of high energy positrons. On the other hand, no gamma-rays due to de-excitation of a highly excited state other than the one at 2.3 Mev were observed. Thus it seems very likely that, as in the case of Mn^{52}, electron capture leads predominantly to the same state of Ti^{48} as positron emission. With this assumption, results of Good[5] indicate $\lambda_+/\lambda_{cap.} = 1.38 \pm 0.2$, for transitions to the 2.3-Mev level. If other excited states are involved in the capture process, this value is a lower limit for the branching to the 2.3-Mev state.

DECAY OF Sc^{48}

The negatron decay of Sc^{48} with a half-life of 44 hours also leads to the product nucleus Ti^{48}. Smith[11] reported a maximum energy of 0.644 Mev for the beta-ray spectrum emitted by this activity. Mandeville[12] reported a gamma-ray of 1.35 Mev emitted in the decay of Sc^{48} produced by the reactions $Ti(n, p)$ and $Ca(d, 2n)$. We made a preliminary investigation of the gamma-rays of Sc^{48} produced by deuteron bombardment of calcium. Since the sample showed no observable positron emission after two days, we assume that the scandium fraction, separated chemically, was predominantly Sc^{48}, in agreement with the findings of Mandeville and of Hibdon, Pool, and Kurbatov.[13] Two gamma-rays, of 0.98 and 1.33 Mev were definitely identified. Their energies are the same as those of the gamma-rays from V^{48} to about ± 3 percent. There is a strong possibility of other gamma-rays of lower energy, but the sample proved too weak for a thorough investigation. The disintegration scheme indicated by dotted lines in Fig. 7 is, therefore, probably incomplete and serves only to summarize the known radiations.

A few hours after bombardment, the scandium samples showed a strong gamma-ray of 1.05 Mev quantum energy, probably due to Sc^{43} in agreement with the results of Walke[14] and in disagreement with those of Hibdon, Pool, and Kurbatov.[13]

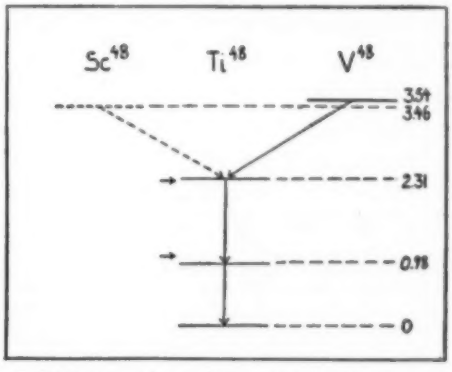

FIG. 7. Disintegration scheme of V^{48}. 58 percent of the disintegrations are by positron emission, the rest by orbital electron capture. The disintegration scheme indicated by the dotted lines is probably incomplete and serves only to summarize the known radiations. Short arrows indicate levels of Ti^{48} found by (α, p) reaction on scandium.

ENERGY LEVELS OF Cr^{52} AND Ti^{48}

The evidence concerning the nuclei Cr^{52} and Ti^{48} presented is incomplete even as far as the possibilities of our present methods are concerned. The disintegration schemes of the 21-minute isomer of Mn^{52}, of V^{52}, and of Sc^{48} should be investigated. Unfortunately the pressure of more essential work prevented the continuation of these studies except for the preliminary observations reported above.

The energy levels of Ti^{48} as found in the decay of V^{48} may be compared with those observed by Pollard[15] in the reaction $Sc^{45}(\alpha, p)Ti^{48}$. In Fig. 7 we have indicated the levels found by Pollard with short arrows. In view of the rather large experimental uncertainty of Pollard's results, all that can be said is that the levels found by the two methods may be identical. In the case of Cr^{52} we may compare our results with those of Dicke and Marshall[16] who observed groups of

[11] G. P. Smith, Phys. Rev. **61**, 578 (1942).
[12] C. E. Mandeville, Phys. Rev. **64**, 147 (1943).
[13] C. T. Hibdon, M. L. Pool, and J. D. Kurbatov, Phys. Rev. **63**, 462 (1943).
[14] H. J. Walke, Phys. Rev. **57**, 163 (1940).
[15] E. Pollard, Phys. Rev. **54**, 411 (1938).
[16] R. H. Dicke and J. Marshall, Jr., Phys. Rev. **63**, 86 (1943).

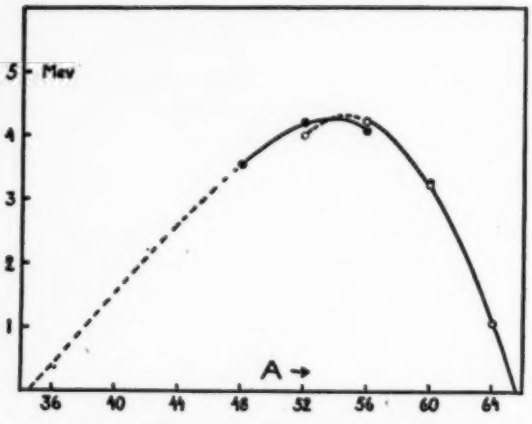

FIG. 8. Disintegration energies of the radioactive neighbors of nuclei with four excess neutrons. Open circles: Negatron emitters. Full circles: Positron emitters. The doubtful decay energy of V^{52} is indicated by a broken circle.

protons scattered inelastically by chromium. Their results are indicated by short arrows in Fig. 4. The agreement with the energies of the levels identified by us is rather less close than in the case of Pollard's results. The evidence favors the assumption that they observed a different set of levels than we did.

Consistent assignments of angular momenta and parity are possible for the decays of Mn^{52} and V^{48}. These assignments are, of course, in no way unique; e.g., the four levels in Cr^{52} might have angular momenta (in order of increasing excitation energy) of 0, 1, 2, and 3 with parity $+, -, -, +$, while the decaying state of Mn^{52} (6.5 day) could be $I=4$, parity $(-)$, similarly in Ti^{48} we might have I values of 0, 1, 2, parity $(+), (-), (+)$, with V^{48} having $I=3$, parity $(-)$.

It is interesting to note that, within the probable error, the gamma-ray energies in the decay of Mn^{52} (6.5 day) are the multiples 3, 4, and 6 of 0.240 Mev. The probability of finding such a combination by chance with an accuracy of two percent and involving no numbers greater than 6 is about one in fifteen. The gamma-rays emitted in the decay of V^{48} are the multiples 3 and 4 of 0.328 Mev. Although these relations are less striking than the one found in Fe^{56} (paper VI), the persistent occurrence of these whole number relationships appears to exceed chance expectance. We wish to call attention to the observations of Wiedenbeck[17] who observed six resonance levels in the nuclear excitation of silver by electrons. The six levels have excitation energies which are the multiples of 3, 4, 5, 6, 7, 8 of 0.392 Mev, with a mean deviation 0.8 percent and a maximum deviation of 1.5 percent which is well within the experimental error. The same author found resonance energies in cadmium which are multiples 3, 4, 5, 6, of 0.420 Mev with the same accuracy as those in silver. In the case of gold he found levels which are the multiples 3, 4, 5, 6, 7 of 0.422 Mev, with comparable accuracy. One should expect that such nuclear absorption spectra will show "series" of levels even more strongly than radioactive decay schemes.

[17] M. L. Wiedenbeck, Phys. Rev. 67, 92 (1945).

ENERGY BALANCE AND MASS DIFFERENCES

From the results presented in this paper we calculate the mass-differences between neutral atoms $Mn^{52}-Cr^{52}=5.10\pm0.15\times10^{-3}$ a.m.u. and $V^{48}-Ti^{48}=4.37\pm0.12\times10^{-3}$ a.m.u. Similarly we find the threshold for the reaction $Cr^{52}(p, n)Mn^{52}$ to be 5.55 ± 0.15 Mev, and that for $Cr^{52}(d, 2n)Mn^{52}$, 7.96 Mev. This takes into account the recoil energy and the mass difference between proton and neutron (1.35×10^{-3} a.m.u.). For the reaction $Ti^{48}(p, n)V^{48}$ we calculate a threshold value of 4.85 ± 0.15 Mev and for $Ti^{48}(d, 2n)V^{48}$ 7.25 Mev.

The calculated value for the proton transmutation threshold of chromium must be compared with the value of 6.2 Mev for the production of the 21-minute isomer, found experimentally by Hemmendinger.[4] The discrepancy is larger than one might expect. It does not seem likely that the two isomers should have an energy difference of almost 0.7 Mev. Possibly selection rules favor the production of the 6.5-day isomer for low proton energies, thus making the apparent threshold for production of the 21-minute isomer higher than the true threshold.

The energy levels identified so far in the nuclei Ti^{48}, Cr^{52}, Fe^{56}, Ni^{60}, and Zn^{64} show no apparent regularity to indicate that these nuclei might be a series of homologues with respect to their level structure. However, if at least the ground states of the sequence of nuclei extending from S^{36} to Zn^{64} show any similar structure, the disintegration energies of their radioactive neighbors should at least show a regular behavior. One or two nuclei in the middle of the sequence

should be its "stablest" member, the disintegration energies of its two radioactive neighbors being about equal. Heavier members of the sequence will tend to have too high a charge for greatest stability so that the disintegration energy of the negatron-emitting neighbor will tend to be less as the mass increases, reaching zero at the end of the stable sequence. On the other hand the disintegration energy of the positron-emitting neighbor should increase as the mass increases. The reverse situation should hold on the low mass side of the "stablest" member of the sequence.

Figure 8 shows a schematic representation of the disintegration energies. It appears that the stablest mass number is 52 or 56. For heavier mass numbers the negatron energies fall off smoothly, reaching zero just beyond the known limit of stability. Less evidence is available concerning the positron-emitters on the light side of the maximum. One might expect their disintegration energies to follow the dotted line shown in Fig. 8. This curve indicates that the positrons emitted by Cl^{36} should be very soft. Also the electron capture process by K^{40} which leads to an excited state of A^{40} at about 2 Mev should have a very low transition energy, so that no positrons could be emitted. This seems to be in agreement with experimental evidence.

Unfortunately no experimental points are available beyond the point of greatest stability. The tentative disintegration scheme for V^{52}, shown in Fig. 7, would indicate a bending-over of the negatron branch, contrary to expectation. Some irregularities in the dependence of the disintegration energy on mass number may be introduced by the fact that the disintegrating state is not necessarily the ground state of the radioactive nucleus. Of the sixteen possible radioactive neighbors of the eight stable nuclei, eleven have been definitely identified.[18] Three of these, Sc^{44}, Mn^{52}, and Co^{60} have been found in two isomeric states. One might expect others to exist in low-lying, relatively long-lived states, and it is not known whether the radioactive states actually observed correspond to the higher or lower member of an isomeric pair.

We wish to thank Professor Robley D. Evans for his continued interest in these studies; Professor M. S. Livingston and the cyclotron crew for making the bombardments; and Professor John W. Irvine, Jr. for help with chemical procedures.

[18] G. T. Seaborg, Rev. Mod. Phys. 16, 1 (1944).

PHYSICAL REVIEW VOLUME 69, NUMBERS 7 AND 8 APRIL 1 AND 15, 1946

Experimental Test of Beta-Ray Theory for the Positron Emitters Na^{22}, V^{48}, Mn^{52}, Co^{58}

WILFRED M. GOOD,* DAVID PEASLEE, AND MARTIN DEUTSCH
Massachusetts Institute of Technology, Cambridge, Massachusetts
(Received December 29, 1945)

The positron branching ratio $\lambda_+/(\lambda_e+\lambda_+)$ has been measured by a coincidence counting method for four isotopes in which radioactive decay involves competition between positron beta-rays and orbital electron capture. The results are $_{11}Na^{22}$: 1.00 ± 0.05, $_{23}V^{48}$: 0.58 ± 0.04, $_{25}Mn^{52}$: 0.35 ± 0.02, $_{27}Co^{58}$: 0.145 ± 0.005. It is shown that these values, as well as the observed shapes of the beta-ray spectra, and the observed lifetimes are in agreement with predictions of the beta-ray theory for nuclear angular momentum changes $\Delta I=0$ or $\Delta I=\pm1$. The type of interaction remains uncertain, as does the parity change, except that the scalar interaction gives consistent results if one assumes the parity change in every case except Mn^{52}.

INTRODUCTION

A NUMBER of attempts have recently been made to refine the theory of beta-decay and to verify it experimentally.[1] In general the conclusion is drawn that the available experimental data can be explained by the Fermi theory which assumes an interaction between the nucleons and the electron-neutrino field depending

* Based in part upon a thesis submitted by Wilfred M. Good to the faculty of the Massachusetts Institute of Technology in partial fulfillment of the requirements for the degree of Doctor of Philosophy in 1944.

[1] E. J. Konopinski, Rev. Mod. Phys. 15, 209 (1943).

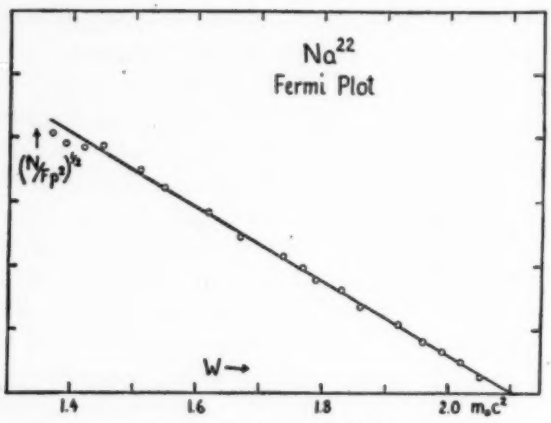

FIG. 1. Positrons of Na^{22}.

only on the position of the particles. It seems preferable, though, to replace the original vector form of the interaction proposed by Fermi by some other form, particularly the tensor form, of combining the wave functions. This has the effect of changing the matrix elements and the energy distribution for particular changes in angular momentum and parity combinations. The behavior of "allowed" transitions is the same for all forms of the Fermi theory. The so-called K-U theory, in which the interaction depends on the derivatives of the wave functions, is ruled out by experiment. The experimental evidence available to test the theory in detail is still inadequate.

Two types of information that are usually considered are the energy distribution of the beta-particles, and the relationship between the half-life and the maximum energy of the particles. Lawsons careful measurement[2] on the beta-ray spectrum of In^{114} has shown excellent agreement with theory in the case of what is undoubtedly an "allowed" transition. This is powerful experimental support for the Fermi theory, but it does not distinguish between the several forms of the interaction. Of the forbidden spectra, only RaE and possibly P^{32} have been studied with sufficient precision to allow comparison with theory. The results, although not conclusive, indicate that either the tensor form or Fermi's original polar vector interaction yields fair agreement.[3]

[2] J. L. Lawson and J. M. Cork, Phys. Rev. **57**, 982 (1940).

[3] E. J. Konopinski and G. E. Uhlenbeck, Phys. Rev. **60**, 308 (1941); Hereafter referred to as K-U II.

There is only one beta-disintegration for which the angular momenta of the initial and final states are known with certainty, namely K^{40}. The disintegrations of Rb^{87}, Lu^{176}, and Be^{10} which are sometimes considered in this connection involve other states besides the ground states of the nuclei concerned, since gamma-rays are emitted. The observed lifetime and maximum beta-ray energy of K^{40} are consistent with either the tensor or the polar-vector interactions, although the tensor interaction seems favored.

In the case of positron emitters there is a third possibility of testing the theory, namely a determination of the relative values of the probabilities of positron emission, λ_+, and orbital electron capture, λ_e. In favorable cases, such an experiment involves a minimum of difficulties and uncertainties of technique. It permits a differentiation between various forms of the theory to about the same extent as a careful measurement of the beta-ray energy distribution. This can be understood qualitatively if we consider positron emission in a formal manner as capture of electrons from negative energy states. Thus we compare the integral of the capture probability for the continuum of electron negative energy states with the integral—or rather the sum—over the discrete bound atomic states. On the other hand a measurement of the beta-ray spectrum compares the probabilities for various intervals of the continuum.

We have measured the ratio, λ_+/λ_e, of the positron emission and electron capture decay constants for four radioactive substances. This quantity together with the total decay constant (half-life), the beta-ray energy distribution, and the maximum positron energy, comprise a set of data for comparison with theory.

The disintegration schemes of the substances discussed in this paper were investigated in this laboratory. Co^{58} has been reported by Deutsch and Elliott,[4] Mn^{52} and V^{48} by Peacock and Deutsch.[5] The results on Na^{22} have not been reported previously. The gamma-ray spectrum of Na^{22} showed only one gamma-ray of 1.30 ± 0.03 Mev energy besides the annihilation radiation.

[4] M. Deutsch and L. G. Elliott, Phys. Rev. **65**, 211 (1944).

[5] W. C. Peacock and M. Deutsch, Phys. Rev. **69**, 306 (1946).

This is in agreement with the result of Oppenheimer and Tomlinson.[6] A Fermi plot of the positron spectrum is shown in Fig. 1. The maximum energy is 0.575 Mev. Coincidence measurements proved that there is one 1.30 Mev gamma-ray accompanying each positron.[7] Details of the methods employed have been published in several papers dealing with the study of disintegration schemes. Figure 2 summarizes the disintegration schemes of the four substances including the branching ratios reported in this paper. It should be mentioned that there is no positive proof for the absence of orbital electron capture transitions of V^{48} to the intermediate excited state of Ti^{48} (such as we have in the case of Mn^{52}) but the absence of high energy positrons is a rather convincing argument.

EXPERIMENTAL METHOD

The method used to determine the ratio λ_+/λ^e of the partial decay constants consists essentially in measuring what fraction of all the gamma-rays emitted is due to annihilation radiation. It has been shown previously that in every case discussed in this paper, except V^{48} and probably for it also, all of the disintegrations, whether by positron emission or by electron capture, lead to the same excited state of the product nucleus. That is, the positron spectra and the "capture spectra" are simple. Therefore we limit our discussion of the method to this case, although it can be extended to more complicated decay schemes.

Consider a sample of the substance under investigation surrounded by enough material to stop all of the positrons in a small space. At some distance from the source there is placed a gamma-ray counter whose efficiency is known as a function of gamma-ray energy. The method for determining this relationship has been discussed elsewhere.[8] Let the efficiency for detecting an annihilation quantum be e_a and the *total* efficiency for detecting the nuclear gamma rays emitted in a disintegration (on the average, if there is gamma-ray branching) be Σe_γ. Let the disintegration rate of the source be N_0 per minute. Then the counting rate will be

$$N = N_0(\Sigma e_\gamma + 2e_a R), \tag{1}$$

where R is the branching ratio for positron decay!

$$R = \lambda_+/(\lambda_e + \lambda_+). \tag{2}$$

The counting rate due to annihilation quanta only is

$$N_a = 2N_0 R e_a. \tag{3}$$

From (1) and (3) we find

$$R = k\Sigma e_\gamma / 2e_a(1-k), \tag{4}$$

where

$$k = N_a/N. \tag{5}$$

To determine k we make use of the fact that the two annihilation quanta are known to be emitted exactly in opposite directions.[9] Thus consider the arrangement shown in Fig. 3 in which the two similar gamma-ray counters are connected to a coincidence circuit and may be placed either in collinear position (A) or at right angles with respect to the source (B). Then, except for some minor corrections which are discussed below, the difference in the coincidence counting rates in the two positions is due entirely to annihilation

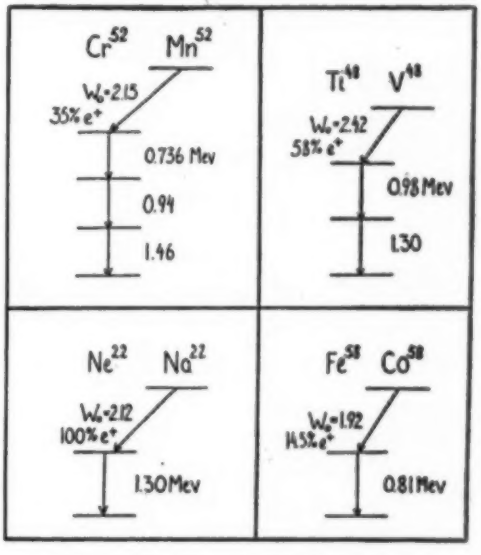

FIG. 2. Disintegration schemes of the substances investigated.

[6] F. Oppenheimer and E. P. Tomlinson, Phys. Rev. **56**, 858 (1939).

[7] Since the first draft of this paper was written, a concordant result has been published by H. Maier-Leibnitz, Zeits. f. Physik **122**, 233 (1944).

[8] A. Roberts, L. G. Elliott, J. R. Downing, W. C. Peacock, and M. Deutsch, Phys. Rev. **64**, 268 (1943).

[9] R. Beringer and C. G. Montgomery, Phys. Rev. **61**, 222 (1942).

quanta. Call this difference the *net* coincidence rate C_a. Then the net coincidence rate per annihilation quantum recorded in one of the counters is

$$C_a/N_a=\eta_a. \tag{6}$$

We call η_a the *intrinsic* efficiency for detecting an annihilation quantum

$$\eta_a=\epsilon_a/\omega, \tag{7}$$

where ω is the solid angle subtended by one of the counters at the source. With a source emitting nuclear gamma-rays as well as annihilation radiation, the net coincidence rate per recorded gamma-ray count (due to either nuclear or annihilation radiation) is

$$C_a/N=k\eta_a, \tag{8}$$

or

$$k=(C_a/N)/\eta_a. \tag{8'}$$

C_a/N is a directly observed quantity. In order to determine η_a directly we need a positron emitter without nuclear gamma-rays so that (8′) reduces to (6). Such a substance is Cu^{64}. We have made a careful search for nuclear gamma-rays of Cu^{64}, using the magnetic lens beta-ray spectrometer and confirm the results of other observers[10] that none are emitted. Thus $k=1$ for Cu^{64} and η_a can be determined directly.

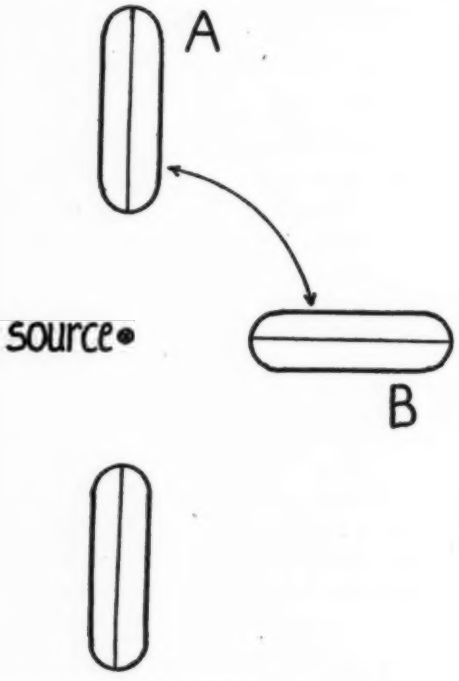

FIG. 3. Arrangement of counters for the determination of the number of positrons.

The gamma-ray counters used in the arrangement in Fig. 3 were seamless copper tubing, 2.50 cm in diameter and 12 cm long, plated with 130 grams of bismuth. These counters were filled with ½ percent water vapor and helium to atmospheric pressure. Figure 4 shows η_a as a function of the distance between source and front end of the cathode. The variation can be readily interpreted by considering the angle of incidence of the gamma-rays on the cathode. The distance actually used in these experiments was 11 cm. The dependence of ϵ_γ on energy for these counters and this geometry was found by comparison with the standard Pt counters used in this laboratory[8] and is shown in Fig. 5. A small correction for absorption in the source was applied where necessary.

As mentioned above, certain small corrections must be applied in determining the net coincidence rate C_a. In general we have four causes for coincidences in position A: (1) Annihilation pairs of quanta, (2) coincidences of nuclear gamma-rays with each other or with annihilation quanta, (3) cosmic-ray coincidences, (4) chance coincidences.

In position B coincidences occur due to all but the first of these causes. The rate of chance coincidences is certainly unaffected by the position. The cosmic-ray coincidence rate is slightly higher in position B, but this effect was made negligible by the strength of the sources used. Effect (2) is expected to be independent of position according to all reliable experimental evidence available. Even if there should be an angular correlation of nuclear gamma-rays the effect on our experiment can be made negligible by making the source-counter distance large enough, i.e., by making the ratio $\eta_a/\Sigma\epsilon_\gamma$ sufficiently large. The cosmic-ray coincidence rate is also reduced by this procedure. Thus it is advantageous to make the distance between source and counters as large as possible with reasonable source strength. A typical set of results, for Co^{58} is shown in Table I.

[10] A. W. Tyler, Phys. Rev. 56, 135 (1939).

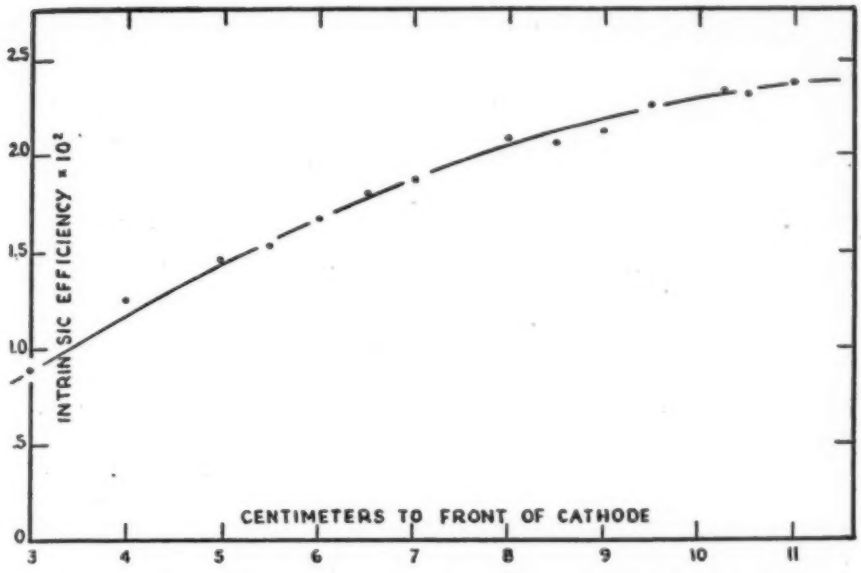

FIG. 4. Intrinsic efficiency of the gamma-ray counters for annihilation radiation *vs.* distance from source.

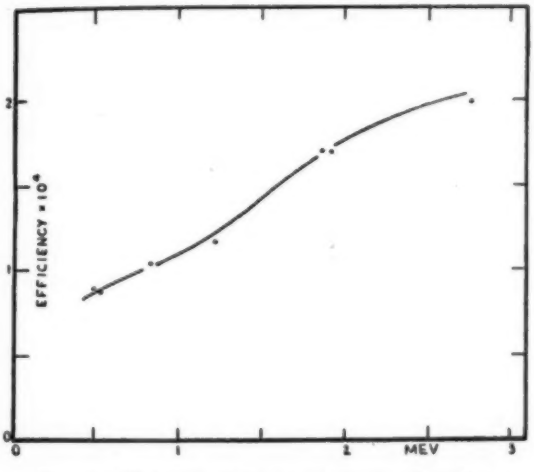

FIG. 5. Efficiency of the counters as a function of gamma-ray energy.

EXPERIMENTAL RESULTS

In Table II we summarize the experimental results for the partial decay constants. In the last two columns we give the total decay constants and the disintegration energies including the rest energy of the positron. The Fermi plot for Na^{22} is given in Fig. 1 and the Fermi plots for V^{48}, Mn^{52}, Co^{58} are given in references 4 and 5.

COMPARISON WITH THEORY

For our purpose the tensor formulation of the Fermi theory as given in K-U II[3] seems better suited than e.g., the spherical harmonic formulation of Marshak.[11] We shall follow the notation of K-U II except where otherwise indicated, and the reader is referred to that paper for the meaning of symbols, selection rules, etc. In this notation one writes for the emission probability of a positron with momentum p, due to any one matrix element M (with the appropriate selection rules)

$$P(p)dp = |M|^2(G^2/2\pi^3)C(-Z') \times F(-Z', p)p^2K^2dp, \quad (9)$$

where Z' is the atomic number of the *product* nucleus, F is the "Fermi function," C the appropriate "correction factor," and G is a universal constant. The total decay probability by positron emission is then

$$\lambda_+ = |M|^2(G^2/2\pi^3)B_+, \quad (10)$$

$$B_+ = \int_0^{p_0} C(-Z')F(-Z', p)p^2K^2dp, \quad (10')$$

where $p_0 = (W_0^2 - 1)^{\frac{1}{2}}$ is the maximum momentum of the particles and $K = (W_0 - W)$ is the neutrino energy. The correction factors C are given in K-U II, except for the inclusion of the matrix element $|M|^2$ which we write as a separate factor in (9) and (10).

[11] R. E. Marshak, Phys. Rev. 61, 431 (1942).

TABLE I. Typical experimental values.

Net counting rate A	1660± 30 counts per minute
Net counting rate B	1690± 30 counts per minute
Coincidence rate A	8.50±.24 counts per minute
Coincidence rate B	0.42±.02 counts per minute
Chance coincidences	0.29±.03 counts per minute
Cosmic-ray pos. A	<0.05 counts per minute
Cosmic-ray pos. B	<0.06 counts per minute

We can write similar formulas for orbital electron capture[12]

$$\lambda_c = |M|^2(G^2/2\pi^3)B_c, \tag{11}$$

where M and G have the same values as in (10) for the same transition

$$B_c = (\pi/2)(W_0+W_n)^2\Sigma_n(N_n/2n^2)C^{(n)}(Z_n)F_c, \tag{11'}$$

$$F_c = (1/2)(2\alpha Z_n)^{3-(\alpha Z_n)^2}\rho^{-(\alpha Z_n)^2}\exp(-2\alpha Z_n\rho). \tag{12}$$

B_c represents a summation over the various shells with radial quantum numbers n. N_n is the number of electrons actually present in the nth shell. The summation over the various subshells with orbital angular momentum quantum numbers l is made by the correction factors $C^{(n)}$ which have the same form as those for the continuous spectrum given by K-U II, except that the neutrino energy K now has the value (W_0+W_n) and the radial wave functions of the bound atomic electrons are used instead of those for the continuum. Thus

$$L_l^{(n)} = (F_c)^{-1}\frac{g_l^{(n)^2}+f_{-l-2}^{(n)^2}}{\rho^{2l}}, \tag{13a}$$

$$M_l^{(n)} = (F_c)^{-1}\frac{f_l^{(n)^2}+g_{-l-2}^{(n)^2}}{\rho^{2l+2}}, \tag{13b}$$

$$N_l^{(n)} = (F_c)^{-1}\frac{f_l^{(n)}g_l^{(n)}+f_{-l-2}^{(n)}g_{-l-2}^{(n)}}{\rho^{2l+1}}. \tag{13c}$$

$\rho = 0.0038A^{\frac{1}{3}}$ is the nuclear radius. Z_n is the effective charge of the *initial* nucleus for the nth shell: $Z_K = Z-0.30$, $Z_L = Z-4.15$, etc.[13] $W_n = [1-(\alpha Z_n/n)^2/2]$. If the capture probabilities for the separate shells or subshells are wanted, only the terms involving the corresponding wave functions should be included in Eqs. (11) and (13). These wave functions in approximation good to terms of the order $(\alpha Z)^2$ have the following values at the surface of the nucleus.[14] For the shells K, $L_{\rm I}$, $L_{\rm III}$, $M_{\rm I}$, $M_{\rm III}$, $M_{\rm V}$, etc.

$$\frac{g_l^{(n)^2}}{\rho^{2l}} = \frac{(n+l)!}{2n(n-l-1)![(2l+1)!]^2} \times (2\alpha Z_n/n)^{2l+3-(\alpha Z_n)^2/l+1}\rho^{-(\alpha Z_n)^2/l+1} \times \exp(-2\alpha Z_n\rho/n), \tag{14a}$$

$$\frac{f_l^{(n)^2}}{\rho^{2l+2}} = (\alpha Z_n/2\rho)^2(1/l+1)^2\frac{g_l^{(n)^2}}{\rho^{2l}} \tag{14b}$$

and for the shells $L_{\rm II}$, $M_{\rm II}$, $M_{\rm IV}$, etc.

$$\frac{f_{-l-2}^{(n)^2}}{\rho^{2l}} = \rho^2\frac{n^2-(l+1)^2}{n^2}\frac{f_l^{(n)^2}}{\rho^{2l+2}}, \tag{14c}$$

$$\frac{g_{-l-2}^{(n)^2}}{\rho^{2l+2}} = [(\alpha Z_n/2l)^2+2(\alpha Z_n/2\rho)]\frac{f_{-l-2}^{(n)^2}}{\rho^{2l}}. \tag{14d}$$

In most cases up to second forbidden transitions the single term with $n=1$ (K-capture) contributes over 90 percent of the total capture probability unless the transition energy is very low.

In Table III we have collected the values of B_+ and B_e calculated from Eqs. (10') and (11') for the four transitions investigated, and for the matrix elements of interest. Since the factors multiplying the integral or sum represented by B are the same in Eqs. (10) and (11), the ratio $B_+/(B_e+B_+)$ can be compared directly with the corresponding value of $\lambda_+/(\lambda_e+\lambda_+)$ in Table II. Keeping in mind the selection rules for the various matrix elements, as given in K-U II, it appears immediately that only for transitions with changes in the nuclear angular momentum of $\Delta I=0$ or $\Delta I=\pm 1$ does the theory predict a ratio of the partial decay constants reasonably close to the observed value. The "allowed" term

TABLE II. Experimental partial decay constants.

Nucleus	$\Sigma\epsilon_\gamma/\epsilon_0$	k	$\lambda_+/(\lambda_e+\lambda_+)$	$\lambda_e+\lambda_+$	W_0
Na^{22}	1.54	0.570	1.00 ±0.05	8.7×10^7 sec.$^{-1}$	2.12 mc^2
V^{48}	2.86	0.289	0.58 ±0.04	1.4×10^8 sec.$^{-1}$	2.42 mc^2
Mn^{52}	4.08	0.146	0.35 ±0.02	5.6×10^5 sec.$^{-1}$	2.15 mc^2
Co^{58}	1.18	0.202	0.145±0.005	5.6×10^6 sec.$^{-1}$	1.92 mc^2

[12] After these calculations were completed it came to our attention that a similar treatment was given by E. Greuling, Thesis Indiana University, 1942.

[13] E. Greuling, Phys. Rev. **61**, 568 (1942).

[14] E. L. Hill and R. Landshoff, Rev. Mod. Phys. **10**, 106 (1938).

TABLE III. Types of spectra and values of the theoretical qualities B_+, B_c for different interactions and matrix elements.

Interaction	Matrix elements	Na^{22} B_+	Na^{22} B_c	Na^{22} $\frac{B_+}{B_+ + B_c}$	V^{48} B_+	V^{48} B_c	V^{48} $\frac{B_+}{B_+ + B_c}$	Mn^{52} B_+	Mn^{52} B_c	Mn^{52} $\frac{B_+}{B_+ + B_c}$	Co^{58} B_+	Co^{58} B_c	Co^{58} $\frac{B_+}{B_+ + B_c}$	Spectrum Fig. 6
Tensor Scalar Vector Axial v.	$\int\sigma$, $\int\alpha$ $\int 1$ $\int 1$, $\int\alpha$ $\int\sigma$, $\int\gamma_5$	0.37	0.0295	0.93	0.54	0.43	0.56	0.205	0.36	0.36	0.075	0.410	0.155	*b*
Tensor	$\int\sigma\cdot r$, $\int\alpha\cdot r$	4.67	0.70	0.87	19.5	24.0	0.45	6.75	17.8	0.28	3.30	26.1	0.112	*a*
Tensor	$\int\sigma\times r$	3.50	0.262	0.94	16.0	11.3	0.59	5.7	9.0	0.39	2.92	15.2	0.161	*b*
Scalar	$\int r$				19.8	25.2	0.44	6.90	18.5	0.27				*a*
Vector	$\int r$				16.3	12.2	0.57	5.95	9.6	0.38				*b*
Axial v.	$\int\sigma\cdot r$				16.0	11.1	0.59	5.7	8.8	0.39				*b*
Axial v. Vector	$\int\sigma\times r$ $\int\alpha\times r$				19.6	24.2	0.45	6.8	18.0	0.27				*a*
Tensor Vector	ΣB_{ij}, ΣA_{ij} ΣA_{ij}	0.05	0.025	0.67	0.11	0.42	0.21	0.031	0.29	0.097	0.008	0.27	0.029	*c*
Axial v.	ΣB_{ij}													
Tensor	ΣT_{ij}							0.5	8.5	0.055				*c*
Tensor	ΣS_{ijk}							7×10^{-4}	0.03	0.022				*d*

—identical of all interactions—yields theoretical ratios in satisfactory agreement with observation in all cases investigated. However, as we shall see presently, there is strong evidence from the lifetimes that at least some of the transitions considered are "forbidden."

In the last column of Table III we indicate the theoretically predicted shape of the positron spectrum as calculated from Eq. (9). The letters refer to the curves in Fig. 6 which show the Fermi plots predicted by theory for transitions of Mn^{52} involving various matrix elements. This method of presenting the theoretical spectra, i.e., a plot of $(CK^2)^{\frac{1}{2}}$ *vs.* W has the advantage of being readily compared with the experimental results as they are usually shown. The trend of the predicted spectra for the other transitions is very similar to that for Mn^{52}. Matrix elements marked with the same letter in the last column of Table III do not necessarily give rise to identical spectra but rather the predicted distributions are indistinguishable by present techniques. The observed spectra as shown in Fig. 1 and references 4 and 5 are definitely of type *b* except possibly in the case of Co^{58} where the experimental uncertainty is too great to allow a distinction between types *a* and *b*. This again shows that transitions with $\Delta I=\pm 2$ or more are excluded. Furthermore the single "first forbidden" term $\int r$ of the scalar interaction predicts too small a relative probability of positron emission and a spectrum of type *a* and is therefore excluded by experiment. All other interactions involve several terms in the first forbidden approximation and by proper adjustment of the several matrix elements agreement with experiment can be obtained for transitions with $\Delta I=0$ or $\Delta I=\pm 1$. Since other evidence[1] seems to favor the tensor interaction it is of particular interest to see whether a reasonable estimate of the several matrix elements yields the observed ratio of the partial decay constants and the observed shape of the spectrum. For $0\rightarrow 0$ transitions to which only the matrix element $\int\sigma\cdot r$ contributes, the predicted relative probability of positron emission is too small in all cases. For other transitions with $\Delta I=0$ we have a combination of four matrix elements. Greuling[13] has made an estimate of the magnitudes of these matrix elements. For three of them he finds $|\int\sigma\cdot r|^2 \approx|\int\sigma\times r|^2\approx|\Sigma B_{ij}|^2\approx 2\rho^2$. The magnitude of $|\int\alpha|^2$ is rather more uncertain. It appears that it should be about ten times as large as the others. Using these estimates we can calculate the

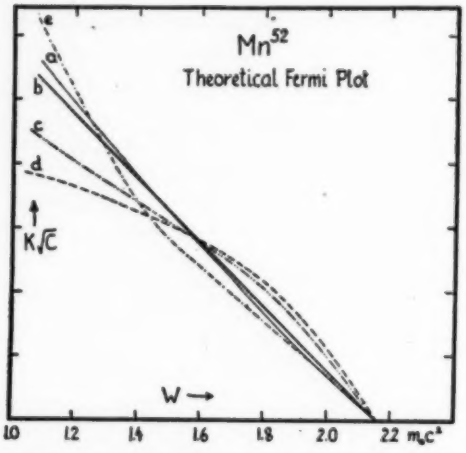

FIG. 6. Fermi plots predicted by theory. See Table III.

predicted ratio $\lambda_+/(\lambda_e+\lambda_+)$ by summing, respectively, the four terms $|M|^2B_+$ and $|M|^2B_e$. These sums should be proportional to the λ's. For $\Delta I=\pm 1$ only three matrix elements $\int a$, $\int \sigma \times r$, and ΣB_{ij} contribute to the decay probability. In Table IV we summarize the predicted values of $\lambda_+/(\lambda_e+\lambda_+)$, together with the observed values. It will be seen that the values for $\Delta I=\pm 1$ are, generally, in better agreement with experiment than those for $\Delta I=0$. The predicted spectra, in both cases are of type *b*. We can use Greuling's estimates of the matrix elements to calculate the predicted lifetimes for $\Delta I=0$ or $\Delta I=\pm 1$. For this it is necessary to make some assumptions concerning the lifetime for allowed transitions, for which the matrix element is conventionally taken as unity. Equations (10) and (11) apply strictly only to transitions within the same supermultiplet, i.e., practically only to very light elements because of the greater complexity of heavy particle states in heavier nuclei. We shall, therefore, follow the empirical approach of Konopinski[1] which essentially replaces $(G^2/2\pi^3)$ in Eqs. (10) and (11) by a different constant for each region of the periodic table, determined by the half-lives of the most nearly "allowed" transitions in that region. In Table IV we summarize the predicted half-lives, obtained by this

TABLE IV. Observed and calculated values of half-lives and positron branching ratios for the tensor interaction.

	Calculated					
	Allowed	First forbidden $\Delta I=0$	First forbidden $\Delta I=\pm 1$	First forbidden $\Delta I=\pm 2$	Observed	
Na^{22}	0.93	0.90	0.93	0.67	1.00 ±0.05	$\lambda_+/(\lambda_e+\lambda_+)$
V^{48}	0.56	0.51	0.575	0.21	0.58 ±0.04	
Mn^{52}	0.36	0.32	0.375	0.097	0.35 ±0.02	
Co^{58}	0.155	0.133	0.158	0.029	0.145 ±0.005	
Na^{22}	2.5 hr.	20 d.	30 d.	30 yr.	3 yr.	Half-life
V^{48}	14 hr.	35 d.	70 d.	10 yr.	16 d.	
Mn^{52}	1 d.	70 d.	130 d.	25 yr.	6.5 d.	
Co^{58}	1 d.	40 d.	70 d.	23 yr.	65 d.	

method, together with the observed values. Mn^{52} is probably an allowed transition because it is easier to understand that the lifetime belengthened by unfavorable heavy particle wave functions than that it be shortened by a factor of ten compared with expectation. V^{48} and Co^{58} may well be first forbidden transitions (i.e., parity change) with $\Delta I=\pm 1$. Since the evidence of partial decay constants and positron energy distribution excludes $\Delta I=2$ for Na^{22} we must assume that ΔI is 0 or ± 1 with particularly unfavorable nuclear configurations. It is true, of course, that by admitting a reduction of the decay probability by a factor of 30 in the case of Na^{22}, we also admit the possibility that all of the other three transitions may be allowed, with unfavorable heavy particle configurations.

We may summarize the evidence by stating that the angular momentum change in all four transitions appears to be one or zero. The form of the interaction and the parity change are not certain.

It is obvious that more, highly forbidden transitions should be studied with a view to deciding between the several forms of interaction. A program of such studies was interrupted by the pressure of war work which also delayed publication of these results.

It is a pleasure to acknowledge the interest and encouragement of Professor Robley D. Evans and the cooperation of the members of the Radioactivity Center and the cyclotron crew.

PHYSICAL REVIEW VOLUME 69, NUMBERS 7 AND 8 APRIL 1 AND 15, 1946

The Origin of Large Cosmic-Ray Bursts

R. E. LAPP
Ryerson Physical Laboratory, University of Chicago, Chicago, Illinois
(Received November 30, 1945)

Integral size-frequency distribution curves for cosmic-ray bursts of more than 100 particles were obtained by using an ionization chamber shielded by 1.25, 12, and 35 cm of iron. These distribution curves can all be represented by an inverse power law with exponent $=2.0\pm0.2$. The transition curve plotted from these data shows a pronounced maximum. Five G-M counter coincidence sets were arranged to register on the ionization chamber trace so that coincidences between bursts and air showers could be measured. For a thickness of 1.25 cm of iron, about 85 percent of the bursts were coincident with air showers, while for 12 cm of iron, this fraction was about 20 percent and for 35 cm of iron, only 5 percent of the bursts were observed to be coincident with extensive showers. A discussion is given to account for the origin of the bursts which were not coincident with air showers. For the analysis of the transition curve three different types of bursts are considered: bursts due to extensive atmospheric showers, bursts produced by narrow air showers or single high energy electrons, and bursts produced by mesotrons (knock-on and bremsstrahlung processes). Data for bursts of more than 500 particles under 12 cm of lead are compared with the corresponding data obtained under 35 cm of iron in order to determine the dependence of burst frequency on atomic number; the results are in substantial agreement with production of these bursts by bremsstrahlung of the mesotron. Integral size-frequency distribution curves are also plotted for data obtained during a five-year period at Huancayo (3350-meters elevation) and at Cheltenham (72 meters) for bursts under 12 cm of lead. The Cheltenham data are compared with the theoretical calculations of Christy and Kusaka for burst production by mesotrons of spin 0, ½, and 1 and it is concluded that either the spin 0 or the spin ½ curve fits the experimental data but the evidence definitely excludes spin 1. The altitude dependence for burst under 12 cm of lead shows that the ratio of the burst frequencies at Huancayo and Cheltenham is constant for bursts up to 2400 particles, but increases sharply for still larger bursts. This increase is discussed on the basis that bursts under thick shields at higher altitudes may be caused either by extensive showers or by possible spin 1 mesotrons having so short a mean life that most of them fail to reach sea level.

INTRODUCTION

As early as 1938 several investigators[1] pointed out that large cosmic-ray bursts which occur under thick shields are associated with the mesotron component of cosmic rays. Indeed, Christy and Kusaka[2] were able to demonstrate that the burst data of Schein and Gill[3] were in substantial agreement with the theoretical calculations which they carried out for burst production for mesotrons of spin 0. For comparison with such theoretical calculations it is essential that burst data be obtained with an ionization chamber and shield of the proper geometry. A spherical ionization chamber surrounded by a uniform spherical shield of sufficient thickness to exclude all but the mesotron initiated bursts is an excellent geometrical arrangement. With a cylindrical chamber, however, comparison of experimental data with calculation is very difficult for the number of particles observed in each burst will depend on the angle at which the particles intercept the chamber. Furthermore, if flat layers of shielding material are placed above the chamber, the effect of scattering of the burst particles in this absorber is also very difficult to calculate. For experiments concerned with burst production by mesotrons, a shield that uniformly surrounds the chamber on all sides is necessary since the mesotrons which can initiate large[4] bursts are essentially isotropically distributed with respect to the zenith angle.

The importance of obtaining reliable burst data under thick[5] shields lies in the fact that, at present, this is the most feasible method by which the electromagnetic interaction of high energy mesotrons with nuclei and electrons can be studied. In particular, such burst data constitute the only experimental evidence that the majority

[1] H. Euler, Naturwiss. 26, 382 (1938); H. Euler and W. Heisenberg, Ergeb. exakt. Naturwiss. 17, 1 (1938); M. Schein and P. S. Gill, Phys. Rev. 55, 1111 (1939).
[2] R. F. Christy and S. Kusaka, Phys. Rev. 59, 414 (1941).
[3] M. Schein and P. S. Gill, Rev. Mod. Phys. 11, 267 (1939).
[4] In this paper only large cosmic-ray bursts are considered and these are arbitrarily taken as bursts containing more than 100 particles as measured in a spherical ionization chamber of 35-cm diameter.
[5] By a thick shield, it is meant a shield of thickness sufficient to assure that the majority of the bursts observed under it are produced by mesotrons. This corresponds to a thickness of about 20 radiation units at sea level.

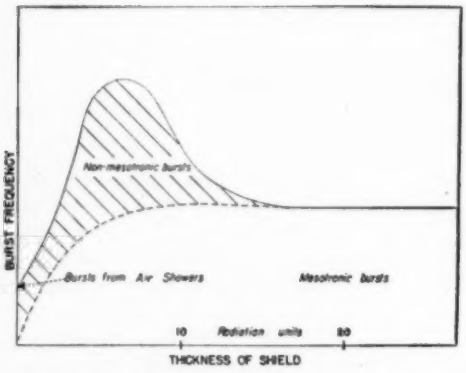

FIG. 1. Schematic curve representing a typical transition curve in which the relative burst frequency (in arbitrary units) is plotted against the thickness of the absorbing shield which surrounds the ionization chamber.

of the very large bursts under thick shields are initiated by the bremsstrahlung of a mesotron in the electromagnetic field of a nucleus. At energies above 10^{10} ev, this radiation process (bremsstrahlung) of the mesotron predominates over the close collision (knock-on process) of a mesotron with an electron. For both the bremsstrahlung and the knock-on process the forces which act are strongly spin-dependent, hence comparison of burst data with the theoretical results for burst production by mesotrons may yield an experimental determination of the spin of the mesotron. Such a comparison was first made by Christy and Kusaka[2] who compared the results of their calculations with the burst data[3] obtained under a 12-cm lead shield at sea level. Because of the fact that bursts produced by the bremsstrahlung of the mesotron are actually photon initiated showers localized in the shield surrounding the ionization chamber, then in accordance with the cascade theory for such showers, the observed bursts should depend upon the square of the atomic number of the shielding material. In the present experiments, the dependence of the bursts upon atomic number was investigated by comparing the bursts under 35 cm of iron with the 12-cm lead burst data of Schein and Gill[3] as well as with more recent data discussed in this paper.

Since practically all the large bursts observed at sea level under thick shields are due to mesotrons of energy greater than 10^{10} ev, there should be no altitude dependence for such bursts if bursts under thick shields at higher altitudes have the same origin as those at sea level. The reason for this is that the mesotrons above 10^{10} ev having a lifetime of a 10^{-6} second undergo negligible decrease in intensity in traversing the atmosphere. However, it is well known[3] that bursts under thick shields show a marked altitude dependence. For example, the number of bursts of more than 200 particles observed under 12 cm of lead at Huancayo, Peru (elevation 3350 meters) is 4.5 times greater than the number of bursts observed at sea level under the same experimental conditions. Thus one is led to the conclusion that there is present at higher altitudes a burst producing radiation which does not exist with measurable intensity at sea level. The fact that this radiation is so strongly absorbed in the atmosphere between Huancayo and sea level suggests that it may be associated with the high energy soft component of cosmic-rays. The theory of cascade showers initiated by primary electrons predicts that the extensive atmospheric showers[6] should have a broad region which contains a high density of energetic electrons and photons. Recently, it was shown[7] that at sea level such atmospheric showers actually possess a region (core) of sufficiently high particle density to record as a burst of more than 100 particles in an unshielded ionization chamber of 995-sq. cm cross-sectional area. More recently,[8] it has been found that even when the ionization chamber was shielded with as much as 12 cm of lead, about 5 percent of the total bursts were observed to be coincident with a high density core of an atmospheric shower. This result is in agreement with the hypothesis that a few of the most energetic air showers may contain particles of energy sufficient to multiply under 12 cm of lead.

It is well known that if one varies from 0 to 20 radiation units the thickness of the shielding material around an ionization chamber at sea level, the burst frequency first increases from an initial finite value, then passes through a maximum, and finally attains a fairly constant value which is independent of any further increase in the thickness of the shield. Such a generalized

[6] P. Auger, R. Maze, and T. Grivet-Meyer, Comptes rendus **206**, 1721 (1938); W. Kolhorster, J. Matthes, and E. Weber, Naturwiss. **26**, 576 (1938); P. Auger and R. Maze, Comptes rendus **207**, 228 (1938); P. Auger, R. Maze, P. Ehrenfest, Jr., and A. Freon, J. de phys. et rad. **10**, 39 (1939).

[7] R. E. Lapp, Phys. Rev. **64**, 129 (1943).

[8] R. E. Lapp, Phys. Rev. **64**, 254 (1943).

transition curve for large bursts is shown in Fig. 1. In order to facilitate the discussion of the origin of bursts under different thicknesses of shielding, three critical values of the thickness will be considered and the bursts corresponding to those measured under these thicknesses are designated as:

(a) t_0-bursts—those bursts observed in an unshielded chamber with negligible heavy material in the vicinity.

(b) t_m-bursts—the bursts measured under a thickness of shield that gives the maximum burst frequency.

(c) t_μ-bursts—those found under thick shields. (This thickness will have to be larger for higher altitudes in order to exclude those bursts originating from very energetic atmospheric showers.)

Three different explanations were offered to account for the origin of the t_0-bursts. It was first[9] suggested that these bursts could be produced by extremely large fluctuations in the cascade multiplication of an incident electron or photon. Second, Heisenberg[10] proposed that these bursts might be created by a new type of multiple process, the so-called explosion shower. Finally, it was suggested that a large number of particles might be simultaneously incident upon an ionization chamber, giving rise to a burst in the chamber. Very recently,[7] however, it was directly demonstrated that the t_0-bursts were coincident with the high density core of an atmospheric shower as measured by the simultaneous coincidence of several G-M counter sets. This definitely proved that the last of the three suggestions is the correct one.

Thus, it is now established that the t_0- and t_μ-bursts are of entirely different origin at sea level, the t_0-bursts being produced by a core of an atmospheric shower and the t_μ-bursts being created by high energy single mesotrons. One would then think that the t_m-bursts would be of a complex nature, containing a mixture of t_0- and t_μ-bursts with bursts of other (unknown) origin not being excluded.

[9] D. K. Froman and J. C. Stearns, Rev. Mod. Phys. **10**, 133 (1938).

[10] W. Heisenberg, Zeits. f. Physik **113**, 61 (1939).

APPARATUS

The ionization chamber used for the following experiments was a Carnegie model C meter which has been described elsewhere.[11] It will suffice to mention here that the chamber is a steel sphere of 17.5-cm inside radius with walls 1.25 cm thick. It is filled with very pure argon to a pressure of 50 atmospheres. As it is usually used, the chamber is mounted within a 3-mm walled spherical shell which is then filled with lead shot so that there is an equivalent of 12 cm of lead around the chamber. By means of a small auxiliary ionization chamber located within the main chamber, the ionization current due to cosmic radiation is compensated so that only the variations in the ionization due to cosmic rays are registered. A Lindemann electrometer was used to measure the ionization current and the image of the electrometer needle was focused upon a continuously moving strip of photographic paper. For the present experiments, the collecting electrode system of the chamber was automatically grounded every 15 minutes and once every hour a voltage of 0.40 volt was applied to the electrometer needle in order to check the sensitivity of the instrument. A synchronous clock drive fed the photographic paper through the recording camera at a rate of 8 cm/hr. and for convenience a time reference mark was registered on the paper every 6 hours.

A very simple system was devised to register coincidences of G-M counter sets on the same

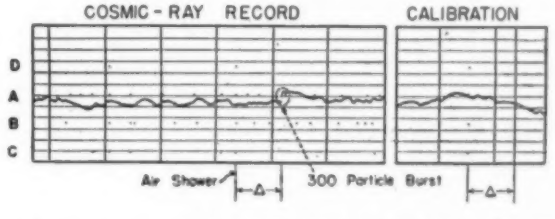

FIG. 2. A representative portion of the cosmic-ray ionization trace is shown. The distance between each of the vertical lines represents a time interval of 15 minutes. As explained in the text, each spot appearing on the record represents a coincidence of a G-M counter set, *A*, *B*, *C*, or *D*. These spots are off-set from the instantaneous ionization trace by an amount (Δ) which is determined by the calibration shown in the second frame from the right on the above record. In the fifth frame from the left a 300-particle burst is shown coincident with an extensive air shower.

[11] A. H. Compton, E. O. Wollan, and R. D. Bennett, Rev. Sci. Inst. **5**, 415 (1934).

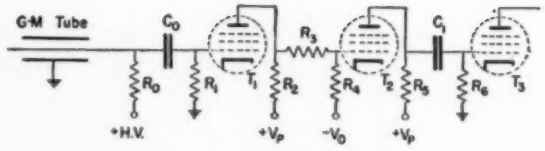

FIG. 3. The general principle of the twofold coincidence circuit is illustrated; only 1 arm of the circuit is shown since the other is identical and both arms are joined together by putting the last tubes in parallel in the usual manner. Circuit constants are: (resistances in megohms, condensers in micro-micro-farads)

$R_0=R_1=0.5 \quad R_2=R_4=R_5=0.1 \quad R_3=0.075 \quad R_6=0.010$

Plate resistor of tube $T_3=0.2$ (not shown above)

$C_0=100 \quad C_1=10$

T_1, T_2, T_3=1LD5, 6SJ7, or 7C7

Typical operating conditions: $V_p=150$ volts, $V_{Screen}=100$ volts, V_0 adjusted to give a grid potential on T_2 in the range of from -3 to -5 volts.

record as that on which the ionization trace was registered. Five pre-focused Mazda lamps were so mounted on the camera back that each lamp was focused onto a 0.007-inch aperture in a brass plate that rested against the back of the photographic paper in the camera. There was sufficient light intensity from this source so that when the lamps were flashed at rated voltage for $\frac{1}{10}$ of a second, a small spot was recorded on the photographic paper. Because of the design of the camera mechanism, it was not practical to locate the lamp apertures exactly at the point where the ionization trace was recorded; instead, the apertures were displaced $\frac{1}{2}$ inch from this point. To determine accurately this displacement Δ, the system was calibrated by simultaneously flashing all the lamps and interrupting the electrometer lamp circuit momentarily. This process is illustrated in Fig. 2 where an actual ionization record is shown. In the actual process of determining whether a burst were coincident with any of the G-M coincidences, it was found that the bursts and atmospheres showers were both so infrequent that it was relatively easy to detect the coincidences. It should be pointed out that the present arrangement for registering coincidences of G-M counter sets has distinct advantages for the investigation of atmospheric showers, for one can see at once for any given shower just how many and which G-M counter sets are triggered by the shower.

The twofold coincidence circuit used in these experiments has a resolving power of 1.2 microseconds and with the G-M counter tubes that were used only one chance coincidence would occur every two hours. The circuit is given in Fig. 3 where it is seen that it is a three-stage amplifier with pure resistance coupling between the first and second stages. The low resolving time is attained by suitable choice of circuit constants between the second and third stage. The three-, four-, and fivefold circuits were of the usual design and in each circuit a sensitive relay in the plate circuit of the power output tube activated a micro-switch which in turn completed a lamp circuit in the camera back.

t_μ-BURSTS[12]

The t_μ-bursts were measured under a 35-cm iron shield,[13] the details of which have already been given.[8] The upper iron hemisphere was such that it presented a traversal distance of 35 cm for mesotrons which were radially incident upon the chamber. For most of the experiments, the apparatus was located on the top floor (greenhouse) of the Botany building on the campus of the University of Chicago. There was no heavy material above or to the side of the ionization chamber.

The data obtained during a time interval of 1754 hours are presented in Table I. Here the cumulative burst frequency (cm^{-2} $sec.^{-1}$) is given for different burst sizes[14] (S). To obtain the burst frequency given in column 4 of Table I, the total number of bursts greater than a certain size (S) was divided by the product of the total elapsed

TABLE I. Integral number of bursts (cm^{-2} $sec.^{-1}$) with more than S particles produced in 35 cm of iron.

Burst size (in mm)	Burst size (S) (No. of particles)	Integral number of bursts (1754 hr.)	Burst frequency (cm^{-2} $sec.^{-1}$)
1.0– 2.0	100	372	$6.16\cdot10^{-8}$
2.0– 3.0	200	152	$2.52\cdot10^{-8}$
3.0– 4.0	300	78	$1.29\cdot10^{-8}$
4.0– 5.0	400	49	$8.12\cdot10^{-9}$
5.0– 6.0	500	42	$6.42\cdot10^{-9}$
6.0– 7.0	600	25	$4.14\cdot10^{-9}$
7.0– 8.0	700	18	$2.98\cdot10^{-9}$
8.0– 9.0	800	14	$2.32\cdot10^{-9}$
9.0–10.0	900	11	$1.82\cdot10^{-9}$
>10	>1000	5	$8.29\cdot10^{-10}$

[12] Both Dr. R. F. Christy and Dr. S. Kusaka were very generous in discussing the results of this experiment with the writer.

[13] The author acknowledges the cooperation of Dr. W. P. Jesse in making the iron shield available for this experiment.

[14] Unless otherwise specified, the burst size refers to the number of particles contained in the burst.

time (in seconds) multiplied by the cross-sectional area of the chamber (995 cm²). Schein and Gill[8] have given the procedure for determining the number of particles in bursts for the type of ionization chamber used here. For the 35-cm iron experiment, the electrometer sensitivity was such that a 1-mm deflection corresponded to a burst of 100 particles. Before considering in detail the results given in Table I, it is necessary to proceed to a discussion of the relation of air showers to t_μ-bursts.

1. Relation to Air Showers

To detect any atmospheric showers which might be coincident with the t_μ-bursts, two sets of twofold coincidence arrangements of G-M counters were used. These G-M counters were placed on light wooden racks suspended over the ionization chamber. Each counter had an effective surface of 100 cm² and they were separated by distances of from 2 to 10 meters. As has already been reported,[15] the coincidence experiments for the t_μ-bursts showed that they were not coincident with extensive air showers within the accuracy of the experiment. However, more recent experiments[16] carried out with an equivalent thickness of 20 radiation units of lead around the ionization chamber showed that approximately 5 percent of the total bursts were coincident with air showers. There are two definite conclusions to be drawn from this result:

First, since the number of energetic air showers which could produce more than 100 particles below 20 radiation units is certainly small compared with the total number of the energetic air showers which are incident upon the chamber, one can conclude that most of these air showers at sea level do not contain particles of energy sufficient to traverse 20 radiation units of material. This is equivalent to stating that the cores of these air showers do not contain particles with energy greater than 2×10^{10} ev which is the minimum energy required for a single electron or photon to produce unit multiplication after traversing 20 radiation units.

Second, showers which do contain particles of energy more than 2×10^{10} ev capable of penetrating 20 radiation units of material are found to be extremely rare, occurring with a frequency of only one in four days as measured with the present experimental set-up. For such extremely rare showers, the primary particle initiating the shower, independent of its point of origin in the atmosphere, must have an extremely high energy which can be estimated from its high penetrating power and very low frequency of occurrence to be of the order of 10^{16} ev.[17]

The fact that only 5 percent of the bursts under thick shields are associated with air showers can be considered as direct evidence that the great majority of the t_μ-bursts at sea level are owing to single high energy particles. It was necessary to establish this point before proceeding to a comparison of the t_μ-burst data with the calculations of Christy and Kusaka for burst production by mesotrons. It also allows one to proceed with a discussion of the t_μ-burst data presented in Table I and facilitates the comparison of these data with other t_μ-burst data obtained by using a 12-cm lead shield around the ionization chamber.

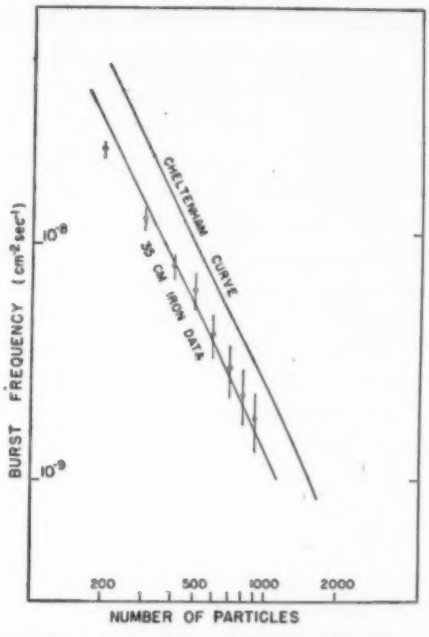

FIG. 4. The integral burst frequency (cm^{-2} sec.$^{-1}$) for bursts observed at sea level under 35 cm of iron is plotted against the size of the bursts in number of particles. The Cheltenham curve represents a very accurate integral size-frequency distribution for t_μ-bursts observed under 12 cm of lead. Statistical errors are shown for the lower curve, those for the Cheltenham curve are shown in Fig. 6.

[15] R. E. Lapp, Phys. Rev. **63**, 60 (1943).
[16] R. E. Lapp, Phys. Rev. **65**, 347 (1944).
[17] L. Wolfenstein, Phys. Rev. **67**, 238 (1945).

2. Dependence on Atomic Number

In Fig. 4, the lower curve represents the data given in Table I for t_μ-bursts observed under 35 cm of iron. This curve, plotted on a double logarithmic scale, is called the cumulative or integral size-frequency distribution curve. It will be noted that the experimental points for the smallest burst sizes fall below the curve drawn in Fig. 4; this discrepancy has been noted by others and it is explained by the fact that many of the smallest bursts are confused with the statistical fluctuations of the cosmic-ray ionization occurring in the ionization chamber and are thus overlooked. That this explanation is actually correct is seen from the fact that the data of Steinke[18] and Schmid[19] for bursts of from 30 to 230 particles under thick shields are represented by a cumulative size-frequency distribution which is a direct continuation of the 35-cm iron curve in Fig. 4 and which has the same slope as this curve.

The cumulative size-frequency distribution curve for the t_μ-bursts under 35 cm of iron is represented by a simple power law of the form:

$$F(>S)=\text{const.}(1/S^{\gamma}), \qquad (1)$$

where $F(>S)$ is the frequency of bursts of size greater than S; S refers to the burst size in number of particles; γ has the value 2.0 ± 0.2 for $200<S<1000$.

In the same Fig. 4, there is also plotted the integral size-frequency distribution curve for bursts observed at Cheltenham[20] (72-meter elevation) with a Carnegie meter shielded by 12 cm of lead. This cumulative size-frequency distribution for bursts in lead can be compared with the 35-cm iron burst data to determine the dependence of burst frequency upon the atomic number of the shielding material. As pointed out in the *Introduction*, the t_μ-bursts originate in the shielding material surrounding the ionization chamber as a result of the interaction of mesotrons with this material. Two different mechanisms are involved in this interaction whereby a mesotron transfers a large fraction of its energy to an electron or photon. First, a high energy mesotron may make a very close collision with an electron (knock-on process) and thus transfer to the electron a large part of its energy. Second, a photon may be produced by the electromagnetic interaction of a mesotron with a nucleus and thus carry away most of the mesotron's energy (bremsstrahlung process). The cross sections for these processes were calculated by Christy and Kusaka[21] and others.[22]

Comparison of the 35-cm iron distribution curve with the 12-cm lead curve can be made on the following basis. The cascade theory predicts that if the initial energy of the photon (for t_μ-bursts produced by bremsstrahlung) initiating the burst in lead or iron is measured in units of the critical shower energy (β) of the shielding material, and if the thickness of the shield is measured in radiation units, then the burst frequency should be nearly independent of the nature of the shielding material for thicknesses greater than 20 radiation units. As a result, for bursts of more than 500 particles ($E>5\times10^{10}$ ev) one should, therefore, expect that the size-frequency distribution curves for bursts measured under an equivalent thickness of lead and iron would be parallel to each other but horizontally displaced by an amount equal to the ratio of the critical energies: $\beta_{Fe}/\beta_{Pb}=22.4/8=2.8$. Actually one finds that the curves in Fig. 4 are essentially parallel but are displaced from one another by a factor of only 1.4 for bursts greater than 500 particles which are practically all initiated by the bremsstrahlung process as will be shown later. That the experimentally determined ratio is considerably smaller than the predicted ratio is caused by the fact that the t_μ-burst data for lead are obtained by using an ionization chamber with a 1.25-cm iron wall surrounded by 10.7 cm of lead whereas the t_μ-burst data for iron is obtained with a homogeneous iron shield. Thus for the lead (Cheltenham) burst data a transition effect occurs which results in an appreciable absorption of the burst particles which are produced in the

[18] E. G. Steinke and H. Schmid, Zeits. f. Physik **115**, 740 (1940).

[19] H. Schmid, Zeits. f. Physik **117**, 452 (1941).

[20] Dr. Jno. A. Fleming of the Carnegie Institution at Washington, D. C. kindly made available to the author some five years of burst data from the Cheltenham, Maryland cosmic-ray station. In Fig. 4 only the smoothed curve for these data is shown; the statistical errors for the experimental points are given in Fig. 6.

[21] R. F. Christy and S. Kusaka, Phys. Rev. **59**, 405 (1941).

[22] H. J. Bhabha, Proc. Roy. Soc. **164**, 257 (1938); H. S. W. Massey and H. C. Corben, Camb. Phil. Soc. **35**, 463 (1939); J. R. Oppenheimer, H. Snyder, and R. Serber, Phys. Rev. **57**, 75 (1940).

TABLE II. Integral number of bursts (cm^{-2} $sec.^{-1}$) with more than S particles produced in 20 radiation units of material calculated for mesotrons of spin 0, ½, and 1. The burst frequencies due to knock-ons and bremsstrahlung in lead are given in (a) and (b) while those for iron are given in (c) and (d). The total frequencies in lead are found in (e) and (f), respectively.

Lead

(a) Knock-on Bursts (cm^{-2} $sec.^{-1}$)

βS $\times 10^9$	Spin 0	Spin ½	Spin 1
1	$6.8\cdot10^{-8}$	$8.7\cdot10^{-8}$	$1.2\cdot10^{-7}$
2	$1.3\cdot10^{-8}$	$1.8\cdot10^{-8}$	$3.2\cdot10^{-8}$
4	$2.3\cdot10^{-9}$	$3.3\cdot10^{-9}$	$8.1\cdot10^{-9}$
8	$3.5\cdot10^{-10}$	$5.4\cdot10^{-10}$	$2.1\cdot10^{-9}$
16	$5.1\cdot10^{-11}$	$8.1\cdot10^{-11}$	$5.5\cdot10^{-10}$
32	$7.1\cdot10^{-12}$	$1.2\cdot10^{-11}$	$1.5\cdot10^{-10}$
64	$9.7\cdot10^{-13}$	$1.6\cdot10^{-12}$	$3.9\cdot10^{-11}$

Lead

(b) Bremsstrahlung Bursts (cm^{-2} $sec.^{-1}$)

Spin 0	Spin ½	Spin 1
$2.0\cdot10^{-7}$	$3.2\cdot10^{-7}$	$1.0\cdot10^{-6}$
$7.3\cdot10^{-8}$	$1.2\cdot10^{-7}$	$4.8\cdot11^{-7}$
$2.2\cdot10^{-8}$	$3.8\cdot10^{-8}$	$2.1\cdot10^{-7}$
$6.0\cdot10^{-9}$	$1.0\cdot10^{-8}$	$8.7\cdot10^{-8}$
$1.4\cdot10^{-9}$	$2.5\cdot10^{-9}$	$3.3\cdot10^{-8}$
$2.9\cdot10^{-10}$	$5.1\cdot10^{-10}$	$1.2\cdot10^{-8}$
$5.0\cdot10^{-11}$	$9.0\cdot10^{-11}$	$3.7\cdot10^{-9}$

Iron

(c) Knock-on Bursts (cm^{-2} $sec.^{-1}$)

βS $\times 10^9$	Spin 0	Spin ½	Spin 1
1	$2.1\cdot10^{-7}$	$2.7\cdot10^{-7}$	$3.8\cdot10^{-7}$
2	$4.1\cdot10^{-8}$	$5.6\cdot10^{-8}$	$1.0\cdot10^{-7}$
4	$7.2\cdot10^{-9}$	$1.0\cdot10^{-8}$	$2.5\cdot10^{-8}$
8	$1.1\cdot10^{-9}$	$1.7\cdot10^{-9}$	$6.6\cdot10^{-9}$
16	$1.6\cdot10^{-10}$	$2.5\cdot10^{-10}$	$1.8\cdot10^{-10}$
32	$2.2\cdot10^{-11}$	$3.8\cdot10^{-11}$	$4.7\cdot10^{-10}$
64	$3.0\cdot10^{-12}$	$5.0\cdot10^{-12}$	$1.2\cdot10^{-10}$

Iron

(d) Bremsstrahlung Bursts (cm^{-2} $sec.^{-1}$)

Spin 0	Spin ½	Spin 1
$2.0\cdot10^{-7}$	$3.2\cdot10^{-7}$	$1.0\cdot10^{-6}$
$7.3\cdot10^{-8}$	$1.2\cdot10^{-7}$	$4.8\cdot10^{-7}$
$2.2\cdot10^{-8}$	$3.8\cdot10^{-8}$	$2.1\cdot10^{-7}$
$6.0\cdot10^{-9}$	$1.0\cdot10^{-8}$	$8.7\cdot10^{-8}$
$1.4\cdot10^{-9}$	$2.5\cdot10^{-9}$	$3.3\cdot10^{-8}$
$2.9\cdot10^{-10}$	$5.1\cdot10^{-10}$	$1.2\cdot10^{-8}$
$5.0\cdot10^{-11}$	$9.0\cdot10^{-11}$	$3.7\cdot10^{-9}$

Lead

(e) Knock-on +Bremsstrahlung Bursts (cm^{-2} $sec.^{-1}$)

βS $\times 10^9$	Spin 0	Spin ½	Spin 1
1	$2.7\cdot10^{-7}$	$4.1\cdot10^{-7}$	$1.1\cdot10^{-6}$
2	$9.0\cdot10^{-8}$	$1.4\cdot10^{-7}$	$5.1\cdot10^{-7}$
4	$2.5\cdot10^{-8}$	$4.1\cdot10^{-8}$	$2.2\cdot10^{-7}$
8	$6.4\cdot10^{-9}$	$1.1\cdot10^{-8}$	$8.9\cdot10^{-8}$
16	$1.5\cdot10^{-9}$	$2.6\cdot10^{-9}$	$3.3\cdot10^{-8}$
32	$2.9\cdot10^{-10}$	$5.2\cdot10^{-10}$	$1.2\cdot10^{-8}$
64	$5.0\cdot10^{-11}$	$9.2\cdot10^{-11}$	$3.7\cdot10^{-9}$

Iron

(f) Knock-on +Bremsstrahlung Bursts (cm^{-2} $sec.^{-1}$)

Spin 0	Spin ½	Spin 1
$4.2\cdot10^{-7}$	$5.9\cdot10^{-7}$	$1.4\cdot10^{-6}$
$1.1\cdot10^{-8}$	$1.8\cdot10^{-7}$	$5.8\cdot10^{-7}$
$2.9\cdot10^{-8}$	$4.8\cdot10^{-8}$	$2.3\cdot10^{-7}$
$7.1\cdot10^{-9}$	$1.2\cdot10^{-8}$	$9.3\cdot10^{-8}$
$1.6\cdot10^{-9}$	$2.8\cdot10^{-9}$	$3.5\cdot10^{-8}$
$3.1\cdot10^{-10}$	$5.5\cdot10^{-10}$	$1.2\cdot10^{-8}$
$5.3\cdot10^{-11}$	$9.5\cdot10^{-11}$	$3.7\cdot10^{-9}$

lead shield. Christy and Kusaka made a correction for this effect by calculating an effective absorbing thickness of iron. This correction was applied by introducing a critical energy $\beta=13\times10^6$ ev instead of $\beta=8\times10^6$ ev which is the value for pure lead. Using this value for the critical energy for the lead curve in Fig. 4, one arrives at the following ratio:

$$\frac{\beta_{Fe}}{\beta_{Pb-Fe}}=\frac{22.4\times10^6 \text{ ev}}{13\times10^6 \text{ ev}}=1.7,$$

which is in as good agreement with the experimental value of 1.4 as can be expected if one considers the fact that statistically exact data for bursts greater than 500 particles require at least several years for collection. On the other hand, changing the critical energy from an estimated value of 13×10^6 ev to 16×10^6 ev results in very good agreement between the theoretical and experimental values for the burst frequencies in iron and in lead. Since the dependence of burst frequency upon atomic number is thus in first approximation in agreement with the predictions of the cascade theory, this definitely indicates that t_μ-bursts greater than 500 particles must be predominantly produced by the bremsstrahlung process.

3. The Spin of the Mesotron

As a result of the experimental data presented above, one is now in a position to compare the t_μ-burst data with the theoretical calculations for burst production by knock-on and bremsstrahlung processes. The recent and more extensive burst data from Cheltenham permit this comparison to be made even for very large bursts ($S>1000$ particles). Table II contains the calculated values for burst frequency as a function of the quantity βS where β represents the critical energy of the shielding element and S is the burst size; the values for lead are taken directly from Christy and Kusaka[3] while the values for iron were calculated by the author. Sections (e) and (f) in Table II give the total frequency for bursts in lead and in iron for mesotrons of spin 0, ½, and 1. The burst frequencies are given for corresponding values of the quantity βS for the following reason: if one plots the calculated burst frequency *versus* the quantity βS, it follows from the cascade theory of showers that experimental data for any value of β can be directly compared with this theoretical curve. This comparison will be valid for all values of $\beta S>5\times10^9$ where the effect of knock-on processes is negligible (see Table II). From the data given in Table II, the percentage of bursts in iron and in lead due to knock-ons (from mesotrons of spin 0 and ½) is calculated as a function of βS and the results are given in Fig. 5. Since, however, the Cheltenham which are to be compared with the theoretical burst frequencies in Table II involve a transition effect which is introduced by the 1.25-cm iron chamber wall, one has to consider a curve which is intermediate between the lead and the iron curves (Fig. 5) in order to see the contribution of bursts due to knock-ons. Taking into consideration this transition effect, the lead-iron curve (Fig. 5) shows that for $\beta S=1.5\times10^9$ corresponding to a 200-particle burst the percentage of

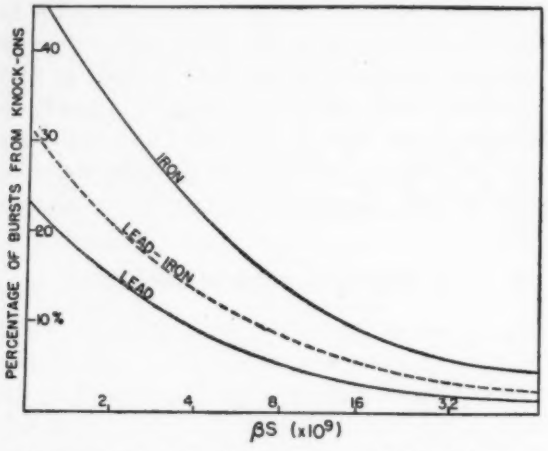

FIG. 5. The contribution to the total t_μ-burst frequency by bursts produced by knock-ons from mesotrons of spin 0 and $\frac{1}{2}$ is illustrated. The quantity βS is the product of the critical shower energy β multiplied by the size S as given by the number of particles in the burst. The dotted curve labeled Lead-Iron is drawn for burst data obtained with 1.25 cm of iron and 11 cm of lead.

bursts due to knock-ons is 25 percent while for a 600 particle burst it is only 10 percent. Thus for bursts larger than about 500 particles the effect of knock-ons does not seriously affect the comparison of the theoretical burst frequencies with the experimental data as was discussed earlier in connection with the dependence of burst frequency on atomic number.

A direct comparison of the theoretical values for burst production by mesotrons given in Table II is now made with the experimental t_μ-burst data for the Cheltenham station. This comparison is given in Fig. 6, where the solid curves represent the theoretical curves calculated for t_μ-bursts produced by mesotrons of spin 0, $\frac{1}{2}$, and 1. On the same graph, the total knock-on contribution to the burst frequency averaged for spin 0 and $\frac{1}{2}$ is plotted (see the lower dotted curve). The Cheltenham data have been plotted in Fig. 6 with the estimated value of $\beta = 13\times10^6$ ev. It is seen that these experimental points are in excellent agreement with the size-frequency distribution curve for bursts produced by mesotrons of spin 0. However, in discussing the dependence of burst frequency on atomic number it was noted that a value of $\beta = 16\times10^6$ ev yielded better agreement between theory and experiment. The effect of using this higher value of β for the Cheltenham data would be to shift the experimental points upward on the graph to a position intermediate between the spin 0 and spin $\frac{1}{2}$ curves. On the other hand, it has to be noted that in the theoretical calculation of the spin $\frac{1}{2}$ curve, a mesotron mass $= 200m_e$ (m_e = electron mass) was used; by assuming a larger mesotron mass, the spin $\frac{1}{2}$ curve can be shifted downward to coincide with the experimental points for the Cheltenham data. For a value of $\beta = 13\times10^6$ ev, such a displacement of the spin $\frac{1}{2}$ curve would require a mesotron mass $= 230m_e$. At present, the mass of the mesotron is not even determined to be within these limits (177 to $230m_e$) and, indeed, it has not been experimentally demonstrated that the mesotron is a particle of unique mass.

Therefore, on the basis of the present experimental results, it does not seem possible to determine whether the t_μ-bursts observed at sea level are produced by mesotrons of spin 0 or if they originate from spin $\frac{1}{2}$ mesotrons. The very great divergence of the experimental data from the theoretical values for burst production by mesotrons of spin 1 does show, however, that at sea level no appreciable fraction of the t_μ-bursts can be due to mesotrons of spin 1.[23]

4. Comparison with Underground Data

If, in place of the βS scale used for the abscissa in Fig. 6, one is to substitute an energy scale, then one has to calculate the average energy per burst particle. This calculation is complicated by the fact that whenever a burst is measured in the chamber, only a single measurement is made of the total number of ions collected in the burst. From this measurement the number of particles in the burst has to be derived. It has been estimated[2] that for the chamber used here, the most probable energy per burst particle is 6β. If this value of 6β is used and β is taken to be 13×10^6 ev, then the probable energy per burst particle is 7.8×10^7 ev. This enables one to assign a definite energy scale to the abscissa of Fig. 6. On the assumption[24] that the fractional energy transfer of a high energy mesotron to an electron or photon is independent of its energy, the size-frequency distribution for t_μ-bursts should represent the integral energy spectrum for mesotrons at sea level.

The underground cosmic-ray intensity meas-

[23] R. E. Lapp, Phys. Rev. **64**, 255 (1943).
[24] J. R. Oppenheimer, Rev. Mod. Phys. **11**, 264 (1939).

urements[25] also provide an approximate evaluation of the integral energy spectrum for mesotrons at sea level and it is of interest to compare Wilson's depth curve with the Cheltenham curve. Assuming that the particles which Wilson measured were mesotrons which lose energy predominantly by ionization loss, one can assign an energy scale to the depth curve. It is understood that for exact calculation of the energy, losses other than ionization must be considered.[26] The Cheltenham curve and Wilson's depth curve are plotted in Fig. 7. For these curves, the same energy scale is used but the ordinates are chosen so as to bring the curves arbitrarily close together to facilitate comparison of their slopes. For energies greater than 6×10^{10} ev corresponding to 250 meters of water equivalent, the slopes of the two curves are nearly the same, indicating that the cosmic radiation producing the large t_μ-bursts at sea level consists of the same particles (mesotrons) which are able to penetrate deep into the earth's surface.

5. Altitude Dependence

To investigate the origin of the t_μ-bursts occurring at higher altitudes, burst data collected over five years at Huancayo (altitude 3350 meters) were studied. A preliminary analysis[27] of these data has been completed, and the integral size-frequency distribution curve derived from these data is given in Fig. 8 where the Cheltenham curve is given again for purposes of comparison. Comparison of the curves given in Fig. 8 is best accomplished by taking the ratio of the frequencies at the two given altitudes and plotting this ratio as a function of burst size. This is done in Fig. 9. It will be noticed that this ratio is essentially constant for burst smaller than 2400 particles and thereafter it increases almost linearly. Schein and Gill[3] have discussed this phenomenon at some length and if one compares their curve for the ratio of burst frequencies at the same two altitudes with Fig. 9, it is noted that the point at which the ratio departs from being constant is shifted to larger burst sizes for the curve given in Fig. 9. This is caused by the fact that more data have been incorporated into the curve in Fig. 9 and greater statistical accuracy for the largest burst sizes is thus attained.

In order to discuss in detail the increase in the ratio of burst frequencies at the two given altitudes, the theoretical curves for burst production by mesotrons of different spin are again considered. For this purpose, the Huancayo data were given on the same graph in Fig. 6. From these curves, it is apparent that if spin 1 mesotrons exist at higher altitudes and become decreasingly important at lower altitudes (since spin 1 mesotrons are assumed to be short lived and therefore are rapidly absorbed in the atmosphere between the two altitudes), then the ratio of the burst frequencies at the two altitudes should increase with energy as given by the

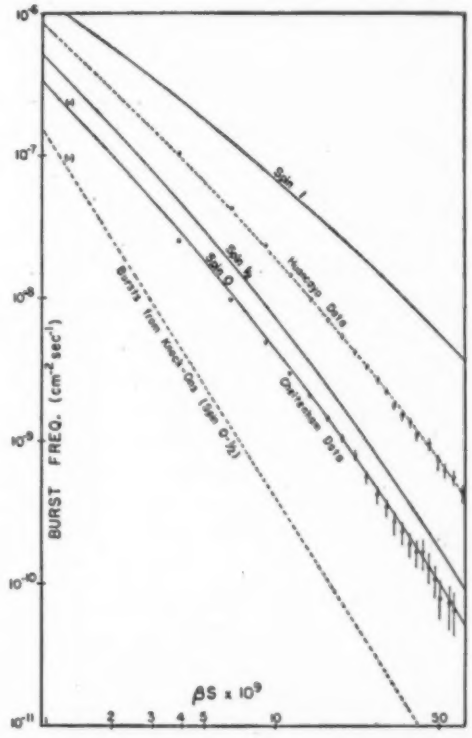

FIG. 6. The integral size-frequency distributions (solid curves above) for burst production by mesotrons of spin 0, ½, and 1 as given in Table II are plotted as a function of the quantity βS. β is the critical shower energy and S is the burst size in number of particles. With this abscissa, the point $\beta S=5\times10^9$ corresponds to a burst of 400 particles where β is taken as 13×10^8 ev. In addition, the burst frequency due to knock-ons for spin 0 or ½ is given by the lower dotted curve. Two sets of experimental data are plotted for comparison with the theoretical curves; the lower set (Cheltenham Data) gives the burst frequency for sea level, while the upper set (Huancayo Data) represents the frequency for an altitude of 3350 meters.

[25] V. C. Wilson, Phys. Rev. **53**, 337 (1938); J. Clay and A. V. Gemert, Physica **6**, 497 (1939); A. Ehmert, Zeits. f. Physik **106**, 751 (1937).
[26] D. Lyons, Physik. Zeits. **42**, 166 (1941).
[27] M. Schein and R. E. Lapp, Phys. Rev. **65**, 63 (1944).

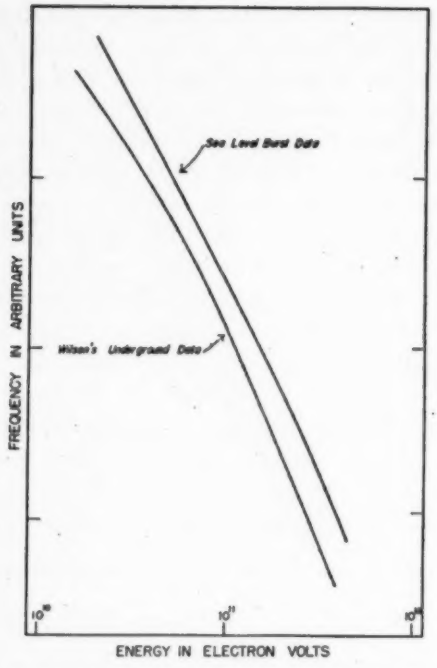

FIG. 7. The integral size-frequency distribution curve for Cheltenham (upper curve labeled Sea Level Burst Data) is compared with the underground data of V. C. Wilson (see reference 25). For the purpose of comparison the abscissa is given in terms of energy measured in electron volts. The two curves are plotted arbitrarily close together to facilitate comparison of their slopes.

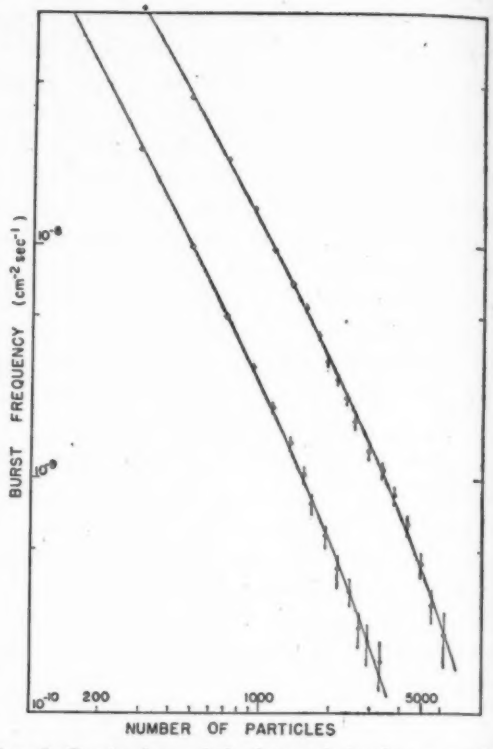

FIG. 8. Comparison of the integral size-frequency burst distributions for Cheltenham (72-m elevation) and Huancayo (3350-m elevation). Both size-frequency distributions incorporate about 5 years of burst data; the upper curve for Huancayo is based on data from 35,000 bursts larger than 200 particles.

number of particles in the bursts. From nuclear theory, it is predicted[28] that spin 1 mesotrons should have a lifetime of about 10^{-9} second.

Another explanation was suggested[3] to account for this phenomenon by considering the possibility that energetic air showers might give rise to t_μ-bursts at higher altitudes. Since the number of these air showers was found to be extremely small at sea level and since air showers of very high energy (10^{16} ev) should increase considerably slower[17] with altitude than the corresponding burst frequencies, it seems rather improbable that burst production by such giant air showers could account for the observed altitude dependence.

t_0-BURSTS

Several observers[18,29] have noted that the frequency of large bursts measured in thin-walled ionization chambers depends rather strongly on the amount of dense material which is close to the chamber. For results that can be clearly interpreted it is essential that experiments on bursts in thin-walled chambers, *viz.*, t_0-bursts, be carried out in a location where the horizon is not obstructed by dense material. One should use a structure which has not only a thin roof but also has thin walls. The experiments on t_0-bursts described here were carried out in the glass greenhouse located on the fifth floor of the Botany building on the campus of the University of Chicago. The greenhouse roof and side structure were entirely of glass construction with light metal reinforcement and there were no nearby buildings to obstruct the horizon. Racks used to support the G-M counters used in these experiments were of light wooden construction.

1. Relation to Air Showers

The primary object of the t_0-bursts experiment was to determine whether or not these bursts

[28] W. Heisenberg, *Kosmische Strahlung* (Verlagsbuchhandlung, Julius Springer, Berlin, 1943).
[29] D. Heyworth and R. D. Bennett, Phys. Rev. 50, 589 (1936); H. Nie, Zeits. f. Physik 99, 453 (1936); C. G. Montgomery and D. D. Montgomery, Phys. Rev. 56, 640 (1939).

were coincident with air showers. Some of the results of these coincidence experiments have already been published.[7] As the initial set-up for the coincidence experiments, two twofold coincidence sets of G-M counter tubes were used to detect air showers. These were used in order to have the highest probability for detecting extensive air showers. It was then found that the majority of the t_0-bursts were coincident with a simultaneous triggering of both twofold sets, but there was a small number of t_0-bursts that were accompanied by a triggering of only 1 set and a few which were not coincident with a triggering of either set. The quantitative investigation of these t_0-bursts is made difficult because of their low frequency, only 1 or 2 such bursts being recorded per day. For the purpose of investigating more accurately the relation of the t_0-bursts to air showers, three additional counter sets were utilized. Using these additional counter sets (a threefold, a fourfold, and a fivefold coincidence set) large t_0-bursts were observed which were coincident with a simultaneous triggering of all 5 of the G-M sets.[30] The data obtained from these coincidence experiments may be summarized as follows:

(1) The larger the burst size, the greater is the probability that the burst is coincident with an extensive shower.
(2) In most cases, the larger bursts trigger more of the G-M sets than the smaller bursts.
(3) About 1/7 of the total bursts[31] were not coincident with a triggering of any of the G-M sets.

These results are discussed later in this section in connection with the density distribution of particles in atmospheric showers. It may be pointed out at this time, however, that those t_0-bursts which were not coincident with extensive showers might produced by narrow angle air showers or by local showers generated in the small amount of dense material in the vicinity of chamber.

2. Size-Frequency Distribution

Table III shows the t_0-burst data obtained during a time interval of 2063 hours. Since the size-frequency distribution curve for these data has already been given,[7] it is not reproduced separately[32] here. It is obvious that the 1.25-cm iron wall of the chamber will tend to produce some multiplication of the particles which are incident on it. This wall is equal to 0.7 radiation units (r.u.) and this thickness of material is sufficient also to cause some of the incident particles to be absorbed. If the incident particles are selectively more absorbed than they are multiplied by the 0.7 r.u. there will be correspondingly fewer small bursts recorded, thus causing a flattening of the integral size-frequency distribution curve. In comparing the t_0-burst data obtained with different ionization chambers, it must be born in mind that the following factors will have an appreciable effect on the observed burst frequency:

(1) The thickness and material of the chamber wall.
(2) The altitude at which the t_0-bursts are measured.
(3) The geometry of the ionization chamber.
(4) Presence of dense material in the vicinity of the chamber.

In general, it is almost impossible to accurately correct t_0-burst data for variations in these four factors and it is therefore very difficult to compare the burst data of different experimenters. Migdal[33] and others[34] have directly compared various t_0-burst data. An extensive survey of the litera-

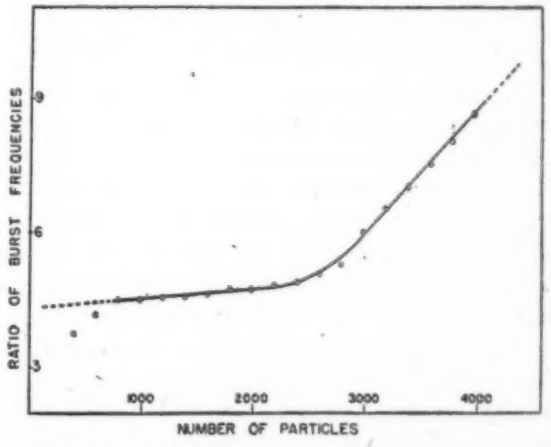

FIG. 9. Ratio of the burst frequencies at Huancayo and Cheltenham as a function of burst size.

[30] The G-M sets were arranged as shown in Fig. 1 of reference 7.
[31] It is not possible to express this fraction more exactly because in a completely unshielded condition, the ionization chamber records considerable fluctuation in the cosmic-ray ionization and due to this fact, many of the smaller bursts may be overlooked.
[32] The t_0-burst curve is shown later in Fig. 12 of this paper.
[33] A. Migdal, J. Phys. U.S.S.R. 9, 183 (1945).
[34] G. Hoffmann, Zeits. f. Physik 119, 35 (1942); K. L. Kingshill and L. G. Lewis, Phys. Rev. 68, (1946).

TABLE III. Integral number of bursts (cm^{-2} $sec.^{-1}$) with more than S particles produced in 1.25 cm of iron.

Burst size (in mm)	Burst size (S) (No. of particles)	Integral number of bursts (2063 hr.)	Burst frequency (cm^{-2} $sec.^{-1}$)
1.0–1.5	100	170	$2.30 \cdot 10^{-8}$
1.5–2.5	150	138	$1.86 \cdot 10^{-8}$
2.5–3.5	250	84	$1.14 \cdot 10^{-8}$
3.5–4.5	350	43	$5.82 \cdot 10^{-9}$
4.5–5.5	450	24	$3.25 \cdot 10^{-9}$
5.5–6.5	550	13	$1.76 \cdot 10^{-9}$
6.5–7.5	650	10	$1.35 \cdot 10^{-9}$
7.5–8.5	750	8	$1.08 \cdot 10^{-9}$
8.5–9.5	850	6	$8.12 \cdot 10^{-10}$
>9.5	>950	5	$6.75 \cdot 10^{-10}$

ture has revealed a lack of t_0-burst data with which the data obtained here could be compared for burst sizes greater than 200 particles. Using a chamber with 0.3-mm steel walls but otherwise similar to the one used here, Kingshill and Lewis[34] have recently obtained t_0-burst data for bursts smaller than 200 particles. It is interesting to note that for 200 particle bursts, they found a frequency of 1.1×10^{-8} burst cm^{-2} $sec.^{-1}$ as compared with the value 1.6×10^{-8} burst cm^{-2} $sec.^{-1}$ found here for bursts of the same size. This approximate agreement indicates that the 1.25-cm iron wall in the Carnegie chamber does not drastically affect the observed burst frequency apparently because there is a compensation between the number of particles being absorbed in the iron and those being multiplied by it.

3. Density *vs.* Extension in Air Showers

Extensive air showers have been generally investigated by determining the coincidence counting rate for two or more G-M counters as a function of the lateral distance separating the counters. From these and similar experiments in which the extension of the shower was the experimental quantity observed, values were deduced both for the density of particles in the shower as well as for the energy of these particles. These values, however, could only be obtained by using the cascade theory applied to multiplicative processes for electrons and photons, for which an energy spectrum was assumed to be valid to energies up to 10^{16} ev. It is now known that these first[35] calculations on cascade multiplication in the atmosphere neglected important considerations. Such factors, as the zenith angle dependence and the diffusion effect[36] for electrons and photons in the shower cannot be neglected, and if they are taken into consideration, the results then obtained[17] are in disagreement with the assumption that most of these showers could originate close to the top of the earth's atmosphere.

The coincidence experiments on t_0-bursts described here show definitely that the great majority of the large bursts observed in unshielded ionization chambers at sea level are produced by a high density core of an atmospheric shower striking the chamber. For the range of burst sizes observed, the density of particles in the cores of these showers is of the order of 10^3 to 10^4 particles per square meter. If the region of such high particle density in an atmospheric shower had considerable extension, then it would have been observed that all of the G-M sets would have been simultaneously triggered when such a shower was centered upon the ionization chamber. The coincidence data show that many of the t_0-bursts did not trigger all of the G-M sets, thus indicating that high density cores of such showers do not exhibit very great lateral extension. This point will be amplified after considering the t_m-burst coincidence data.

t_m-BURSTS

For large cosmic-ray bursts, it is well known that a maximum burst frequency is obtained for a thickness of shielding material around the chamber equivalent to 6 or 7 radiation units. For iron, 7 r.u. corresponds to about 12 cm.[37] The 12-cm iron shield was made up of two mating hemispherical caps of 3-cm wall thickness which fitted around the chamber and in addition a uniform layer of No. 22 iron shot equivalent to 7.7 cm of solid iron was placed around these caps.

1. Relation to Air Showers

For the t_m-burst coincidence experiments, the G-M counter sets were arranged as shown in Fig. 10. By use of this arrangement of counters, coincidence data were collected for 568 hours during which time 197 bursts were observed. In

[35] H. Euler, Zeits. f. Physik 116, 73 (1940).

[36] J. A. Richards and L. W. Nordheim, Phys. Rev. 61, 735 (1942).

[37] H. Nie (reference 29) reports that he finds a maximum frequency of bursts in iron for a thickness between 10 and 15 cm.

Table IV, these data are presented and it is seen that of the total of 197 t_m-bursts, 39 were observed to be coincident with one or more of the G-M counter coincidences. Additional information on these coincident bursts is given in Table V in which the number of coincident bursts is tabulated as a function of the burst size. Moreover, the total number of t_m-bursts for each burst size is also listed in the Table V and the ratio of coincident bursts to total bursts is given as a function of the burst size.

Analysis of the data presented in Tables IV and V allows the following conclusions to be drawn. Coincident t_m-bursts have the highest probability for triggering the threefold G-M set *C*, the next highest probability for fourfold set *D*, and the least for twofold set *B*. Thus while the twofold set should have the highest probability for detecting an extensive shower, it has a lower rate of coincidence with the t_m-bursts than do the three and fourfold G-M sets which essentially measure a higher density but less extensive shower. This means that a large fraction of the t_m-bursts have their origin in the incidence of narrow air showers on the ionization chamber. In good agreement with conclusion are the data of Kingshill and Lewis[34] who observed very infre-

TABLE IV. G-M counter coincidence data for t_m-bursts.

Counter set—Type		No. of coincident t_m-bursts >150 particles
B	twofold	18
C	threefold	34
D	fourfold	30
E	fivefold	10
Total	—	39

$$\text{Ratio: } \frac{\text{total coincident bursts}}{\text{total bursts}} = \frac{39}{197} = 20 \text{ percent}$$

TABLE V. G-M counter coincidence data for t_m-bursts as a function of burst size.

Burst size	Total bursts	Coincident bursts	Ratio
2	58	13	0.22
3	48	5	0.10
4	41	6	0.15
5	19	3	0.16
6	7	1	0.14
7	4	2	0.50
8	9	4	0.45
9	2	1	0.50
10	2	1	0.50
>10	7	3	0.43

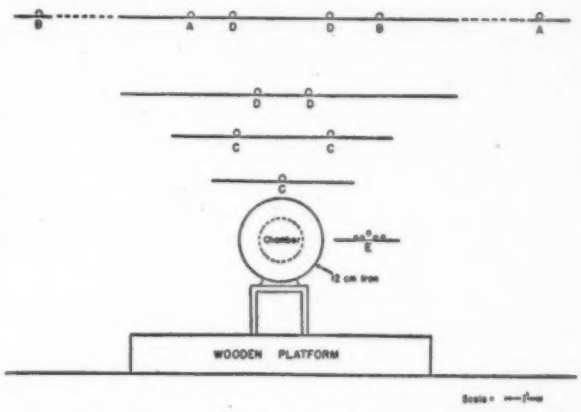

FIG. 10. Arrangement of ionization chamber and G-M counters for the t_m-burst experiment. G-M tube dimensions are: G-M *A* 2″×19″, *B* 2″×15″, *C* 2″×10″, *D* 2″×10″, *E* 1″×10″.

quent coincidences between t_0-bursts in two thin-walled chambers separated by a distance of one meter. Furthermore, it is evident from Table V that the probability for a t_m-burst to be coincident with an air shower increases with increasing burst size. For a burst larger than 500 particles, there is about a 50 percent probability for the burst to be coincident with an air shower. This can be interpreted as meaning that these air showers not only have higher densities of particles in their cores and thus trigger the G-M counter sets, but also contain particles of higher energy necessary to traverse the 12 cm of iron and produce large bursts in the chamber.

So far, the origin of only 20 percent of the t_m-bursts has been discussed. Before proceeding to a discussion of the other t_m-bursts, it is necessary to consider the integral size-frequency distribution curve for the t_m-bursts in relation to the t_0- and t_μ-bursts so that the transition effect for large bursts in iron may be studied.

2. Size-Frequency Distribution

Burst data collected during 1411 hours of recording time are tabulated in Table VI. For these observations, the Lindemann electrometer was operated at a higher sensitivity than for the t_0- and t_μ-experiments so that more data for the smaller bursts were obtained as indicated by the fact that during the 1411 hours, 965 bursts were recorded. The integral size-frequency distribution curve for these data is plotted in Fig. 11. This t_m-burst curve conforms to an inverse exponential

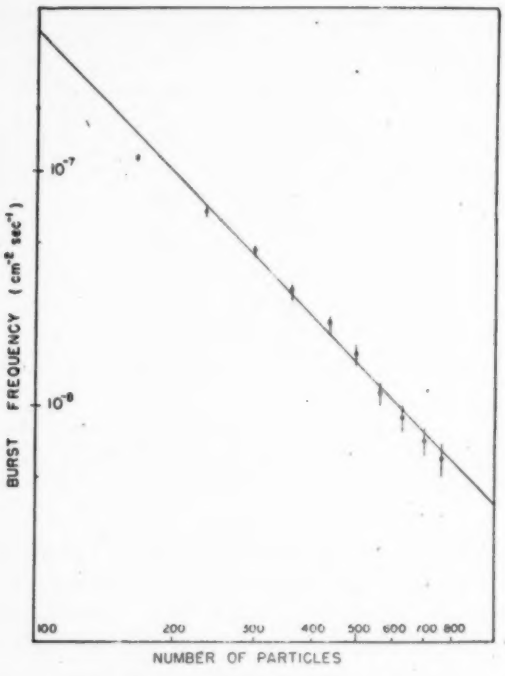

FIG. 11. Integral size-frequency distribution curve for bursts measured under 12 cm of iron at sea level.

power law with exponent = 2.0±0.15, and it is in satisfactory agreement with the value of 1.82 found by Sittkus[38] for large bursts measured under a 10-cm iron shield.

The t_0-, t_m- and t_μ-burst curves which have already been given are compared in Fig. 12. Within the experimental accuracy of these curves, they can all be represented by an integral size-frequency distribution obeying an inverse exponential power law with exponent = 2.0. In other words, the three curves corresponding to size-frequency distributions for bursts under 1.25, 12, and 35 cm of iron are nearly parallel; thus integral size-frequency distribution for burst measured under a shield of iron is independent of the thickness of the shield. Since the ratios of the frequencies of the $t_0:t_m:t_\mu$ bursts is independent of burst size, these ratios can be directly evaluated by taking the intercept of each curve with the ordinate in Fig. 12. In this way, $t_0:t_m:t_\mu$ is found to be 1:6.5:2.3 where the t_0-burst frequency has been taken equal to unity. These values have been used to plot the three-point transition curve given in Fig. 13.

[38] A. Sittkus, Zeits. f. Physik **112**, 626 (1939).

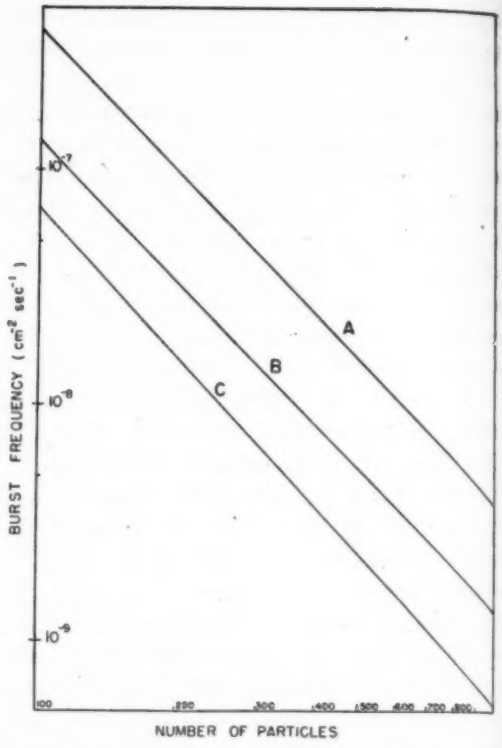

FIG. 12. Comparison of t_0-, t_m-, and t_μ-burst curves (integral size-frequency distributions). The integral size-frequency distribution curves for bursts measured under 1.25, 12, and 35 cm of iron are given. Curve *A* is a duplication of Fig. 11, while curve *B* is redrawn from Fig. 4. Curve *C*, plotted from the data given in Table III, was given in an earlier publication (see reference 7).

3. Transition Effect

The prohibitive length of time required for obtaining additional data for other intermediate points on the transition curve (Fig. 13) precluded their investigation at this time. In addition, transition curves should be plotted for various

TABLE VI. Integral number of bursts (cm^{-2} $sec.^{-1}$) with more than S particles produced in 12 cm of iron.

Burst size (in mm)	Burst size (S) (No. of particles)	Integral numbers of bursts (1411 hr.)	Burst frequency (cm^{-2} $sec.^{-1}$)
1.5– 2.5	100	965	1.84×10^{-7}
2.5– 3.5	167	557	1.12×10^{-7}
3.5– 4.5	234	360	6.85×10^{-8}
4.5– 5.5	300	244	4.65×10^{-8}
5.5– 6.5	367	158	3.02×10^{-8}
6.5– 7.5	434	118	2.25×10^{-8}
7.5– 8.5	500	87	1.66×10^{-8}
8.5– 9.5	567	59	1.12×10^{-8}
9.5–10.5	634	47	8.95×10^{-9}
10.5–11.5	700	37	7.04×10^{-9}
11.5–12.5	767	31	5.92×10^{-9}

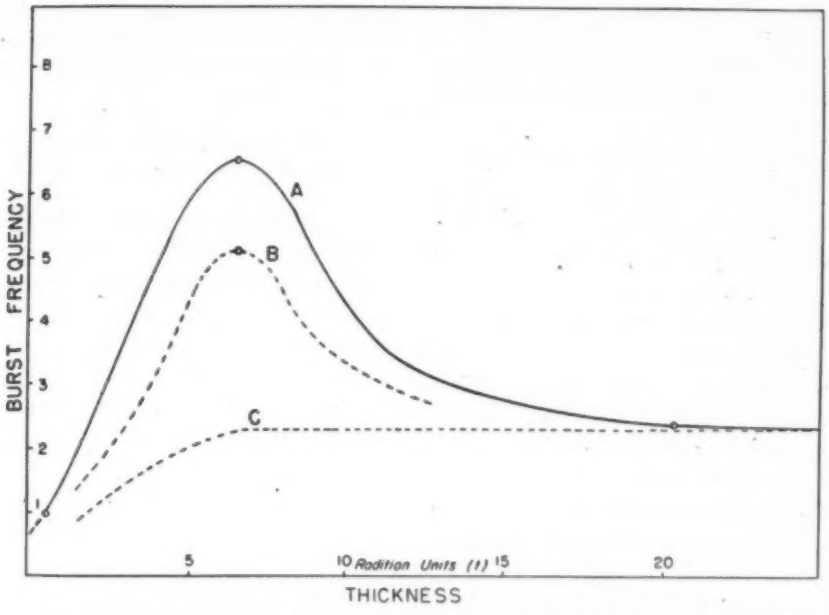

FIG. 13. Analysis of the transition curve for large bursts in iron. From the data given in Fig. 12, the frequency of the bursts observed under 1.25, 12, and 35 cm of iron is plotted as a function of the iron shield thickness as measured in radiation units. The G-M counter coincidence data have been used to effect the decomposition of the transition curve *A* into three components. Thus curve *B* represents the transition effect that would be observed if the effect of extensive air showers was not considered and curve *C* gives the transition expected for bursts originating from knock-on and bremsstrahlung processes in mesotron collisions.

burst size intervals, say from 100 to 300 particles, from 300 to 500, etc. This procedure, if applied to comprehensive burst data covering a wide range of burst size and having high statistical accuracy, could be used to verify the prediction of cascade theory that for the larger burst sizes the maximum in the transition curve should shift to a point corresponding to a greater thickness of shielding material. Such a shift in the maximum cannot be verified from the present experiments because of the lack of sufficient data.

The transition curve given in Fig. 13 exhibits a pronounced maximum. Nie[29] also observed a maximum for large bursts at about the same thickness of iron, but the maximum was not as pronounced as that found here. It is believed that this discrepancy can be explained by the fact that the transition curve for large bursts does not represent a simple transition effect involving only one type of cosmic-ray burst. It is, on the contrary, a complex transition and integrates the effect of three burst-producing cosmic-ray components, for each of which the burst frequency is dependent not only upon the geometry of the chamber and shield but also upon the presence of adjacent dense material. Thus a spherical ionization chamber surrounded by a symmetric shield located in a site free from obstruction by dense material is essential for obtaining interpretable transition curves for large bursts.

Curve *C* is drawn in Fig. 13 to represent the transition effect for bursts produced by knock-on and bremsstrahlung processes of the mesotron. Where the thickness of the chamber shield is greater than 6 or 7 r.u., these t_μ-bursts should, in general, be independent of any further increase in this thickness. Thus, at a point on the transition curve corresponding to 12 cm of iron, the contribution to the t_m-burst frequency by bursts produced by mesotrons should be equal to the t_μ-burst frequency; this would amount to 35 percent of the t_m-frequency. Since 20 percent of the total t_m-bursts have already been shown to be coincident with extensive showers, there are 45 percent of the t_m-bursts which must be of different origin. Curve *B* (Fig. 13) is sketched to show a possible transition effect for these bursts. It is supposed that these bursts originate from:

(1) Either the incidence of a very narrow air shower on the ionization chamber.
(2) Or from single high energy electrons which produce a high multiplication of electrons and photons in the 12 cm of iron.

Supporting the first possibility is the evidence obtained from the coincidence of G-M counter sets with the 20 percent coincident bursts, which shows that many of these bursts are coincident with relatively narrow air showers. Therefore, one could assume that there exist even narrower showers which would not give coincidences with the G-M sets but which would produce bursts under the 12 cm of iron. If these very narrow showers contain a few high energy photons or electrons, these particles would undergo great multiplication in the iron and thus one would not have to postulate high particle densities for these showers. Regarding the second possible origin, it is suggested that single high energy electrons at sea level might arise from the disintegration of short-lived mesotrons. There is, however, no experimental evidence to substantiate this supposition. In order for single electrons to account for the t_m-bursts at sea level, these particles would have to have energies in the range from 10^{10} to 10^{11} ev.

Since for any given thickness of shield less than about 20 r.u., there are three distinct contributions to the observed burst frequency, each of which for a given burst size may have a different total energy associated with it, it is not possible to assign an energy scale to the abscissa of the transition curve. Neither is it possible to select a mono-energetic band of burst producing radiation by merely shielding an ionization chamber with an arbitrary thickness of absorber.

DISCUSSION

The results of the t_0-, t_m- and t_μ-burst experiments can be summarized in part as follows:

At sea level, the observed cumulative burst frequency $R(t)$ of bursts containing more than 100 particles as observed under a thickness (t) of absorbing shield, is given as:

$$R(t)=R_0(t)+R_s(t)+R_\mu(t), \qquad (2)$$

where

$R_0(t)$ is the frequency due to bursts caused by extensive air showers. $R_0(t)$ yields the contribution[39] obtained by subtracting curve B from A in Fig. 13.

$R_s(t)$ represents the frequency assumed to be due to either narrow air showers or single high energy electrons. $R_s(t)$ represents[39] the difference between curves B and C in the transition curve.

$R_\mu(t)$ is the frequency arising from bursts due to knock-on electrons and bremsstrahlung of mesotrons, as represented by curve C in Fig. 13.

For example, it is seen from Fig. 13 that at a thickness of absorber equal to 7 r.u., $R_0(7)$ contributes approximately 20 percent; $R_s(7)$, 45 percent; and $R_\mu(7)$, 35 percent, respectively, to the observed frequency $R(7)$.

If one excludes burst of origin other than the above three types, then it is obvious that the frequency $R(h, t)$ for any altitude (h) can be given as:

$$R(h, t)=R_0(h, t)+R_s(h, t)+R_\mu(h, t), \qquad (3)$$

where the quantities on the right-hand side of the above expression are similar to those defined in Eq. (2), except that they are taken as valid for any altitude (h). Both h and t are measured in r.u. and sea level is defined as $h=0$ r.u.

Since there has been no measurement of the complete transition curve carried out at a higher altitude, say, $h=7$ r.u., one cannot make a thorough comparison of the altitude dependence of the transition curve. However, there have been several experiments performed at higher altitudes from which one can roughly estimate the values for the following ratios:

$$\frac{R(7, 0)}{R(0, 0)}\sim 50 \quad \text{(Kingshill and Lewis[34])},$$

$$\frac{R(7, 7)}{R(0, 7)}\sim 15 \quad \text{(Montgomery and Montgomery[40])},$$

$$\frac{R(7, 20)}{R(0, 20)}=4.5\pm 0.3 \quad \text{(Fig. 9)}.$$

Since the ratios $R(0, 0)$[41]$:R(0, 7):R(0, 20)$ have already been given here as 1:6.5:2.3, it can accordingly be estimated that the approximate values of the ratios at altitude $h=7$ r.u. are 50:100:10. These values could be used to indi-

[39] This is only approximate since curve B is extrapolated to thicknesses greater than 7 r.u.
[40] C. G. Montgomery and D. D. Montgomery, Phys. Rev. 47, 429 (1935).
[41] Actually the value used is $R(0, 0.7)$ but for the present comparison this is approximately $R(0, 0)$.

cate the approximate shape of the transition curve for bursts of more than 100 particles at an altitude of $h=7$ r.u. The fact that the t_s-burst frequency for such a transition curve is very small compared with the t_0- and t_m-burst frequencies shows that the great majority of the extensive atmospheric showers at higher altitudes do not contain electrons or photons of energies sufficient to create high multiplication under 20 r.u. (i.e., $E>10^{11}$ ev).

It is with sincere gratitude that the writer acknowledges the counsel of Professor Marcel Schein who suggested the problem and guided all phases of the investigation. The author is also grateful to Chancellor A. H. Compton for his support and advice. The work was facilitated by a fellowship granted by the Henry Strong Educational Foundation. Appreciation is likewise expressed to the Carnegie Institution of Washington for its cooperation.

PHYSICAL REVIEW VOLUME 69, NUMBERS 7 AND 8 APRIL 1 AND 15, 1946

Structure in the X-Ray *K* Absorption Edge of Metallic Potassium

JOSEPH B. PLATT*
Cornell University, Ithaca, New York
(Received December 26, 1945)

For the alkali metals sodium and potassium the free electron approximation should give the energy states in the conduction band closely. Calculations based on this approximation predict an arctangent shape for the potassium *K* absorption edge. By use of a two-crystal vacuum x-ray spectrometer, the absorption edge of metallic potassium has been explored with high resolving power. Details of the experimental procedure are given. The shape of the absorption edge is in satisfactory agreement with the theoretical arctangent curve, and the width of the edge agrees with the predicted value. Some evidence is found of a secondary structure not given by the simple theory and the free electron approximation. The wave-length of the midpoint of the edge has been redetermined.

INTRODUCTION

RECENT theories of the solid state have predicted the distribution in energy of the conduction electrons in metals. Knowledge of the electronic energy states in the conduction band of a metal makes possible a theory of the structure to be found in the neighborhood of an x-ray absorption edge for that metal, and this derived theory can be tested experimentally. The photoelectric ejection of an electron from the *K* state of the metal atom, with absorption of the quantum, is permissible if the quantum has sufficient energy to raise the electron to the lowest unoccupied state in the conduction band. Variation of the absorption coefficient for quantum energies starting at this critical value and increasing by a few ev must be due to the nature and density of the energy states in the conduction band.

The experimental requirement is that the absorption coefficient of the metal be investigated carefully over a range of quantum energies of several electron volts including the absorption edge. Since the energy of the absorption edge itself is in general of the order of electron kilovolts, this puts a stringent requirement on the resolving power of the apparatus used. Such resolving power can be obtained without prohibitive loss in x-ray intensity with the two-crystal x-ray spectrometer. A number of investigators have used this research tool to study the structure of absorption edges in metals.[1,2]

The alkali metals, and especially sodium and potassium, are of particular interest because the theory of their solid state has been developed in some detail. The present study is of the absorption structure in the region of the potassium *K*

* Now at the University of Rochester.

[1] H. Friedman and W. W. Beeman, Phys. Rev. 58, 400 (1940).
[2] L. G. Parratt, Phys. Rev. 54, 99 (1938).

edge. Sodium, on which the most complete theoretical work has been done,[3] has recently been reported on by another investigator.[4]

THEORY OF ABSORPTION STRUCTURE IN POTASSIUM *K* EDGE

The methods of wave mechanics have been used to study three questions which are of interest in predicting the variation of the absorption coefficient of potassium in the region of the *K* edge. The first of these questions is the determination of the density of energy states, within the conduction band, to which an electron may be ejected. The second is the behavior of the probability of a transition from the *K* shell to one of the states in the conduction band. The third is the "smearing" of the detail of the absorption curve caused by the fact that the energy of the atom in a state of *K* excitation is not exactly defined.

Density of Energy States

The Schroedinger equation for the wave function of an electron is

$$\frac{\hbar^2}{2m}\nabla^2\psi+(E-V(\mathbf{r}))\psi=0,$$

where E is the total energy of the electron and $V(\mathbf{r})$ is its potential energy. For a conduction electron in potassium metal, the potential function $V(\mathbf{r})$ is nearly constant over most of the volume within the lattice (the volume outside the ionic cores). To a first approximation $V(\mathbf{r})=0$, if the zero of energy be taken as the mean potential energy of a conduction electron. This leads to the "free electron" solution

$$\psi=\exp[i\mathbf{k}\cdot\mathbf{r}],$$

where $\mathbf{r}$ is the position vector of the electron, and the wave vector $\mathbf{k}$ has the magnitude $(2mE/\hbar^2)^{\frac{1}{2}}$. For this solution, the number of electronic energy states between E and $E+dE$ is proportional to $E^{\frac{1}{2}}dE$. The energy of the highest occupied state in the conduction band is

$$E_{\max}=\frac{\hbar^2R_{\max}^2}{2m}=\frac{\hbar^2}{2m}\left(\frac{3\pi^2}{\Omega}\right)^{\frac{2}{3}},$$

where Ω is the volume occupied by one atom. For potassium the value of $E_{\max}$ is 2.06 ev.

In second approximation one includes in the potential term $V(\mathbf{r})$ the part of the potential that is not constant. A good deal of information may be secured without knowing the exact variation of the potential simply from the fact that the potential must be identical at corresponding points within the lattice. $V(\mathbf{r})$ may therefore be expanded in a three-dimensional Fourier series the fundamental space periods of which correspond to the lattice vectors for metallic potassium. The problem may then be treated by perturbation methods, in which the "free electron" solutions are taken for the unperturbed wave functions. The result is that the electron energies are very closely those of the unperturbed case except for values of the wave vector $\mathbf{k}$ which fall near the boundary of one of the Brillouin zones in $\mathbf{k}$ space. If these zones were bounded by spherical shells, there would be certain energy values within the electron energy spectrum which would not occur. Since the zones are actually bounded by polyhedra, one can say only that there will be regions in the energy spectrum for which the $E^{\frac{1}{2}}$ law will not be obeyed. In the case of metallic potassium, one expects deviations from the $E^{\frac{1}{2}}$ law in the region from three to five ev, due to the influence of the boundary of the first Brillouin zone. The extent of these deviations should be small if the approximation of constant potential (unperturbed theory) is nearly valid. Effects due to other Brillouin zones than the first should be greatest in the energy regions of 10 ev and 36 ev, and should be smaller than those at the first boundary.

Transition Probability

The variation in absorption coefficient depends not only on the density of states within the conduction band to which the electron can be ejected, but also on the probability than an electron makes the transition from the *K* shell of the atom to a particular state in the conduction band, under the influence of the radiation.

[3] E. Wigner and F. Seitz, Phys. Rev. **43**, 804 (1933); **46**, 509 (1934).
[4] K. C. Rule, Phys. Rev. **66**, 199 (1944).

The probability of transition from a state in which the wave function of the electron is ψ_i to a state in which the wave function of the electron is ψ_f is proportional to the absolute square of the matrix element $\mathbf{M}$,[5] where

$$\mathbf{M}=\int \psi_i \mathbf{r} \psi_f^* dv.$$

Here $\mathbf{r}$ is the coordinate vector with respect to which the integration is performed, and dv is an element of volume. Exact evaluation of the matrix element involves the precise functional form of ψ_i and ψ_f. A good deal of information may be secured, however, merely from a qualitative knowledge of the behavior of the wave functions.

It suffices to note that $r\psi_i$, where ψ_i is the wave function of the K electron, varies with the increasing distance from the nucleus roughly as shown in Fig. 1.[6] The maximum occurs at a distance of about 2.5×10^{-10} cm from the nucleus, and from this region on the wave function decreases rapidly with increasing distance. The quantity $r\psi_i$ is only appreciable for a radial distance between 5×10^{-11} and 10^{-9} cm.

To find the behavior of the wave function ψ_f of the ejected electron one makes use of an approximate solution of the Schroedinger equation. As previously, one may neglect in first approximation the periodic variation in the potential of an electron within the lattice. There is one deviation from constant potential, however, which may not be neglected. Upon ejection from the K shell the photoelectron leaves behind it an atomic core which is ionized in the K shell. In the neighborhood of the ion from which it was ejected, then, the electron moves in a potential due to one positive charge. One must add to the expression for the potential a term $-Z'e^2/r$, where Z' has the value unity for large r, and has the value of the effective atomic charge for r within the ion itself. The Schroedinger equation becomes

$$\frac{\hbar^2}{2m}\nabla^2\psi_f+\left(E+\frac{Z'e^2}{r}\right)\psi_f=0.$$

The solution is most conveniently obtained in terms of spherical coordinates since the potential term is spherically symmetric. It is readily shown that the solution may be written

$$\psi_f(r)=A_0\frac{R_0(r)}{r}+\frac{R_1(r)}{r}\sum_{m=-1}^{1}A_{1m}P_{1m}(\phi,\theta)+\frac{R_2(r)}{r}\sum_{m=-2}^{2}A_{2m}P_{2m}(\phi,\theta)+\cdots$$

where the A_{jm} are constants, the $P_{jm}(\phi,\theta)$ are spherical harmonics, and the $R_j(r)$ are solutions of the radial equation

$$\frac{d^2R_j(r)}{dr^2}+\left[\frac{2m}{\hbar^2}\left(E+\frac{Z'e^2}{r}\right)-j\frac{(j+1)}{r^2}\right]R_j(r)=0.$$

The boundary condition to be imposed on the solution $\psi_f(r)$ is that for large values of r, i.e., large distances from the ionized atom, the wave function must be identical with the previous solution,

$$\psi_f(r)=\text{constant}\cdot\exp(i\mathbf{k}\cdot\mathbf{r}).$$

This is equivalent to requiring the electron to assume its normal role in the lattice once it is removed from the influence of the ion. This requirement makes one simplification immediately possible, for, if the polar axis (z axis) of the spherical coordinates be chosen parallel to $\mathbf{k}$, only those spherical harmonics for which m is zero can appear in the expression for $\psi_f(\mathbf{r})$.

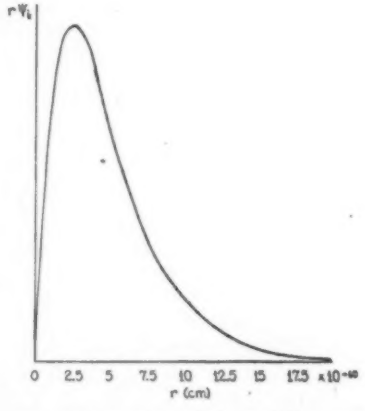

FIG. 1. $r\psi_i$ as a function of the radial parameter r for the potassium K electron.

[5] F. Seitz, *The Modern Theory of Solids* (McGraw-Hill Book Company, Inc., New York, 1940), p. 219.
[6] H. A. Bethe, *Handbuch der Physik* (Verlagsbuchhandlung, Julius Springer, Berlin, 1933), Vol. 24/I, p. 285.

A further simplification results from the fact that the wave function ψ_i of the electron in the K shell is spherically symmetric. It can be shown[6] that under this condition the only spherical harmonics in $\psi_f(\mathbf{r})$ which contribute to the matrix element are those for which j is unity. In this problem one is interested only in the coefficient of $P_{10}(\phi, \theta)$.

An approximate method of solving the radial equation has been developed by Wentzel, Kramers, and Brillouin.[7] If one makes the substitution for the case $j=1$,

$$\Phi(r)=\frac{2m}{\hbar^2}\left(E+\frac{Z'e^2}{r}\right)-\frac{2}{r^2},$$

the radial equation becomes

$$\frac{d^2R_1(r)}{dr^2}+\Phi(r)R_1(r)=0,$$

the approximate solution of which is

$$R_1(r)=C\Phi^{-\frac{1}{4}}(r)\cos\left(\int_{r_0}^{r}\Phi^{\frac{1}{2}}(\lambda)d\lambda-\pi/4\right)+\cdots$$

where the constant C is independent of r, and $\Phi(r_0)=0$. The solution holds for r greater than r_0. If we assume $E=10$ ev and $Z=19$ for potassium, then we find r_0 is in the region of the K shell. Thus the W-K-B method leads to the solution

$$\psi_f(r)=\cdots+P_{10}(\phi, \theta)\times(C/r)\Phi^{-\frac{1}{4}}(r)\cos\left(\int_{r_0}^{r}\Phi^{\frac{1}{2}}(\lambda)d\lambda-\pi/4\right)+\cdots.$$

This must be identical with $\exp[i\mathbf{k}\cdot\mathbf{r}]$ for large r. The expansion of this function in spherical harmonics approaches for large r the value

$$\underset{r\to\infty}{\exp}[i\mathbf{k}\cdot\mathbf{r}]=\frac{\sin kr}{kr}+P_{10}(\phi, \theta)\left(\frac{\cos kr}{kr}-\frac{\sin kr}{(kr)^2}\right)+\cdots.$$

To compare the two expansions, one notes that for large r, $\Phi(r)$ approaches $2mE/\hbar^2$. Writing the energy E as $\hbar^2k^2/2m$, one finds for large r

$$\Phi(r)=k^2,\quad \int_{r_0}^{r}\Phi^{\frac{1}{2}}(\lambda)d\lambda=kr+\text{constant},$$

$$\psi_f(r)=\cdots+P_{10}(\phi, \theta)\times(C/r)k^{-\frac{1}{2}}\cos(kr+\text{constant})+\cdots.$$

Comparing, we find that in order for the two expressions to be identical, C must be proportional to $k^{-\frac{1}{2}}$.

For small values of r, in the region of the K shell of the ion where the major contribution to the matrix element occurs, $\Phi(r)$ is practically independent of k, since the term involving E is negligible compared to the other two terms. Over this region ψ_f involves $\mathbf{k}$ only in the normalization constant C. The matrix element is therefore proportional to $k^{-\frac{1}{2}}$, and the transition probability is proportional to k^{-1}, or $E^{-\frac{1}{2}}$. Thus the probability of an electron transition from the K state to a state in the conduction band in which it has the kinetic energy E is inversely proportional to the square root of E.

Effect of Radiation Width of K State

The effect of radiation width of the K state must also be taken into account in predicting the variation of the absorption coefficient. Consider a photoelectric process in which the atom initially has the energy E_i. Upon absorption of a quantum of energy $h\nu$, an electron is ejected from the K shell of the atom to some unoccupied electron state. Let the energy of the new state of the atom be E_f. The following energy equation holds:

$$h\nu=E_f-E_i.$$

If the energy of the atom before and after the absorption act could be known exactly, the frequency of the absorbed quantum could be specified exactly.

Actually, however, the energy E_f cannot be known precisely. The reason is that the atom does not remain long in a state of K excitation because of the high probability of the subsequent emission of a K series quantum. According to the Heisenberg uncertainty principle, one cannot know simultaneously the energy of a system and the time at which it has this energy. The product

[7] W. Voss, Zeits. f. Physik **83**, 581 (1933).

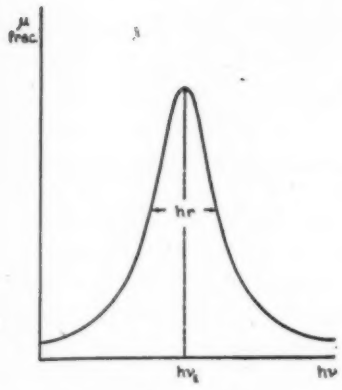

FIG. 2. Fractional absorption coefficient as a function of the energy of the absorbed quantum.

of the uncertainties in these two variables must be of the order of Planck's constant. The energy E_f is therefore uncertain by an amount which is inversely proportional to the lifetime of the atom in a state of K excitation.

Weisskopf and Wigner[8] have shown that the probability of absorption of a quantum of frequency between ν and $\nu+d\nu$, causing transition of an electron between two states whose energy separation is $h\nu_E$ is given by

$$P(\nu)d\nu=\frac{C_1\Gamma d\nu}{(\nu-\nu_E)^2+(\Gamma/2)^2}.$$

Here C_1 is a constant, and $2\pi\Gamma$ is the reciprocal of the mean lifetime of the atom in the excited state.

The fraction of the absorption coefficient for the atom due solely to transitions between these two states, which is proportional to this probability, is therefore given by a classical dispersion curve (Fig. 2) with a peak at $h\nu_E$ and a full width at half-maximum equal to $h\Gamma$.

For K absorption in metallic potassium, the total absorption coefficient $\mu(\nu)$ is simply the sum of these fractional absorption coefficients for transitions from the K shell to the various unoccupied states in the conduction band, if each fractional absorption coefficient is weighted by its relative probability.

$$\mu(\nu)=C_1\sum_i\frac{P(i)\Gamma}{(\nu-\nu_i)^2+(\Gamma/2)^2},$$

where the index i denotes the particular state in the conduction band, and $P(i)$ is the relative probability of an electron transition from the K state to the ith band state. Γ is the same for all band states.

There are actually a great number of states in the conduction band, and the energy gap between any two states is very small, so the summation may be replaced by an integral. If the zero of energy be taken as the energy of the initial state, let $h\nu_i$ be the energy of the atom with a K electron ejected to the ith band state. Let $N(h\nu_i)$ be the number of states per unit energy interval in the neighborhood of the ith band state, and the summation may then be written

$$\mu(\nu)=C_2\int\frac{P(i)N(h\nu_i)d\nu_i}{(\nu-\nu_i)^2+(\Gamma/2)^2},$$

where C_2 is another constant. The integration extends over all unoccupied band states. It has been shown, however, that for metallic potassium in the approximation of constant potential within the lattice, the quantity $N(h\nu_i)$ is proportional to the square root of the kinetic energy of the ith electron, and the square of the matrix element is inversely proportional to the same quantity. The transition probability $P(i)$ is proportional to the square of the matrix element and to the quantity[9] $(\nu_0/\nu_i)^{8/3}$ where $h\nu_0$ is the energy of the electron of lowest energy in the conduction band. Thus the product $P(i)N(h\nu_i)$ is simply proportional to $(\nu_0/\nu_i)^{8/3}$. This quantity varies very slowly over the region where the integrand is appreciable, and is essentially equal to unity over the entire region of the absorption edge. The integral therefore becomes

$$\mu(\nu)=C_3\int_{\nu_F}^{\infty}\frac{d\nu_i}{(\nu-\nu_i)^2+(\Gamma/2)^2},$$

where C_3 is another constant. The integration extends from ν_F, where $h\nu_F$ is the energy of the electron in the highest occupied state, to infinity. It was shown above that $h(\nu_F-\nu_0)$ is about 2.06 electron volts.

Carrying out the integration, we find the following expression for the absorption coefficient:

$$\mu(\nu)=C_4\left\{\frac{\pi}{2}+\tan^{-1}\frac{(\nu-\nu_F)}{\Gamma/2}\right\}.$$

[8] V. Weisskopf, Physik. Zeits. **34**, 1 (1933).

[9] Reference 6, page 475.

Additional Absorption Processes

These calculations deal only with the fraction of the absorption coefficient caused by transitions from the K shell to the conduction band. There is a further contribution due to ejection of electrons from the L and M shells. This contribution, small compared to the K absorption and practically constant over the region of the K edge, may be included by adding a constant term to the expression for the absorption coefficient. A slight diminution of the transmitted beam, and hence a slight addition to the measured absorption coefficient, is caused by scattering of radiation in other than the forward direction. This effect may also be accounted for by the use of an additive constant. The value of the total additive constant may be determined from experimental data. No such data are available for metallic potassium, but for neighboring elements in the periodic table this constant, representing an unchanging background of absorption, is about one-tenth of the maximum value of $\mu(\nu)$ over the immediate region of the K absorption edge. Upon adding such a term to the expression previously derived for the absorption coefficient of metallic potassium, one obtains:

$$\mu(\nu)=C_4\left\{\frac{11\pi}{18}+\tan^{-1}\frac{(\nu-\nu_F)}{\Gamma/2}\right\}. \qquad (I)$$

Summary of Theoretical Predictions

An expression may be obtained for the absorption coefficient of metallic potassium in the region of the K edge if the conduction electrons are assumed to move in a region of constant potential within the lattice. Under these circumstances the density of states to which an electron may be ejected is proportional to the square root of its kinetic energy, and the probability of a given transition is inversely proportional to the square root of this kinetic energy. Upon including the effect of the radiation width of the K state, an analytic expression was derived for the absorption coefficient due to transitions from the K state to the conduction band. An additive term was inserted to include the effect of other absorption processes.

The approximation of constant potential within the lattice, under which the analytic expression was derived, should be poorest for energies corresponding to electron momenta which give rise to Bragg reflection of the electron within the lattice.

EXPERIMENTAL MEASUREMENTS

The apparatus used in the measurements consisted of an x-ray tube and power supply, a two-crystal vacuum x-ray spectrometer, an ionization chamber and d.c. amplifier, and a number of thin potassium foils.

The power supply was of the standard full-wave rectifier type with filtered output. The voltage output of the power supply was stabilized by an electronic device reported elsewhere.[10] This device not only reduced voltage fluctuations caused by "ripple" but also those due to change in the primary voltage and to variations in characteristics of circuit elements. The voltage across the x-ray tube was found to be constant to within 0.1 percent over the eighteen hour period of the average "run." The tube was operated at 10 kv and 100 ma. Over the same period of time the maximum variation in the tube current was one milliampere.

The x-ray tube has been described elsewhere.[11] The focal spot was rectangular, 3 mm×6 mm. The target was made of an alloy of 12 percent antimony and 88 percent lead. The alloy was "tinned," or coated, on the copper face of the target carrier. The lead gave rise to a high background of continuous radiation, needed for measurements distant from the edge, and the strong antimony $L\alpha_1$ line at 3432 x.u. gave high intensity in the immediate region of the potassium K edge (3429 x.u.).

The absorbers were prepared by the evaporation method. The backing material was Kodapak, 2×10^{-3} cm thick. A protective layer of aluminum, 2×10^{-6} cm thick, was condensed on the Kodapak. Next, a layer of metallic potassium, 8×10^{-4} cm thick, was condensed on the aluminum. Lastly, a protective coating of ceresine was condensed over the metallic potassium surface. The techniques used have been described in some detail elsewhere.[12]

[10] J. W. Trischka and L. G. Parratt, Rev. Sci. Inst. 13, 17 (1942).
[11] L. G. Parratt, Phys. Rev. 54, 99 (1938).
[12] J. B. Platt and D. H. Tomboulian, Rev. Sci. Inst. 12, 612 (1941).

Data were taken with three of the absorbers. Uniformity of thickness of the absorbers was checked by measuring percent transmission at a fixed wave-length for each of several areas of a typical absorber. The wave-length used was on the high energy (and hence the high absorption) side of the potassium *K* edge. No variation as large as 1 percent of the incident intensity was found. A sample of the potassium metal used, analyzed spectroscopically,* contained an impurity of 0.2 percent of sodium. No detectable trace of other impurities was found. Since the evaporation process was completed in fifteen minutes in a vacuum system maintaining a pressure of 10^{-5} mm Hg, no appreciable oxygen contamination was possible.

The spectrometer was of the two-crystal type, with calcite crystals. A vacuum instrument was used to eliminate air absorption of the x-ray beam. Details of the construction have been given elsewhere.[13] A study was made of the physical resolving power of the crystals. It was found that at 710 x.u. the width of the $(1, -1)$ rocking curve was 5.2 seconds of arc, and the $(1, -1)$ percent reflection was 61 percent. At 3598 x.u. the $(1, -1)$ width was 26 seconds of arc, and the $(1, -1)$ percent reflection was 60 percent. In the spectral region in which the potassium *K* edge occurs, the spectrometer had a computed physical resolving power of 11,700. This is the limiting factor in the resolving power of the instrument, since the geometrical resolving power is approximately 60,000.

Changes in the angular position of each of the crystals could be read to the nearest fifth of a second of arc, which corresponds at the wave-length of the potassium *K* edge to 0.005 x.u.

The determination of intensity was made with an ionization chamber. This was filled with argon at a pressure of 26 cm Hg. Dimensions were so chosen in the design of the chamber that wall effects were negligible and electric fields were intense in the region of maximum ionization, thus insuring satisfactorily linear response of the ionization chamber.

The d.c. amplifier was of the modified Barth[14] type, using a Western Electric D96475 tube. The maximum voltage sensitivity of the amplifying circuit was 142,000 mm/volt, with a scale at a distance of two meters and a galvanometer of sensitivity 2.6×10^{-9} ampere/mm at one meter. With the 3×10^{11} ohm grid resistor with which most of the data were taken, the over-all current sensitivity for the amplifier was 2.3×10^{-17} ampere/mm. Random fluctuations of the galvanometer spot were of the order of one centimeter, and the mean position of the spot could be read to an estimated accuracy of three millimeters.

The ionization current produced by the direct beam of continuous radiation alone (without the contribution from the Sb $L\alpha$ lines) was 9.2×10^{-15} ampere, and could be measured with an error of one percent.

The term "random fluctuations" is not intended to include the slow continuous shift of position of the galvanometer spot which occurred with no signal on the grid. This will be called "zero drift" and was the source of the largest single error in the measurement of ionization current. In the best set of data obtained the zero drifted at the rate of two cm/hour, and a drift of the order of eight cm/hour was more usual.

Method of Making Measurements

Measurements were made in the following manner:

1. The spectrometer was so adjusted that the crystals reflected the particular wave-length desired.
2. A lead stop was inserted in the x-ray beam, and the "zero" position of the galvanometer spot was recorded.
3. The lead stop was removed, permitting the direct beam to enter the ionization chamber, and the galvanometer deflection was noted.
4. The potassium absorber was inserted in the beam, and the position of the galvanometer spot was noted.

For subsequent zero drift correction, the time was noted at which each reading was made. In the spectral region in which the chief contribution to the intensity of the beam was that of continuous radiation, several measurements were made on the absorber for each measurement of the direct beam, and a determination of the zero position of the galvanometer spot was made every twenty minutes.

* The writer is indebted to Professor A. W. Laubengayer of Cornell University for the spectroscopic analysis of the potassium metal.

[13] L. G. Parratt, Phys. Rev. **54**, 99 (1938).

[14] D. B. Pennick, Rev. Sci. Inst. **6**, 115 (1935).

All intensity measurements were corrected for zero drift. The measured intensity of the direct beam was then plotted as a function of wave-length. The curve thus obtained was the contour of the Sb $L\alpha_1$ line and the neighboring spectral region on the short wave-length side. From this curve was determined the intensity incident on the absorber at each wave-length setting.

At the completion of a "run," a plot was made of the negative of the logarithm of the fractional transmission of the absorber, as a function of wave-length. Six runs extending 40 x.u. from the edge, and one run over only the 10 x.u. region including the edge, are included in the data presented here.

Since the thickness of the potassium layer and of the ceresine coating could not be assumed to be the same from one absorber to another, corrections were necessary to eliminate the effect of materials other than potassium in the absorber, and to adjust the results to correspond to the same thickness of potassium in each case. The negative of the natural logarithm of the fractional transmission of the absorber may be written

$$\log_e Q=\mu_1x_1+\mu_2x_2+\mu_3x_3+\mu_4x_4,$$

where the μ's are the linear absorption coefficients, the x's the corresponding thickness in centimeters, and the subscript 1 refers to the Kodapak, 2 to the aluminum, 3 to the potassium, and 4 to the ceresine. Within the spectral region investigated, only one element other than potassium has an absorption edge. That element is palladium, which has its L_1 edge at 3421 x.u. The probability of the existence of a detectable trace of palladium in the absorber is very small, and there is only a 10 percent change in transmission at this edge in any case, so one would expect no structure to be introduced into the plot by rapid variation in μ_1, μ_2, or μ_4. Furthermore, the fractional change in wave-length over the spectral region investigated was 1 percent, so the variation in each of these μ's, assuming the validity of the λ^3 law,[15] is only three percent over this spectral region. If one writes

$$\log_e Q=\mu_3x_3+C,$$

where C is a constant, the error can be at most three percent of the value of C.

The value of C, or in other words the baseline, was determined for each absorber by adjusting the baseline to give a "jump ratio" of 10 for potassium. The jump ratio is defined as the ratio of the absorption coefficient on the high absorption side of the edge to that on the low absorption side. No data are given in the literature on the jump ratio for potassium, but interpolation between values for elements of near atomic numbers indicates the value 10. For adjusting baselines, the jump ratio was made 10 for quantum energies five electron volts greater and five electron volts less than that of the midpoint of the edge. As a check, "dummy" absorbers, containing no potassium but prepared otherwise in the same way as the actual absorbers, were used for experimental determination of C. The values of C so determined could not, of course, be taken as those for the actual absorbers, but none of the indirectly determined values of C differed by more than six percent from that for the average of the "dummies."

Having determined μ_3x_3 as a function of wave-length for each of the three absorbers, it remained only to adjust these absorption curves for the same thickness of potassium. This was done by multiplying x_3 for two of the absorbers by constants so chosen as to make the curves coincide at a wave-length corresponding to a quantum energy five electron volts greater than that of the edge.

The x-ray spectrometer used in this research is incapable of absolute wave-length measurements but capable of measuring small wave-length intervals with a high degree of precision. For gross adjustment, the calcite crystals could be moved relative to the scales, but once clamped to the scale mechanism further motion of either crystal could be determined to one-fifth of a second of arc. Comparison of data taken in two "runs" between which the position of a crystal was shifted relative to its scale was possible only if some reference point is determined within each "run." The reference point chosen for comparison of data was the midpoint of the absorption edge.

[15] A. H. Compton and S. K. Allison, *X-Rays in Theory and Experiment* (D. Van Nostrand Company, Inc., New York, 1936), p. 533.

Errors and Corrections

The largest source of uncertainty in relative wave-length measurements was the determination of reference wave-length positions for successive "runs." This potential error, a possible linear shift of one curve relative to another, is a maximum of two seconds of arc, or 0.05 x.u. Absolute determination of wave-lengths was made by reference to the known wave-length of the peak of the Sb $L\alpha_1$ line. This wave-length is given by Hjalmar[16] as 3431.8±0.1 x.u. It was located to within 0.05 x.u. on each of two "runs," and therefore the wave-length scale on any one "run" is known to within 0.1 x.u. with reference to the Sb $L\alpha_1$ line and to within 0.2 x.u. absolutely. It may be argued that the position of the peak of the Sb $L\alpha_1$ line is in question because the target material was an alloy rather than pure antimony. Detectable shifts of the peaks of lines have been observed due to the presence of other elements in the target.[17] The Sb $L\alpha_1$ line, however, results from an electron transition from the *M* shell of the atom to the *L* shell. Since both of these shells lie deep within the antimony atom, the effects of neighboring atoms cannot be expected to shift the energy value of either level, and hence of the emitted quantum, appreciably.

The main source of error in intensity measurements was zero drift. In the best data obtained, the combined effect of zero drift and random fluctuations gave rise to an error in intensity measurements of one percent of the direct beam. For these data, the estimated probable errors caused by zero drift and random fluctuations were each three millimeters. In general, the estimated probable error caused by zero drift was five millimeters. The final results are weighted averages of the data taken on various "runs." Correction was made for the effect of second-order radiation, third and higher orders being ruled out because the tube was operated below the corresponding excitation potentials. The incident beam contained three percent of second-order radiation in the continuum, as determined from absorption measurements on three thicknesses of aluminum foils. A correction was made for second-order radiation in the absorption measurements on potassium. This correction was negligible in the region of the absorption edge because of the high intensity of characteristic radiation.

No correction was attempted for the finite resolving power of the spectrometer. Any such correction for absorption measurements, lacking quantitative knowledge of the diffraction patterns of the two crystals, would be hazardous. Since the measured width of the absorption edge is large compared to the width of the $(1, -1)$ rocking curve at the same wave-length, there is reason to believe that the correction for finite resolving power would be negligible in any case.

The results are presented in Figs. 3 and 4. Figure 3 shows the absorption structure over the entire spectral region investigated, while Fig. 4 includes only the immediate region of the edge. Data were taken every 0.2 x.u. over most of the spectral region investigated, and every 0.07 x.u. over the immediate region of the edge. Probable errors are indicated by vertical lines. The dotted curve is the theoretically predicted absorption structure.

The theoretical curve based on the free electron approximation is in fairly satisfactory agreement with the experimental results. Deviations are less than ±10 percent and are slightly greater than the experimental uncertainty. The fit is achieved with the aid of two arbitrary constants representing the wave-length of the edge and the thickness of the absorber. The constant determining the width of the edge, i.e., the energy separation between points whose absorption coefficients lie at one-quarter and three-quarters of the height of the absorption edge, is not arbitrary. This is the constant Γ in Eq. (I). It is determined by the mean lifetime of the state of *K* excitation, and cannot be evaluated theoretically with precision. However, if this constant is known for some neighboring element in the periodic table for which the possible transitions are similar, it can be calculated for potassium. The calculation, based on the Weisskopf-Wigner theory of line widths and the Dirac radiation theory, assumes that Γ is proportional to the square of the energy of the atom due to *K* excitation. From measurements on argon line

[16] Reference 15, page 528.

[17] A. E. Lindh, *Handbuch der Experimentalphysik* (Akademische Verlagsgesellschaft, M. B. H., Leipzig, 1930), Vol. 24/II, pp. 314–325.

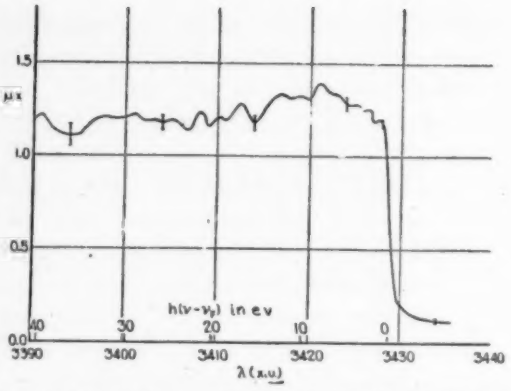

FIG. 3. Absorption coefficient for metallic potassium, in arbitrary units, as a function of the energy of the absorbed quantum. Entire spectral region investigated.

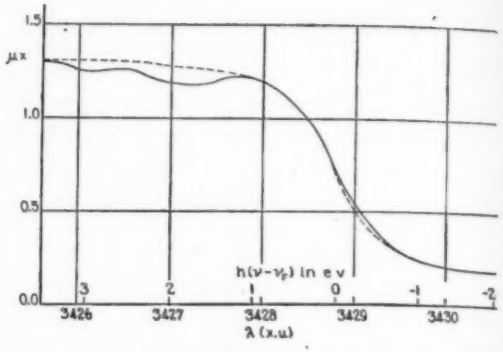

FIG. 4. Absorption coefficient for metallic potassium, in arbitrary units, as a function of the energy of the absorbed quantum. Immediate region of the absorption edge.

widths[18] $h\Gamma$ is known to have the value 0.58 ev for argon. Hence, for potassium, $h\Gamma$ is 0.73 ev. The value found from experimental measurement on the width of the potassium K edge is 0.75 ev.

The experimentally determined values of the absorption coefficient are lower than those predicted on the free electron approximation in just the region (one to three electron volts) corresponding to the first Brillouin zone. The deviation may or may not be meaningful, but should be pointed out.

The wave-length of the midpoint of the absorption edge, where the midpoint is defined to have an absorption coefficient equal to the average of the mean absorption coefficients on the two sides of the edge, has been found to be 3428.8 $\pm$0.2 x.u. This does not agree with the value of 3431.0$\pm$1.0 x.u. given by Lindh.[19]

The author is deeply indebted to Professor Lyman G. Parratt of Cornell University, who suggested this problem, for his continued interest and advice. Much of the theoretical material presented is the result of discussion with Professor Hans A. Bethe of Cornell University, whose guidance the author acknowledges with gratitude.

[18] L. G. Parratt, Phys. Rev. **56**, 295 (1939).

[19] A. E. Lindh, Ark. Mat., Astr. o. Fys. **18**, 14 (1924).

Metastable Ions Formed by Electron Impact in Hydrocarbon Gases

J. A. HIPPLE, R. E. FOX, AND E. U. CONDON*
Westinghouse Research Laboratories, East Pittsburgh, Pennsylvania

(Received January 12, 1946)

It has been recently reported that the non-integral masses appearing in the mass spectra of various hydrocarbons may be explained by the spontaneous dissociation of some of the ions into fragments of lighter mass after they have been accelerated and emerge from the ion gun. By means of an energy filter, an energy analysis of the non-integral masses in *n*-butane, butadiene, and ethane has been made and the values obtained agree with those predicted on the basis that they arise from metastable ions. Variation of the pressure and electrode potentials confirms that the dissociation is spontaneous. The formation of metastable ions appears to be a general occurrence in the ionization and dissociation of hydrocarbons and is shown here to occur in ethane, propane, 1,3-butadiene, butene-1, *cis*-butene-2, isobutylene, normal butane, iso-butane, pentene-2, normal pentane, iso-pentane, and methyl-cyclo-pentane.

INTRODUCTION

A PRELIMINARY report[1] has been made on evidence obtained with the mass spectrometer indicating that some kinds of primary ions formed by electron impact in several hydrocarbon gases are metastable. They are apparently stable enough to hold together for a time of the order of 10^{-6} sec. during which they are drawn out of the ion source region and accelerated, but dissociate before completing their trip through the analyzing magnetic field. The observed facts are in accord with the interpretation that the metastable ions simply fall apart so that the fragments have a small energy of relative motion. This "small" energy may amount to some volts but is small compared to the 500 to 1000 electron volts of energy which the ions are given for analysis in the mass spectrometer.

This paper reports further data obtained by means of the mass spectrometer with energy analysis of the ions which fully confirms and considerably extends the results given earlier. Broadly the phenomenon here discussed bears some resemblance to pre-dissociation, first discovered by Henri[2] in optical band spectra, but it should be observed that when pre-dissociation results in broadening of the lines in the band spectrum, the mean life of the molecule for pre-dissociation must be short compared to the usual radiative life of 10^{-8} sec. Hence optical pre-dissociation studies deal with cases in which the mean life is much smaller than in the cases described in this paper. The range of values of the mean life which may be studied in a particular mass spectrometer is of course dependent on potentials of the electrodes and the dimensions of the tube in the ion source and ion accelerating regions.

These studies grew out of a desire to understand the origin of several broad peaks, some of which occur at positions corresponding to non-integral masses, which were observed in the mass spectrometer. In the first experiments, reported

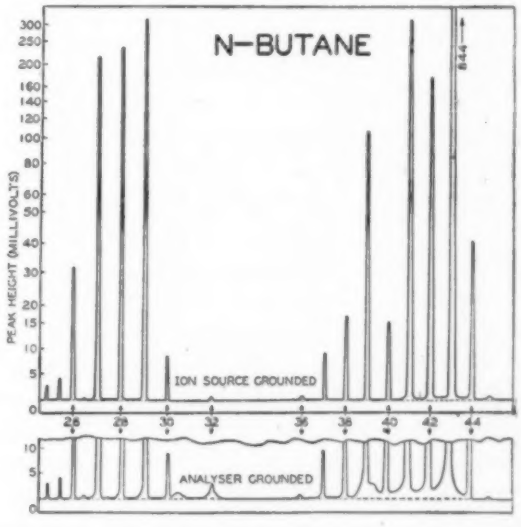

FIG. 1. Showing effect on observed mass spectrum of *n*-butane of operating with ion source grounded instead of with analyzer grounded.

* At present Director of National Bureau of Standards, Washington, D. C.

[1] J. A. Hipple and E. U. Condon, Phys. Rev. 68, 54 (1945).

[2] V. Henri, Comptes rendus 177, 1037 (1923).

earlier, an experiment was performed on the effect on the mass spectrum of operating with the ion source and the collector both at ground while the main accelerating potential was applied to the analyzer section of the tube. Since the ions are formed in a region that is one or two volts above ground, only those ions reach the collector which have essentially as much energy on leaving the analyzer as they acquired on entering it.

Figure 1 shows the mass spectrum of normal butane taken in the two ways, the ion source grounded curve being superposed above the curve taken in the more familiar way in which the analyzer is grounded. Comparing the two curves, the following differences are at once evident:

(a) The broad background from mass 38 to 44 is removed.
(b) The hump on the side of the mass 39 peak is removed.
(c) The mass 32 peak is considerably reduced and sharpened indicating that in the usual spectrum it is really compounded of a broad peak, which is removed when the ion source is grounded, together with a small sharp peak which is unaffected by the change. In later experiments with a tube that was vacuum-tight this mass 32 peak (O_2) was entirely eliminated when the ion source was grounded.
(d) The broad peak at mass 30.5 is removed.

The material which is not collected with the ion source grounded must consist of ions which lose energy in some way in going through the tube. Of course, it is possible that some energy losses occur by impact with the residual gas in the tube but it was thought that this could only account for a general raising of the background around regions of intense ionization.

The hypothesis was considered that these effects might be due to unstable ions which hold together long enough to be accelerated through all or most of the accelerating potential drop but which dissociate, perhaps with a small release of internal energy, somewhere in the tube before they have entered the analyzer, or at least before they have gone through the field. Let the potential be reckoned as zero at the place where the ion is first formed, and suppose the ion has mass m_0 which it retains until it has moved to a place where the potential is V_1. At this place suppose it dissociates with negligible release of internal energy into an ion of mass m and a neutral fragment of mass (m_0-m). The new ion will continue on with little immediate change of velocity, but will in turn be accelerated by the electric field in going from the region of potential V_1 to that of the full voltage V of the accelerating field.

Its kinetic energy just before dissociation is eV_1 but after dissociation the ion fragment has only the kinetic energy, $(m/m_0)eV_1$, the other part being carried off by the neutral fragment. After traversing the whole accelerating field the kinetic energy of the ion fragment is

$$T=(m/m_0)eV_1+e(V-V_1).$$

Now the radius in which it moves in the analyzer is determined by the usual formula,

$$R=\frac{c}{eH}(2mT)^{\frac{1}{2}}.$$

Therefore the ion fragment will appear at the collector for the same combination of V and H as does a normal ion of mass m^* where

$$m^*=\frac{m^2}{m_0}\frac{V_1}{V}+m\left(1-\frac{V_1}{V}\right).$$

If dissociation occurs before the ion is accelerated, then its effective mass is m. However, if dissociation occurs after full acceleration but before entering the analyzer then $(V_1=V)$

$$m^*=m^2/m_0.$$

It has been found that the observations correlate with this expression. The peaks have width which is partly due to the fact that some dissociations occur elsewhere and partly to the effect of the neglected release of internal energy. An additional reason for the diffuseness of the metastable peaks is the focusing property of the instrument. The instrument has been designed to focus ions that maintain a constant m/e in passing through the analyzer. Thus it is probable that the observed diffuse peaks are caused by transitions occurring very close to the exit slit of the ion gun and before the ion has traversed very far into the analyzer. This is confirmed by the spectrum of n-butane obtained by Washburn, Wiley, and Rock[3] on an instrument employing a deflection in the magnetic field of 180°. Although there is no field-free

[3] H. W. Washburn, H. F. Wiley, and S. M. Rock, Ind. Eng. Chem. Anal. Ed. **15**, 541 (1943).

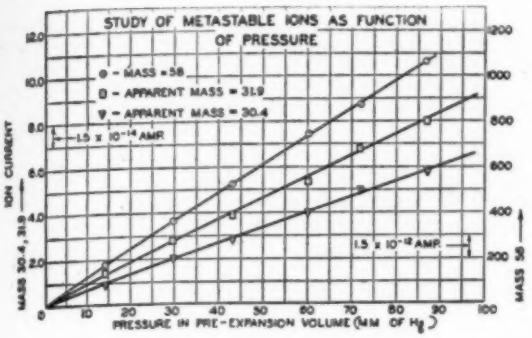
STUDY OF METASTABLE IONS AS FUNCTION OF PRESSURE
O - MASS = 58
□ - APPARENT MASS = 31.9
▽ - APPARENT MASS = 30.4
1.5 x 10⁻¹⁴ AMP.
1.5 x 10⁻¹² AMP.
ION CURRENT
MASS 30.4, 31.9
MASS 58
PRESSURE IN PRE-EXPANSION VOLUME (MM OF Hg)

FIG. 2. Variation of ion current with pressure. The linearity of the curves shows that the peaks at 30.4 and 31.9 are not induced by ion-molecule collisions.

region between the ion source and the analyzer, the diffuse peaks at mass 32 and 39.2 are quite prominent, and there is some indication that those at 25.2 and 30.4 are also present. The ions dissociating elsewhere in the tube will contribute to the background with no pronounced peaks appearing.

Of course, an observation of m^* alone does not suffice to determine both m_0 and m and hence to fix the particular dissociation process responsible for a peak. This was done by arranging to measure the kinetic energy of the ions after they have gone through the analyzer by adjusting the retarding field between the analyzer region and the ion collector, as explained in a later section.

Peaks arising from reactions occurring during the transit of the ions through the mass spectrometer have previously been reported. Smyth reported two peaks in hydrogen[4] having an apparent mass less than one (throughout this paper singly charged ions are being discussed unless explicitly stated). Smyth[5] also reported a peak at mass 7 in N_2 which occurred at low electron voltages. The size of these peaks relative to the parent ion was very sensitive to the pressure in the instrument and they were attributed to collisions with other molecules during the transit through the instrument. Discussing the case of N_2, Smyth[6] concludes "that there are N_2^+ ions, probably those formed at the first ionization potential which dissociate on collision after acquiring large kinetic energies." Hogness and Lunn[7] reported a similar effect in NO—". . . some of the NO^+ ions are unstable toward collision with gas molecules, and on collision dissociate into either N^+ or O^+."

Dissociation of molecules during transit has been observed in several mass spectrographs by the appearance of diffuse traces at non-integral mass numbers on the photographic plate. These are greatly enhanced by increasing the pressure in the field-free region between the electrostatic energy filter and the magnetic analyzer. A very careful study of these "bands" has been made by Mattauch and Lichtblau,[8] who have described 28 different processes of dissociation of this type induced by collision. All of these processes differ from those reported in the present work which it is believed are not induced by collision.

With the improved techniques now available, mass spectrometers are now operated at a pressure 100 to 1000 times lower than in the early experiments and the possibility of dissociation induced by collision is remote. For instance, Smyth found a peak at mass 7 with 30-volt electrons amounting to 3 percent of mass 28 in N_2 in one experiment.[5] Hagstrum and Tate[9] reported the same peak having an appearance potential of 64 ± 2 volts and an abundance relative to N_2^+ of 0.006 percent. This relative abundance was confirmed approximately in the course of the present investigation using 100-volt electrons and no ionization was evident at 50 volts. This work was done with an automatic recorder without pushing the sensitivity beyond 1 part in 20,000, but the ionization below 50 volts at mass 7 must be less than the above figure in our equipment. The conclusion is that mass 7 ($m/e=7$) in N_2 must be attributed to N^{++} in present instruments at the usual operating pressures and the large peak at this mass observed in the early experiments arises from dissociation induced by ion-molecule collisions.

In order to show that the ions at non-integral masses occurring in the spectra of hydrocarbons are caused by spontaneous dissociation and are

[4] H. D. Smyth, Phys. Rev. **25**, 452 (1925).
[5] H. D. Smyth, Proc. Roy. Soc. **A104**, 121 (1923).
[6] H. D. Smyth, Rev. Mod. Phys. **3**, 373 (1931).
[7] T. R. Hogness and E. G. Lunn, Phys. Rev. **30**, 26 (1927).
[8] J Mattauch and H. Lichtblau, Physik. Zeits. **40**, 16 (1939); see also F. W. Aston, *Mass Spectra and Isotopes* (Edward Arnold and Company, London, 1942), page 61.
[9] H. D. Hagstrum and J. T. Tate, Phys. Rev. **59**, 354 (1941).

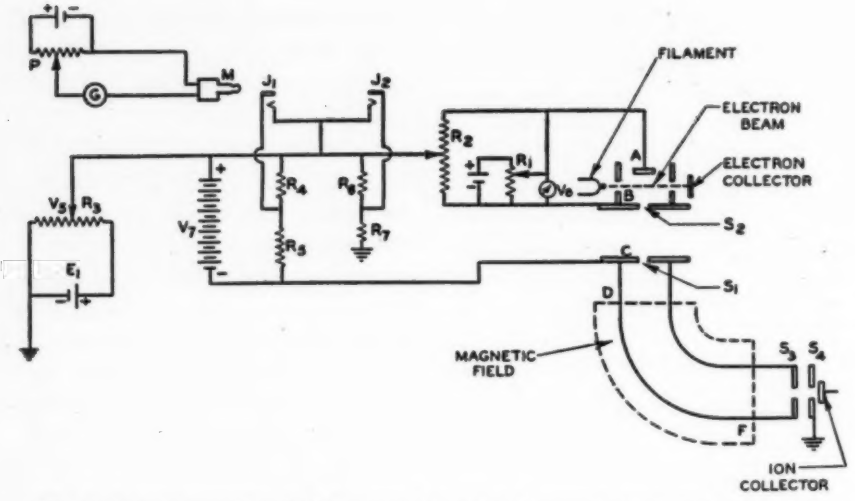

FIG. 3. Arrangement for studying energies of ion fragments from metastable ions.

not to be attributed to ion-molecule collisions, the spectrum of *n*-butane was studied as the pressure in the tube was varied. This tube did not have differential pumping[6] and the analyzer section was not pumped separately; therefore, the pressure in the analyzer varied in the same manner as that in the ion source and any peaks conditioned by collisions in the analyzer should not vary linearly with the pressure. The pressure in back of the leak bleeding the gas into the mass spectrometer tube was used as a measure of the pressure in the tube—the leak had previously been found to have a linear flow characteristic in the range used. The pressure in the large gas reservoir used for stabilizing the flow through the leak was determined by measuring the pressure in a smaller pre-expansion volume with a manometer before the sample was expanded into the larger reservoir. In this way the pressure could be measured accurately. In Fig. 2 the pressure in the pre-expansion reservoir is taken as the abscissa since it is a linear function of the pressure in the tube. This is evident by the linearity of the ion current corresponding to the parent ion $C_4H_{10}^+$ in normal butane. The other curves show that the peaks arising from the metastable ions

$$C_4H_{10}^+ \rightarrow C_3H_7^+ + CH_3, \quad m^* = 31.9,$$
$$C_4H_{10}^+ \rightarrow C_3H_6^+ + CH_4, \quad m^* = 30.4,$$

also vary linearly with the pressure and are, therefore, to be attributed to a primary process. Other strong evidence for this is the effect of the ion-draw-out voltage (V_6 in Fig. 3) on the intensity of the metastable ions relative to the rest of the spectrum which is described in detail later. When less time is spent in the ion source, the abundance of the metastable ions rises rapidly as compared with the rest of the spectrum.

APPARATUS AND EXPERIMENTAL PROCEDURE

The mass spectrometer employed in these experiments was of the type with a sectored magnetic field in which the ions were deflected through 90 degrees on a five-inch radius. An ion accelerating voltage variable from 300–1300 volts was available. The electron energies could be varied by changing the accelerating voltage on the electrons from 0–100 volts.

The ions were measured with a pen recording system whose sensitivity enabled signals of 0.2 millivolts to be recorded. This represented an ion current of about 5×10^{-15} ampere. This recorder, along with certain features of the mass spectrometer has been previously described.[10]

In order to obtain the retarding potential which formed the energy filter, the electrical circuit was arranged as shown in Fig. 3.

An electron beam creates the ions in the region *AB*. By means of a small potential V_6 these ions are drawn through slit S_2 into the accelerating field *BC*. The ions emerging from slit S_1 pass through a field-free region *CD* into the magnetic

[10] J. A. Hipple, D. J. Grove, and W. M. Hickam, Rev. Sci. Inst. **16**, 69 (1945).

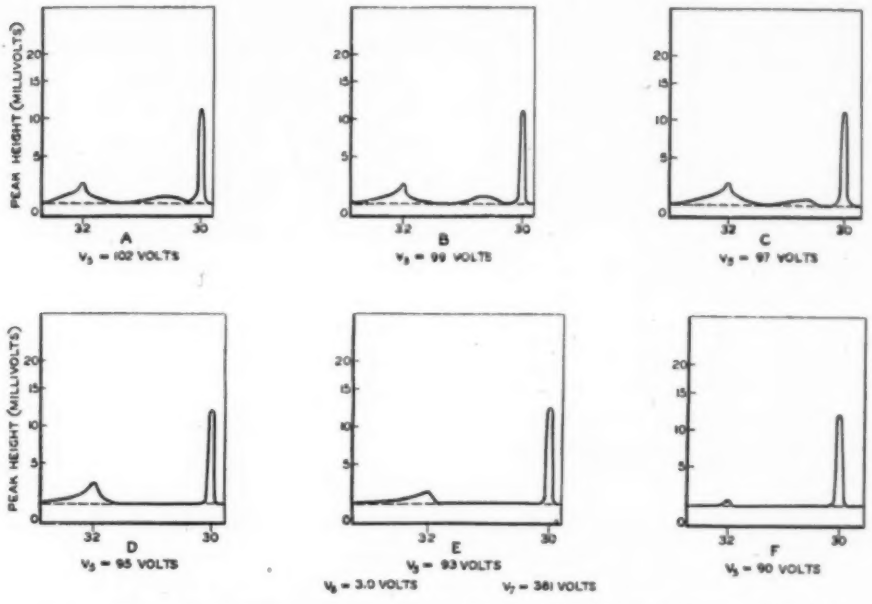

FIG. 4. Effect of energy filter on mass spectrum of *n*-butane in the mass 30 region.

field *DF*. After leaving the magnetic field, they pass through a slit S_3 into the retarding field which is applied between S_3 and S_4. Those ions which are able to penetrate this retarding field are caught by the ion collector and measured with the recording system.

An ion accelerating voltage V_7 was applied between slits S_1 and S_2 in which S_1 was negative with respect to S_2. The ion source was connected to ground through a variable voltage supply V_5. S_4 was maintained at ground potential. Since the potential of the ion source and analyzer could be varied with respect to ground potential by means of R_3, the retarding potential between S_3 and S_4 could be adjusted so as to allow the metastable ions to be completely filtered. A measure of the voltage V_5 which would just enable these ions to get through to the ion collector would then be a measure of the energy lost in the dissociation. The potentials V_5 and V_7 were obtained with banks of batteries.

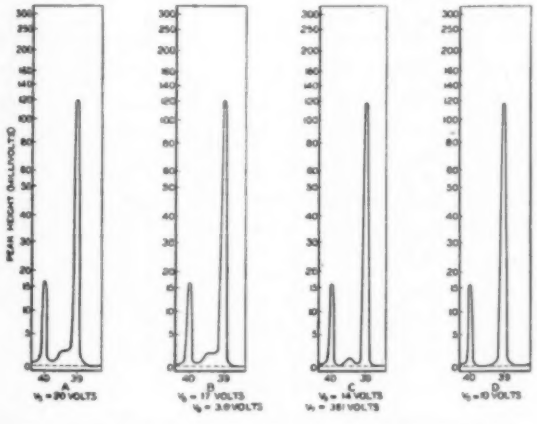

FIG. 5. Effect of energy filter on mass spectrum of *n*-butane in the mass 39 region.

Since the ions are drawn out of AB with about 3 volts, it was necessary to take this voltage into consideration as the ions would then not be formed at ground potential. This was done by means of the resistor R_2. This resistor was placed across plates A and B and in parallel with the source of potential used to draw out the ions from that region. R_3 was adjusted so that V_5 was zero. R_2 was then adjusted until the primary ions were just beginning to be cut off. Thus the voltage V_5 which just cut off the ions in question was then a good measure of the energy lost.

The voltages V_5 and V_7 were measured with a potentiometer P. This potentiometer measured the voltage drop across the bleeder resistors R_4 and R_6. The potential drop across the resistor R_4 gave a value of the voltage V_7 while that across R_6 gave the voltage V_5. R_4 and R_6 were 1500 ohms each while R_5 and R_7 were 3×10^6 ohms each. The resistors in each bleeder were matched to better than 0.1 percent. The potentiometer

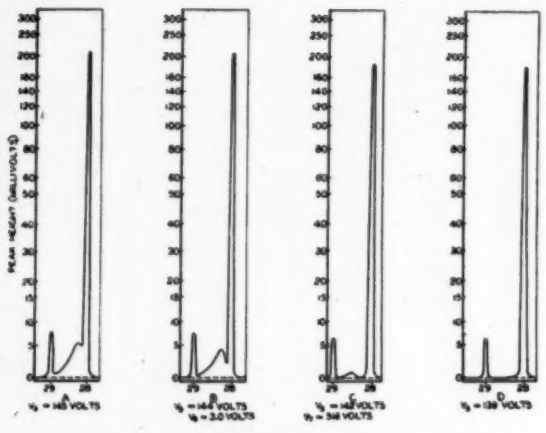

FIG. 6. Effect of energy filter on mass spectrum of 1,3-butadiene in the mass 28 region.

circuit measured each of the voltages by means of the two jacks J_1 and J_2, the accuracy being about 0.2 volt.

With this arrangement the spectra of *n*-butane, 1,3-butadiene and ethane were studied to determine the transitions giving rise to the metastable ions. The spectra were scanned by varying the magnetic field.

DISCUSSION OF SOME HYDROCARBON SPECTRA

1. Normal Butane

In addition to the normal sharply defined peaks in the mass spectrum, there are broad peaks at effective masses about 32 and 30.5 and a large hump on the side of the 39 peak which appears to be superposed on the normal 39 peak. There is also a slight hump at 25.2.

The peak at 32 is associated with the transition

$$C_4H_{10}^+ (58) \rightarrow C_3H_7^+ (43) + CH_3 (15),$$

for which $m^* = (43)^2/58 = 31.9$. This assumption has in its favor the fact that mass 43 is a very prominent peak in the normal spectrum. If the assumption is correct, then the ions responsible have only (43/58) of the kinetic energy corresponding to the total applied potential of 361 volts. This means that in the energy filter this peak should disappear if the ions are caused to go against a retarding field of more than

$$(43/58) \times 361 = 268 \text{ volts}.$$

They, therefore, will have lost 93 electron volts of kinetic energy, which actually went to the unobserved neutral methyl radical.

Figure 4 shows the effect of the energy filter on the mass 32 region as V_5, the potential of the ion source with respect to ground is varied. The diffuse peak is present for $V_5 = 95$ volts but begins to go out as V_5 is further diminished and is quite gone at $V_5 = 90$ volts. In curve *F* of Fig. 4 the remaining small sharp peak at mass 32 is due to O_2^+ from a small trace of that gas in the tube.

Similarly the diffuse peak at $m^* = 30.5$ also shown in Fig. 4 may be associated with

$$C_4H_{10}^+ (58) \rightarrow C_3H_6^+ (42) + CH_4 (16),$$

for which $m^* = (42)^2/58 = 30.4$. In this transition 16/58 of the original energy is lost to the ion fragment on dissociation. This is 99.5 volts and in Fig. 4 it is clearly seen that the 30.5 peak starts to disappear at 99 volts and is cleaned out at 95 volts—a higher value of V_5 than the diffuse 32 peak, in accord with this interpretation.

The hump at $m^* = 39$ is associated with the transition

$$C_3H_7^+ (43) \rightarrow C_3H_5^+ (41) + H_2 (2)$$

giving a calculated $m^* = 39.2$. The calculated energy loss of the ion fragment is 2/43 of 361 or 16.3 volts. Figure 5 shows the effect of the energy filter on this region of the mass spectrum. Again the expected behavior is obtained, a considerable portion of the hump being removed in going from 17 to 14 volts.

The weak ion current appearing at 25^+ may be explained by the transition

$$C_2H_5^+ (29) \rightarrow C_2H_3^+ (27) + H_2 (2)$$

from which $m^* = (27)^2/29 = 25.1$. It has been found that this diffuse peak may be erased from the spectrum when $V_5 = 24.0$ which agrees well with the deduced value of $(2/29) \times 361 = 24.8$ volts.

It should be emphasized that these experiments do not reveal the nature of the neutral fragment that is formed. Thus, in the preceding equations what we write as CH_4 may possibly represent production of this material in dissociated form such as $CH_3 + H$ or $CH_2 + H_2$, etc.

2. Propane

It is interesting that the two transitions observed with propane are the same as two of those

found in *n*-butane. Diffuse peaks were observed at 39.2 and 25.2 corresponding to the transitions

$$C_3H_7^+ (43) \rightarrow C_3H_5^+ (41) + H_2 (2), \quad m^* = 39.2,$$

and

$$C_3H_5^+ (29) \rightarrow C_2H_7^+ (27) + H_2 (2), \quad m^* = 25.2.$$

These transitions were not studied with the energy filter.

3. Ethane

Diffuse peaks are observed at 24^+, 25^+, and 26^+. These may be explained by the transitions

$$C_2H_6^+ (30) \rightarrow C_2H_4^+ (28) + H_2 (2), \quad m^* = 26.2, \quad V_L = 34.4,$$

$$C_2H_5^+ (29) \rightarrow C_2H_3^+ (27) + H_2 (2), \quad m^* = 25.2, \quad V_L = 35.4,$$

$$C_2H_4^+ (28) \rightarrow C_2H_2^+ (26) + H_2 (2), \quad m^* = 24.2, \quad V_L = 36.8,$$

where V_L is the energy lost by the ion to the neutral fragment.

In this study an ion accelerating voltage of 516 volts was used and the measured value of voltages at which the peaks started to disappear were 35.0, 36.0, and 37.0 volts, respectively—in nice agreement with the values of V_L given above.

4. 1,3-Butadiene

In the mass spectrum of 1,3-butadiene,

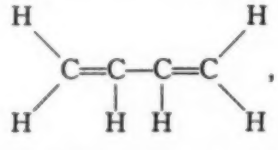

there is a large diffuse peak at about mass 28.2 and a smaller one at about mass 13.8. The parent mass is 54 and the large diffuse peak at 28.2 can be associated with the transition $54^+ \rightarrow 39^+ + 15$ for which the calculated m^* is $(39)^2/54 = 28.2$ although not immediately evident from the structure. However, 39^+ and 54^+ are the largest peaks in 1,3-butadiene.

Figure 6 shows the effect of the energy filter on the mass 28 region which shows that the peak begins to disappear for $V_5 = 144$ volts and is removed when $V_5 = 139$ volts. The expected loss is $(15/54) \times 516 = 143$ volts.

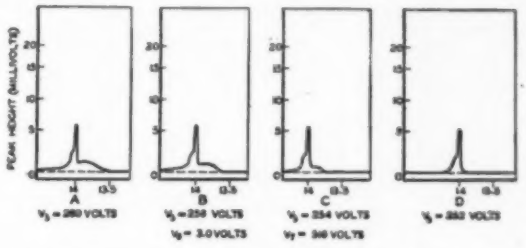

FIG. 7. Effect of energy filter on mass spectrum of 1,3-butadiene in the mass 14 region.

The diffuse peak at mass 13.5 is shown in Fig. 7 for various values of V_5. This peak is associated with a simple splitting in half of the parent ion, $54^+ \rightarrow 27^+ + 27$, which leads to a calculated m^* of 13.5. On this view the ion fragment has only one-half of the original energy and so can be stopped by a retarding potential of 258 volts in good agreement with the experimental value ($V_5 = 256^+$ volts) shown in the figure. The remaining asymmetry on mass 14 is caused by the production of CH_2 with kinetic energy.

These interpretations indicate that there are two different ways in which the parent ion can break up, the dropping off of a methyl group being considerably more probable than the process of splitting in half.

5. Iso-butane

Iso-butane shows the same broad peaks as normal butane except for some differences in relative intensity. The peaks at 31.9 and 30.5 are much weaker than those from *n*-butane, and the "hump" at 39.2 is about twice as strong as in the case of *n*-butane.

These differences correlate with the fact that 58^+, which is interpreted as giving rise to 31.9 and 30.5, is relatively stronger in *n*-butane than isobutane, whereas 43^+, which is interpreted as the source of the 39.2 hump, is relatively stronger in isobutane than *n*-butane.

6. The butenes

The spectra of butene-1, *cis* butene-2, and isobutylene were studied and no important differences were noted with respect to peaks due to metastable ions.

A broad diffuse peak appears at mass 30 similar in appearance to the 31.9 peak in the butanes.

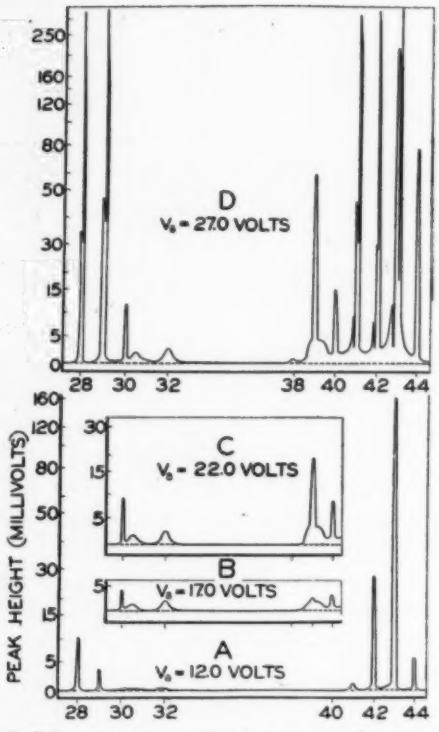

FIG. 8. Mass spectrum of *n*-butane in the mass 28–44 region showing the effect of variation of the electron voltage. The discontinuities indicate a change to $\frac{1}{10}$ sensitivity to record the tops of the large peaks.

This is interpreted as being due to decomposition of the parent ion by the dropping of a methyl group,

$$56^+ \rightarrow 41^+ + 15,$$

the calculated m^* being $(41)^2/56 = 30.0$.

The "hump" now appears at mass 37 instead of mass 39 and may be associated with the transition,

$$41^+ \rightarrow 39^+ + 2.$$

7. Normal pentane

With normal pentane there is a very diffuse peak at mass 24.5. This peak can be associated with the transition

$$72^+ \rightarrow 42^+ + 30, \quad m^* = 24.5.$$

There is also a very broad peak between 29 and 30 which can be regarded as due to

$$57^+ \rightarrow 41^+ + 16, \quad m^* = 29.5.$$

A "hump" is also present on the 39 peak as in the butanes.

This spectrum has not been studied with the energy filter to give detailed confirmation of the suggested transitions. It might be expected that the parent 72^+ ion could drop a methyl group. This would lead to a predicted diffuse peak at $m^* = 45.3$ but there is no indication of such a process in our observations.

TABLE I. Peak heights in normal butane spectrum.

Mass	V_e=1.0	2.0	3.0	4.0	5.0
58	246.0	425.6	437.9	431.3	430.2
57	41.08	68.67	71.22	70.25	69.55
43	1243	2016	2129	2119	2129
42	174.6	278.2	291.6	288.2	287.2
41	349.0	541.1	563.4	553.5	553.5
40	15.38	24.16	25.66	25.93	26.00
39	114.0	178.9	189.5	187.6	189.7
39.2	1.28	2.84	3.36	3.99	4.26
31.9	0.88	1.94	2.39	2.61	2.89
30.5	0.27	1.03	1.37	1.49	1.64

8. Iso-pentane

The same diffuse peaks are observed here as with *n*-pentane, presumably arising from the same transitions. In iso-pentane the 57 peak is about twice that for *n*-pentane and correspondingly the diffuse 29.5 peak is about twice as intense as in *n*-pentane. On the other hand the situation is reversed with regard to the parent ion 72^+ and its associated diffuse peak at 24.5 where the *n*-pentane intensity is about four times that in iso-pentane.

9. Pentene-2

Pentene-2 shows diffuse peaks at masses 24, 15.3, 27.8, and 51. These peaks can be interpreted by the following transitions, with the corresponding calculated m^*,

$$70^+ \rightarrow 41^+ + 29, \quad m^* = 24.0,$$

$$55^+ \rightarrow 39^+ + 16, \quad m^* = 27.7,$$

$$55^+ \rightarrow 29^+ + 26, \quad m^* = 15.3,$$

$$55^+ \rightarrow 53^+ + 2, \quad m^* = 51.1.$$

TABLE II. Relative peak heights at various voltages.

Ion-draw-out voltage	Mass 58	57	43	42	41	40	39	39.2	31.9	30.5
1.0	1.00	1.00	1.00	1.00	1.00	1.00	1.00	1.00	1.00	1.00
2.0	1.73	1.67	1.62	1.59	1.55	1.57	1.57	2.22	2.21	3.82
3.0	1.78	1.73	1.71	1.67	1.61	1.67	1.66	2.62	2.72	5.26
4.0	1.75	1.71	1.70	1.65	1.59	1.69	1.65	3.11	2.97	5.52
5.0	1.75	1.70	1.71	1.65	1.59	1.69	1.66	3.33	3.29	6.07

10. Methyl Cyclo-Pentane

Diffuse peaks are observed in methyl cyclopentane at 56.8 and 37.4. The following transitions could account for these:

$$C_6H_{12}^+ (84) \rightarrow C_5H_7^+ (69) + CH_3 (15), \quad m^* = 56.7,$$

$$C_6H_{12}^+ (84) \rightarrow C_4H_8^+ (56) + C_2H_4 (28), \quad m^* = 37.4.$$

EFFECT OF ION-DRAW-OUT POTENTIALS

Since the ions spend a considerable portion of their lifetime in the ion source, it should be possible to change the magnitude of those peaks originating from the metastable ions by changing the time spent in this region. This can be accomplished by changing the potential with which the ions are drawn from the ion source into the main accelerating field. This potential is represented by V_6 in Fig. 3. With an increase in this voltage the ions are drawn out faster and hence they spend a shorter time in this region. Thus more ions have a chance to dissociate in the regions where the effect can be detected.

A complication arises, however, in that an increase in V_6 not only increases these metastable peaks, but also affects all of the peaks in general because of the change in the focusing conditions. In order to obtain some idea as to the effect of V_6 on the dissociation phenomenon, it is necessary to look at the peak ratios.

Table I presents the peak heights in arbitrary units of some masses in the normal butane spectrum taken at several values of V_6.

Table II is derived from Table I. The data are normalized to show more clearly the relative change in the peak heights as V_6 is increased. From this table it is noted that from 2.0 through 5.0 volts, peaks 58, 57, 43, 42, 41, 40, and 39 remained fairly constant, and that they all changed by approximately the same percentage between 1.0 and 2.0 volts. However, those peaks which are attributed to the metastable ions changed by a greater percentage between 1.0 and 2.0 volts, and they continued to increase as V_6 was increased. In fact it is noted that the 30.5 peak is six times as large at 5.0 volts as at 1.0 volt, while the 31.9 peak is over three times as large.

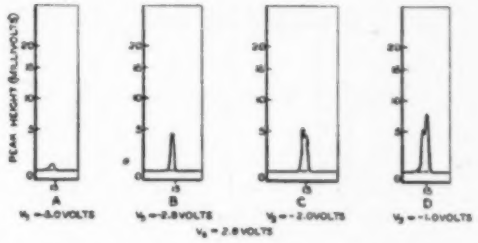

FIG. 9. Study of mass 15 in *n*-butane with the energy filter to show that the doublet is caused by the formation of CH_3^+ with kinetic energy and not by a metastable ion.

EFFECT OF ELECTRON ENERGY

A study of the metastable ions in *n*-butane[11] as a function of the electron voltage V_8 is shown in Fig. 8. The spectrum in the 28–44 mass region is shown with $V_8 = 12$, 17, 22, and 27 volts. With 12-volt electrons the metastable ions at 30.5 and 31.9 are just appearing whereas the "hump" at 39.2 has not appeared. At 17 volts the 39.2 peak has appeared, although the true mass 39 peak is barely evident. Since the metastable peaks are weak, it is difficult to measure their appearance potentials accurately. However, it is interesting that mass 43 and the apparent mass 31.9 appear at the same voltage within the accuracy of the measurements (about 0.5 volts); in the former case the reaction

$$C_4H_{10}^+ \rightarrow C_3H_7^+ + CH_3$$

occurs before the acceleration in the ion gun (region *AB* in Fig. 3), and in the latter case after this acceleration (after *BC* in Fig. 3). The appearance potential of 39.2 is about 2.5 volts higher than that for 31.9.

IONS FORMED WITH KINETIC ENERGY

Since the mass spectrometer of the type used in this work will not focus ions of the same m/e which differ in energy, those ion fragments which are formed from the parent molecule with appreciable kinetic energy will give rise to asymmetrical peaks. A measurement of the kinetic energy released in the ionization and dissociation of some less complicated molecules has provided a greater insight into the dissociation processes involved in these molecules.[12,9] Part of the

[11] D. P. Stevenson and J. A. Hipple, J. Am. Chem. Soc. **64**, 1588 (1942).
[12] W. Bleakney, Phys. Rev. **35**, 1180 (1930).

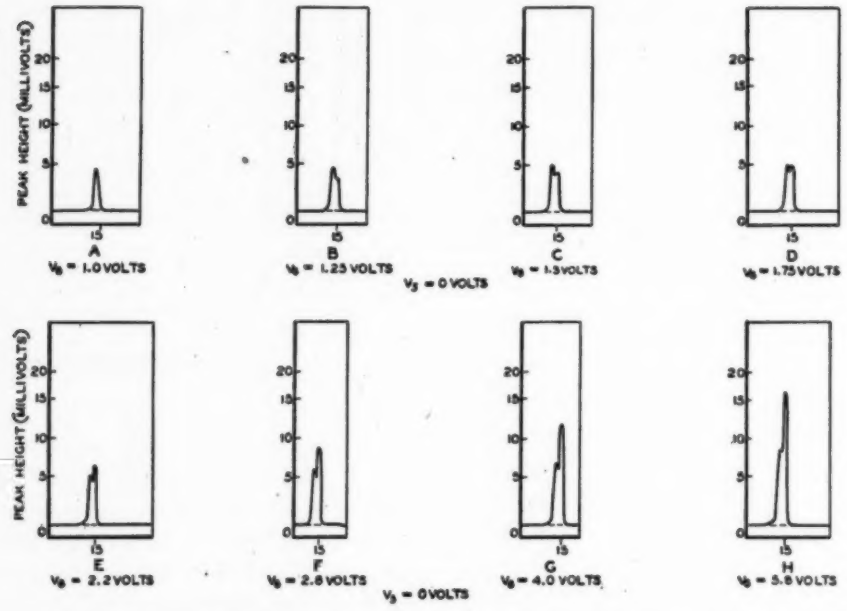

FIG. 10. Showing the difference in the effect of the ion-draw-out voltage (V_6) on the CH_3^+ in *n*-butane formed with considerable kinetic energy as compared with the fragment formed with little or no kinetic energy.

asymmetry in Fig. 7 was ascribed to the formation of CH_2^+ with kinetic energy in butadiene. Similarly, in *n*-butane there appears to be a weak kinetic energy peak at mass 14 and a pronounced one at mass 15. These ions still reached the ion collector when electrode *A* (Fig. 3) was grounded, eliminating all the other peaks in the spectrum between mass 15 and mass 60. Under this condition only those ions formed initially with kinetic energy can reach the ion collector. Although this is not a metastable effect, the investigation of mass 15 is described in this paper as there is a non-integral mass involved here which might be mistakenly interpreted as arising from a metastable ion unless proven otherwise. If the ion formed with kinetic energy is designated $*CH_3^+$, it is seen in Fig. 9 that this ion is relatively unaffected when V_5 is varied from -1.0 volts to -2.8 volts whereas CH_3^+ disappears at -2.8 volts. In fact, $*CH_3^+$ is still present when $V_5 = -5.0$ volts. Figure 10 shows that $*CH_3^+$ is less affected by V_6 in the range studied than CH_3^+ which is reasonable on geometrical considerations. Similar studies have shown the presence of ions formed with considerable kinetic energy in the C_2 and C_3 regions.

Heat Treatment of Semi-Conductors and Contact Rectification*

B. SERIN
Randal Morgan Laboratory of Physics, University of Pennsylvania, Philadelphia, Pennsylvania
(Received December 21, 1945)

It is suggested that the heat treatment results in the formation of a layer low in impurity concentration near the surface of the semi-conductor. This is the result of a rapid evaporation of impurity atoms from the surface and a slower influx by diffusion from the interior. The conditions for the formation of this layer are discussed, and an expression for the ratio of the evaporation coefficient to the diffusion coefficient is derived. The effect of the depleted layer on the electrical characteristics of a semi-conductor-metal rectifying contact are calculated on the basis of the diode theory of rectification; and it is shown that the heat treatment results in increased back resistance and decreased contact capacity. The effect of these changes on the efficiency of rectification is discussed.

INTRODUCTION

THE preparation of semi-conductor-metal contact rectifiers usually involves the heating of the semi-conductor before the rectifier is assembled. In particular, in making silicon-tungsten point contact rectifiers, the silicon is heated at approximately 1000°C for about one hour. The silicon in these rectifiers has semi-conducting properties by virtue of the presence of impurities, small quantities of aluminum or boron, which are deliberately added to the original silicon melt.

We propose that one of the effects of the heating is to cause evaporation of the impurities from the surface of the semi-conductor. If the diffusion rate of the impurity in the bulk of the semi-conductor is slow enough, the decrease in impurity content near the surface will not be compensated by an influx of impurities from the bulk material. After some time, a layer low in impurity concentration will form near the surface of the semi-conductor. This change in impurity concentration near the surface, in turn, changes the electrical characteristics of a metal-semi-conductor contact.

The latest procedures of silicon preparation also involve polishing the surface and sometimes etching the surface. Further, the silicon is heated in air, and the resulting oxide layer is then dissolved away. These procedures undoubtedly change the surface and thus the character of the rectifying contact. These changes are hard to treat theoretically and are not understood, and we shall neglect them.

We shall treat only the simple case of heating in a vacuum, so as to avoid the complication introduced by the oxide surface layer. Heating in air probably produces effects of the same general nature as those that we discuss.

PRODUCTION OF A SURFACE LAYER DEPLETED OF IMPURITY ATOMS

We consider a semi-infinite, homogeneous, isotropic block of semi-conductor with its plane face at $x=0$, containing initially a uniform concentration N_0 of impurity atoms. The concentration of impurities in the semi-conductor at a distance x from the surface at a later time t is given by the solution of the diffusion equation

$$\mathfrak{D}\partial^2 N/\partial x^2 = \partial N/\partial t, \qquad (1)$$

subject to the appropriate boundary conditions, where $\mathfrak{D}$ is the diffusion coefficient.

We assume that the rate of loss of impurity atoms per unit area from the surface is proportional to the surface concentration, i.e., equal to $kN(0, t)$, where we call k the evaporation coefficient. If the concentration of impurities outside the semi-conductor is maintained equal to zero, it follows from the equation of continuity that

$$-\mathfrak{D}(\partial N/\partial x)_{x=0} + kN(0, t) = 0.$$

This is the first boundary condition. The other

* This work was done in part under Contract No. OEMsr-388, with The Trustees of the University of Pennsylvania under the auspices of the Office of Scientific Research and Development, which assumes no responsibility for the accuracy of the statements contained herein.

boundary conditions are clearly

$$N(x,0)=N_0, \quad x>0;$$
$$N(\infty,t)=N_0.$$

The solution of the analogous problem in heat flow (a semi-infinite body initially at uniform temperature losing heat by radiation into a region of zero temperature) is known,[1] so that by the proper substitution of variables, the solution of Eq. (1) is

$$N/N_0=F\{2^{-1}x(\mathfrak{D}t)^{-\frac{1}{2}}\}$$
$$+[1-F\{2^{-1}x(\mathfrak{D}t)^{-\frac{1}{2}}+(\mathfrak{D}t)^{\frac{1}{2}}k\mathfrak{D}^{-1}\}]$$
$$\times\exp(xk\mathfrak{D}^{-1}+\mathfrak{D}tk^2\mathfrak{D}^{-2}),$$

with

$$F\{u\}=2\pi^{-\frac{1}{2}}\int_0^u dy\cdot\exp(-y^2).$$

For large values of $(\mathfrak{D}tk^2\mathfrak{D}^{-2})$, this solution may be approximated by the simpler form

$$N/N_0=F\{2^{-1}\pi^{\frac{1}{2}}\alpha_0xk\mathfrak{D}^{-1}\}$$
$$+[\exp(-4^{-1}\pi\alpha_0^2x^2k^2\mathfrak{D}^{-2})]$$
$$\times[2^{-1}\pi\alpha_0k\mathfrak{D}^{-1}x+\alpha_0^{-1}]^{-1}, \quad (2)$$

where

$$(N/N_0)_{x=0}=\alpha_0\equiv[(\pi\mathfrak{D}t)^{\frac{1}{2}}k\mathfrak{D}^{-1}]^{-1},$$

so that α_0 is the relative surface concentration. This approximation is valid in the limit that we may neglect α_0^3 compared with α_0. Physically, we are interested only in the case of low surface concentration, so that Eq. (2) is the form of solution which is most useful.

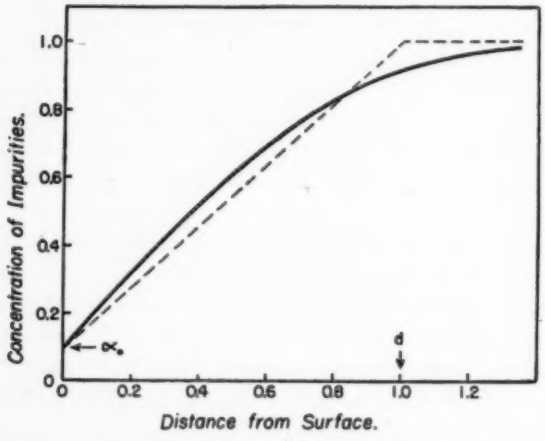

FIG. 1. The relative concentration of impurities is plotted as a function of the distance from the surface in units of the total thickness of the depleted layer. The dashed curve shows the linear approximation.

Substituting for x in Eq. (2) the value

$$d\equiv(\alpha_0k\mathfrak{D}^{-1})^{-1},$$

we obtain

$$(N/N_0)_{x=d}\simeq 0.9.$$

We call d the thickness of the depleted layer. Figure 1 shows a plot of N/N_0 as a function of x in units of d, for $\alpha_0=0.1$. We note that this curve may be roughly approximated by the linear relationship shown by the dotted curve.

If we require that $\alpha_0=0.1$, then for values of the thickness of the depleted layer $d\geqslant 10^{-6}$ cm, we obtain that $k/\mathfrak{D}\leqslant 10^7\,\mathrm{cm}^{-1}$. However, the smaller $k/\mathfrak{D}$, the longer the time it takes to realize a given α_0 and d. In the next section we discuss the factors which determine the magnitude of $k/\mathfrak{D}$.

RATIO OF EVAPORATION COEFFICIENT TO DIFFUSION COEFFICIENT

The diffusion coefficient may be expressed in terms of atomic parameters[2] as

$$\mathfrak{D}=a\delta^2\cdot\exp(-\epsilon'/KT), \quad (3)$$

where a is the "jumping frequency" of a substituted impurity atom in the bulk crystal lattice, δ is the distance between adjacent bulk atoms, ϵ' is the activation energy for diffusion, K is Boltzmann's constant, and T is the absolute temperature.

To derive an analogous expression for the evaporation coefficient we note that the rate at which impurity atoms leave the surface equals the product of the number of impurities on the surface and the probability per second that an atom will leave. We assume that the number of impurities on the surface is the number contained in the first atomic layer, and the probability that an atom will leave is given by

$$a\cdot\exp(-\epsilon''/KT),$$

where a is the same jumping frequency and ϵ'' is the activation energy for evaporation; thus

$$k=a\delta\cdot\exp(-\epsilon''/KT). \quad (4)$$

[1] H. S. Carslaw, *Introduction to the Theory of Fourier Series and Integrals and the Theory of the Conduction of Heat* (The Macmillan Company, New York, 1906), pp. 245–247.

[2] F. Seitz, *Modern Theory of Solids* (McGraw-Hill Book Company, Inc., New York, 1940), pp. 494–496.

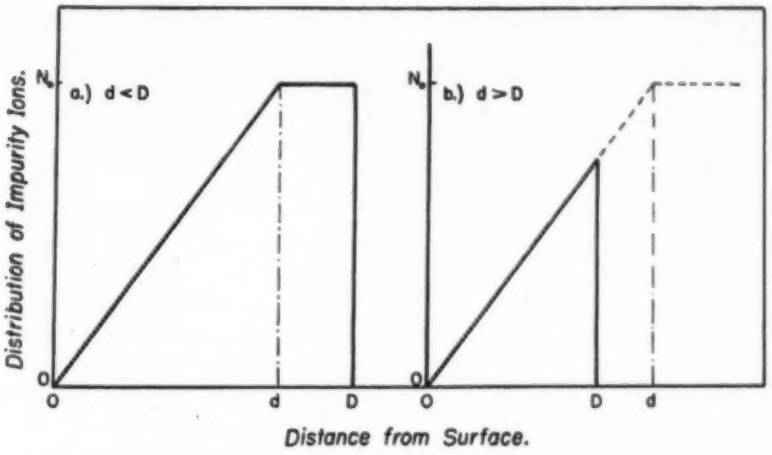

FIG. 2. The effective distribution of ions at the rectifying contact is shown for the two cases $d<D$ and $d>D$, where d is the thickness of the depleted layer. The potential goes to zero at D.

Combining Eqs. (3) and (4) we obtain

$$k/\mathfrak{D}=\delta^{-1}\cdot\exp\left[-(\epsilon''-\epsilon')/KT\right].$$

In most substances δ is of the order of a few Angstrom units, so that for $\epsilon''\simeq\epsilon'$, $k/\mathfrak{D}$ is of the order of 10^7 cm^{-1}. Since ϵ'' is probably greater than ϵ',[3] it is reasonable that $k/\mathfrak{D}\lesssim 10^7$ cm^{-1} and that a depleted layer thickness of $\gtrsim 10^{-6}$ cm is readily attainable for a sufficient heating time.

EFFECT OF THE DEPLETED LAYER ON THE ELECTRICAL CHARACTERISTICS OF A RECTIFYING CONTACT

The theory of silicon-metal contact rectification for a uniform distribution of impurities was given by Bethe.[4] The impurity energy levels in silicon lie close enough to the conduction band for all the impurities to be ionized at room temperature. When a metal having a different work-function than the silicon is put in contact with the latter, a potential barrier is established at the contact, the voltage being equal to the contact potential difference at the surface and falling to zero at a distance D_0 inside the semi-conductor. The distance at which the potential falls to zero is found by solving Poisson's equation for the electron potential V,

$$d^2V/dx^2=4\pi e^2(n_+-n_-)/\epsilon,$$

where e is the electronic charge, ϵ is the dielectric constant, and n_+ and n_- are, respectively, the density of positive and negative charges at x; subject to the boundary conditions $V=e\varphi$ at $x=0$, and $dV/dx=0$, $V=0$ at $x=D_0$, where φ is the potential at the contact. It is assumed that the density of electrons is zero and $n_+=N_0$ in the region where the potential is greater than zero ($x<D_0$) and the total charge density is zero for $x>D_0$. We obtain

$$D_0=(\epsilon\varphi/2\pi eN_0)^{\frac{1}{2}}.$$

To this potential we must add the potential due to the image force of the metal, which lowers the potential by an amount $-e^2/4\epsilon x$. This lowers the peak of the potential barrier approximately by

$$\Delta\varphi_0=(2e\varphi/\epsilon D_0)^{\frac{1}{2}}. \tag{5}$$

The position of the maximum of potential is also shifted into the semi-conductor by an amount

$$x_m=(eD_0/8\epsilon\varphi)^{\frac{1}{2}}.$$

Equation (5) is valid in the approximation that $(x_m/D_0)^2$ is negligible compared with (x_m/D_0).

If we assume that the electrons are not stopped by collisions in passing over the barrier (diode theory), we find the current density through the contact is

$$j=j_0[\exp -e(\varphi_0-\Delta\varphi_0)/KT][(\exp e\varphi'/KT)-1],$$

[3] J. Steigman, W. Schockley, and F. C. Nix, *Phys. Rev.* **56**, 13 (1939).

[4] Complete references will be found in the OSRD technical reports of the University of Pennsylvania: Div. 14 No. 282, May 29, 1944, and Div. 14 No. 304, August 3, 1944. Copies of these reports may be obtained from the Publications Board of the Department of Commerce, Washington, D. C.

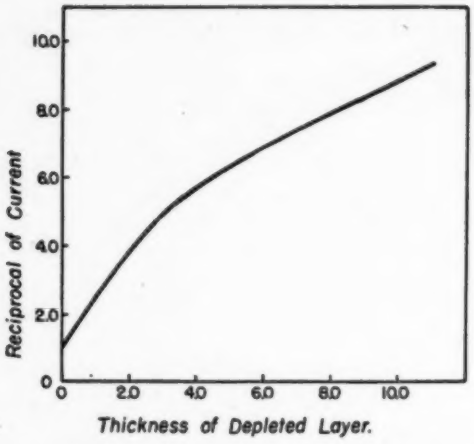

FIG. 3. The back current for an applied potential of -1.0 v is shown as a function of the thickness of the depleted layer in units of D_0. The current is in units of the current through a contact with no depleted layer.

where j_0 is the current density of electrons approaching the contact, φ_0 is the contact e.m.f., and φ' is the applied potential. The potential at the contact φ is the difference between φ_0 and φ'. The current density is very small for negative applied voltages and increases rapidly with positive values of φ'. The effect of the tunneling of electrons through the barrier is neglected in the derivation of the expression for the current density.

To calculate the effect of the depletion of impurities on the electrical characteristics of the contact, we assume that the heat treatment results in a linear distribution of impurity atoms of the form

$$N=N_0x/d, \quad x\leqslant d; \quad N=N_0, \quad x>d;$$

where d is the thickness of the depleted layer (see Fig. 1). We neglect the concentration at the surface since this is small and only complicates our equations without adding to their significance. If D is now the distance at which the potential falls to zero, we must distinguish between two cases, $d<D$ and $d>D$. The effective distributions of impurity ions for these two cases are shown schematically in Fig. 2. The effective distribution of ions is zero at distances greater than D, because the ions are effectively neutralized by the conduction electrons of the semiconductor.

Solving Poisson's equation for these distributions of positive ions, subject again to the boundary conditions $V=e\varphi$ at $x=0$; $V=0$, $dV/dx=0$ at $x=D$, we obtain for the thickness of the potential barrier

$$\begin{aligned} &\text{(a)}\ D=(D_0^2+d^2/3)^{\frac{1}{2}}, \quad d<D, \\ &\text{(b)}\ D=(3D_0^2d/2)^{\frac{1}{2}}, \quad d>D. \end{aligned} \tag{6}$$

The depleted layer increases the thickness of the potential barrier. We note that $d=D$, when $d=(3/2)^{\frac{1}{2}}D_0$.

The increased thickness of the potential barrier decreases the amount that the top of the barrier is lowered by the image force. To the approximation that $(x_m/D)^2$ is negligible compared with (x_m/D), the height of the barrier is lowered by an amount

$$\begin{aligned} &\text{(a)}\ \Delta\varphi=\Delta\varphi_0[(1+d^2/3D_0^2)^{\frac{1}{2}}-d/2D_0]^{\frac{1}{2}}, \quad d<D, \\ &\text{(b)}\ \Delta\varphi=\Delta\varphi_0(2D_0/d)^{1/6}\cdot 3^{\frac{1}{2}}/2, \quad d>D, \end{aligned}$$

where $\Delta\varphi_0$ is given by Eq. (5). The reciprocal ratio of the current density through a contact with a depleted layer to the current density through a contact with no layer is

$$\exp\left[-e(\Delta\varphi_0-\Delta\varphi)/KT\right].$$

Figure 3 shows this ratio plotted as a function of the thickness of the depleted layer in units of D_0, where we have taken $N_0=5.0\cdot 10^{18}$ cm^{-3} (impurity content 0.01 percent), $\varphi_0=0.5$ v, $\varphi'=-1.0$ v, and $\epsilon=13$; this choice gives $\Delta\varphi_0=0.125$ v and $D_0=2.08\cdot 10^{-6}$ cm.

The effect of increasing the thickness of the depleted layer is to increase the resistance of the contact for negative applied voltages (back resistance).

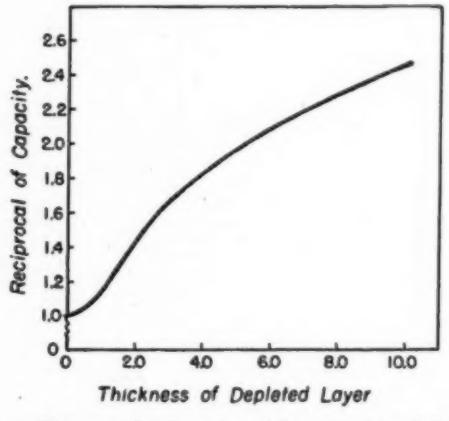

FIG. 4. The capacity in units of the capacity of the same contact with no depleted layer is shown as a function of the thickness of the depleted layer in units of D_0.

The depleted layer also changes the capacity of the contact. The capacity is determined by calculating the total charge in the barrier and then differentiating with respect to the applied voltage; it may be expressed by the usual formula

$$C = \epsilon A / 4\pi D,$$

where A is the area of the contact and where now for D we must substitute the appropriate expression given by (6). Thus the effect of the depleted layer is to decrease the capacity of the contact; this is shown in Fig. 4.

Both these effects (the increase in back resistance and the decrease in capacity) contribute to improved rectifying performance at high frequencies. A model of a crystal rectifier is shown in Fig. 5. R is the resistance of the contact which varies rapidly with applied voltage, being very large for negative applied voltages and very small for positive voltages. C is the capacity of the contact which varies slowly with applied voltage. The quantity R_s is the resistance of the bulk of the semi-conductor. Bethe[4] has pointed out that in the forward direction R is very small, and the total impedance is R_s. In the back direction R is very large (in our case still larger), so that the total impedance is $R_s + (iC\omega)^{-1}$ where ω is the angular frequency of the applied voltage. Thus a decrease in capacity gives a larger ratio of back impedance to front impedance, thereby increasing the efficiency of rectification.

DISCUSSION

The neglect of the tunnel effect contribution to the current through the contact in the previous calculations does not affect the general conclusions. Courant[4] has shown that this effect may be regarded as producing a further decrease in the height of the potential barrier at the contact. The magnitude of the decrease can be of the same magnitude as the image force lowering of the potential barrier. The increased thickness of the potential barrier produced by a depleted layer will cause a decrease in the number of electrons tunneling through the barrier compared with the number tunneling through a normal barrier. Thus, the resistance of a contact with a depleted layer will be still larger than the resistance of a normal contact.

It is hard to say how changes in the surface properties of the semi-conductor affect the rectification characteristics. It is conceivable that

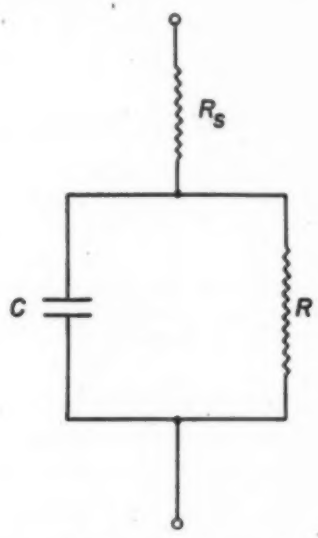

FIG. 5. The model of the crystal rectifier consists of a variable resistance R, a capacity C, and the resistance R_s of the bulk semi-conductor.

polishing results in the production of a liquid-like layer near the surface. The impurities would probably diffuse faster in this layer than in the crystalline solid. Even if the layer were only 10^{-7} cm thick, it is believed that polishing distorts the lattice to a depth[5] as great as 10^{-4} cm, assuming no recrystallization upon heating. Hence the impurity diffusion rate may be a function of depth, increasing as the surface is approached. The thickness of the depleted layer would then depend on the nature of the polishing procedure. This effect has been observed in copper.[6] A polish layer also could change the work function of the surface by more strongly adsorbing gases.

Considering these difficulties, all that we may reasonably conclude is that one of the functions of heating semi-conductors for use in contact rectifiers is to form a layer depleted of impurities near the surface, where contact is made. This

[5] C. S. Barrett, *Structure of Metals* (McGraw-Hill Book Company, Inc., New York, 1943), p. 505.
[6] G. I. Finch, A. G. Quarrell, and J. S. Roebuck, Proc. Roy. Soc. **145**, 676 (1934).

layer increases the back resistance and decreases the capacity of the contact, improving the rectification efficiency. The quantitative results of these calculations have been used only to demonstrate the reasonableness of the assumptions and to illustrate the direction of the effects.

The author wishes to thank Dr. W. E. Stephens and Dr. L. I. Schiff for suggesting the problem and for their interest and aid.

PHYSICAL REVIEW VOLUME 69, NUMBERS 7 AND 8 APRIL 1 AND 15, 1946

On the Electronic Structure of the Nitrogen Molecule

G. HERZBERG
Yerkes Observatory, Williams Bay, Wisconsin
(Received January 5, 1946)

It is shown that the Lyman-Birge-Hopfield bands of nitrogen represent a forbidden $^1\Pi_g - {}^1\Sigma_g^+$ transition. A considerable difficulty in the interpretation of the electronic states of N_2 by electron configurations is thus removed. A revised electronic energy level diagram of N_2 is given.

THE Lyman-Birge-Hopfield ($a-X$) bands of nitrogen have been considered a $^1\Pi_u - {}^1\Sigma_g^+$ transition ever since it was established[1] that each band has a P, a Q, and an R branch. However, on this basis a serious difficulty arises in the interpretation of the upper state of the $a-X$ bands by means of electron configurations. The lower state (X) of these bands is the ground state of the N_2 molecule whose electron configuration is

$$KK(\sigma_g 2s)^2(\sigma_u 2s)^2(\pi_u 2p)^4(\sigma_g 2p)^2, \quad (1)$$

where KK stands for the two K shells. The two lowest unoccupied orbitals are $(\pi_g 2p)$ and $(\sigma_u 2p)$, in this order, both of which are antibonding. Since, as shown by the N_2^+ spectrum, the orbitals $(\pi_u 2p)$ and $(\sigma_g 2p)$ have nearly the same energy, the lowest excited states of N_2 would be expected to belong to the following configurations:

$$KK(\sigma_g 2s)^2(\sigma_u 2s)^2(\pi_u 2p)^4(\sigma_g 2p)(\pi_g 2p)\,;\ {}^1\Pi_g, {}^3\Pi_g, \quad (2)$$

$$KK(\sigma_g 2s)^2(\sigma_u 2s)^2(\pi_u 2p)^3(\sigma_g 2p)^2(\pi_g 2p)\,;\ {}^1\Sigma_u^+, {}^3\Sigma_u^+, {}^1\Delta_u, {}^3\Delta_u, {}^1\Sigma_u^-, {}^3\Sigma_u^-, \quad (3)$$

$$KK(\sigma_g 2s)^2(\sigma_u 2s)^2(\pi_u 2p)^4(\sigma_g 2p)(\sigma_u 2p)\,;\ {}^1\Sigma_u^+, {}^3\Sigma_u^+, \quad (4)$$

$$KK(\sigma_g 2s)^2(\sigma_u 2s)^2(\pi_u 2p)^3(\sigma_g 2p)^2(\sigma_u 2p)\,;\ {}^1\Pi_g, {}^3\Pi_g. \quad (5)$$

They give rise to the states indicated at the right. Two of these, $^3\Sigma_u^+$ and $^3\Pi_g$, account readily for the two lowest observed triplet states $A\ {}^3\Sigma_u^+$ and $B\ {}^3\Pi_g$ of N_2 (compare the energy level diagram in Fig. 1) but a $^1\Pi_u$ state cannot be accounted for in this way. An electron configuration of higher energy would be required, which contradicts the fact that $a\ {}^1\Pi$ is a low, if not the lowest, excited singlet state.[1a]

This difficulty can now be resolved by a new interpretation of the Lyman-Birge-Hopfield bands made necessary by recent findings of new singlet band systems of nitrogen by Herman,[2] Gaydon,[3] and Worley.[4,5]

As has been recognized by Herman, the upper state of the new singlet bands found by her is identical with the upper state of the ultraviolet emission bands $h-X$ found by Watson and Koontz[1] while their lower state is the upper

[1] E. T. S. Appleyard, Phys. Rev. **41**, 254 (1932); W. W. Watson and P. G. Koontz, Phys. Rev. **46**, 32 (1934); J. W. T. Spinks, Can. J. Research **A20**, 1 (1942).

[1a] Compare R. S. Mulliken [Rev. Mod. Phys. **4**, 1 (1932)] and A. Recknagel [Zeits. f. Physik **87**, 375 (1934)] who have calculated the energies of the predicted low lying states. Both authors have emphasized the importance of the above mentioned difficulty.

[2] R. Herman, Comptes Rendus **217**, 141 (1943).

[3] A. G. Gaydon, Proc. Roy. Soc. **182**, 285 (1944).

[4] R. E. Worley, Phys. Rev. **64**, 207 (1943); **65**, 249 (1944).

[5] A. G. Gaydon and R. E. Worley, Nature **153**, 747 (1944).

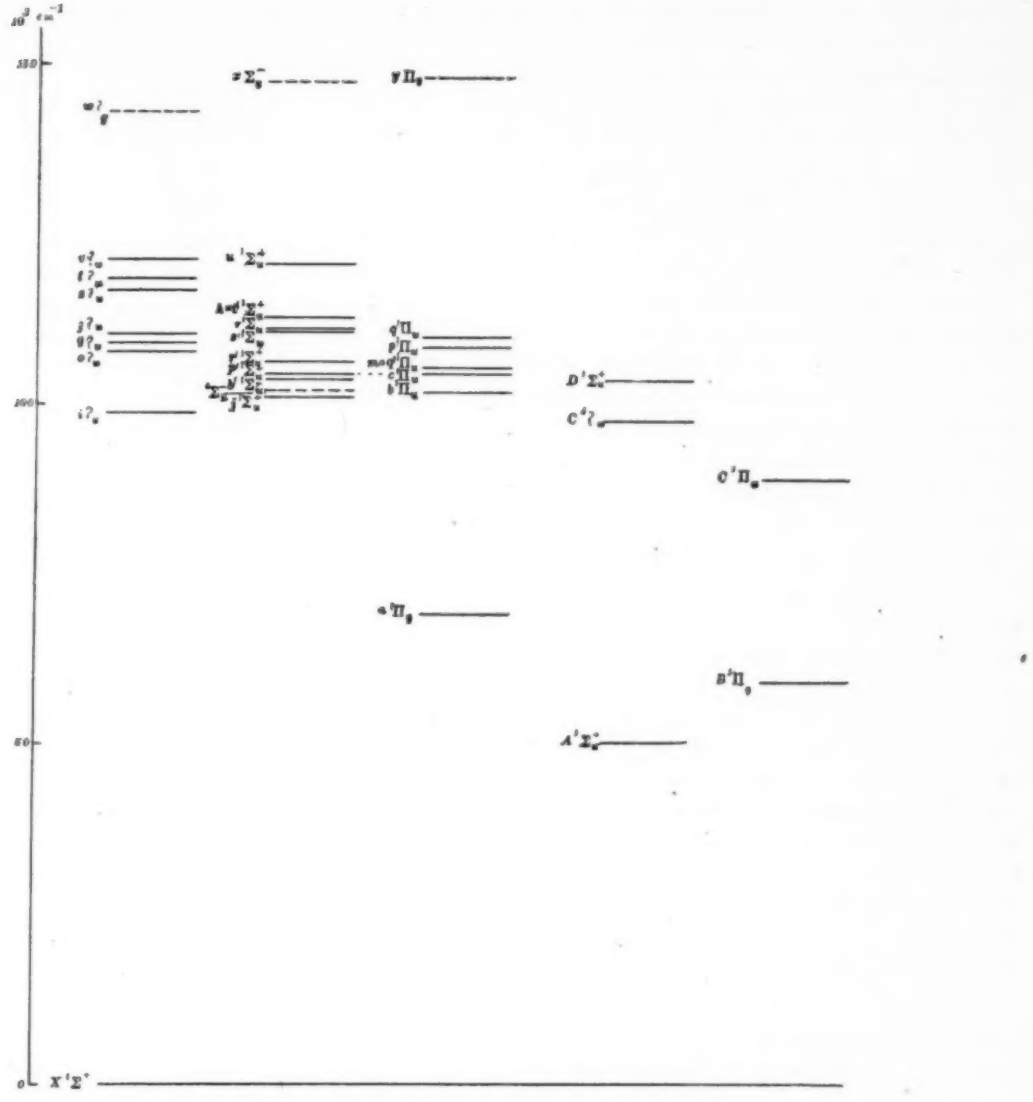

FIG. 1. (The lowest broken-line level in the second column is $a'\ ^1\Sigma_u^-$.)

state a of the $a-X$ bands (see Fig. 1). The $0-0$ band of the $h-X$ system has also been found in absorption by Worley[4] at 112,778.5 cm^{-1} while the $h-a$ bands of Herman have also been found independently by Gaydon[3, 5] who designates them $t'-a$ and gives 112,774.2 cm^{-1} for the energy of the t' state above the ground state. The difference between the two figures is within the accuracy of band head measurements in the far ultraviolet. Gaydon has analyzed the fine structure of the $h-a$ bands and finds the upper state to be a $^1\Sigma$ state while the lower state is $^1\Pi$.

The upper state of another new singlet system, $q'-a$, found by Gaydon at 105,351.1 cm^{-1} is identical with the upper state of the far ultraviolet system $m-X$ found by Worley at 105,349.6 cm^{-1}. In this case Worley has been able to determine the rotational constant B' of the upper state obtaining the value 1.36 cm^{-1} which closely agrees with that found by Gaydon for the q' state (1.36_8). The identity of the two states q' and m is therefore beyond all reasonable doubt.[6]

[6] To be sure Worley (references 4, 5) assumes the $0-0$ band of the $m-X$ system to be unobserved and to lie at considerably longer wave-lengths. However, the agreement

Thus there are in N_2 two sets of three states $-X, a, h(\equiv t')$ and $X, a, m(\equiv q')$—such that all three transitions in each set are observed (see Fig. 1). Such a situation is possible in a homonuclear molecule like N_2 only if one of the three transitions is a forbidden transition violating the (g, u) rule (i.e., the rule that even states combine only with odd). The question then arises which transition in each set is forbidden. Herman, who realized the necessity of a forbidden transition for the group X, a, h, assumed the $h-a$ transition to be forbidden. However, since the $h-X$ bands have a very high transition probability as shown by their occurrence in absorption with a path of only 0.2 mm at atmospheric pressure (see Worley[4]), it seems quite impossible that the $h-a$ bands could be observed in emission with moderate intensity if they represent a transition violating the (g, u) rule. An allowed transition to the ground state would take place long before the forbidden transition to the a level could occur. A corresponding difficulty arises for the assumption that the transition $m-a$ of the second set contradicts the (g, u) rule. These difficulties do not arise if it is assumed that the forbidden transition in either set is $a-X$, that is, that *the Lyman-Birge-Hopfield bands represent a* $^1\Pi_g-^1\Sigma_g^+$ *transition not* $^1\Pi_u-^1\Sigma_g^+$ as hitherto assumed. Unlike the previous cases there is here no other transition that competes with $a-X$ in depleting the number of molecules in the a state. The effect of collisions in reducing the number of molecules in the $a\,^1\Pi_g$ state probably accounts for the comparatively low intensity of the $a-X$ bands in emission particularly at high pressure.

There is possibly a third set of the type described above: The upper state c of one of the systems found by Birge and Hopfield[7] in emission and by Worley[4] in absorption may be identical with the upper state p' of one of Gaydon's systems whose lower state is $a\,^1\Pi_g$. While Gaydon's p' state is fairly definitely a $^1\Sigma$ state, the c state is considered by Worley to be $^1\Pi$. However, it appears that the far ultraviolet data can also be accounted for on the assumption of a $^1\Sigma$ state so that p' and c could be identical. The B value of the c state which does agree with that of the p' state is somewhat in doubt since on its basis it is difficult to account for the great length of the v'' progression observed in emission.

The interpretation of the $a-X$ bands as a forbidden $^1\Pi_g-^1\Sigma_g^+$ transition is also in satisfactory agreement with the observed intensity of absorption. The absorption spectrogram published by Birge and Hopfield[7] was obtained with an absorbing path of as much as 40 cm at atmospheric pressure and even at that the bands do not appear to be particularly strong. A $^1\Pi_g-^1\Sigma_g^+$ transition can occur as magnetic

TABLE I. Singlet states of the nitrogen molecule[a] (revision of Gaydon and Worley's table, reference 6).

State	A_0(cm^{-1})[b] (excitation energy of lowest observed vibrational level)	B_0(cm^{-1})	$\Delta G_{\frac{1}{2}}$(cm^{-1})
$y^1\Pi_g$	$a'+46{,}420$	1.80	1705
$x^1\Sigma_g^-$	$a'+45{,}463$	1.73_5	1869
$w?_g$	$a'+40{,}914$	>1.47	1711?
$v?_u$	$121{,}247H$	$\lesssim 1.9$	925
$u^1\Sigma_u^+$	$120{,}584.6H$	1.07	533
$t?_u$	$118{,}487.3H$	1.16	482
$s?_u$	$116{,}683H$	1.11	522
$h\equiv t'^1\Sigma_u^+$	112,774.2	1.63	
$r^1\Sigma_u^+$	$110{,}944.5H$	1.07	640
$s'^1\Sigma_u^+$	110,662.0	1.58_5	
$f?_u$	$110{,}190H$	$\lesssim 1.9$	
$q^1\Pi_u$	$109{,}832.8H$	1.11	697
$g?_u$	$108{,}950H$	<1.99	
$p^1\Pi_u$	$108{,}372.2H$	1.21	749
$o?_u$	$107{,}657.0H$[c]	$\lesssim 1.8$	1918
$r'^1\Sigma_u^+$	106,373.5	1.67	
$m\equiv q'\,^1\Pi_u$	105,351.1	1.36_5	760
$p'^1\Sigma_u^+$	104,327.9	1.93	
$c^1\Pi_u?$	$104{,}316.1H$	1.92	2180
$b'^1\Sigma_u^+$	$103{,}678H$[d]	1.144	741
$b^1\Pi_u$	$101{,}456.0H$	1.41	698
$a'^1\Sigma_u^-$	?	1.47	1504
$j^1\Sigma_u^+$	100,821.4?	1.45	
$i?_u$	98,486H	~ 1.5?	670
$a^1\Pi_g$	68,956.6	1.62	1666.7
$X^1\Sigma_g^+$	0	1.99_5	2330.7

[a] Upper states of Rydberg series are not included.
[b] An H indicates a value obtained from the measurement of band heads (Worley's Table IV). Gaydon has given band origins for his new bands and has based his energy values for the upper states on the value 68,956.6 for $a\,^1\Pi$. He does not state how this value was obtained. From Birge and Hopfield's value for ν_{00} of the $a-X$ bands which refers to band heads the writer obtains 68,954.3 cm^{-1} referred to band origins. The difference is probably within the accuracy of the ultraviolet measurements and no change from Gaydon's data was made in Table I.
[c] Or 105,694.5 and $\Delta G_{\frac{1}{2}}=1962$.
[d] This is Birge and Hopfield's value. Tschulanowsky (Bull. Acad. Sci. USSR, p. 1313 (1935)) gives a considerably higher value (103,767.06) which, though based on band origins, depends on a rather long extrapolation.

of the upper state of the first observed $m-X$ band with the upper state of Gaydon's emission bands is evidence that the first observed $m-X$ band is the 0–0 band. The occurrence in absorption of this band in spite of the large difference of the equilibrium internuclear distances is caused by the shallowness of the upper state (very small ω_e) which leads to a great width of the vibrational eigenfunction of the upper state.

[7] R. T. Birge and J. J. Hopfield, Astrophys. J. 68, 257 (1928).

dipole radiation. As is well known, the atmospheric oxygen bands represent a magnetic dipole transition which is at the same time a singlet-triplet intercombination. They occur weakly in an absorbing path of 1000 cm. To obtain them with an intensity comparable to that of the $a-X$ bands of N_2 on Birge and Hopfield's spectrogram would require an absorbing path about 10,000 cm long. According to Van Vleck[8] a magnetic dipole transition that is not an intercombination is expected to be about 10^4 times brighter than one that is an intercombination. Therefore about 1-cm absorbing path would be required for a non-intercombination magnetic dipole transition. The fact that the observed absorption intensity of the Lyman-Birge-Hopfield bands is even less than this theoretical estimate[9] makes it rather certain, even apart from the previous argument, that they represent a forbidden ($^1\Pi_g - {}^1\Sigma_g^+$) transition. The allowed transitions from the ground state found by Worley are observed to be about 2000 times stronger than the Lyman-Birge-Hopfield bands.

It should perhaps be pointed out that the rotational fine structure of a magnetic dipole $^1\Pi_g - {}^1\Sigma_g^+$ transition is the same (including the intensity alternation) as that of an ordinary dipole $^1\Pi_u - {}^1\Sigma_g^+$ transition except that the opposite Λ-doubling components form the upper states of Q and P, R branches. Since in none of the bands discussed here the Λ-type doubling has been resolved, the observed fine structure is equally compatible with either interpretation. If very precise data were available one would find that the combination differences of the lower state obtained from the P and R branches of the $h-a$ and $m-a$ bands would not agree exactly with those of the upper state obtained from the P and R branches of the $a-X$ bands.

From all these reasons the conclusion that the a state of nitrogen is $^1\Pi_g$ not $^1\Pi_u$ seems to be well established. At the same time the difficulty with the electron configuration mentioned at the beginning is removed. A low $^1\Pi_g$ is expected from the electron configuration (2) above, the same electron configuration that accounts for the $B\,{}^3\Pi_g$ state. In agreement with expectation the $^3\Pi$ state is lower than the $^1\Pi$ of the same electron configuration. Also the two states have very similar ω_e and B_e values (1694.7 and 1.642 for $a\,{}^1\Pi$ and 1732.8 and 1.6430 for $B\,{}^3\Pi$) as expected if they have the same electron configuration. In this way one of the most unsatisfactory points in the interpretation of electronic states of diatomic molecules by electron configurations is cleared up.

On the basis of the above discussion the interpretation of the upper states of the new singlet bands found by Gaydon has of course to be changed. In particular the states t' and q' of Gaydon (see above) are $^1\Sigma_u^+$ and $^1\Pi_u$, respectively, not $^1\Sigma_g^-$ and $^1\Pi_g$ as assumed by Gaydon. These are the term types indicated in Fig. 1. The revised types are indeed easier to account for on the basis of electron configurations than were Gaydon's types.

For the convenience of the reader, Table I lists the known data about the singlet states of nitrogen in the revised version. Unlike the similar table by Gaydon and Worley,[5] Table I gives the energy of the lowest observed vibrational level rather than that of an extrapolated $v=0$ level since at least in the case of the m state such an extrapolation seems to lead to erroneous results.[6] The states $a'\,{}^1\Sigma_u^-$ and $j\,{}^1\Sigma_u^+$ very probably belong to the same electron configuration [(3) above] as $A\,{}^3\Sigma_u^+$ thus accounting for three of the six states resulting from this configuration. Again the constants ω_e and B_e of these three states are very similar. The exact position of the a' state cannot be derived from the observations. In Fig. 1 it has been placed above $j\,{}^1\Sigma_u^+$ since theoretical calculations by Recknagel[10a] indicate such an order. Gaydon[3, 5] has assumed it to be as low as 60,000 cm^{-1}.

I would like to express my appreciation to Professor R. S. Mulliken for a stimulating discussion of the subject of this paper.

Note added in proof: A more detailed paper by R. Herman-Montagne (Ann. de physique **20**, 241, (1945)) has just been received here. In this paper a number of further band systems of N_2 are found and further energy levels established. Unfortunately these could not be included in Fig. 1 and Table I.

[8] J. H. Van Vleck, Astrophys. J. **80**, 161 (1934).

[9] For a more accurate estimate the difference in frequency of the atmospheric oxygen bands and the $a-X$ nitrogen bands would have to be considered. It would increase the theoretical intensity of the latter by about a factor 5.

Letters to the Editor

PROMPT publication of brief reports of important discoveries in physics may be secured by addressing them to this department. The closing date for this department is the third of the month. Because of the late closing date for the section no proof can be shown to authors. The Board of Editors does not hold itself responsible for the opinions expressed by the correspondents. Communications should not in general exceed 600 words in length.

Atomic Energy from U^{238}

LOUIS A. TURNER
Palmer Physical Laboratory, Princeton University, Princeton, New Jersey
May 29, 1940*

THE recent experiments of Nier, Booth, Dunning, and Grosse[1] and of Kingdon, Pollock, Booth, and Dunning[2] have confirmed Bohr's prediction[3] that the nuclear fission produced in U by thermal neutrons is to be attributed practically entirely to the rarer isotope of mass 235. This is present in an amount only 1/139 as great as that of the 238 isotope, so it is natural to conclude that only 1/140 of any quantity of U can be considered as a possible source of atomic energy if slow neutrons are to be used. It seems likely, however, that this is wrong, that the energy of a large part of the U^{238} nuclei can also possibly be made to undergo fission by slow neutrons in an indirect way. This is of obvious importance for practical utilization of the atomic energy of U.

The indirect use of U^{238} can come about through the fission either of the U^{239} nuclei formed by the capture of neutrons, or of the nuclei descending from U^{239}. In a forthcoming paper[4] it is shown that $_{93}$EkaRe^{239} and $_{94}$EkaOs^{239}, the probable long-lived descendants from U^{239}, would be expected to undergo fission upon capture of thermal neutrons. A similar argument leads to the conclusion that U^{239} itself would probably also give fission with thermal neutrons. For such fission to be of consequence it is necessary that nearly one U^{239} atom be produced for every U^{235} atom lost. That this condition can be satisfied may be seen as follows. Consider N secondary neutrons. A number Np will suffer resonance capture by U^{238} to give U^{239}, p being the probability for such capture. The remaining $N(1-p)$ neutrons will become thermal. Of these, $N(1-p)w$ will produce fission of U^{235} nuclei and $N(1-p)(1-w)$ will be captured by U^{238} nuclei, w being the probability that a thermal neutron will produce fission. It is assumed that no other capture processes are important for the thermal neutrons, that a non-capturing method of slowing the neutrons needed for developing the divergent chain reaction has been found. The total number of U^{239} nuclei formed is thus $Np+N(1-p)(1-w)$ and the number of U^{235} nuclei lost is $N(1-p)w$. The condition that every U^{235} nucleus be replaced by a U^{239} or descendant nucleus becomes $Np+N(1-p)(1-w)>N(1-p)w$ which reduces to $1/(1-p)>2w$. Since $w<1$ this condition can be met if $p\sim0.5$ as it was in the experiments of Halban, Joliot, Kowarski, and Perrin.[5] Presumably it can be made so with other methods of slowing down the neutrons. Some concentration of the U^{235} isotope may be necessary if p is to be ~0.5. Since the number of neutrons evolved per fission[6] is ~3 the divergent chain can develop if more than one on the average gives fission and the present condition be satisfied if more than one gives U^{239}.

It seems likely, however, that of the three nuclei $_{92}U^{239}$, $_{93}$EkaRe^{239}, and $_{94}$EkaOs^{239} only the last might be expected to have a large cross section for fission. The excess energy in the $_{93}U^{240}$ and $_{93}$EkaRe^{240} nuclei after capture of neutrons by $_{93}U^{239}$ and $_{93}$EkaRe^{239}, respectively, would be small compared to what it is in the $_{93}U^{236}$ nuclei coming from $_{92}U^{235}$. The cross sections for fission would thus be correspondingly small. In $_{94}$EkaOs^{240}, on the other hand, the excess energy would be even larger than in $_{93}U^{236}$ and a large cross section for fission would be expected. It might thus be necessary to allow U from which the $_{93}U^{235}$ had been used up to lie idle for several times the as yet unknown half-life of $_{93}$EkaRe^{239} until a sufficient quantity of $_{94}$EkaOs^{239} had developed in it, after which it could again be used. This could be repeated until all of the $_{92}U^{238}$ had been converted.

* This letter was received for publication on the date indicated but was voluntarily withheld from publication until the end of the war.
[1] Nier, Booth, Dunning, and Grosse, Phys. Rev. 57, 748 (1940).
[2] Kingdon, Pollock, Booth, and Dunning, Phys. Rev. 57, 749 (1940).
[3] N. Bohr and J. A. Wheeler, Phys. Rev. 56, 426 (1940).
[4] L. A. Turner, Phys. Rev. 57, 951 (1940).
[5] Halban, Joliot, Kowarski, and Perrin, J. de phys. et rad. 10, 428 (1939). See also L. A. Turner, Phys. Rev. 57, 334 (1940).

Radioactive Element 94 from Deuterons on Uranium

G. T. SEABORG, E. M. MCMILLAN, J. W. KENNEDY, AND A. C. WAHL
Department of Chemistry, Radiation Laboratory, Department of Physics, University of California, Berkeley, California
January 28, 1941*

WE are writing to report some results obtained in the bombardment of uranium with deuterons in the 60-inch cyclotron.

The uranium was bombarded in the form of U_3O_8 and the deuterons had to pass through a 2-mil thickness of aluminum foil before hitting the uranium target. The carefully purified element 93 fraction contained a beta-activity whose aluminum absorption curve (taken on an ionization chamber connected to an FP-54 tube and also on a Lauritsen electroscope) was distinctly different from the absorption curve of a sample of the 2.3-day 93^{239} (formed from uranium plus neutrons) taken under identical conditions. The upper energy limit of the beta-particles from this new 93 activity is about 1 Mev, compared with about 0.5 Mev for 93^{239}. The ratio of gamma-ray to beta-particle ionization is about five times larger than for 93^{239}. The initial part of the absorption curve of this 93 from uranium plus deuterons is very similar to the initial part of the absorption curve of 93^{239}. Of course the production of 93^{239} is expected in the deuteron bombardment of ura-

nium, from the reaction U^{238} $(d, n)93^{239}$. It is impossible to deduce from the absorption curve the relative intensities of the new 93 and of 93^{239}, since the initial parts of the individual absorption curves of these two activities might well be nearly identical. The rate of decay of the high energy beta-particles (0.5–1 Mev) and gamma-rays from the 93 of uranium plus deuterons was determined. This gave a half-life of about 2 days for the new 93. This activity is probably to be assigned to 93^{238}, 93^{236}, or 93^{235} formed in the reaction $U^{238}(d,2n)93^{238}$, $U^{235}(d,n)93^{236}$, or $U^{235}(d,2n)93^{235}$, respectively.

The growth of alpha-particles, which might be due to the element 94 daughter of the 2-day 93, was then looked for. We did observe the growth of alpha-particles in the very carefully purified, as well as in the semi-purified 93 fractions, and the growth curves indicate a half-life of roughly 2 days for the parent of the alpha-emitter. The final alpha-particle count amounts to several hundred counts per minute for a bombardment of 200 microampere-hours. This work was done with a proportional type counter. We plan to re-determine the alpha-particle growth curve more accurately using an ionization chamber and linear amplifier with the help of a magnetic field to bend out the very strong beta-particle background. The alpha-particles have a range of approximately 3.9 cm in air.

This alpha-activity is chemically separable from uranium and 93. The chemical experiments so far indicate a similarity to thorium and the activity has not yet been separated from thorium. More chemical experiments definitely must be performed before it can be regarded as proved that the alpha-particles are due to an isotope of element 94.

* This letter was received for publication on the date indicated but was voluntarily withheld from publication until the end of the war.

Radioactive Element 94 from Deuterons on Uranium

G. T. Seaborg, A. C. Wahl, and J. W. Kennedy
Department of Chemistry, Radiation Laboratory, Department of Physics University of California, Berkeley, California
March 7, 1941*

We should like to report a few more results which we have found regarding the element 94 alpha-radioactivity formed in the 16-Mev deuteron bombardment of uranium. We sent a first report[1] of this work in a Letter to the Editor of January 28, 1941. We have in the meantime performed more experiments in order to study the chemical behavior of this alpha-radioactive isotope. The radioactivity can be precipitated, in what is probably the +4 valence state, as a fluoride or iodate by using a rare earth or thorium as carrier material and as a peroxyhydrate by using thorium as carrier material. However, in the presence of the extremely strong oxidizing agent persulfate ion ($S_2O_8^{--}$), plus Ag as a catalyst, this radioactive isotope is oxidized to a higher valence state which does not precipitate as a fluoride. The oxidizing agent bromate ion (BrO_3^-) is not sufficiently powerful to oxidize it to this higher valence state and hence the radioactivity comes down as a fluoride even in the presence of bromate ion. With the help of persulfate ion it has been possible to separate quantitatively this radioactivity from thorium, by using the beta-active UX_1 as an indicator for thorium. These experiments make it extremely probable that this alpha-radioactivity is due to an isotope of element 94. The experiments are being continued.

* This letter was received for publication on the date indicated but was voluntarily withheld from publication until the end of the war.
[1] G. T. Seaborg, E. M. McMillan, J. W. Kennedy and A. C. Wahl, Phys. Rev. 69, 366 (1946).

Search for Spontaneous Fission in 94^{239}

Joseph W. Kennedy and Arthur C. Wahl
Berkeley, California
December 4, 1941*

This report describes the experimental procedure and gives the results obtained in our search for spontaneous fission in 94^{239}. The observations were made on a 3.5-microgram sample of 94^{239}, the preparation of which was described in a report of July 24, 1941, from this laboratory. This sample, when placed on one electrode of an ionization chamber connected to a linear amplifier adjusted to record counts due to fissions, gave zero counts in 139 hours. In another, independent experiment, done in a similar manner with entirely different apparatus, this sample gave zero counts in 209 hours. These experiments set a lower limit of the order of 10^{14} years for the "half-life" of 94^{239} with respect to spontaneous fission. These results show that it is probable that the half-life for spontaneous fission of 94^{239} is as long or longer than that of U^{235}, assuming the British results (40 spontaneous fissions per min. per g of pure U^{235}).

The details follow: The 3.5-microgram sample of 94^{239} was mounted on a platinum-coated copper disk, along with its cerium fluoride carrier in which the thickness amounted to $\sim$0.3 mg per cm^2. All the measurements described herein were made with shallow ionization chambers so constructed that this disk could be inserted to serve as one of the electrodes. Consideration of this geometry indicates that ionizing particles emitted from a sample on the disk could be counted with an efficiency of about 45 percent; tests of the alpha-particle counting rate with a thin, weighed uranium sample on a similar disk confirmed this estimate when the gain of the linear amplifier used was set sufficiently high. Since in each fission process two ionizing particles are emitted in opposite directions, an upper limit of about 90 percent efficiency for fission counting is set by the geometrical arrangement. Actually, because of the fluctuating background ionization due to alpha-particles from the sample, it was expedient to adjust the amplifier gain in such a way that a slightly lower counting efficiency was obtained. With the use of a neutron source and a thin uranium sample mounted like the 94^{239} sample, two independent calibrations of this efficiency were made, as follows: (1) oscillographic observation of pulses showed the fraction of fission pulses too small to actuate the thryatron recording circuit; (2) the recorded fission rate was compared with the expected rate calculated from the weight of the thin uranium sample, the slow neutron fission cross

section of uranium, and the density of slow neutrons as determined with an indium detector.

Both these calibrations gave the result that about 70 percent of the fissions were being recorded under the operating conditions of our experiments. This slight reduction in counting efficiency is no doubt to be attributed to discrimination against those fission fragments which traverse only a corner of the ionization chamber. It is of course apparent that high precision in the evaluation of this percentage efficiency is not required for our interpretation of the final result; however, the effect of small variations (±10 percent) in amplifier gain on this efficiency calibration was investigated and found negligible, showing that the working region approximated a plateau.

Two separate linear amplifier and ionization chamber outfits were used for two independent series of spontaneous fission experiments. At frequent intervals during all measurements the over-all gain of the amplifier was checked by the use of a pulse generator and voltage divider box or by re-testing the efficiency of counting slow-neutron induced fissions in uranium.

The series of measurements with one amplifier and chamber gave zero spontaneous fission counts in 139 hours of operation. With the other amplifier set-up, 209 hours of observation gave zero counts. These results enable us to say something about the spontaneous fission disintegration constant of 94^{239}, or, more conveniently, about the half-life for spontaneous fission corresponding to this disintegration constant. In the two experiments taken together zero counts were obtained in 348 hours. From the weight of the sample (3.5 micrograms) and the efficiency of the apparatus for counting fissions (70 percent), one can calculate that for a half-life of 10^{13} years the mean time between counts would be about 20 hours and for a half-life of 10^{14} years the mean time between counts would be about 200 hours. The probability of obtaining zero counts in 348 hours is about 10^{-8} for 20 hours mean time between counts, and about 0.2 for 200 hours mean time between counts. Therefore, it seems fairly safe to say that the half-life of 94^{239} for spontaneous fission is of the order of 10^{14} years or greater.

* This letter was received for publication on the date indicated but was voluntarily withheld from publication until the end of the war.

Determination of Absolute Neutron Intensities

R. D. O'Neal and G. Scharff-Goldhaber
Department of Physics, University of Illinois, Urbana, Illinois
February 24, 1942*

We have developed a method of measuring the number of neutrons emitted from a given source and used it to determine the neutron intensity of a laboratory standard consisting of 100 mg of radium surrounded by 85 g of beryllium metal. We made use of the main principle of Amaldi and Fermi's well-known method, which consists in slowing down all the neutrons emitted from the source before they are counted. However, we avoided the use of a number of constants and some difficult approximations, which appeared in the original form of this method.

Our procedure consisted essentially of two steps.

(*a*) *Determination of the ratio R of the number of neutrons activating a* $MnSO_4$ *solution*[1] *with and without the presence of an absorber* (consisting of finely powdered manganese).—The volume of the solution was chosen so large that 1 percent of the neutrons was allowed to escape. After irradiation the solution was thoroughly stirred and the decay of its radioactivity observed by means of a large thin-walled Geiger counter (initial activity without absorber 1110 counts/min. above the background of 200 counts/min., with absorber 850 counts/min.).

(*b*) *Determination of the number of neutrons* (N_a) *captured by the absorber per unit time.*—After irradiation a fraction of the well-mixed Mn powder was filled into paper shells. These "thick" samples were placed alternately around a thin-walled Geiger counter and their initial activities were determined (6185 counts/min.).

In order to determine the number of disintegrations per gram of manganese (specific activity), we irradiated some manganese powder with neutrons from a very strong source and filled a known amount of it into a paper shell as before. With another part we prepared a thin layer (16 mg/cm²) between two pieces of scotch tape, which was placed in a defined position relative to the counter. A similar layer, made of a known amount of fine uranium metal powder, was placed in the same position for standardization. For the calculation of the specific activity of the managanese samples the number of UX_2 nuclei decaying per sec. per gram of uranium was assumed to be 12220.[2] A correction of 2.5 percent was found to be necessary to allow for the slightly stronger absorption of the UX_2 beta-rays in the glass wall of the Geiger counter and in the scotch tape. By multiplying the specific activity of the manganese absorber with the total weight of the absorber (523 g), we obtained N_a and $N=N_a/(1-R)$ where N is the total number of neutrons emitted from our source.

The result was $N=(8.6\pm0.8)\times10^4$ neutrons per sec. The error was calculated by adding up all standard deviations from the mean of the several measurements, which were made for each individual quantity.

The intensity of this laboratory standard has been compared with that of a Ra-α-Be source (see following letter by Gamertsfelder and Goldhaber).

* This letter was received for publication on the date indicated but was voluntarily withheld from publication until the end of the war.

[1] The method of "physical integration" was first described by H. L. Anderson, E. Fermi, and L. Szilard, Phys. Rev. 56, 284 (1939).

[2] Calculated from data given by A. F. Kovarik and N. J. Adams, Jr., J. App. Phys. 12, 296 (1941), and by A. O. Nier, Phys. Rev. 55, 150 (1939).

A Reproducible Neutron Standard

G. R. Gamertsfelder and M. Goldhaber
Department of Physics, University of Illinois, Urbana, Illinois
February 24, 1942*

For some time a need has been felt for a simple, reproducible standard of neutron intensity. It is known that the most commonly used neutron sources, those obtained by mixing Rn or Ra with Be powder, are not reproducible.[1] By contrast it would appear that a photoneutron source, obtained by irradiating Be with Ra γ-rays under exactly defined geometrical conditions, could

be reproduced without difficulty. For a high intensity neutron standard it would seem best to *surround* the γ-ray source with Be. However, such a procedure would be impracticable, since the Ra sources available to different investigators are not of uniform shape. Therefore, if one wishes to construct a reproducible standard, one has to choose an arrangement in which the dimensions of the Ra source—as long as they remain within reasonable limits—are not of paramount importance.

With this in mind, we have devised the following "reproducible neutron standard." The Ra source used consisted of 100-mg Ra, enclosed in a glass tube and surrounded by a Monel tube of 1-mm wall thickness, 4.85-mm external diameter and 2-cm length. With this source a solid cylindrical Be block 1.5" in diameter and 1.5" high was irradiated. The center of the source was placed 4 cm above, and its axis parallel to, the upper face of the Be cylinder.

To determine the number of neutrons emitted by this photo-neutron source, its intensity *relative* to a "laboratory neutron standard" was measured with an arrangement similar to that of Frisch, v. Halban, and Koch.[2] The *absolute* neutron intensity of the "laboratory neutron standard" was determined by O'Neal and Scharff-Goldhaber by a new method (described in the preceding letter), by which they found that it emits $N=(8.6\pm0.8)\times10^4$ neutrons per sec. In our relative measurement we obtained for the intensity of the "reproducible neutron standard" $(0.072\pm0.002)N$. In this result we have already allowed for the number of neutrons emitted by the Ra source itself (about $0.01N$). The "reproducible neutron standard" therefore emits 62 ± 7 neutrons per millicurie Ra per sec.

Other investigators who might like to use this "reproducible neutron standard" may find it more advantageous to put the Ra source closer to the Be cylinder, when its intensity is comparatively small, or further away when its shape is comparatively bulky. The following table, showing the variation of the neutron intensity with the distance d between the center of the source and the upper face of the Be cylinder might therefore prove useful.

d in cm	2	3	4	5	6
Relative neutron intensity	2.35	1.52	1.00	0.716	0.567

We have also determined the neutron intensity of a Ra-α-Be source in terms of the "laboratory neutron standard," and have obtained a value of 6.8×10^3 neutrons per millicurie Ra per sec.

* This letter was received for publication on the date indicated but was voluntarily withheld from publication until the end of the war.

[1] See E. J. Murphy, W. C. Bright, M. D. Whitaker, S. A. Korff, and E. T. Clarke, J. Frank. Inst. 231, 357 (1941).

[2] O. R. Frisch, H. v. Halban, and J. Koch, Proc. Danish Acad. 15, 10 (1938).

Resonance Scattering of Fast Neutrons

DAVID C. GRAHAME
Amherst College, Amherst, Massachusetts
March 3, 1942*

THERE are a number of experimental facts pertaining to the scattering of fast neutrons by atomic nuclei that do not appear to be explainable in an altogether satisfactory manner on the basis of current nuclear theory. It is the purpose of this communication to point out some of these facts and to suggest a possible modification of the theory which appears capable of explaining them.

The facts to which we refer are as follows. (1) Fast neutrons are back-scattered to a measurable extent by such substances as lead and iron without losing the major part of their energy,[1,2] as required by theory.[3] The amount of such back-scattering varies from element to element in a manner suggestive of a resonance phenomenon. (2) Fast neutrons (2.5 Mev) passing through lead emerge with energies intermediate between what one would expect for neutrons inelastically scattered and what one would expect for neutrons elastically scattered or unscattered.[4] (3) Cross sections for inelastic scattering with large energy loss of 2.5 Mev neutrons do not vary monotonically with atomic weight or atomic number.[5] For light elements this might be attributed to resonance of the usual kind, but for heavy elements the spacing of resonance levels is expected to be much too close to permit the observation of resonance phenomena with neutrons whose energies vary by many Kev in even the most favorable cases.[6,7] (Even when the incident neutrons have a very great spread of energies, cross sections for inelastic scattering with large energy loss differ markedly for such near-neighbors as mercury and bismuth.[3]) (4) Inelastic scattering cross sections of most of those nuclei which have been studied show a marked dependence upon neutron energy.[8] The width of the levels observed demands a level spacing greater than that expected from theoretical considerations. (5) Total interaction cross sections for 2.5-Mev neutrons also vary markedly from element to element and otherwise exhibit typical resonance behavior.[9] Since most of the investigations dealing with this problem have been concerned chiefly with the lighter elements, it is not yet certain that resonance phenomena are to be found among the heavy elements, where the disagreement with theory would be the most pronounced. Present indications are that such phenomena are to be found even in elements as heavy as lead, however.

It was suggested by Grahame and Seaborg[3] that a form of neutron scattering might occur in which there is an incomplete amalgamation of the incident neutron with the nucleus which could give rise to scattering of a type involving only small energy loss. Dunlap and Little[4] have pointed out that their results require some such explanation, and the hypothesis which follows is an extension of that idea.

Let us consider that a fast neutron striking a nucleus interacts at first with only a few particles close to the surface. Let it be assumed that the compound nucleus so formed, which we shall call a locally excited or "hot-spot" nucleus, shares its energy with the remainder of the nucleus sufficiently slowly that one may consider the locally excited nucleus as a separate entity with its own set of energy levels. Because of the small number of particles interacting, these levels will be widely spaced by comparison with the levels of a similarly excited compound nucleus of the usual kind. (In this respect the locally excited nucleus will re-

semble a highly excited light nucleus.) Since the lifetime of the locally excited nucleus will be expected to be small, the resonance levels will be wide, in agreement with experiment. The locally excited nucleus may either re-emit a neutron or share its energy to form the usual type of compound nucleus. In the former case, the re-emitted neutron will generally have the greater part of the energy of the original neutron, since that energy has not been shared with any large number of particles. This we believe to be the mechanism for the process of inelastic scattering with small energy loss. Such scattering will be expected to be nearly isotropic.

If the locally excited nucleus distributes its energy to form the ordinary type of compound nucleus, inelastic scattering with large energy loss or other types of nuclear transformation may ensue in the usual manner. But these phenomena will be dependent upon the resonance levels of the locally excited nucleus which was first formed as well as upon the resonance levels of the compound nucleus, because both sets of energy levels affect the outcome of the initial encounter. For this reason resonance phenomena may be expected in all types of fast neutron interaction, with the possible exception of elastic scattering.

* This letter was received for publication on the date indicated but was voluntarily withheld from publication until the end of the war.

[1] H. H. Barschall and R. Ladenburg, Phys. Rev. **61**, 129 (1942).
[2] D. C. Grahame and G. T. Seaborg, Phys. Rev. **53**, 799 (1938).
[3] V. Weisskopf and D. H. Ewing, Phys. Rev. **57**, 472 (1939).
[4] H. F. Dunlap and R. N. Little, Phys. Rev. **60**, 693 (1941).
[5] H. Aoki, Proc. Phys. Math. Soc. Japan **19**, 369 (1937).
[6] H. A. Bethe, Rev. Mod. Phys. **9**, 71 (1937). See Table XXI.
[7] H. Margenau, Phys. Rev. **59**, 627 (1941).
[8] I. Nonaka, Phys. Rev. **59**, 681 (1941).
[9] S. Kikuchi and H. Aoki, Proc. Phys. Math. Soc. Japan **21**, 75 (1939); Phys. Rev. **55**, 108 (1939); H. Aoki, Phys. Rev. **55**, 795 (1939); W. H. Zinn, S. Seely, and V. W. Cohen, Phys. Rev. **56**, 260 (1939); M. R. MacPhail, Phys. Rev. **57**, 669 (1940).